EPA/600/2-86/099

LIMESTONE BED CONTACTORS FOR CONTROL OF CORROSION AT SMALL WATER UTILITIES

by

Raymond D. Letterman
Charles T. Driscoll, Jr.
Marwan Haddad
H. Alan Hsu
Syracuse University
Syracuse, New York 13210

Cooperative Agreement No. CR-809979-01-3

Project Officer

Gary S. Logsdon
Drinking Water Research Division
Water Engineering Research Laboratory
Cincinnati, Ohio 45268

WATER ENGINEERING RESEARCH LABORATORY
OFFICE OF RESEARCH AND DEVELOPMENT
U.S. ENVIRONMENTAL PROTECTION AGENCY
CINCINNATI, OHIO 45268

PB87-112058

FOREWORD

The U.S. Environmental Protection Agency is charged by Congress with protecting the Nation's land, air, and water systems. Under a mandate of national environmental laws, the agency strives to formulate and implement actions leading to a compatible balance between human activities and the ability of natural systems to support and nurture life. The Clean Water Act, the Safe Drinking Water Act, and the Toxic Substances Control Act are three of the major congressional laws that provide the framework for restoring and maintaining the integrity of our Nation's water, for preserving and enhancing the water we drink, and for protecting the environment from toxic substances. These laws direct the EPA to perform research to define our environmental problems, measure the impacts, and search for solutions.

The Water Engineering Research Laboratory is that component of EPA's Research and Development program concerned with preventing, treating, and managing municipal and industrial wastewater discharges; establishing practices to control and remove contaminants from drinking water and to prevent its deterioration during storage and distribution; and assessing the nature and controllability of releases of toxic substances to the air, water, and land from manufacturing processes and subsequent product uses. This publication is one of the products of that research and provides a vital communication link between the researcher and the user community.

Use of limestone contactors to raise the pH, calcium content, and alkalinity of low pH, soft water was evaluated in this project. Studies were conducted in pilot plant columns at Syracuse University, and field evaluations of three types of contactors were carried out at Big Moose Lake in the Adirondacks. The limestone contactors were shown to be capable of reducing the corrosive tendency of water, as measured by copper and lead concentration increases in water held in plumbing of cottages at Big Moose Lake. The model for water quality changes in a limestone column hold promise for application to design of limestone beds placed in upwelling zones (submerged springs) on the beds of acidified lakes.

DISCLAIMER

The information in this document has been funded in part by the United States Environmental Protection Agency under assistance agreement number CR-809979-01-3 to Syracuse University. It has been subject to the Agency's peer and administrative review, and it has been approved for publication as an EPA document. Mention of trade names or commercial products does not constitute endorsement or recommendation for use.

ABSTRACT

A study was conducted to investigate the use of limestone contactors as a technique for mitigating corrosion in small water supply systems that use dilute acidic water. As water is transported through a packed bed of crushed limestone, calcium carbonate dissolves and the pH, calcium ion concentration, and alkalinity increase.

A mathematical model was derived for use in contactor design. The model is based on the interfacial transport of calcium ion and relates the depth of limestone required in the contactor to the desired effluent water chemistry, influent water chemistry, limestone particle size and shape, limestone bed porosity, and water temperature, and superficial velocity. The model was calibrated and tested using laboratory column experiments.

In a contactor monitored for 2.5 years (except for the initial few months) the water quality following treatment was essentially constant. No gradual, long-term degradation in performance was noted. After several months of operation, however, the rate of $CaCO_3$ dissolution was not as high as that observed in the laboratory using fresh limestone. The rate of dissolution is possibly reduced by an alumino-silicate residue that remains after the $CaCO_3$ is dissolved from the limestone matrix. A microbiological film may also have been a limiting factor.

Field study results indicated that limestone contactors can be used to effectively reduce the tendency of water to take up corrosion byproducts (copper, lead, and zinc) from surfaces in piping systems. Copper and lead concentrations in first-flush samples of cottage tapwater receiving untreated spring water were 1.9 ± 0.31 mg Cu/L and 0.046 ± 0.004 mg Pb/L, respectivley. Contactor-treated water at Bay Side cottage contained copper concentrations of 0.030 ± 0.037 mg Cu/L and lead concentrations of 0.0084 ± 0.0084 mg Pb/L.

This report was submitted in fulfillment of Cooperative Agreement CR-809979-01-3 by Syracuse University under the sponsorship of the U.S. Environmental Protection Agency. This report covers the period August 1, 1982 to July 31, 1985 and work was completed as of July 31, 1985.

CONTENTS

Foreward....ii
Abstract....iv
List of Figures....vii
List of Tables....xii
Acknowledgments....xiv

Section 1
Introduction....1
Statement of Problem....1
Study Objective....1

Section 2
Conclusions....3

Section 3
Recommendations....5

Section 4
Literature Review....6
Introduction....6
Limestone Properties....6
Kinetics of Limestone Dissolution....8
Packed Bed Reactors....22
Metal Release from Pipes....24

Section 5
Methods and Materials....32
Apparatuses - Laboratory and Field Contactor Units....32
Laboratory contactors....32
Field Contactors....34
Limestone Characteristics....40
Limestone Bed Characteristics....45
Pipesection Procedures....55
Sampling and Analytical Procedures....55
General Procedures....55
Laboratory contactors....57
Quality Assurance/Quality Control Information Data....57
Computative Analysis....65

Section 6
Derivation of Contactor Design Equations....69
Equilibrium Calcium Concentration....71

Section 7
Results and Discussion....74
Model Verification....74
Equilibrium Calcium Concentration....74
Contactor Design Equations....81

Section 7 (con't)
Field Study Results....94
Baffled Box Contactor....94
Bayside Cottage Wound Fiberglass Column....116
Culligan (Cullneu®) Contactor....119
Evaluation of Contactor Design Equations Using Field Measurements....127
Sensitivity Analysis - Design Equations....133
Thermodynamic Calculations of Trace Metal Chemistry....138
Pipe Leaching Experiments....156
Metal Release from Field Site....164
Spring Contactor Treatment....164
Lake Contactor Treatment....167

References....177

Appendices
A - Chemical Equilibrium Model used in Contactor Design Equation....184
B - Dissolution Rate Data from Column Experiments....199
C - Estimates of Limestone Contactor Costs....205

FIGURES

Number		Page
1	Locations of major chalk and limestone deposits in the continental United States	9
2	Schematic representation of the calcium carbonate dissolution process	13
3	Initial rate of calcite dissolution as a function of the bulk solution pH from Sjoberg and Rickard (1984a)	18
4	Initial rate of calcite dissolution as a function of bulk solution pH and partial pressure of carbon dioxide (Plummer et al., 1975)	19
5	Initial rate of calcite dissolution as a function of the square root of rotating disk rotational speed	21
6	Laboratory columns with water supply and flow control system	33
7	Baffled-box contactor used in the field study	35
8	Wound-fiberglass and Culligan contactors used in the field study	36
9	Map of the Covewood lodge property located near Old Forge, N.Y. Site of the field study	38
10	Diagram showing the installation of the baffled-box contactor in the spring at Covewood	39
11	Measured porosity plotted as a func tion of container surface area to volume ratio for four limestone particle effective diameters	46
12	Measured effluent tracer concentration plotted as a function of time elapsed after tracer injection for four values of the superficial velocity	50
13	Mean residence time calculated using the superficial velocity and measured porosity plotted as a function of the mean residence time from the tracer experiments	53
14	Measured effluent tracer concentration plotted as a function of the time elapsed after tracer injection for the baffled-box contactor (Figure 7)	54
15	Measured and calculated alkalinity for field measurements	61
16	pH plotted as a function of the axial distance to the sampling port and influent pH, pH_o	75

Number		Page
17	Calcium concentration plotted as a function of the axial distance to the sampling port and influent pH, pH_o	76
18	Dissolved inorganic carbon concentration plotted as a function of the axial distance to the sampling port and influent pH, pH_o	77
19	Equilibrium pH, dissolved inorganic carbon and calcium concentrations plotted as a function of the influent pH and the following conditions; Curve A - closed systen and C_{bo} = 0; Curve B closed system and C_{bo} = 28 mgCa/L; Curve C - closed/ open system and C_{bo} = 0; Curve D - closed/open systen and C_{bo} = 28 mgCa/L	79
20	Influent calcium concentration plotted as a function of the influent dissolved inorganic cargon concentration and the equilibrium pH for an influent pH of 6.0	80
21	Sum of the square of the difference between the observed and the model predicted calcium concentration plotted as a function of the dissolution rate constant for run number 32, Appendix B	83
22	Model predicted and measured calcium concentrations plotted as a function of the axial distance to the sampling port for run number 32 and K_o = 0.032 cm/min	84
23	ln $[C_{bL} - C_{eq})/(C_{bo} - C_{eq})]$ plotted as a function of the axial distance to the sampling port for runs 29, 31 and 32	85
24	Dissolution rate constant determined by the least squares method (Method II) plotted as a function of the value obtained using plots such as Figure 23 (Method I)	86
25	Mass transfer factor, j_D, plotted as a function of a modified Reynold's number using the equations derived by Chu and Khalil (1953)	88
26	Values of the dissolution rate constant calculated using the model equations plotted as a function of the experimental (best-fit) values listed in Appendix B	90
27	Observed calcium concentration plotted as a function of the model predicted value. The points include all sampling port locations for the runs listed in Appendix B	91
28	Model predicted and measured pH plotted as a function of the axial distance to the sampling port for run number 32 and K_o = 0.032 cm/min	93
29	Observed pH plotted as a function of the model predicted values for all sampling port locations for the runs listed in Appendix B	95

Number		Page
31	Model predicted and measured alkalinity plotted as a function of the axial distance to the sampling port for run number 32 and K_o = 0.032 cm/min	98
32	Measured change in alkalinity within the laboratory contactors plotted as a function of the model predicted change	99
33	Water temperature plotted as a function of time for the baffled-box contactor	100
34	Influent and effluent pH plotted as a function of time for the baffled-box contactor	101
35	Influent and effluent calcium concentration plotted as a function of time for the baffled-box contactor	103
36	Influent and effluent alkalinity plotted as a function of time for the baffled-box contactor	104
37	Influent and effluent dissolved inorganic carbon concentration plotted as a function of time for the baffled-box contactor	105
38	Influent and effluent standard plate count bacteria concentration plotted as a function of time for the baffled-box contactor	106
39	Influent and effluent total coliform bacteria concentration plotted as a function of time for the baffled-box contactor	107
40	Calculated partial pressure of carbon dioxide plotted as a function of time for the influent and effluent of the baffled-box contactor	111
41	X-ray energy spectra for the following samples: A - fresh limestone, B - limestone after prolonged dissolution in the baffled-box contactor, compartment 1, C - same as B except compartment 5, D - limestone after prolonged dissolution in the laboratory	117
42	Influent and effluent pH plotted as a function of time for the wound-fiberglass contactor in Bayside Cottage	120
43	Influent and effluent calcium concentration plotted as a function of time for the wound-fiberglass contactor in Bayside Cottage	121
44	Influent and effluent alkalinity plotted as a function of time for the wound-fiberglass contactor in Bayside Cottage	123
45	Influent and effluent dissolved inorganic carbon concentration plotted as a function of time for the wound-fiberglass contactor in Bayside Cottage	123

Number		Page
46	X-ray energy spectrum for a limestone sample taken from the wound-fiberglass contactor at the end of the experiment	125
47	X-ray energy spectra for fresh Cullneu® medium (A) and Cullneu® used in the Culligan contactor for 9 months (B)	128
48	Total depth of limestone required to obtain an effluent pH of 8.5 plotted as a function of the ionic strength	140
49	Predominance area diagram for the stability of lead passivation films over a range of pH and dissolved inorganic carbon concentrations at 25°C $p*K_{so}$ = -8.15	142
50	Predominance area diagram for the stability of lead passivation films over a range of pH and dissolved inorganic carbon concentrations at 250°C $p*K_{so}$ = -13.07	143
51	Lead concentrations calculated with the chemical equilibrium model MINEQL as a function of pH for several concentrations of dissolved inorganic carbon	144
52	Predominance area diagram for the stability of lead passivation films over a range of pH and partial pressures of CO_2 at 25°C $p*K_{so}$ = 8.15	146
53	Predominance area diagram for the stability of lead passivation films over a range of pH and partial pressures of CO_2 at 25°C $p*K_{so}$ = 13.07	147
54	Lead concentrations calculated with the chemical equilibrium model MINEQL as a function of pH for several partial pressures of CO_2	148
55	Predominance area diagram for the stability of copper passivation films over ranges of pH and dissolved inorganic carbon concentrations at 25°C	149
56	Copper concentrations calculated with the chemical equilibrium model MINEQL as a function of pH for several concentrations of dissolved inorganic carbon	150
57	Copper concentrations calculated with the chemical equilibrium model MINEQL as a function of pH for several partial pressures of CO_2	151
58	Predominance area diagram for the stability of zinc passivation films over a range of pH and dissolved inorganic carbon concentrations at 25°C	152

Number		Page
59	Zinc concentrations calculated with the chemical equilibrium model MINEQL as a function of pH for several dissolved inorganic carbon concentrations	153
60	Predominance area diagram for the stability of zinc passivation films over ranges of pH and partial pressures of CO_2 at 25°C	154
61	Zinc concentrations calculated with the chemical equilibrium model MINEQL as a function of pH for several partial pressures of CO_2	155
62	Lead concentrations from lead pipe sections leaching experiments	157
63	Zinc concentrations from galvanized steel pipe section leaching experiments	158
64	Total and filtered concentrations of lead from lead pipe section leaching experiments	159
65	Variations in pH (a), dissolved inorganic carbon (DIC) concen tration (b) and measured copper (c) and lead (d) concentrations from pipe section leaching experiments as a function of column treatment by $CaCO_3$	160
66	Copper concentrations from copper pipe section leaching experiments at various levels of $CaCO_3$ treatment (variations in pH)	162
67	Lead concentrations from copper pipe section with lead-tin solder leaching experiments at various levels of laboratory $CaCO_3$ treatment (variations in pH)	163
68	The probability of copper concentrations in untreated and $CaCO_3$ treated lake and spring waters exceeding a given concentration	168
69	The probability of lead concentrations in untreated and $CaCO_3$ treated lake and springwaters exceeding a given concentration	169
70	A comparison of measured copper concentrations from first flush tapwater derived from $CaCO_3$ treated lakewater and calculated values from the chemical equilibrium model MIEQL as a function of pH	173
71	A comparison of measured copper concentrations from first flush tapwater derived from $CaCO_3$ treated lakewater and calculaated values from the chemical equilibrium model MINEQL	174
72	A comparison of measured lead concentrations from first flush tapwater derived from $CaCO_3$ treatment and calculated values from the chemical equilibrium model MINEQL as a function of pH	176

TABLES

Number		Page
1	Representative Chemical Analysis of Different Types of Limestone (from Boynton, 1980)	7
2	Major Impurities in High Calcium Limestone (45 U. S. Samples (from Murray et al., 1954)	10
3	Minor Impurities in High Calcium Limestone (25 U. S. Samples) (from Murray et al., 1954)	11
4	Oxidation Potential of Metallic Materials	26
5	Passivation Film Minerals That May Be Important In Regulating Metal Solubility to Water Distribution Systems	29
6	Effective Solubility of Crushed Limestone Experimental Results.	42
7	Limestone Particle Size and Sphericity Analysis Results	44
8	Bed Porosity and Limestone Particle Surface Area Per Unit Volume of Interstitial Water.	48
9	Results of Tracer Response Measurements Obtained Using Laboratory Columns (Figure 6)	51
10	Analytical Methods.	56
11	Summary of Sampling and Analytical Precision from Sample Triplicate Program	59
12	Estimates of Sample Collection and Analytical Precision from 4 x 4 Analysis for Big Moose Lake.	60
13	Summary of Blind Sample Analysis Obtained from USEPA Clinic Municipal Environmental Research Laboratory.	62 & 63
14	Summary of USEPA CERL of Blind Audit Analysis. All Values in eq l^{-1} Except Where Indicated.	64
15	Equilibrium Constants at 25°C for the Solids Considered in the MINEQL Calculations.	66
16	Reactions and Equilibrium Constants at 25°C for the Aqueous Complexes Considered in the MINEQL Calculations.	67
17	Summary of Baffled-Box Contactor Results Field Measurements	109

Number		Page
18	Baffled-Box Contactor - Limestone Dissolution June 28, 1982 September 26, 1983	114
19	Summary of Bay Side Cottage Wound Fiberglass Column Results.	124
20	Culligan Contactor - Summary of Results November 3, 1983 July 31, 1984.	126
21	Baffled-Box and Wound Fiberglass Contactors - Special Test of Model Equations. Experimental Conditions and Results.	129
22	Special Test of Model Equations Calculated Equlibrium pH and Calcium Concentration.	130
23	Results of Field Test of Model Equations.	131
24	Results of Chemical Equilibrium Model Calculations.	135
25	Sensitivity Analysis Results.	137
26	Effect of Ionic Strength on the Equilibrium and Contactor Effluent (pH = 8.5) Calcium Concentrations	139
27	Comparison of Trace Metal Concentration (as mg/l) in Spring Water and from the First Flush of Treated (Hillside, Bay Side) and Untreated (Covewood) Cottages.	165
28	Comparison of Copper and Lead Concentrations (Mean ± Std. Dev. as mg/l) from First Flush and Three Minutes of Flowing Tapwater Derived from the Box Contactor Treated Spring.	166
29	Metal Concentrations (as mg/l) in Lake Influent, Untreated and Treated First Flush Tapwater at Bay Side	171
30	Comparison of Copper and Lead Concentrations (Mean ± Std. Dev,. as mg/l) from First Flush and After Three Minutes of Flowing Tapwater Derived from Both $CaCO_3$ Treated and Untreated Lakewater.	172

ACKNOWLEDGMENTS

The field study part of this project was conducted with the help and cooperation of C.V. "Major" Bowes, proprietor of Covewood Lodge on Big Moose Lake. The first contactor at Covewood was built and installed by Major Bowes and it was his interest in water quality that led to our first measurements and eventually to this research project. We would also like to acknowledge Dr. Gary S. Logsdon of the U.S. Environmental Protection Agency for his continuous assistance, review comments and patience.

SECTION 1

INTRODUCTION

STATEMENT OF PROBLEM

In many areas of the United States individual homeowners and small public and private water supply systems use water that is potentially corrosive to the materials used in the water distribution system. Corrosion is a concern to the owners and users of small water supply systems because of the potential health problems associated with the ingestion of corrosion byproducts, the degradation of the esthetic quality of the water and the significant economic consequences of piping system deterioration.

Corrosion and the contamination of the water by corrosion by-products may be caused by the use of dilute acidic waters that generally have low pH, alkalinity and concentrations of dissolved solids. Dilute acidic ground and surface waters are found in a number of regions of the country, particularly in regions underlain by siliceous bedrock. These waters are naturally low in buffering capacity and they are corrosive. They are also prone to acidification by atmospheric deposition of strong acids (acid precipitation) or other factors such as changes in land use. In some areas (for example the Adirondack Region of New York State) it is possible that the corrosivity of water has been increased by acidic deposition. In any event, until recent concern developed about acidic deposition and the deterioration of water quality as a result of acidification residents and visitors tolerated or ignored the problems caused by the use of corrosive water. Now this indifference has changed to a significant concern, and many home and resort owners as well as those responsible for village water supplies have begun to adopt techniques designed to mitigate drinking water corrosivity.

Low cost is a very important criterion in establishing the feasibility of a corrosion mitigation technique for a small water supply system. Also the maintenance required should be minimal, and the technique should present a low potential for public health hazard resulting from improper construction, installation or maintenance. Limestone contactors are water treatment devices that tend to meet these requirements.

In a limestone contactor water flows through under a closed-to-the-atmosphere condition and dissolves a packed bed of crushed limestone. The chemistry of the water is altered as the limestone dissolves. Sources of $CaCO_3$ other than high calcium limestone (eg., seashells,) are sometimes used. Limestone contactors are simple but effective devices with low capital cost and minimum maintenance requirements. They have been used for the neutralization of acid mine drainage, acidic industrial wastes, and dilute acidic surface waters.

STUDY OBJECTIVES

The overall objective of this project was to investigate the use of limestone contactors as a technique for the mitigating corrosion in small

water supply systems that use dilute acidic water. The research plan included the development and testing of a rational method for contactor design and the evaluation of the field operation of a contactor with respect to corrosion control and operation and maintenance problems. The study had the following specific objectives:

(1) to derive and test (using laboratory, column-type reactors) a mathematical model for limestone contactor design,

(2) to develop design objectives by experimentally determining the relationship between contactor-treated water quality and metal release from pipes, and

(3) to evaluate the practical application of the design equations and objectives by monitoring the field performance of full-scale contactors and to determine the feasibility of long-term operation and the type and frequency of maintenance required.

SECTION 2

CONCLUSIONS

As dilute acidic water is transported through a packed bed of crushed limestone, calcium carbonate in the limestone dissolves, the pH, calcium ion concentration, and alkalinity increase, and the tendency may decrease for water to dissolve corrosion by-products from surfaces in piping systems.

The depth of limestone, L, required to achieve a given level of treatment can be calculated using a mathematical model based on interfacial transport of calcium ion,

$$L = \frac{\ln[(C_{eq} - C_{bL})/(C_{eq} - C_{bo})]}{\frac{K_o\, a\, \varepsilon}{U_s} - 2\,\bar{d}\left[\frac{K_o\, a\, \varepsilon}{U_s}\right]^2}$$

where a is the interfacial area of limestone per unit volume of interstitial water, ε is the bed porosity, U_s is the superficial velocity, $\bar{d}$ is the effective diameter of the limestone particles, and K_o is the overall $CaCO_3$ dissolution rate constant. C_{bo} is the influent calcium concentration. The results of this study indicate that K_o can be estimated using an existing correlation of dimensionless mass transfer parameters. The quantity "a" can be estimated using $\bar{d}$ and the particle sphericity. The equilibrium and effluent calcium concentrations, C_{eq} and C_{bL}, are determined using a chemical equilibrium model. The magnitudes of these parameters are a function of the characteristics of the influent solution, particularly the temperature, pH, and calcium and dissolved inorganic carbon (DIC) concentrations. As the influent calcium and/or DIC concentrations increase the maximum pH (pH_{eq}) that can be attained in a contactor decreases, and the depth of limestone required to reach a given effluent pH ($< pH_{eq}$) increases. The depth of limestone required to achieve a given treatment objective also increases with decreasing influent pH, increasing superficial velocity, and increasing limestone particle size.

An evaluation of a limestone contactor in the field suggests that except for the initial few months, water quality following treatment was constant through the 2.5-year study period. There was no evidence of a gradual, long-term reduction in performance. However, after 3 or 4 months of continuous operation, the rate of $CaCO_3$ dissolution was not as high as that predicted by the laboratory results obtained with fresh limestone. Analysis of the limestone surfaces by x-ray energy spectrometry indicated that prolonged operation altered the surface of the limestone; the relative abundance of calcium on the surface decreased, and aluminum and silicon increased. Apparently, alumino-silicate impurities in the limestone remained as a thin "residue" after the $CaCO_3$ was leached from the limestone surface matrix. This residue may have slowed the dissolution rate. Also possible is that the dissolution process was adversely affected by a microbiological film on the limestone.

The model developed for contactor design assumes that the water flows through the limestone under a closed-to-gaseous carbon dioxide condition.

Equilibration of the column effluent with atmospheric carbon dioxide can have a significant effect on the pH of the solution and hence on the tendency to dissolve corrosion by products. When the influent DIC is high, (e.g., greater than 10 mg C/L), equilibration with the atmosphere may cause the pH to increase. When the influent DIC concentration is less than several mg C/L, the pH tends to decrease.

Results of the study suggest that dilute acidic waters facilitate the release of elevated concentrations of trace metals from metal piping systems. Passivation films of most significance include $Cu_2(OH)_2\ CO_3$ and $Cu(OH)_2$ for copper, $PbCO_3$, $Pb_3(OH)_2(CO_3)_2$ or $Pb(OH)_2$ for lead and $Zn_5(OH)_6(CO_3)_2$ for zinc. Because of the pH and inorganic carbon-dependent solubility of these minerals, metal corrosion can generally be mitigated by increases in pH and dissolved inorganic carbon concentrations. However, elevated inorganic carbon concentrations coupled with high pH values can facilitate the solubilization of trace metals through the formation of soluble metal carbonate complexes. This problem is most significant for lead, as copper and zinc do not form strong aqueous complexes with carbonate.

Laboratory pipe section experiments using copper pipe with lead-tin solder indicate that limestone contactor treatment reduces copper, and to a smaller extent, lead leaching. Theoretical thermodynamic calculations were consistent with measured copper concentrations in the neutral pH (pH 6.5 to 7.5) region. However, copper concentrations in acidic waters ($pH \leq 6.0$) were substantially undersaturated with respect to theoretical metal solubility. Lead derived from lead-tin solder in pipe section experiments was highly undersaturated with respect to the solubility of lead passivation films.

Trace metal field results were generally consistent with laboratory observations. Spring and lake waters with and without limestone contactor treatment were corrosive. Elevated metal concentrations were observed in first-flush tapwater from both treated and untreated cottages. Running tapwater (3 minutes) significantly reduced copper, lead, and zinc concentrations. Although treated waters were generally corrosive, trace metal concentrations were significantly reduced in both treated spring and lake water, relative to untreated water. For example, first-flush copper and lead concentrations in cottage tapwater receiving untreated spring water were 1.9 ± 0.31 mg Cu/L and 0.0046 ± 0.004 Pb/L, respectively. While treated spring water at Bay Side cottage contained copper concentrations of 0.030 ± 0.037 mg Cu/L and lead concentrations of 0.0084 ± 0.0084 mg Pb/L. Likewise, $CaCO_3$ treatment of acidic lakewater at Bayside cottage significantly reduced copper concentrations in first-flush tapwater from 1.9 ± 0.35 mg Cu/L to 0.54 ± 0.30 mg Cu/L and reduced lead concentrations from 0.033 ± 0.009 mg Pb/L to 0.015 ± 0.014 mg Pb/L. Limestone treatment greatly reduced the probability of metal concentrations exceeding the secondary MCL of 1.0 mg Cu/L from greater than 75% to less than 15%. The probability of consuming elevated lead concentrations in first-flush tapwater was also reduced by $CaCO_3$ treatment.

Measured trace metal concentrations from first-flush tapwater were compared with theoretical calculations from the chemical equilibrium model. Generally untreated lakewater was highly acidic (pH 4.6), and measured copper concentrations were highly undersaturated with respect to the theoretical solubility of $Cu_2(OH)_2CO_3$. However, following treatment, measured copper values were in close agreement to thermodynamic predictions. Concentrations of lead largely derived from lead-tin solder were highly undersaturated with respect to the solubility of lead passivation films.

SECTION 3

RECOMMENDATIONS

The results of this study suggest that as calcium carbonate is dissolved from the limestone particle matrix a layer of residue forms. It appears that transport across this layer eventually limits the overall rate of dissolution. This has important implications for the design of a contactor for long term use. In this study there was limited evidence that the performance of a contactor operated for two years in the field was influenced by the formation of a residue layer.

It seems reasonable to assume that the rate of build-up of a residue layer will be a function of the level of insoluble impurities in the limestone. Additional research is needed to determine this relationship. Long-term experiments should be conducted using contactor columns filled with limestones of varying purity. The rotating disk apparatus has been used to effectively study the kinetics of calcite dissolution and should be considered for use in measuring the effect of limestone purity on the rate of dissolution. Until the significance of the residue layer has been determined the results of this study should be used with an awareness that limestone purity may be an important variable.

SECTION 4
LITERATURE REVIEW

INTRODUCTION

This review of the literature is divided into three parts. In the first section the characteristics of limestone are discussed. Limestone is, in most parts of the country, a readily available and inexpensive source of $CaCO_3$. However because it is a natural material, its physical and chemical characteristics are variable and this variability may affect its use as a neutralizing substance.

The engineering design of a limestone contactor requires an understanding of the kinetics of the neutralization ($CaCO_3$ dissolution) reaction. This topic is covered in the second part of the literature review.

In the third part of the literature review the effect of water chemistry on the release of corrosion by-products such as lead from lead-tin solder and copper from copper pipes is discussed.

LIMESTONE PROPERTIES

Limestone is a general term used to describe sedimentary rock composed primarily of calcium carbonate or combinations of calcium and magnesium carbonate with varying amounts of impurities, the most common of which are silica and alumina. There are numerous forms and types of limestone, varying in chemical composition, mineralogy, crystallinity, color, texture and hardness. Next to sand and gravel, limestone, including all of its carbonate forms, is the second greatest tonnage material produced in the United States.

The two most fundamental types of limestone are high calcium and dolomitic limestone. Pure high calcium limestone is 100 percent calcium carbonate (calcite or aragonite). Pure dolomite is 54.3% $CaCO_3$ and 45.7% $MgCO_3$. High-quality, high calcium limestone is 97-99% $CaCO_3$. (54-56% CaO). Chemical analyses for a number of U.S. limestones are summarized in Table 1.

High calcium limestone was used exclusively in this study. Since there is considerable evidence to suggest that the dissolution rate of dolomitic limestone is substantially less than high calcium limestone (Pearson and McDonnell 1975a, 1975b) the results of this study should therefore, only

Table 1 Representative chemical analyses (percentage composition) of different types of limestone (from Boynton, 1980)

	Limestone Sample*							
	1	2	3	4	5	6	7	8
CaO	54.54	38.90	41.84	31.20	29.45	45.65	55.28	52.48
MgO	0.59	2.72	1.94	20.45	21.12	7.07	0.46	0.59
CO_2	42.90	33.10	32.94	47.87	46.15	43.60	43.73	41.85
SiO_2	0.70	19.82	13.44	0.11	0.14	2.55	0.42	2.38
Al_2O_3	0.68	5.40	4.55	0.30	0.04	0.23	0.13	1.57
Fe_2O_3*	0.08	1.60	0.56	0.19	0.10	0.20	0.05	0.56
SO_3	0.31	--	0.33	--	--	0.33	0.01	--
P_2O_5	--	--	0.22	--	0.05	0.04	--	--
Na_2O	0.16	--	0.31	0.06	0.01	0.04	--	--
K_2O	--	--	0.72	--	0.01	0.03	--	--
H_2O	--	--	1.55	--	0.16	0.23	--	n.d.
Other	--	--	0.29	--	0.01	0.06	0.08	0.20

*

1 = Indiana high calcium stone.

2 = Lehigh Valley, Pa. "cement rock."

3 = Pennsylvania "cement rock."

4 = Illinois Niagaran dolomitic stone.

5 = Northwestern Ohio Niagaran dolomitic stone.

6 = New York magnesium stone.

7 = Virginia high calcium stone.

8 = Kansas cretaceous high calcium (chalk).

be applied to the use of high calcium stone. Active sources (quarries and mines) of high calcium limestone are present in essentially every state (See Figure 1).

Care must be taken in selecting a high calcium stone for use in a limestone contactor. Some states have either high calcium or dolomitic or abundant quantities of both types. The distribution of these materials is however without a predictable pattern, in some cases they occur in separate broad expanses, while in other cases both types may be present in close proximity, for example, on opposite sides of a quarry.

Limestone may contain a number of impurities. Clay, silt and sand (or other forms of silica) may have become incorporated in the stone when it was first deposited or material may have collected later in crevices and between strata. These mineral contaminants are the sources of the major impurities, silica and alumina. Other impurities, in a rough order of relative amounts are iron, phosphorus and sulfur. Trace substances such as manganese, copper, titanium, sodium, potassium, fluorine, arsenic and strontium may be present.

Murray et al. (1954) analyzed 45 different high calcium limestones from the United States. The principal impurities are listed in Table 2. All stone analyzed contained measurable amounts of silica, alumina and magnesium oxide. Potassium, sodium and sulfur were present in some samples.

Murray et al. (1954) also examined 25 high calcium limestones spectrographically for 25 metallic elements. The findings obtained for elements other than calcium, magnesium, silicon and iron are listed in Table 3. Aluminum, barium, manganese,phosphorus, potassium, sodium, strontium and tin were detected in all 25 samples. Titanium, zinc and chromium were detected in 20 of the samples. The metals present at a concentration greater than 1000 ppm in at least one sample are aluminum, manganese, potassium, sodium, strontium, titanium and zinc.

KINETICS OF LIMESTONE DISSOLUTION

The engineering design of a limestone contactor requires an understanding of the kinetics of the $CaCO_3$ dissolution process and the effect of this dissolution on the chemistry of the bulk solution. The overall neutralization/dissolution reaction is given by

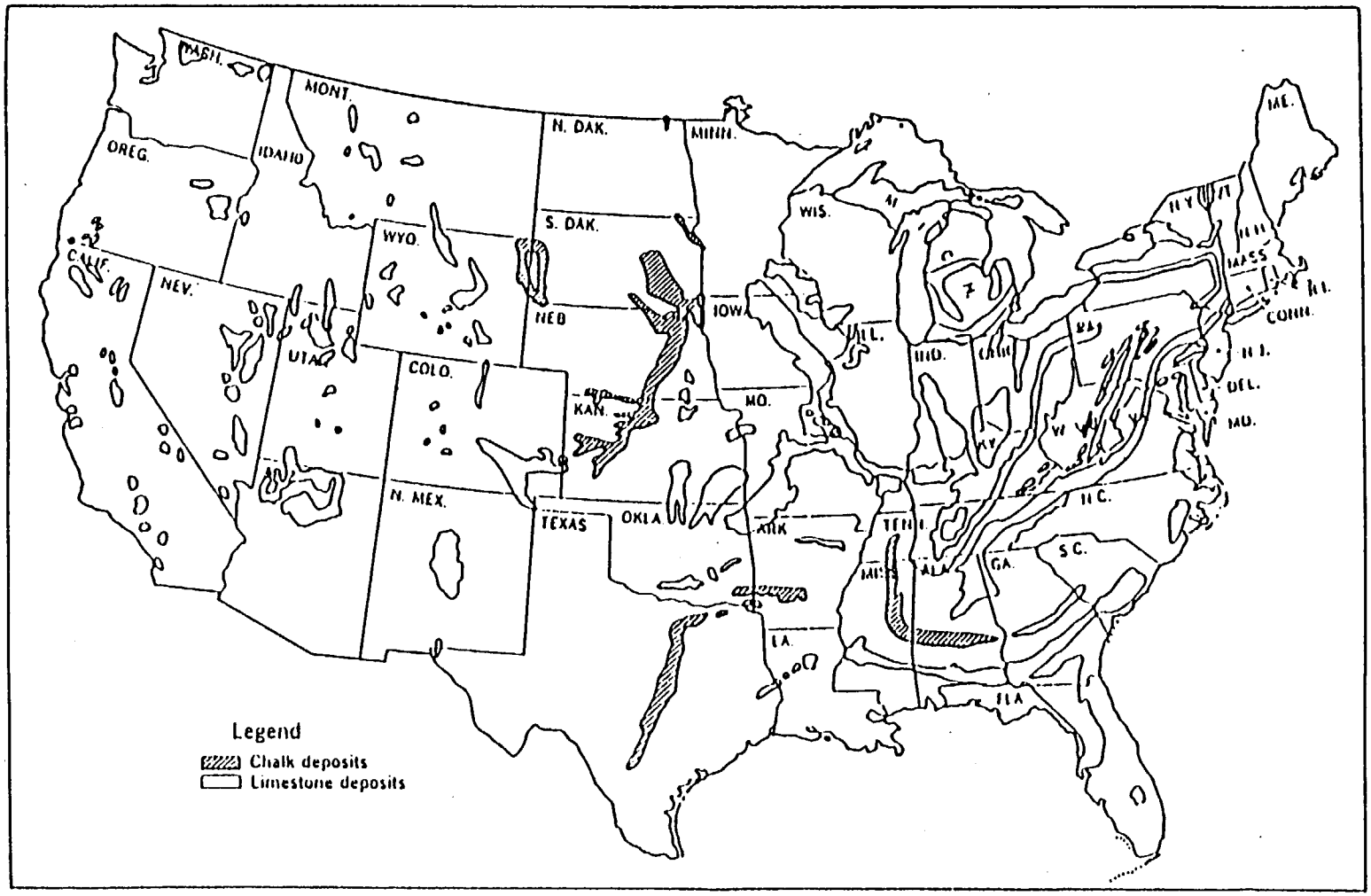

Figure 1. Locations of major chalk and limestone deposits in the continental United States.

Table 2 Major Impurities in High Calcium Limestone (45 U.S. Samples) (from Murray et al., 1954)

SiO_2	0.10 - 2.89%
Al_2O_3	0.13 - 0.92%
K_2O	0.00 - 0.21%
Na_2O	0.00 - 0.16%
SO_3	0.00 - 0.56%
MgO	0.12 - 3.11%

Table 3 Minor Impurities in High Calcium Limestone (25 U.S. Samples) (from Murray et al., 1954)

Element	Number of Samples With Detectable Amount	Maximum Amount
Al	25	0.35-0.60% (5 samples)
Ba	25	not given
B	3*	
Cr	20	10 ppm+ (3 samples)
Co	9	10 ppm+ (2 samples
Pb	15*	
Mn	25	0.1%+ (1 sample)
Hg	4	
Mo	8*	
Ni	22	0.01% (1 sample)
P	25	0.001-0.01% (2 samples)
K	25	0.2% (1 sample)
Ru	17*	
Ag	13*	
Na	25	0.1%+ (3 samples)
Sr	25	0.01-0.1% (all samples)
Sn	25*	
Ti	23	0.1%+ (1 sample)
Zn	23	0.1%+ (1 sample)

*trace amounts only

$$CaCO_3 + H^+ \longrightarrow Ca^{++} + DIC$$

where, DIC, the dissolved inorganic carbon, includes the species, $H_2CO_3^*$ ($CO_2 + H_2CO_3$), HCO_3^- and $CO_3^=$.

The dissolution reaction at the solid surface is influenced by the transfer of the reactants (e.g., hydrogen ion) to the interface and the products (calcium and DIC species) away from it. In addition, if the objective is to understand the effect of dissolution on the chemistry of the bulk solution, the rates of homogeneous reactions involving dissolution products in the solution and, if a gas phase is present, the rate of transport of inorganic carbon to or from the aqueous phase must be considered.

A schematic diagram illustrating the overall dissolution process in a system which includes a $CaCO_3$ solid phase, the aqueous solution and a gas phase which may contain carbon dioxide or may act as an infinite sink for CO_2 released from the aqueous phase is presented in Figure 2. The rate of change in bulk solution chemistry is affected by one or more of the reactions shown.

Reaction A in Figure 2 represents the decomposition of the solid phase, i.e., the net release of calcium and carbonate to the solution. This step might be a combination of reactant adsorption (e.g., H^+ or H_2O) on the $CaCO_3$ surface, chemical reaction with the surface and desorption of reaction products.

The rate of decomposition of the surface (and the rate of change in the bulk solution chemistry) may be controlled by the transport of hydrogen ions to the surface (reaction C) or the transport of reaction products (Ca^{++}, $CO_3^=$, HCO_3^-, and H_2CO_3) away from the surface (reaction B). If a gas phase is present, as shown in Figure 2, the bulk solution chemistry may be affected by the transport of reaction products or gas phase components to or from the bulk solution (reactions D and E). It is also possible, as indicated by reaction E, that a homogeneous solution phase reaction such as the protonation of the bicarbonate ion or the dehydration of carbon dioxide may effect the time varying chemical characteristics of the bulk solution and the solution within the boundary layers.

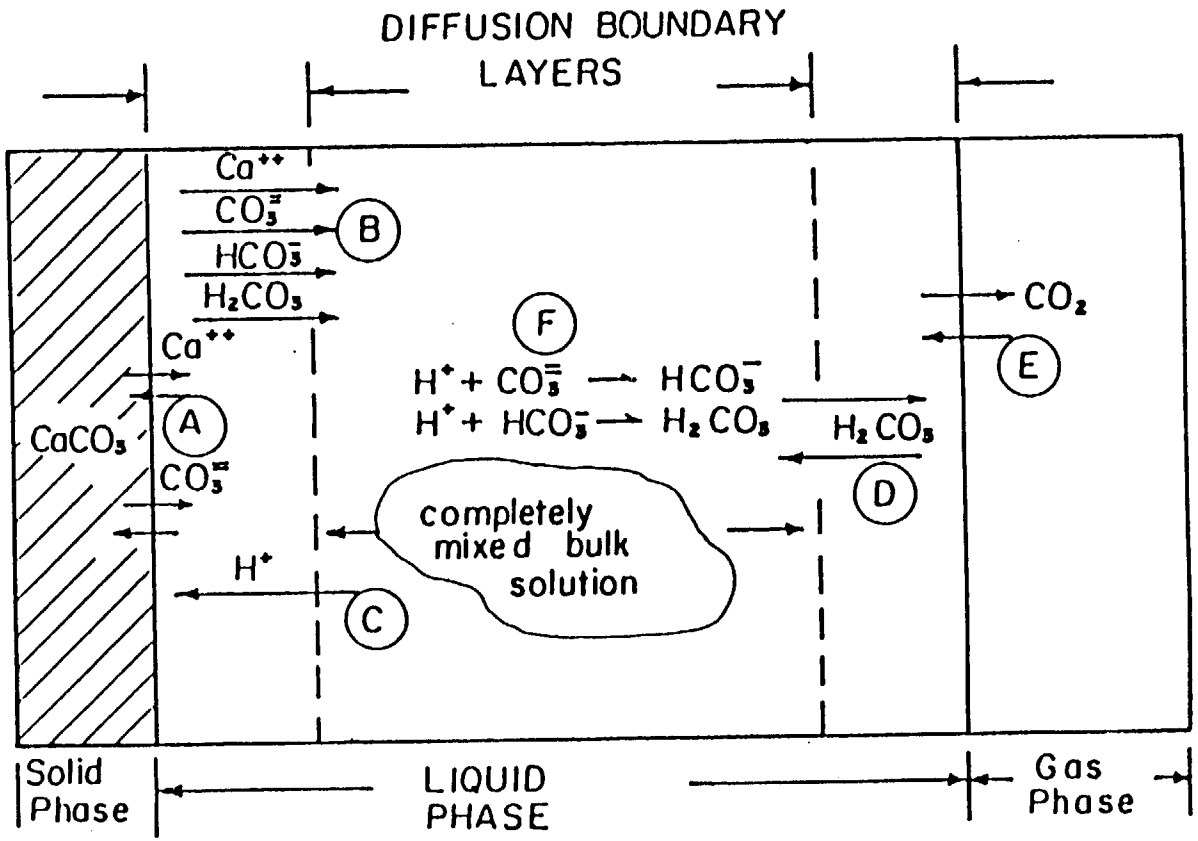

Figure 2. Schematic representation of the calcium carbonate dissolution process.

A significant amount of research has been conducted on mineral dissolution kinetics. The dissolution of calcite and limestone has been investigated for applications such as the formation of antacids (Lund et al., 1975), the neutralization of pickling acids (Eden and Truesdale, 1950; Gehm, 1944; Hoak et al., 1944, 1945, 1947; Reidl, 1947; Galloway and Colville, 1970), the neutralization of acid mine drainage (Pearson and McDonnell, 1975a, 1975b; Jarret, 1966, Mihok et al., 1968; Vatanatham, 1975), the effect of $CaCO_3$ sediments on the pH of sea water (Morse, 1978; Morse, 1974; Morse and Berner, 1972; Berner and Morse, 1974), the neutralization of CO_2-saturated waters (Frear and Johnson, 1929; Erga and Terjesen, 1956; Terjesen et al., 1961; Plummer et al., 1978; Plummer and Wigley, 1976), the neutralization of dilute acidic ground and surface waters (Bjerle and Rochelle, 1982, Vaillancourt, 1981; Sverdrup and Bjerle, 1982; Driscoll et al., 1982; Haddad, 1983), the neutralization of nitric acid solutions (Wentzler, 1971), sulfuric acid solutions (Vatanatham, 1975) and hydrochoric acid solutions (Lund et al., 1975; Tominaga, 1939).

It has been recognized for a long time that mass transport to or from the dissolving $CaCO_3$ surface has at least some effect on the kinetics of the process and therefore most recent, investigators have been careful to control (to some extent) the hydrodynamic conditions in their experimental reactor. A number of experimentors controlled the mixing intensity in mechanically agitated batch reactors containing suspensions of powdered calcite (Erga and Terjesen, 1956; Terjesen et al., 1961; Berner and Morse, 1974; Sjoberg, 1976; Sverdrup and Bjerle, 1982; Rickard and Sjoberg, 1983). Others have mounted rotating cylinders (King and Liu, 1933) or rotating disks (Wentzler, 1972; Lund et al., 1975; Rickard and Sjoberg, 1983; Sjoberg and Rickard, 1983) made of $CaCO_3$ in batch reactors. A few investigators have studied the dissolution reaction using flow-through packed-bed reactors (Pearson and KcDonnell, 1975a, 1975b; Vaillancourt, 1981; Haddad, 1983). In one case (Weyl, 1958) a fluid jet was directed against a calcite crystal.

In the cases where a batch reactor is used the rate of $CaCO_3$ dissolution is usually monitored by either a "pH stat" or "free drift" technique. The pH stat technique involves maintaining the bulk solution at a set-point pH by the controlled addition of mineral acid. The rate of $CaCO_3$ dissolution

is then related to the rate of hydrogen ion addition. The free drift technique involves measuring the pH and/or calcium ion concentration as a function of time as the suspended particles, rotating disk, etc. dissolve in the batch reactor.

Most batch reactor studies have been conducted using an "open" system, where the solution is in contact with a gas phase with a carbon dioxide partial pressure ranging from 0 to 100%. The packed column is usually operated as a closed system; inorganic carbon does not enter or leave the solution during the course of the dissolution reaction. The closed system is less complicated than the open system to model because, as noted in regard to Figure 2, the open system model may require an understanding of the rates of transport and reaction at the gas-solution interface (reactions D and E in Figure 2). There is no gas/liquid interface in an ideal closed system.

A review of the literature suggests that many investigators have recognized the complexity of the $CaCO_3$ dissolution process. Most have attempted to simplify the modeling of this process by delineating the rate limiting steps. It is, however, apparent that in making assumptions and interpretations of experimental data the various investigators have often been limited by the type of apparatus used and the experimental conditions. Consequently, it is difficult to generalize results.

Various processes have been proposed to regulate the dissolution of $CaCO_3$:

- The diffusion of hydrogen ion to the solid surface (King and Liu, 1933, Tominaga et al., 1939, Kaye, 1957, Gortikova and Panteeva, 1937, Neirode and Williams, 1971, Berner and Morse, 1974, Wentzler, 1972, Vaillancourt, 1981, Haddad, 1983).
- A heterogeneous "dissolution" reaction at the solid surface (Erga and Terjesen, 1956, Terjesen et al., 1961, Plummer and Wigley, 1976, Plummer et al., 1978, Berner and Morse, 1974, Sjoberg, 1976).
- Mixed kinetics in which transport and a heterogeneous reaction at the surface acting in series are important (Pearson and Mcdonnell, 1975, Rickard and Sjoberg, 1983, Lund et al., 1975, Berner and Morse, 1974, Plummer et al., 1978, 1976).
- The diffusion of reaction by-products, e.g. Ca^{++}, away from the solid surface (Weyl, 1958, Bjerle and Rocheele, 1982, Berner and Morse, 1974, Haddad, 1983).

- The dissolution and/or exsolution of carbon dioxide in or from the solution (Volpicelli et al., 1981).

Recent papers by Sjoberg and Rickard (Sjoberg and Rickard, 1983; Sjoberg and Rickard, 1984a; Sjoberg and Rickard, 1984b, Rickard and Sjoberg, 1983) provide a detailed analysis of the dissolution process. Sjoberg and Rickard used a rotating-disk/batch reactor apparatus and determined the initial rate of calcite dissolution using the pH-stat technique.

Rickard and Sjoberg (1983) concluded that in neutral to alkaline solutions at ambient temperature the dissolution of calcite was controlled by a mass transfer resistance and a surface reaction acting in series. In this scheme the observed rate of dissolution is a function of a transport rate, R_L, where

$$R_L = K_L (C_s - C_b) \tag{2}$$

and a first order surface reaction rate, R_c, where,

$$R_c = K_c (C_{eq} - C_s) \tag{3}$$

K_L and K_c are the mass transfer and surface reaction rate constants and C_s, C_b and C_{eq} are the molar calcium concentrations at the calcite surface, in the bulk solution and at equilibrium, respectively. The equations for R_L and R_c can be combined by assuming a steady state condition near the interface. The result is an expression for the overall rate of dissolution, R, i.e.,

$$R = K_o (C_{eq} - C_b) \tag{4}$$

where the overall rate constant, K_o, is given by

$$K_o = \frac{K_c K_L}{K_c + K_L} \quad . \tag{5}$$

According to Eq. (5), when $K_c >> K_L$ the dissolution rate is controlled by mass transfer and when $K_L >> K_c$ the surface reaction controls.

Rickard and Sjoberg (1983) concluded that at low pH the initial rate of calcite dissolution was controlled entirely by the rate of mass transfer of the hydrogen ion to the calcite surface. They determined that for pH < 4,

$$R = K_L' [H^+]_b^{0.9}, \quad (6)$$

where $[H^+]_b$ is the bulk solution hydrogen ion concentration and K_L' is an "apparent" mass transfer coefficient for the hydrogen ion. It is not clear exactly why Rickard and Sjoberg found it necessary to change from calcium ion transport control at neutral pH values and above to hydrogen ion transport at low pH. In any case, their assumptions and rate expression for low pH, Eq. (6), are generally consistent with low pH rate equations presented by a number of other investigators (Miadokova and Bednarova ; Lund et al., 1975; Berner and Morse, 1974; Plummer et al., 1975a; Nierode and Williams, 1971).

A plot from Sjoberg and Rickard (1984a) of the initial rate of calcite dissolution as a function of the bulk solution pH for a batch reactor/rotating disk/pH-stat system operating at 25°C and a disk rotational speed of 1000 rpm is presented in Figure 3. Note, the initial rate of dissolution was highest at low bulk solution pH. The rate decreased with increasing pH and approached a minimum (asymptotically) at pH > 5. Under the conditions used to obtain the data of Figure 3 the minimum initial rate of dissolution was approximately 6.3×10^{-10} moles calcium $cm^{-2}s^{-1}$. Sjoberg and Richard (1984a)concluded that the magnitude of this minimum rate was determined by both the mass transfer and surface reaction rate constants (Eq. 5).

Plummer et al. (1978) obtained the initial calcite dissolution rate as a function of the bulk solution pH. The results are presented in Figure 4. The pH-stat technique was used in conjunction with a mechanically agitated batch reactor containing crushed calcite (Iceland Spar). The CO_2 partial pressure was a controlled parameter and the temperature was 25°C.

The results plotted in Figure 4 are similar to those obtained by Sjoberg and Rickard, (1984a). As the bulk solution pH increased above pH = 4 the initial rate of dissolution asymptomatically approached a minimum value. The minimum rate (for $pCO_2 = 0.00$) was approximately 3×10^{-10} moles $cm^{-2}s^{-1}$.

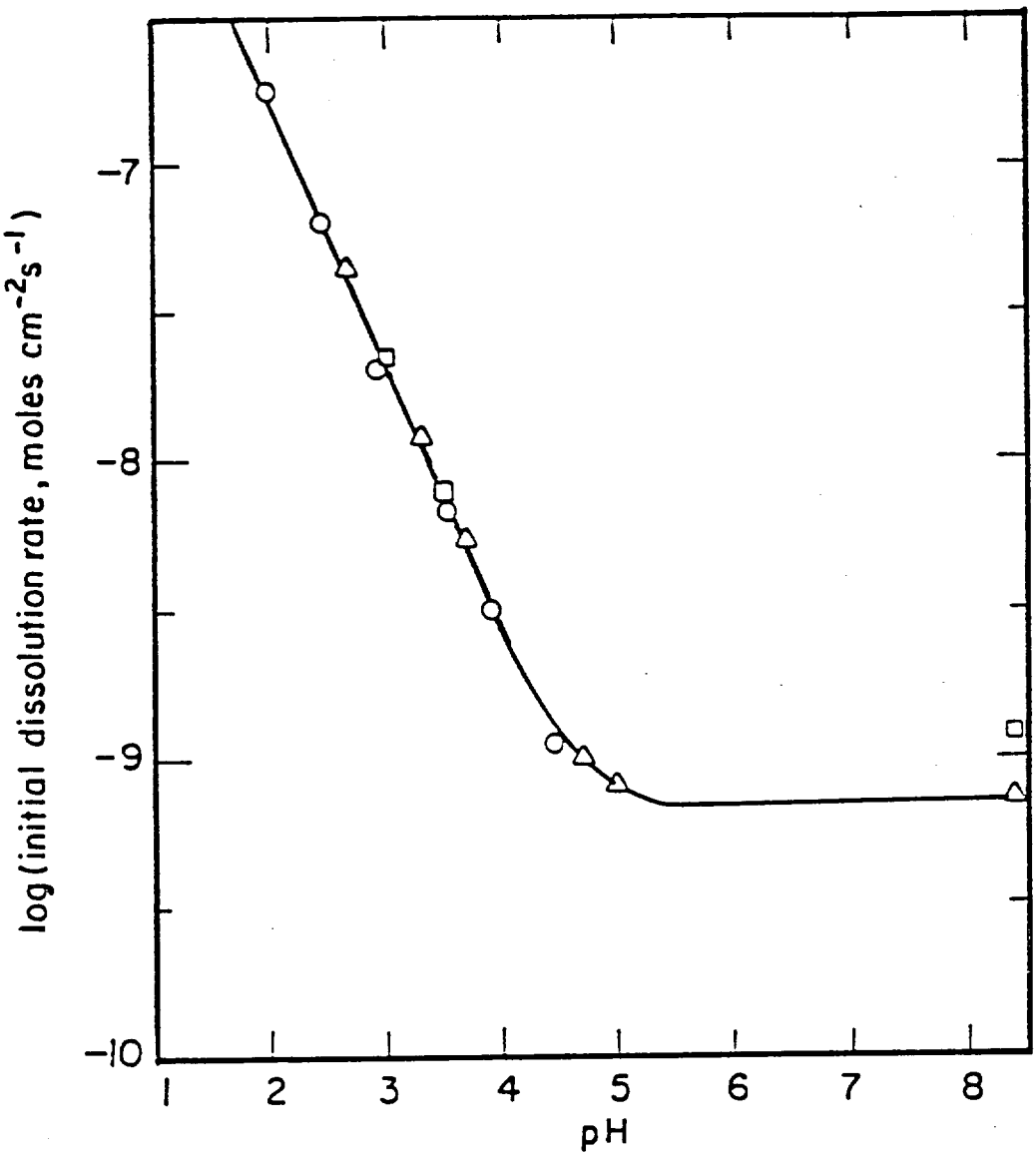

Figure 3. Initial rate of calcite dissolution as a function of the bulk solution pH from Sjoberg and Rickard (1984a). System was closed to atmospheric CO_2.

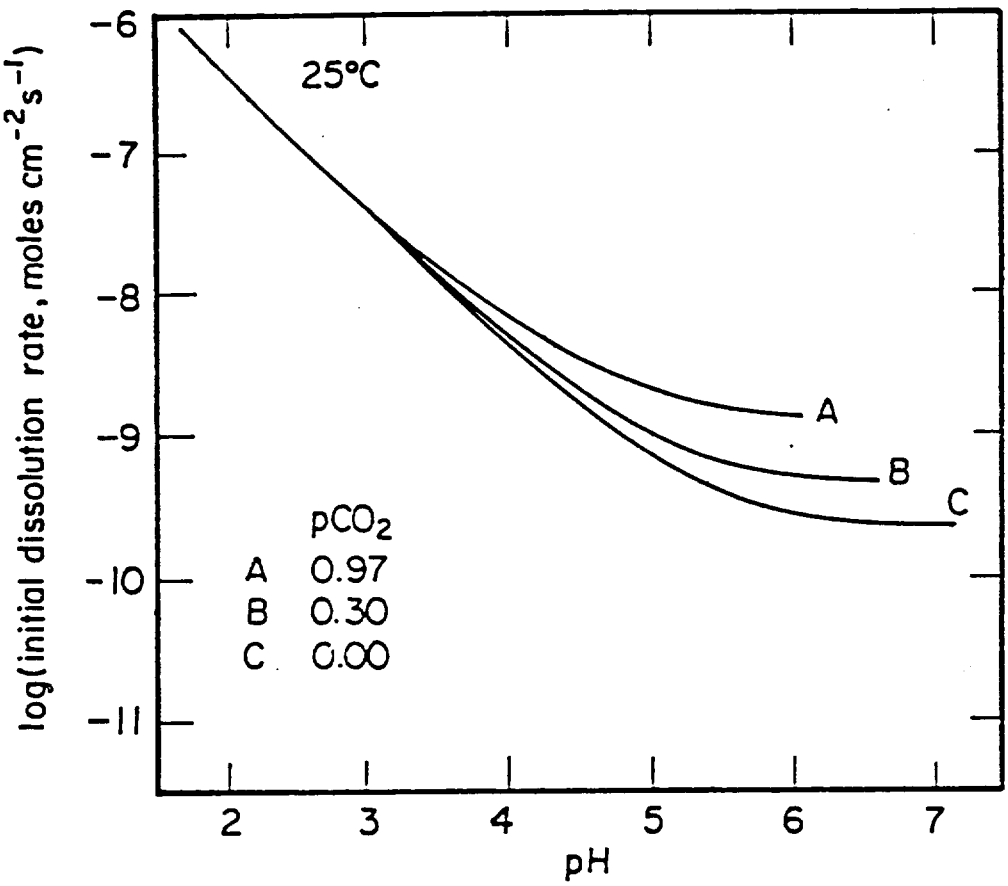

Figure 4. Initial rate of calcite dissolution as a function of bulk solution pH and partial pressure of carbon dioxide (Plummer et al., 1975).

Sjoberg and Rickard (1984b) plotted the initial rate of dissolution as a function of the square root of the disk rotational velocity, $\omega^{\frac{1}{2}}$, to illustrate the effect of the mass transfer coefficient, K_L, on the dissolution rate. An example for carrara marble, a bulk solution pH of 8.4, a background electrolyte of 0.7 M KCl and temperatures of 1 and 25°C is illustrated in Figure 5. In the rotating disk system K_L was directly proportional to $\omega^{\frac{1}{2}}$ and, therefore, if mass transfer was the controlling step, the dissolution rate, R, would be directly proportional to $\omega^{\frac{1}{2}}$. At a bulk solution pH of 8.4 the relationship between R and $\omega^{\frac{1}{2}}$ is linear only at low values of $\omega^{\frac{1}{2}}$. As $\omega^{\frac{1}{2}}$ increased, the surface reaction apparently became an increasingly important factor in determining the initial rate of dissolution.

For the results obtained at 25°C (Figure 5)) the relationship between R and $\omega^{\frac{1}{2}}$ was linear and mass transfer apparently controlled up to $\omega^{\frac{1}{2}} = 5\ s^{-1}$ where R was approximately equal to 7×10^{-10} moles $cm^{2-} s^{-1}$. At 1°C the effect of the surface reaction on R seemed to be even greater than at 25°C. The upper limit for mass transfer control was $R \simeq 1 \times 10^{-10}$ moles $cm^{-2}s^{-1}$ at $\omega^{\frac{1}{2}} = 2\ s^{-1}$.

It will be indicated in a subsequent section that in packed bed limestone contactors operated under the conditions used in this study, the maximum rate of dissolution for bulk solution pH values greater than 4 is generally less than 1×10^{-10} moles $cm^{-2}s^{-1}$. It therefore seems reasonable to assume that, based on Sjoberg and Rickard's results (Figure 3)), the rate of transport of calcium ion away from the interface controlled the dissolution rate throughout the entire depth of the packed columns used in this study.

It has been shown that the presence of certain substances can reduce the rate of calcite dissolution. This effect has been noted for ferric and chromic ions, (King and Liu, 1933), copper (Erga and Terjesen, 1956), aluminum (Volpicelli et al., 1981), scandium (Nestaas and Terjesen, 1969), organic matter, magnesium and orthophosphate (Morse 1974a, 1974b; Berner and Morse, 1974). The effect of contaminants on the rate of dissolution can be significant at very low contaminant concentrations. Nestaas and Terjesen (1969) concluded that metal ions adsorb at active spots or kinks on the surface of the dissolving crystal, blocking the dissolution process at that location. At the present time there are no methods available for quantifying the effect of contaminants

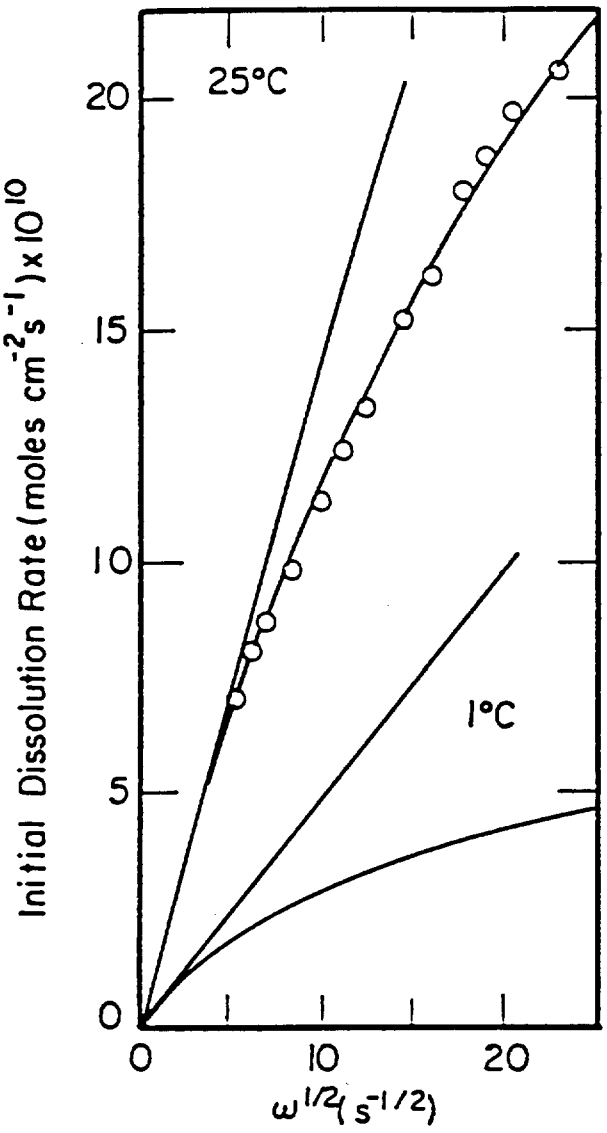

Figure 5. Initial rate of calcite dissolution as a function of the square root of the rotating disk rotational speed. Bulk solution pH was constant at 8.4 and the system was closed to atmospheric CO_2 (Sjoberg and Rickard, 1984b).

on the dissolution rate, particularly the dissolution rate of limestone. Eventually, for example, relationships between the contaminant concentration and K_c, the surface reaction constant, may be developed.

PACKED-BED REACTORS

Only a few studies have involved attempts to model the kinetics of limestone dissolution in continuous flow, packed-bed reactors (Pearson and McDonnell,1975a, 1975b; Barton and Vatanatham, 1976; and Vaillancourt, 1981).

Pearson and McDonnell (1975a, 1975b) studied the neutralization of acidic drainage from coal mines using packed columns and in-stream barriers of large (6.4 to 10 cm. effective diameter) limestone particles. Their open-to-the-atmosphere experiments were conducted at ambient temperature and in the presence and absence of dissolved metal ions.

Pearson and McDonnell (1975a) indicated that a rate equation based on hydrogen ion transport coupled with a surface reaction can be used to describe limestone dissolution kinetics. The proposed model is given by:

$$\frac{V}{A}\frac{dC_o}{dt} = K C_o^{n'} = K_a C_i^{n} = K_d (C_o - C_i) \qquad (7)$$

where V/A is the inverse of the interfacial area per unit volume of fluid in the column, K is an overall rate constant, K_a is a surface reaction rate constant, K_d is the mass transfer coefficient, C_o is the hydrogen ion concentration in the bulk solution, C_i is the hydrogen ion concentration at the limestone/water interface and n' and n are exponents.

Pearson and McDonnell (1975a, 1975b) did not use their experimental data to test the proposed rate equation, Eq. 7, but instead developed an empirical expression which related the rate of limestone dissolution to water temperature, pH, solution ionic strength, the bicarbonate ion concentration and the hydraulic shear stress. Their overall model included an expression for predicting the rate of CO_2 exolution at the air/water interface above the packed bed. The experimental conditions used by Pearson and McDonnell (1975a) to develop their empirical equations are appropriate for the treatment

of acidic drainage from coal mines but not the dilute acidic surface waters used as potable supplies.

Two groups of investigators, Barton and Vatanatham (1976) and Vaillancourt (1981) assumed that the rate of limestone dissolution in closed and open-to-the atmosphere, packed-columns is controlled by the rate of hydrogen ion transport from the bulk solution to the limestone surface. Vaillancourt (1981) used the conventional relationship,

$$\frac{U_s}{\varepsilon}\frac{dH_b^+}{dx} = -K\ a\ (H_b^+ - H_{eq}^+) \qquad (8)$$

where U_s is the superficial velocity, ε is the bed porosity, K is the mass transfer coefficient for hydrogen ion, a is the surface area of limestone per unit volume of interstitial water, x is distance in the axial direction, H_b^+ is the hydrogen ion concentration in the bulk solution and H_{eq}^+ is the hydrogen ion concentration when the solution and limestone solid phase are at equilibrium (under a closed-to-the-atmosphere condition). Vaillancourt (1981) correlated experimentally determined mass transfer coefficients with the limestone particle diameter, superficial velocity and fluid properties using dimensionless parameters.

Unfortunately, Vaillancourt (1981) used very short packed-columns with high Reynolds numbers in his experiments and did not consider the adverse effect these conditions had on his assumption of plug flow. He also did not consider the effect of raw water chemistry on the magnitude of H_{eq}^+. A constant value was incorrectly used for all solutions studied.

Vatanatham (1975) and Barton and Vatanatham (1976) studied the kinetics of limestone dissolution in acidic solutions using an open-to-the-atmosphere batch reactor and a recycle-downflow, packed-bed reactor system. Several models were tested including, zero order reaction controls, carbon dioxide transport controls, surface reaction controls and hydrogen ion transport controls. Barton and Vatanatham (1976) concluded that in the pH range of 2 to 6 hydrogen ion transport controls. They did not determine the rate limiting step outside this range but assumed that the lack of agreement between the experimental data and the hydrogen ion transport model was due to experimental error or the increasing importance of other transport or rate limiting mechanisms.

The kinetic equation used by Barton and Vatanatham (1976) for pH values between 2 and 6 is given by,

$$\frac{dW}{dt} W^{-2/3} = \frac{k\ M\ W_o}{6\ \rho\ D_o} [H_b^+ - H_{eq}^+], \qquad (9)$$

where W and W_o are the mols of $CaCO_3$ present at any time, t, and at t = 0, M is the molecular weight of $CaCO_3$, D_o is the initial diameter of the limestone particles, ρ is the mass density of limestone, H_{eq}^+ is the hydrogen ion concentration in the bulk solution at equilibrium and H_b^+ is the hydrogen ion concentration in the bulk solution at any time. Eq. 9 is essentially a first order (film) transport equation modified to include the change in interfacial area as the particles dissolve and decrease in size. Unfortunately Barton and Vatanatham (1976) made an error in deriving Eq. 9. The number six should appear in the numerator and not in the denominator and therefore all their model calculated results were in error by a factor of 36.

METAL RELEASE FROM PIPES

There is considerable concern over the corrosion of water distribution systems. Elevated corrosion rates may substantially reduce the service period of piping systems resulting in increased operation and maintenance expenses (Anderson and Berry, 1981). Metal release from water distribution systems may also cause water supplies to exceed the U.S. Environmental Protection Agency (U.S. EPA) Standards for maximum contaminant levels (MCL) or secondary maximum contaminant levels (SMCL). Maximum contaminant levels (MCL) are established for concentrations of compounds that may result in human health problems, while SMCL are primarily established for esthetic criteria.

Metal release may occur from copper, galvanized steel, iron and lead pipes, and from lead-tin solder coated on copper piping materials. Human health concerns are largely associated with the leaching of lead from lead pipe or lead-tin solder coated on copper pipe. The toxic effects of lead are well established (NAS 1977; Waldbott, 1978). Lead is an active and cumulative toxicant which alters neurological and metabolic functions. It has been associated with hyperactivity, hypertension, mental retardation and motor disfunctions (NAS 1977; Patterson and O'Brien, 1979). Several studies

have established a link between high concentrations of lead in drinking water, and elevated concentrations of lead in blood and subsequent health problems (Beeners et al, 1976; Campbell et al., 1977; Cameron and Wunderlich, 1976). Because of human health concerns, the U.S. EPA established a MCL for lead of 0.05 mg $Pb \cdot L^{-1}$.

Although copper is an essential trace metal, at elevated concentrations it has been implicated as a gastrointestinal poison (Doull et al., 1980). The U.S. EPA Secondary MCL for copper is 1.0 mg $Cu \cdot L^{-1}$. This standard has largely been established for esthetic considerations, such as the taste and staining characteristics associated with elevated concentrations.

Elevated corrosion rates have been reported for a number of regions (Hudson and Gilcreas, 1976; Dansel, 1976; Patterson and O'Brien, 1979; Karalekas, et al., 1983; Maessen et al., 1985). Of particular concern are soft-water supplies such as in the northeastern, southeastern and northwestern United States (Patterson and O'Brien, 1979).

Corrosion is a deterioration of a metal which usually occurs as a result of an electrochemical reaction. For corrosion to occur, an electrochemical cell must be established including an anode, a cathode, an electrolyte solution, and an electrical (metal) connection between the anode and cathode. As an electrochemical reaction proceeds oxidation occurs at the anode releasing electrons which are transmitted through the electrical connection to the cathode. These electrons are accepted at the cathode through a reduction reaction. The tendency for a metal to oxidize (and subsequently exhibit corrosion) is measured through its oxidation potential (E°). Some values of oxidation potential for some relevant reactions are summarized in Table 4. Note the reaction with the highest oxidation potential will have the greatest tendency to undergo oxidation in an electrochemical reaction. For example, if copper and lead form an electrochemical cell at a copper-lead solder joint, lead would be oxidized (corroded) while copper would be reduced by virtue of their values of oxidation potential.

There are two conditions by which corrosion may be restricted. First, the electrochemical (redox) potential and pH may not thermodynamically favor oxidation. This condition is termed immunity. The second condition involves the formation of a sparingly soluble solid phase with an oxidation by-product,

TABLE 4 Oxidation Potential of Metallic Materials

Anode	Anodic Reactions	Potential E° (volts)
Zinc	$Zn(s) \rightarrow Zn^{2+} + 2e^-$	0.76
Iron Soft Solder	$Fe(s) \rightarrow Fe^{2+} + 2e^-$	0.44
Tin	$Sn(s) \rightarrow Sn^{2} + 2e^-$	0.136
Lead	$Pb(s) \rightarrow Pb^{2+} + 2e^-$	0.126
Copper	$Cu(s) \rightarrow Cu^{2+} + 2e^-$	-0.345

such as an oxide, hydroxide or salt. If this solid adheres as a film on the metal surface, then it may mitigate corrosion. This process is referred to as passivation. The effectiveness of passivation films is highly variable, and depends on the affinity of the solid phase for the metal and whether coverage is complete or partial.

Hilburn (1983) developed two conceptual models for uniform corrosion. The direct-dissolution model is applicable when the metal is oxidized and directly released to solution. Under these conditions the corrosion rate is controlled by either the kinetics of the reaction, or the transport of reactants and products to and from the metal surface through solution. The dissolution-and-film-growth-model applies to metals which form a passivation film. The overall corrosion rate may be regulated by reaction kinetics, transport through the passivation film or solution transport, whichever is the rate-limiting process.

Corrosion is an extremely complicated process. For example factors such as pipe age, pipe length, impurities in the pipe material, interval of solder joints, temperature, turbulence and water chemistry can all contribute to corrosion (Herrera et al., 1982; Hilburn, 1983, 1983; Schock, 1984; Maesson et al., 1985; Treweek et al., 1985). As a result, it is often difficult to evaluate factors regulating metal release from piping systems. Maessen et al. (1984) studied metal mobilization in home well-water systems in Nova Scotia. They assessed bedrock type (e.g. granite, limestone), proximity to the coast, well-type (e.g. dug, drilled) and depth, plumbing data (e.g. length of piping, age of piping, type of piping), as well as solution chemistry on the extent of metal release from water distribution systems. They found significant leaching of copper, lead and zinc occurred in some systems. Concentrations of metals were elevated in water that had been in contact with piping material for a prolonged periods of time (e.g. overnight, standing) relative to running water samples. Although a wide range of bedrock, water chemistry and plumbing conditions were evaluated, no factor could be found to systematically predict the extent of metal leaching. Moreover, indexes commonly used to assess the corrosive tendency of a water (Langelier, Ryznar, Aggressiveness indexes, and the ratio of SO_4^{2} and Cl^{-1} to alkalinity) and pH were poor predictors of metal release.

Meranger et al. (1983) evaluated metal leaching from cottage piping systems that contacted acidic lakewater in northern Ontario. They found elevated leaching of cadmium, copper, lead and zinc. Mobilization rates were greatest during the first two hours of contact time with the pipe, but concentrations continued to increase for a period of up to 10 days. Highest metal concentrations were again obtained with the first sample collected and concentrations decreased by up to 97% in the third liter of water collected. Although the authors were concerned that acidic deposition to the region resulted in surface water acidification and enhanced the corrosivity of lake water, because these waters are naturally soft and corrosive this effect is not clear.

Although it is often difficult to interpret field data because of all the physical and chemical factors which contribute to corrosion, considerable progress has been made in recent years through controlled laboratory experiments in evaluating the chemistry of passivation films and processes regulating the formation of films. Housing and building systems frequently have sections of pipe that remain stagnant for prolonged periods of time. Initially metal release is regulated by mass-transport reactions, however over time concentrations can approach and reach saturation with respect to mineral phase solubility (Schock, 1984). Therefore, solubility calculations may be used as worst-case assessment of metal leaching.

In recent years thermodynamic calculations have been used as a tool to assess trace metal chemistry and the stability of passivation films within water distribution systems. Several types of passivation films may form on metal pipe depending on the chemical characteristics of the water supply (Table 5). Patterson and O'Brien (1979) discussed the role of inorganic carbon in regulating the release of lead from lead pipe. Using thermodynamic calculations, they found that the solubility of lead decreases with increasing inorganic carbon concentrations. Moreover, they suggested that elevated inorganic carbon concentrations result in the formation of an insoluble lead carbonate passivation film. This film not only reduces lead solubility but also strongly adheres to the pipe surface, limiting the release of particulate lead to water. Their calculations suggest that reduced inorganic carbon

TABLE 5

Passivation film minerals that may be important in regulating metal solubility in water distribution systems

COMPOUND	STOICHIOMETRY
Lead Pipe	
Lead hydroxide	$Pb(OH)_2$
Lead carbonate (cerussite)	$Pb\ CO_3$
Basic lead carbonate (hydrocerussite)	$Pb_3(CO_3)_2(OH)_2$
Lead Sulfate	$Pb\ SO_4$
Copper Pipe	
Copper hydroxide	$Cu(OH)_2$
Copper carbonate	$CuCO_3$
Basic copper carbonate (malachite)	$Cu_2(OH)_2CO_3$
Basic copper carbonate (azurite)	$Cu_3(OH)_2(CO_3)_2$
Copper sulfate	$CuSO_4$
Basic copper sulfate(brochantite)	$Cu_4(OH)_6SO_4$
Basic copper chloride(atacamite)	$Cu_2(OH)_2Cl$
Galvanized Steel Pipe	
Zinc hydroxide	$Zn(OH)_2$
Zinc carbonate	$ZnCO_3$
Basic zinc carbonate(hydrozincite)	$Zn_5(OH)_6(CO_3)_2$
Zinc sulfate	$ZnSO_4$
Basic zinc silicate(hemimorphite)	$Zn_4\ Si_2\ O_7(OH)_2 \cdot H_2O$

concentrations facilitate the formation of a lead hydroxide film which does not adhere strongly to the pipe surface and periodically is released to the water supply as particulate lead.

In a series of papers, Schock (1980), Schock and Gardels (1983), and Schock (1984) greatly elaborate on the role of inorganic carbon in controlling trace metal concentrations in water distribution systems. Schock (1980) suggested that the thermodynamic analysis by Patterson and O'Brien (1979) was incorrect due to a failure to consider soluble lead-carbonate complexes. Lead forms strong aqueous complexes with carbonate and therefore elevated dissolved inorganic carbon concentrations can significantly enhance aqueous lead concentrations. As a result, the contention by Patterson and O'Brien (1979) that increases in dissolved inorganic carbon concentration reduce aqueous lead concentrations is incorrect and may suggest counter-productive water treatment strategies.

Due to the relatively high solubility of lead at low pH and the potential to form lead-carbonate complexes at higher pH values the conditions under which the theoretical solubility of lead is below the U.S. EPA MCL of 0.05 mg $Pb \cdot L^{-1}$ are limited to relatively high pH values (8.0 - 10) and low dissolved inorganic carbon concentrations. Schock (1984) indicated that under these conditions the concentrations of lead would be generally regulated by the solubility of hydrocerussite ($Pb_3(CO_3)_2(OH_2)$), a tightly adhering passivation film. These conditions would limit the release of particulate lead to water supplies.

In addition to lead solubility, Schock (1984) evaluated the theoretical solubility of passivation films from copper and galvanized steel pipe. Because both zinc and copper are hydrolyzing metals and form soluble complexes with carbonate, it is reasonable to expect their solubility to mimic lead. Copper exhibits a considerable variation in solubility over a range of pH and dissolved inorganic carbon concentrations. Generally the solubility of copper in the pH range 7 to 11 is well below the U.S. EPA secondary MCL of 1 mg $Cu \cdot L^{-1}$. It is, therefore not as difficult to meet the U.S. EPA secondary MCL for copper as it is to meet the MCL for lead. Like lead, the minimum theoretical solubility occurs at elevated pH values (9-10) and the solubility is enhanced at high pH values due to the formation of soluble carbonate com-

plexes. Schock (1984) indicates that in the pH range of 9-10 the theoretical solubility of copper is regulated by tenorite (CuO).

The theoretical solubility of zinc has a minimum value near pH 9 and in this pH range is thought to be regulated by the solubility of hydrozincite ($Zn_5(CO_3)_2(OH)_6$) (Schock 1984). Hydrozincite is not a strongly adhering passivation film. Therefore, zinc concentrations in water supplies using galvanized steel pipe may be significantly enhanced by the release of particulate Zn. Unlike lead and to a lesser extent copper, zinc does not form strong soluble complexes with carbonate. Therefore, pH is the major factor regulating variations in the solubility of dissolved zinc from galvanized steel pipe. However within the pH range 7 to 11, the theoretical solubility of dissolved zinc is well below the USEPA SMCL of 5 mg $Zn \cdot L^{-1}$ (Schock 1984).

While thermodynamic calculations represent an important tool to assess trace metal solubility and the stability of passivation films, they clearly have many limitations. As indicated previously, thermodynamic calculations should be viewed as an upper-limit of dissolved metal concentrations. Under many conditions, particularly when water has been in contact with piping material for a short period of time, the release of corrosion by-products will be controlled by mass-transport reactions. Physical factors such as the poor adherence of passivation films to piping material and/or erosion of these films due to turbulance can significantly increase metal concentrations through the release of particulate metal. Moreover, our understanding of the temperature dependence (standard enthalpy values) of metal complexation and solubility reactions is limited. So it is difficult to make thermodynamic solubility calculations at temperatures other than 25°C with confidence. Finally, while thermodynamic calculations provide theoretical values of dissolved metal concentration which may be useful in evaluating compliance with U.S. EPA drinking water standards, no information is obtained on the destruction of the metal pipe. While an insoluble passivation film may restrict the release of metal to solution, if it is not impervious to molecular oxygen then oxidation may continue and substantially diminish the lifetime of the metallic piping material.

SECTION 5

METHODS AND MATERIALS

APPARATUSES - LABORATORY AND FIELD CONTACTOR UNITS

Laboratory Contactors

Four downflow, packed-column contactors were used in the laboratory study. Each column contained a different limestone particle size. The column diameters were chosen to yield a column-to-particle diameter ratio of at least ten to minimize the effect of the higher porosity at the wall on the flow through the bed . The four columns and the water feed system are illustrated in Figure 6.

Column A in Figure 6 was constructed of clear acrylic plastic and contained limestone particles with a 0.96 cm mean diameter. The column inside diameter was 15.2 cm and the length was 3.5 m. Columns B, C and D were constructed of polyvinyl chloride pipe. Columns B and C both had inside diameters of 15.2 cm and Column D had an inside diameter of 38.1 cm. The stone sizes (mean diameter) in these columns were 0.54 cm, 1.5 cm, and 3.2 cm for Columns B, C, and D respectively. All three columns were 2.1 m. long.

All four columns in Figure 6 were equipped with through-the-wall sampling tubes. The tubes were spaced in the axial direction at 15.2 cm intervals at the influent end and at 30.4 cm intervals over the remaining portion of each column.

Each sampling tube (0.6 cm diameter acrylic plastic) extended to the center of the column. Five 0.25 cm diameter holes were drilled in the upper part of each tube. Each tube was cemented to a plastic adaptor which was threaded into the column wall. A short length of plastic tubing with a hose clamp was attached to the plastic adaptor. A drawing of a typical sampling tube is included within Figure 6.

The water supply and flow control system used with the four laboratory columns is shown in Figure 6. The raw water was pumped from a 200 L plastic tank to a constant head tank located above Column A. Overflow from the constant head tank returned to the plastic tank. Flow control for each column effluent was accomplished using a flowmeter with a micrometer controlled

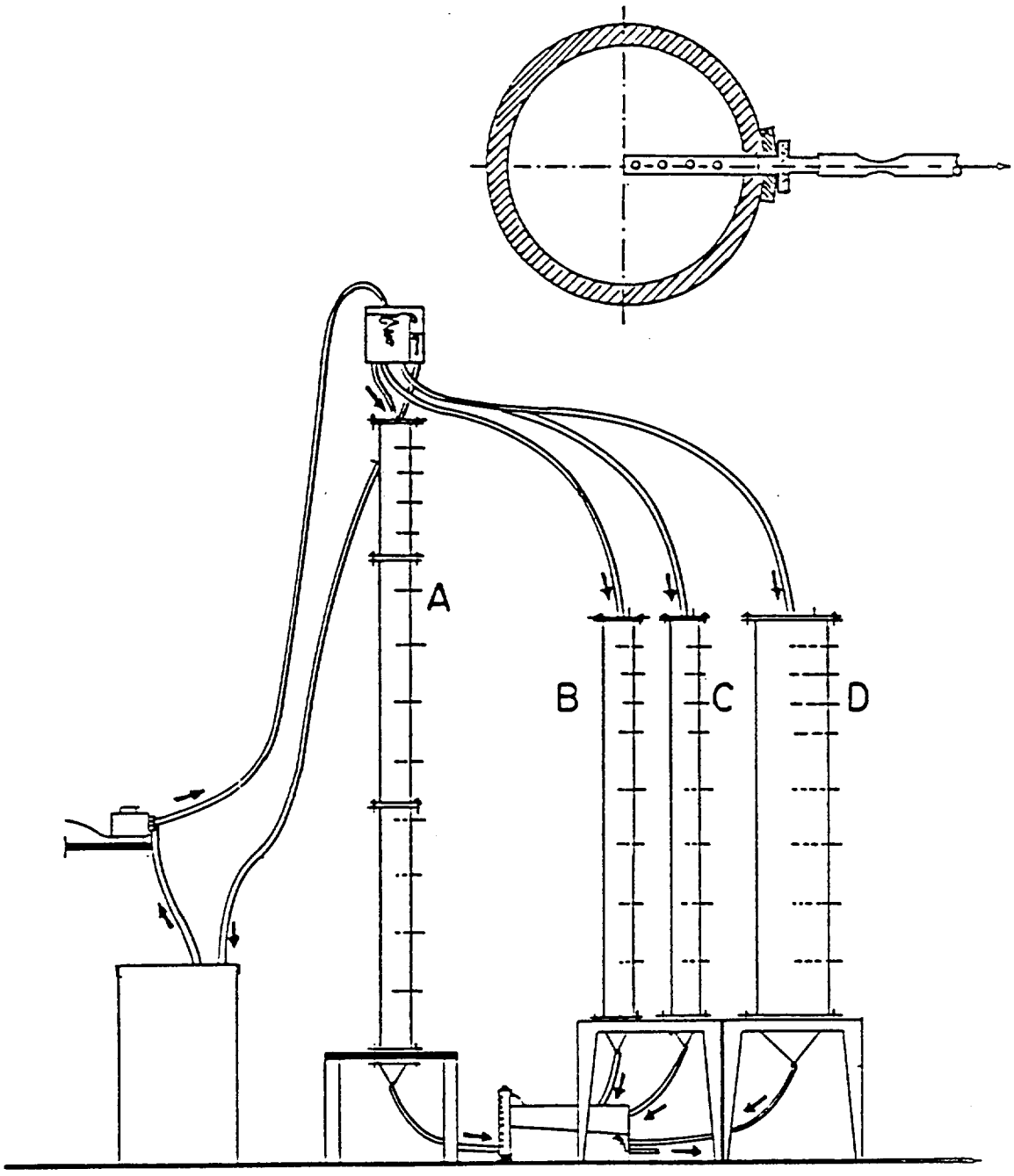

Figure 6. Laboratory columns with water supply and flow control system. Insert is a drawing of a typical through-the-wall sampling tube.

valve assembly. From the flowmeter the water discharged to a small open chamber and from this unit to a floor drain. The flowmeter calibration was checked frequently using a volumetric cylinder and a stopwatch.

The limestone was washed with tap water and placed in each column layer by-layer to facilitate installation of the sampling tubes and to minimize later compaction of the bed. Gentle tapping and shaking of the column were used to consolidate the bed as it was installed.

Field Contactors

Three devices were studied in the field investigation. These included a large baffled-box device which was submerged in a mountainside spring at the head end of a rural resort water supply system and two small column-type units which were used for individual resort cabins. One of these small units was obtained from Culligan, Inc.*

The baffled-box contactor is described in Figure 7. The unit was constructed several years ago at Syracuse University using 1.9 cm thick marine-grade plywood covered with 2 mm thick plexiglass sheets. The overall dimensions are 0.6 x 0.6 x 1.2 m. Sampling cells which also serve as baffles to direct the flow along the bottom of the chambers were constructed of 0.6 and 1.3 cm plexiglass (each is 12.7 cm x 12.7 cm x 0.6 m). The sides and lid were braced with fiberglass resin coated aluminum angles. Fiberglass resin was also used to coat small areas of the contactor not covered by plexiglass sheets. The unit contained approximately 479 Kg. of 0.96 cm mean diameter limestone particles and the length of the flow path through the limestone was approximately 354 cm. The cross-sectional area perpendicular to the direction of flow was approximately 915 cm^2.

The two smaller column type units used in the field study are shown in Figure 8. Column 1 had an inside diameter of 20.2 cm and an overall length of 130 cm. Flow entered this column at the top, passed down through the bed and exited through a cylindrical plastic strainer connected to a 2 cm, inside diameter plastic pipe which passed up through the center of the bed. Column 1 was constructed of wound fiberglass and contained 60 Kg of crushed limestone (0.96 mean diameter particle size). The overall depth of limestone was 122 cm. Column 1 was a slightly modified version of a container used in ion exchange systems.

*Mention of trade names or commercial products does not constitute endorsement or recommendation for use.

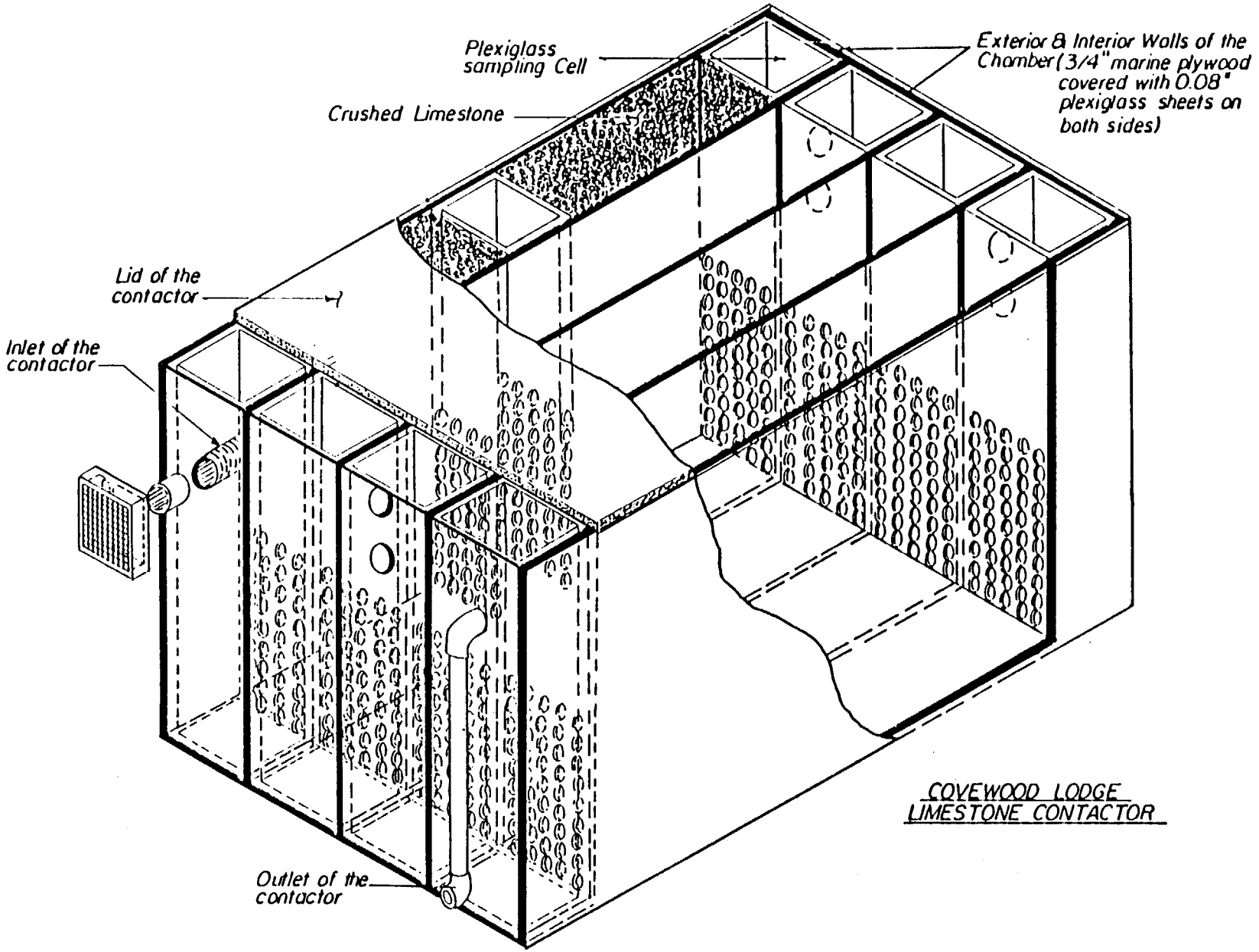

Figure 7. Baffled-box contactor used in the field study. Entire unit was submerged in a mountain-side spring.

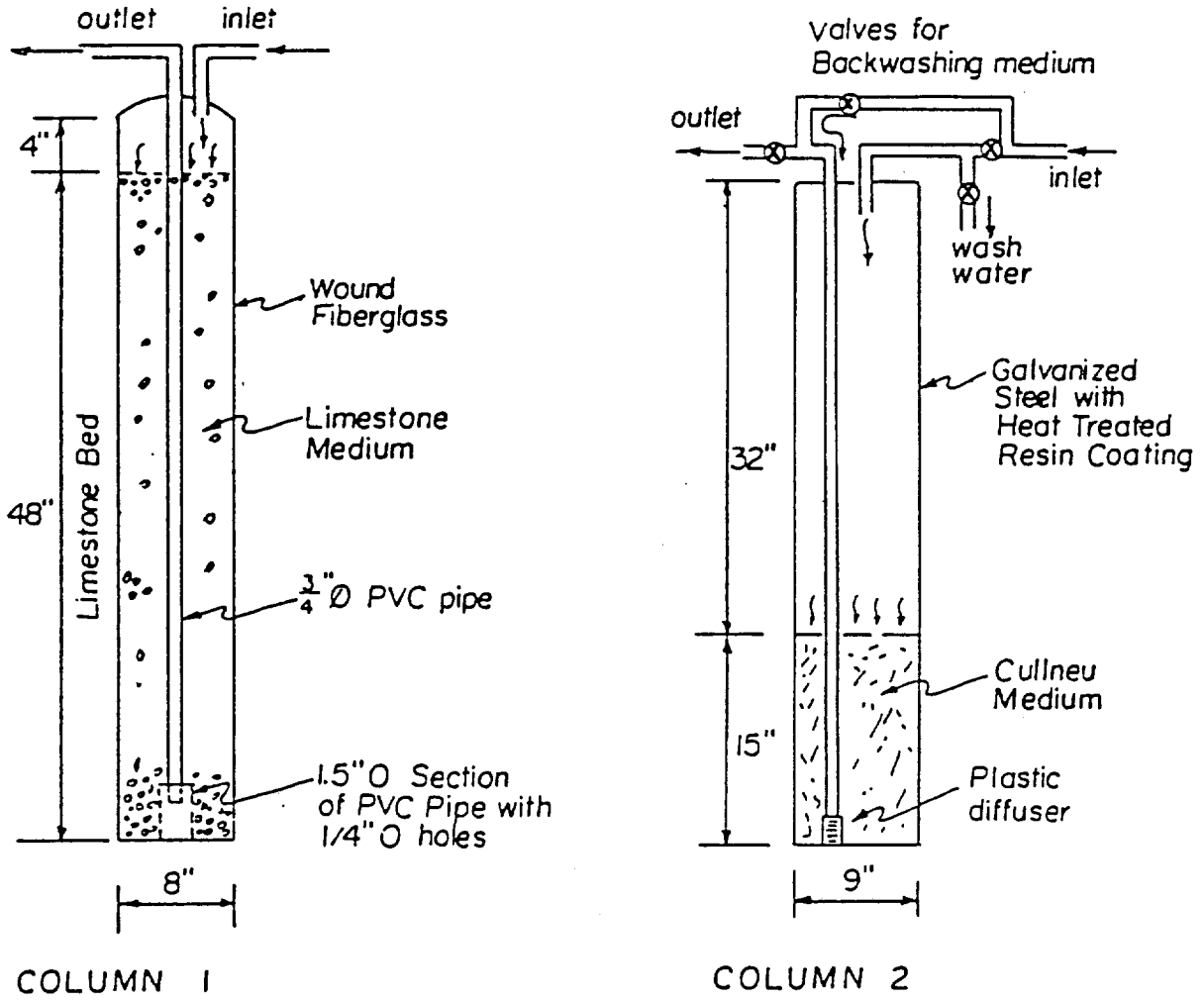

Figure 8. Wound-fiberglass and Culligan contactors used in the field study. The wound-fiberglass contactor was filled with limestone and the Culligan unit contained Cullneu, a form of $CaCO_3$ sold by Culligan, Inc. The wound-fiberglass unit was installed in Bayside cottage and the Culligan unit in Henry Covey cottage. (See Figure 9)

Column 2 illustrated in Figure 8, was rented from Culligan, Inc. It had an inside diameter of 23 cm and a total length of 127 cm. It was constructed of galvanized steel coated with a heat treated epoxy resin.

A granular, calcium carbonate medium (Cullneu®, neutralizing medium, catalog number 1600-10) sold by Culligan, Inc.* was used in place of limestone in Column 2. The column was filled to a depth of 40 cm with Cullneu®. The flow conditions within Column 2 were very similar to those in Column 1, however, Column 2 was equipped with a valve arrangement at the top which allowed one to direct water into the effluent pipe to backwash the medium by upflow through the bed.

The baffled-box contactor and the two column units were installed at the Covewood Lodge, a resort with housekeeping cottages and a rustic lodge located in the Adirondack Region of New York State near Old Forge. A map illustrating the layout of the gravity-fed supply system is presented in Figure 9. The baffled-box contactor was installed, completely submerged, in the spring which serves the seven cottages on the west side of the resort. The spring water elevation was approximately fifteen meters above the ground floors of the cottages. Water flowed for a distance of approximately 20 ft. (6 m) into two, 400 gallon, (1600 L) galvanized steel storage tanks. Flow to the cottages from the storage tanks was through a 3.8 cm diameter plastic pipe. The plumbing in each cottage was copper pipe soldered with 50/50 lead-tin solder. The installation of the baffled-box contactor installed within the spring is illustrated in Figure 10. Bay Side and Hillside cottages contained approximately 30 m (100 ft) and 15 m (50 ft) of 1.3 cm (½ in.) diameter copper pipe, respectively with approximately forty 50/50 lead-tin solder joints per cottage or two joints per meter of copper pipe.

The wound fiberglass column with limestone particles (Column 1, Figure 8) was installed in the heated basement of Bay Side cottage (see Figure 9). The unit was used during the months of January, February, March and April 1984 when the plastic line from the spring and baffled-box contactor became frozen and it was necessary for the resort owner to supply water to the winterized cottages by pumping water directly from Big Moose Lake. The contactor in Bay Side Cottage was installed on the pressure side of a pressure switch activated supply pump. The cottage contains two small living units, each

*Mention of trade names or commercial products does not constitute endorsement or recommendation for use.

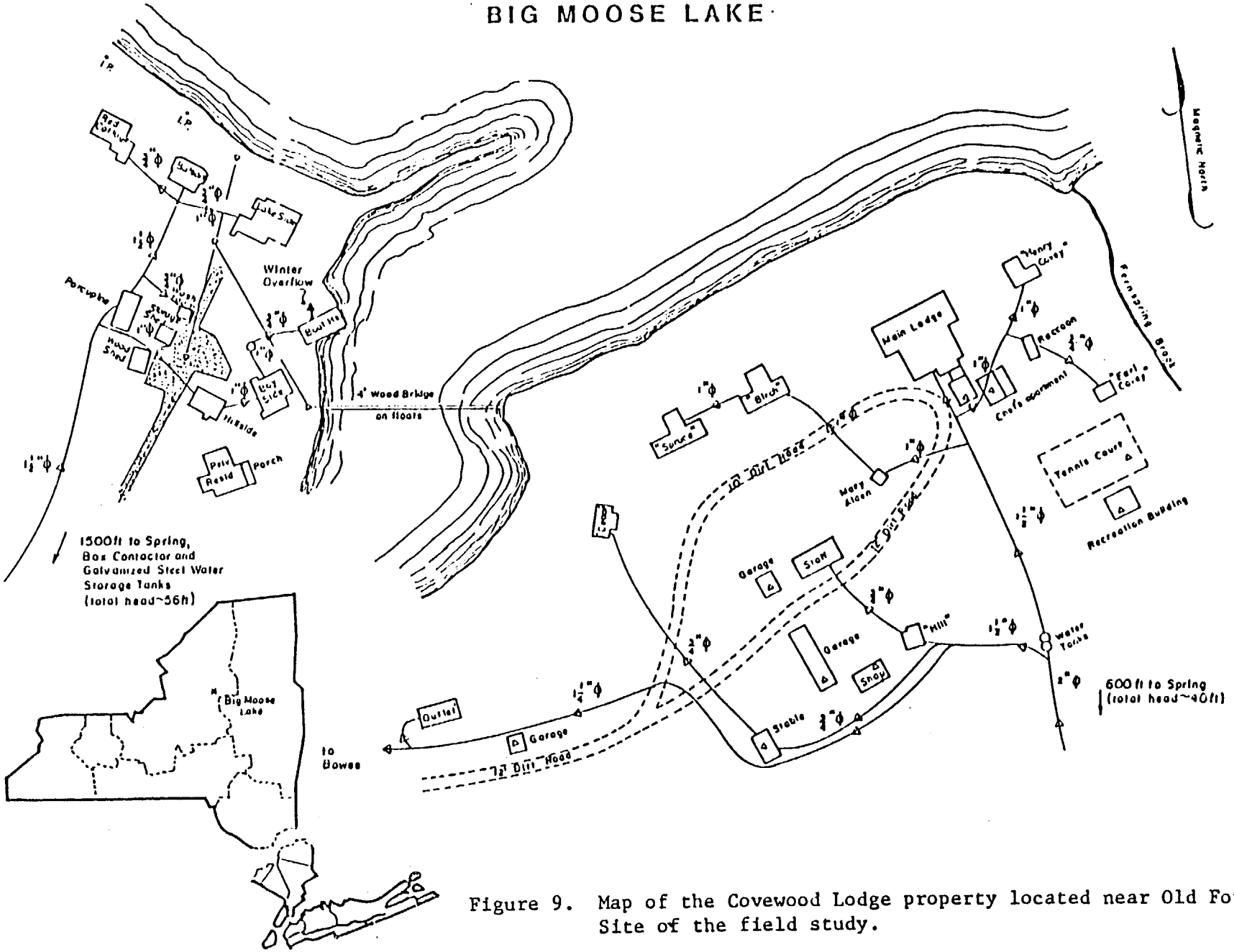

Figure 9. Map of the Covewood Lodge property located near Old Forge, NY. Site of the field study.

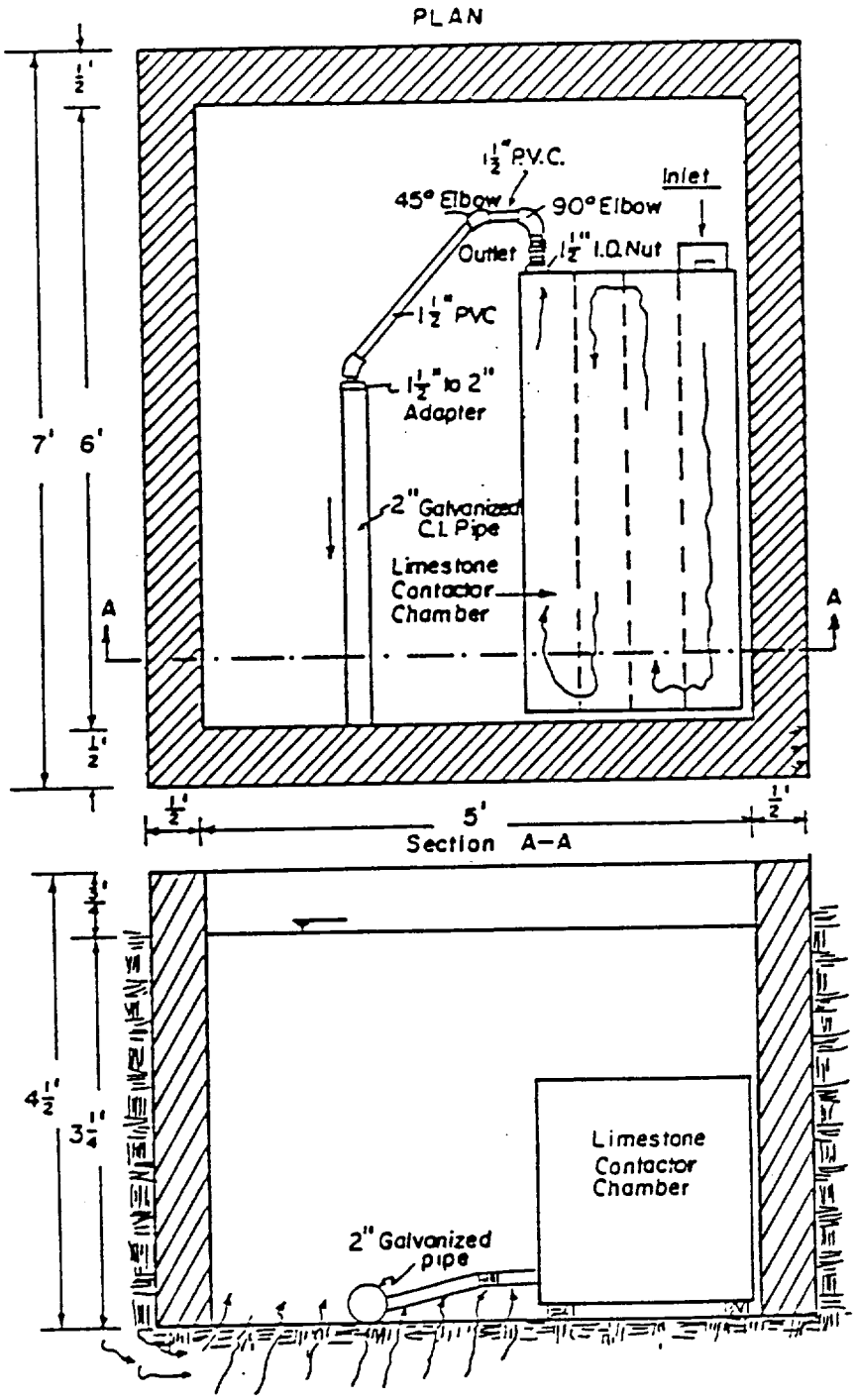

Figure 10. Diagram showing the installation of the baffled-box contactor in the spring at Covewood.

has a kitchen and a bathroom with a toilet, sink and shower. Normal total occupancy during the winter (most but not all guests limit their stay to a weekend) is four adults.

The Culligan column with Cullneu® medium was installed in the basement of a cottage (Henry Covey, Figure 9) on the east side of the resort. The east side of the resort receives water from a spring, which at the time of this study, contained a marginally effective limestone contactor installed by the resort owner. The unit in this spring was somewhat ineffective because of significant short-circuiting. The Henry Covey cottage is winterized and has a kitchen and a bathroom with sink, toilet and shower. Normal occupancy is two persons.

Estimates of limestone contactor cost are given in Appendix C.

Limestone Characteristics

The limestone used throughout the study was obtained from a quarry in Boonville, New York. The limestone was analyzed in the laboratory to determine its physical and chemical characteristics.

Chemical Characteristics - A sample of limestone was ground to a powder (particle diameter less than 0.29 mm) and then washed with tap water and dried 24 hours at 105°C.

Three 0.2 gram portions of the powdered limestone were dissolved in 50 ml 1:1 HCL/HNO_3. After dilution with deionized water elemental analysis was conducted by atomic absorption spectrophotometry.

It was determined that the cation content of the Boonville limestone is (by mass) 85 percent calcium, 12.3 percent aluminum and 2.4 percent magnesium. Iron, Mn, Zn, Cu and Cd were present at less than 0.1 percent and Pb, K and Na were not detected. These results indicate that the Boonville limestone is essentially a "high calcium" limestone.

A supplemental experiment was conducted in which a measured quantity of Boonville limestone was dissolved in concentrated hydrochloric acid in a closed system. The CO_2 evolved was captured and its amount measured. This result combined with the calcium measurement indicates that the Boonville stone contains 79% $CaCO_3$ by mass. Therefore, although it can be labeled a high calcium stone it is not of high purity.

The effective $CaCO_3$ solubility product for the limestone was determined by placing 0.10 gram samples of the powdered limestone in twelve open flasks containing 100 ml of deionized water. Different amounts of acid were added to each flask (between 0.25 to 1000 μeq/L using 1N HCl) so that the initial pH of the samples was between 3.00 and 6.60. The flasks were agitated on a shaker table in the 20°C room for one week. At the end of the equilibration period samples were filtered using 0.45 μm millipore membrane filter and analyzed to determine Ca, Mg, DIC and pH.

The molar concentrations of these constituents for each sample were input to the MINEQL chemical equilibrium computer program (Westall et al., 1976) using the following conditions:

a - Fixed carbon dioxide partial pressure of $10^{-3.5}$ atm.

b - Fixed pH (measured final value for each sample)

c - Total hydrogen ion concentration equal to the molar concentration of acid initially added to the sample.

A solubility product of $CaCO_3$ for the limestone of each sample was calculated as the product of the equilibrium activities of calcium and carbonate computed by the computer program. The average effective solubility product of $CaCO_3$ in Boonville limestone was found to be $10^{-8.71}$ (20°C). The experimental results and the computed values of the effective solubility product are listed in Table 6.

Physical Characteristics - The four size fractions of limestone particles obtained from the Boonville quarry were analyzed to determine particle size, sphericity and mass density.

The median particle size for each size fraction was determined using a standard ASTM (ASTM Manual 447-4) sieve analysis. The percent by weight finer than a given sieve opening was plotted as a function of the size of the sieve opening on arithmetic probability graph paper. The median particle size was determined by interpolation from this graph. In the case of the 0.96 cm median size fraction, 90 percent of the particles were between 0.7 and 1.3 cm.

The volume-weighted mean particle diameter was determined by measuring the volume of at least 1200 particles in each size fraction. Particle volume

Table 6 Effective Solubility of Crushed Limestone
Experimental Results

Sample Number	Acidity Added eq/l HCl	Initial pH pHo	Final pH pHf	Final DIC mgC/L	Final Calcium Conc. mgCa/L	Final Mag. Conc. mgMg/L	Computed pKsp
1	0.25	6.6	7.54	11.9	23.08	0.18	9.663
2	20	4.7	7.85	12.38	23.87	0.18	8.998
3	60	4.22	7.88	12.38	25.61	0.2	8.94
4	100	4.0	7.92	12.38	24.41	0.18	8.881
5	140	3.85	7.89	10.24	21.88	0.18	8.988
6	200	3.7	7.86	10.95	24.57	0.18	8.844
7	260	3.59	7.92	9.29	23.7	0.19	8.894
8	300	3.52	7.94	9.52	24.24	0.19	9.029
9	340	3.4	8.09	10.71	28.3	0.21	8.48
10	400	3.4	8.11	11.43	29.95	0.21	8.416
11	500	3.3	8.11	10.48	31.81	0.23	8.389
12	1000	3.0	8.02	9.29	44.4	0.33	8.422

was measured by drying a random sample of particles at 105°C for 24 hours. Each particle in the sample was weighed and numbered and then carefully suspended in a small volumetric cylinder filled with water. The volume displaced was accurately measured with a 1 ml pipet. The volume-weighted mean diameter, d_p, for each fraction was calculated using

$$d_p = \left[\frac{6\ V_p}{n\ \pi}\right]^{1/3} \tag{10}$$

where V_p is the total measured volume and n is the number of particles included in the measurement. In the case of the size fraction with a 1.01 cm median diameter (sieve analysis) the volume weighted mean diameter was 0.93 cm. The results of the particle size measurements for the four fractions are given in Table 7. The diameter used for a given fraction in model calculations was the average of the value obtained by the sieve analysis and the value obtained by fluid displacement. The sieve analysis results were approximately normally distributed and therefore it is reaonable to assume that the median size from the sieving/weighing procedure and the mean size from the fluid displacment measurements should be nearly the same since the particles all have the same density.

The sphericity of a particle is equal to the surface area of a sphere with the same volume as the particle divided by the measured surface area of the particle. The sphericity of each particle, ψ_i, was determined by

$$\psi i = \frac{(6\ V_i/\pi\ )2/3\ (\ \pi/4)}{A_i} \tag{11}$$

where V_i is the volume of the particle measured by fluid displacment and A_i is the actual surface area measured planimetrically. The sphericity listed in Table 7 for each size fraction is the average value for the particles in the sample. The sample size for each size fraction was approximately fifty particles.

The average sphericity ranged from 0.83 for the 3.20 cm size fraction to 0.78 for the 1.50 cm fraction. In the case of the 0.96 cm fraction the measured sphericities ranged from 0.50 to 0.98, with an average value of 0.79.

TABLE 7 Limestone Particle Size and Sphericity Analysis Results

Size Fraction	Mean Diameter Sieve Analysis (cm)	Volume Weighted Mean Diameter, dp (cm)	Diameter Used in Design Calculations, d(cm)	Particle Sphericity (dimensionless)
I	3.20	----	3.20	0.83
II	1.45	1.55	1.50	0.78
III	1.01	0.93	0.97	0.79
IV	0.55	0.54	0.54	0.81

The mean density of the particles was determined by dividing the sum of the particle weights by the sum of their measured volumes. The calculated density was 2.64 g/cm^3.

Cullneu is described by the manufacturer, Culligan, Inc., as "a specially graded calcium carbonate compound for neutralizing acid waters which provides consistent dissolving rate for treatment." The particle size is 6-30 mesh or a mean effective diameter of approximately 2.2 mm. The bulk density is approximately 1.5 g/cm^3. No other information is available on the Cullneu material.

Limestone Bed Characteristics

A number of tests were conducted to measure pertinent physical characteristics of the packed-bed contactors used in the study. The bed porosity was measured and used with the mean particle diameter and particle sphericity to calculate the area of limestone particle surface per unit volume of interstitial water. This quantity is important in modeling dissolution kinetics. Tracer studies were conducted to measure fluid residence time and axial dispersion in the contactor.

The porosity of a packed bed is the ratio of the void space and the total enclosed volume of the bed. The porosity of each column was determined by measuring the volume of fluid required to displace all the air from the bed. This volume was divided by the total volume of the column to obtain the porosity. The complete procedure was repeated five times.

To evaluate the effect of the column wall on the bed porosity a series of special tests were conducted. Beakers of various sizes and hence various wall plus bottom area to volume ratios were filled with each of four limestone particle sizes and the porosity was measured. The measured porosities have been plotted as a function of the vessel contact area to volume ratio (A/V in cm^{-1}) in Figure 11.

The measured porosity for the column which contained the 0.96 cm limestone particles was 0.41 and the vessel contact area to volume ratio was 2.25 cm^{-1}. From the least square regression line fitted to the 0.96 cm particle size data points in Figure 11, the expected porosity for a vessel contact area to volume ratio of 0.25 cm^{-1} is 0.43 $\pm$ 0.04. The measured porosity of 0.41

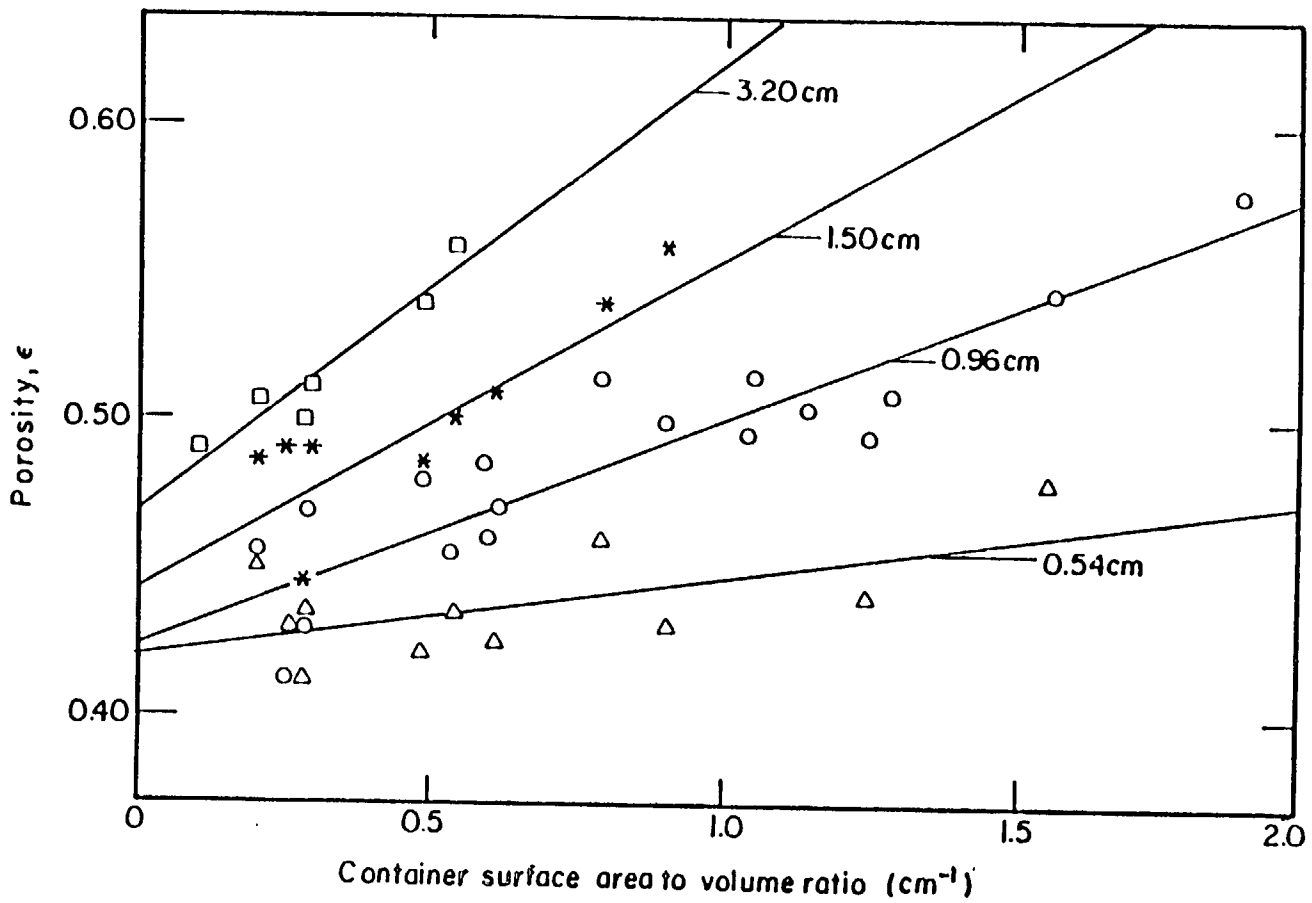

Figure 11. Measured porosity plotted as a function of container surface area to volume ratio for four limestone particle effective diameters. Lines were fitted to the data by the method of least squares.

falls within this range. This result also suggests that under these conditions the column wall has a negligible effect on the overall bed porosity.

The effect of the vessel contact area to volume ratio on the porosity increases with increasing particle size (Figure 11). For example using the four least squares regression lines, for $A/\forall = 1\ cm^{-1}$, the overall porosity is 0.62 for 3.2 cm limestone, 0.55 for 1.5 cm limestone, 0.49 for 0.96 cm limestone and 0.43 for 0.54 cm limestone. The porosities measured (or estimated using Figure 11) for each of the columns used in this study, except the Culligan unit are listed in Table 8.

The limestone particle surface area per unit volume of interstitial water (a, cm^{-1}), which was used in modeling the dissolution process, is also listed in Table 8. This quantity was calculated for each column using the measured or estimated porosity (ε) and the measured mean particle size ($\bar{d}$) and sphericity (ψ). The equation used is

$$a = \frac{6(1-\varepsilon)}{\bar{d}\ \psi\ \varepsilon} \qquad (12)$$

The contactors described in Figure 6 were used in a set of experiments designed to determine the effect of limestone particle size, flowrate and the depth of the packed-bed on axial dispersion and mean fluid residence time. Axial dispersion may be an important factor in modeling the effect of limestone dissolution on effluent chemistry. Tracer studies were conducted to evaluate axial dispersion and to test calculated values of mean fluid detention time within the bed.

Lithium chloride was used as a tracer salt. Lithium is easily detected (by atomic absorption spectrophotometry), it does not react with nor is it significantly adsorbed by the contents of the columns and the background concentration of lithium was negligible in the tap water used in the tracer experiments.

In most experiments a 200 mg quantity of LiCl dissolved in 10 mL of deionized water (20g Li/L) was injected with a syringe into the feed port at the top of the column. Samples from the effluent port were collected every 15-30 seconds around the peak concentration of the tracer curves and every minute for the remainder of the test. The tracer study was repeated

TABLE 8 Bed porosity and Limestone Particle Surface Area per unit volume of Interstitial Water

Column	Limestone Particle Diameter, $\bar{d}$ (cm)	Porosity	Limestone Particle Surface Area Per Unit Volume of Interstitial Water, a (cm^{-1})
A, Figure 6	0.96	0.41	11.4
B, Figure 6	0.54	0.43	18.2
C, Figure 6	1.50	0.49	5.3
D, Figure 6	3.20	0.49	2.6
Wound Fiberglass Figure 8	0.96	0.44*	9.7
Baffled-Box Figure 8	0.96	0.44*	9.7

*Estimated Using Figure 11 and measured vessel contact area to volume ratios.
Wound Fiberglass Column, $A/\forall = 0.21\ cm^{-1}$;
Baffled-Box Contactor, $A/\forall = 0.19\ cm^{-1}$.

three times for each flowrate. The results of four experiments are plotted in Figure 12.

The results from each tracer test were analyzed to determine the total mass of lithium injected passing the sampling port using the following equation:

$$[\text{Mass of Lithium Recovered}] = Q \sum_{i=1}^{n} C_i \; t_i \qquad (13)$$

The quantity $\sum_{i=1}^{n} C_i \; t_i$ is the area under the tracer response curve and Q is the volumetric flowrate.

The mean fluid residence time, $\bar{t}$, was determined using the first moment of the tracer response curve, i.e.,

$$\bar{t} = \frac{\Sigma t_i C_i \; \Delta t_i}{\Sigma C_i \; \Delta t_i} \; . \qquad (14)$$

The axial dispersion number was determined by the second moment matching procedure described by Levenspiel and Smith (1957). For low levels of axial dispersion

$$N_D = \frac{\Sigma t_i^2 \; C_i \; \Delta t_i}{2\bar{t}^2 \; \Sigma \; C_i \; \Delta \; t_i} - 0.5 \qquad (15)$$

where N_D is the dimensionless axial dispersion number.

The axial dispersion number and mean fluid residence time were determined for ranges of superficial velocity, limestone particle size and depth of packed-bed. The results obtained are listed in Table 9. Note that the axial dispersion number was less than 0.02 in all cases and therefore the use of Eq. 15 was reasonably appropriate.

A number of investigators including Edwards and Richardson (1968) and Wilhelm (1962) have compiled data from various researchers and noted that for axial dispersion in liquids in packed beds the Peclet number, i.e.,

$$\text{Peclet number} = \frac{\bar{d} \; U_s}{D \; \varepsilon} = \frac{1}{N_D} \cdot \frac{\bar{d}}{L} \; , \qquad (16)$$

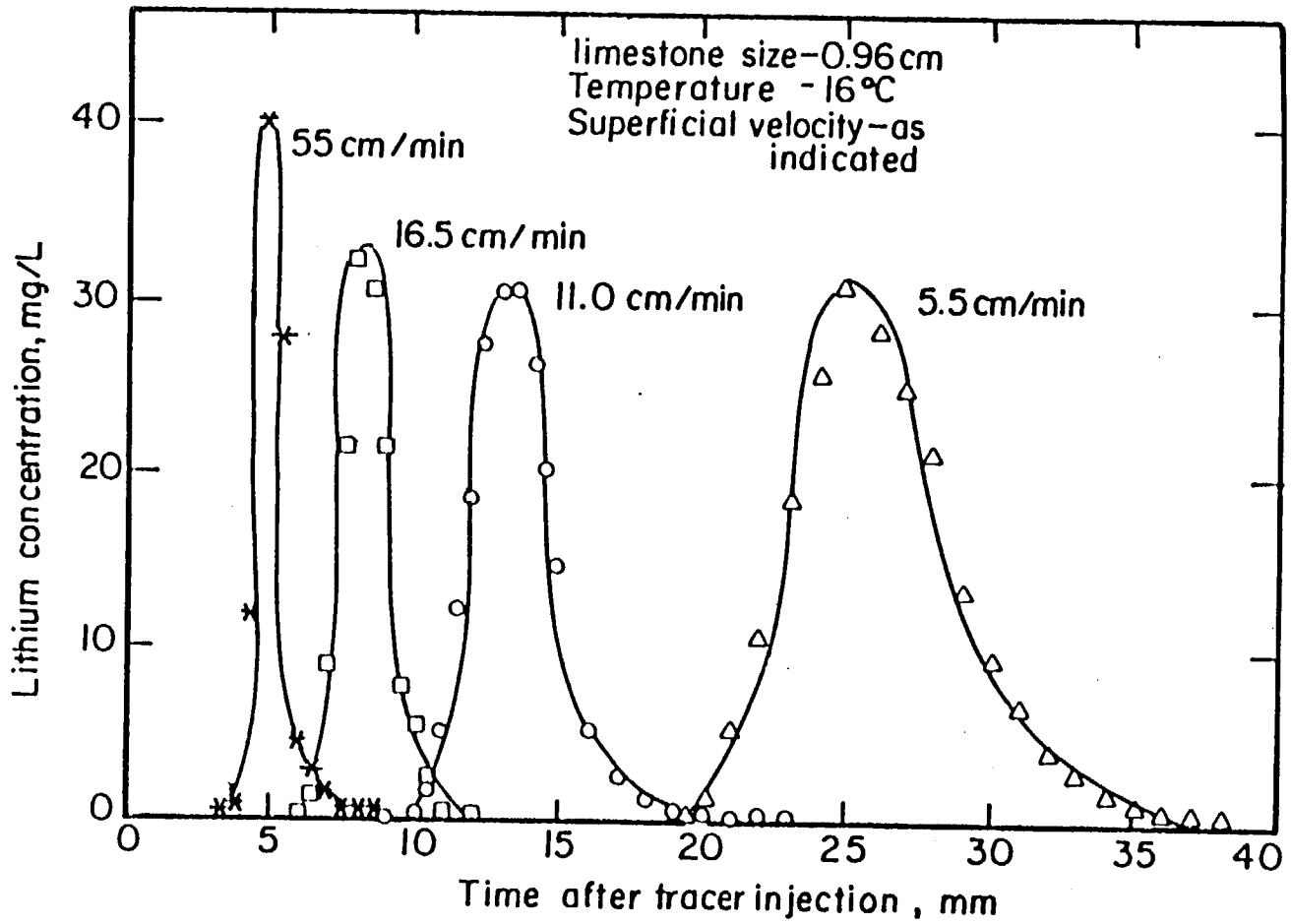

Figure 12. Measured effluent tracer concentration plotted as a function of time elapsed after tracer injection for four values of the superficial velocity. Results were obtained using Column A, Figure 6.

TABLE 9 RESULTS OF TRACER RESPONSE MEASUREMENTS OBTAINED USING LABORATORY COLUMNS (FIGURE 6)

Exp. No.	Depth L, cm	Particle Size $\bar{d}$, cm	Porosity ϵ	Superficial Velocity U_s, cm/min	Observations: Dispersion Number, N_D	Peclet Number, Pe	Mean Residence Time, $\bar{t}$, min	Tracer Mass Recovered %
1	305	0.96	0.41	12.2	0.0181	0.17	12.5	98
2	152.	0.96	0.41	18.2	0.0075	0.84	4.0	96
3	335	0.96	0.41	18.2	0.0034	0.84	8.6	99
4	335	0.96	0.41	6.1	0.0078	0.37	26.6	104
5	335	0.96	0.41	6.1	0.0062	0.46	26.7	105
6	335	0.96	0.41	14.7	0.0106	0.27	14.3	113
7	335	0.96	0.41	22.0	0.0046	0.62	8.8	96
8	335	0.96	0.41	22.0	0.0034	0.84	8.6	99
9	335	0.96	0.41	22.0	0.0069	0.42	8.0	99
10	335	0.96	0.41	29.3	0.0040	0.72	7.4	102
11	335	0.96	0.41	29.3	0.0043	0.67	6.9	127
12	335	0.96	0.41	29.3	0.0065	0.44	7.2	106
13	335	0.94	0.41	37.5	0.0118	0.24	5.6	115
14	335	0.96	0.41	36.7	0.0072	0.40	5.7	103
15	335	0.96	0.41	36.7	0.0045	0.64	5.3	104
16	335	0.96	0.41	5.4	0.0088	0.33	25.9	104
17	335	0.96	0.41	21.4	0.0063	0.45	6.8	108
18	335	0.96	0.41	37.5	0.0051	0.56	3.5	97
19	335	0.96	0.41	53.5	0.0047	0.61	3.0	109
20	61	0.54	0.43	5.4	0.0183	0.48	4.2	119
21	152	0.54	0.43	5.4	0.0079	0.45	12.0	79
22	213	0.54	0.43	5.4	0.0085	0.30	21.1	102
23	213	0.54	0.43	21.5	0.0127	0.20	3.3	81
24	213	0.54	0.43	32.2	0.0085	0.30	3.4	114
25	213	0.54	0.43	53.7	0.0065	0.39	2.2	97
26	213	1.50	0.49	5.3	0.0149	0.47	34.0	108
27	213	1.50	0.49	16.0	0.0183	0.38	4.4	96
28	213	1.50	0.49	37.4	0.0089	0.79	3.4	110
29	213	1.50	0.49	48.1	0.0082	0.86	2.6	108
30	213	3.20	0.49	0.3	0.0200	0.75	111.7	109
31	213	3.20	0.49	1.1	0.0125	0.20	33.3	88
32	213	3.20	0.49	1.9	0.0096	1.56	16.7	76
33	213	3.20	0.49	2.7	0.0073	2.05	13.1	69

is essentially a constant over a wide range of Reynolds numbers and in addition, is only slightly affected by variation in the size of the packing material. For the Reynolds number range of this study ($1 < Re < 100$) all the literature values of the Peclet number analyzed by Wilhelm (1962) and Edwards and Richardson (1968) fall in the interval 0.2 to 2. The range of Peclet numbers for the results listed in Table 7 fall in the range 0.2 to 2 and are therefore consistent with published values.

The mean and standard deviation of the Peclet numbers derived from the quantities listed in Table 7 are 0.50 and 0.21, respectively. These values suggest that a reasonable estimate of the dispersion number for the range of conditions used in this study can be obtained from the following expression,

$$\bar{N}_D = (\overline{Pe})^{-1}(\bar{d}/L) = 2.0\ (\bar{d}/L) \qquad (17)$$

where, $\overline{Pe}$, is the mean value of the Peclet number. Given the standard deviation of 0.21 and the expected value of 2.0, $\bar{N}_D$, should fall in the interval $1.4\ (\bar{d}/L)$ to $3.3\ (\bar{d}/L)$.

The mean fluid residence time in the columns was calculated using the measured bed porosity, ε, (Table 8), the depth of the packed-bed, L, superficial velocity, U_s, and the relationship

$$\bar{t}_c = \frac{L\varepsilon}{U_s} \qquad (18)$$

The mean fluid residence time determined using the tracer response curve, $\bar{t}$, plotted as a function of the value calculated using Eq. 18 is given in Figure 13. The agreement obtained is reasonable, a result which tends to support the method used to measure bed porosity and the quality of the tracer response data.

Before it was installed in the field the baffled-box contactor was subjected to a pulse input, lithium chloride tracer response test. The results of this test are plotted in Figure 14.

According to the dimensions of the contactor, the porosity of the bed and the flowrate used in the test (13.6 L/min) the mean residence time should

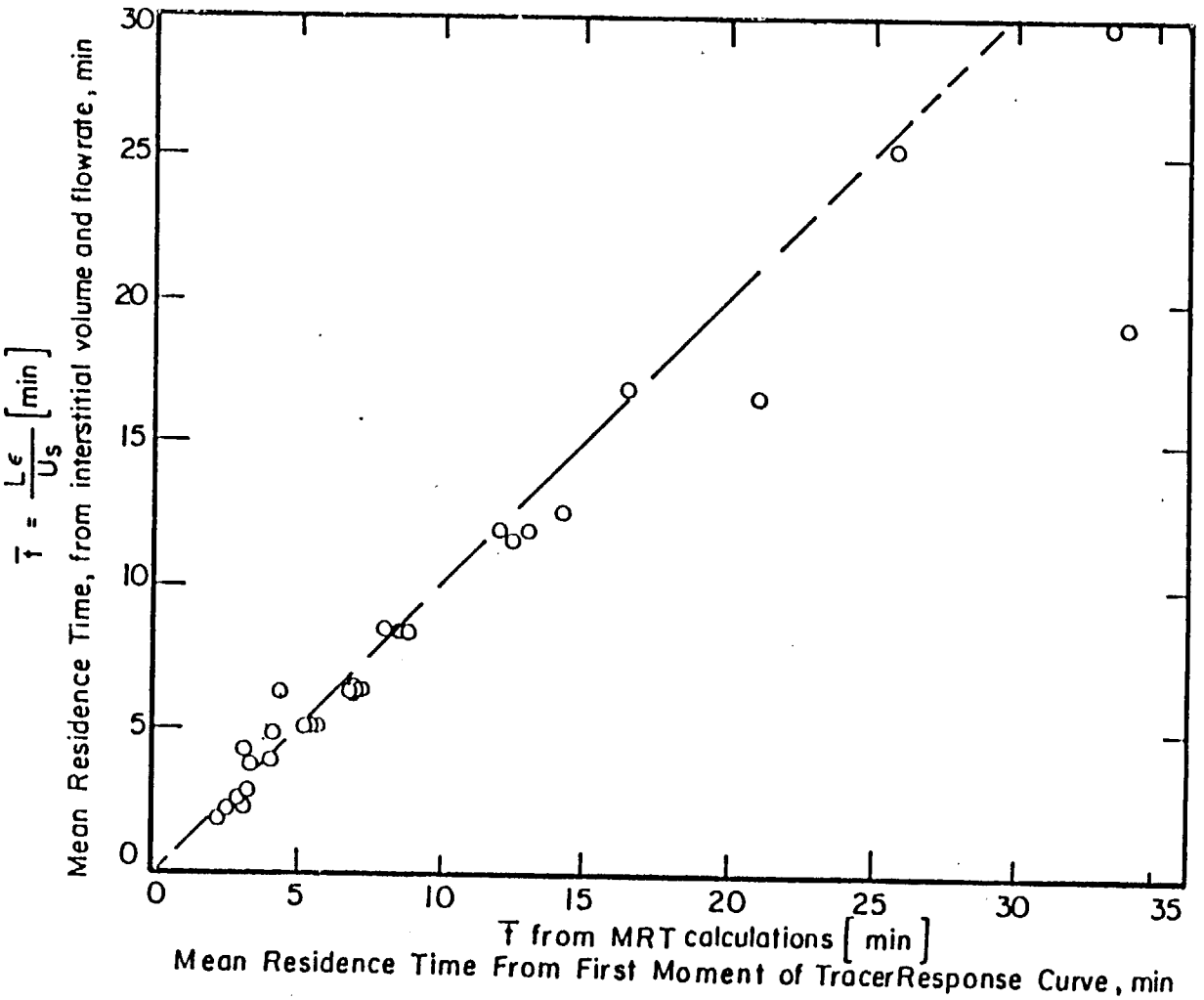

Figure 13. Mean residence time calculated using the superficial velocity and measured porosity plotted as a function of the mean residence time from the tracer experiments.

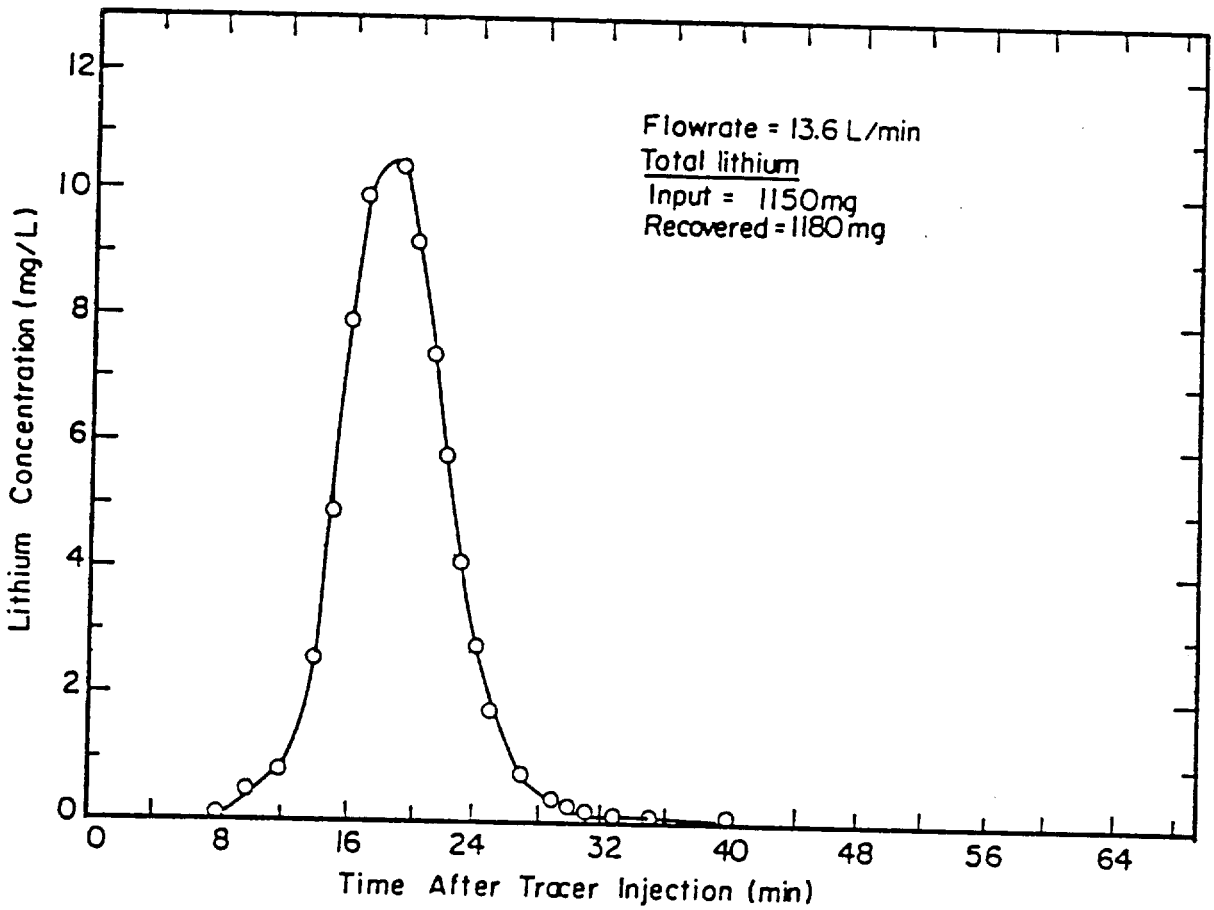

Figure 14. Measured effluent tracer concentration plotted as a function of the time elapsed after tracer injection for the baffled-box contactor (Figure 7).

be 10.4 min in the limestone and a total of 6.5 min in the nine sampling/baffle chambers (see Figure 7). The sum of these two quantities is approximately 17 min, a value which is in reasonable agreement with the mean residence time of 18 min determined using the tracer response data and Eq. 18. Also there was no evidence of significant short-circuiting or dead space.

PIPE SECTION PROCEDURES

To evaluate metal corrosion prior to and following limestone treatment, pipe section leaching studies were conducted in both laboratory and field experiments. Most pipe section experiments were conducted with 1 m (3.3 ft) lengths of 1.27 cm (½ in.)inside diameter copper pipe. Copper pipe was amended with 2.54 cm (1 in.) of 50-50 percent lead-tin solder at both ends of a given section, to simulate Pb corrosion from Pb solder joints. A limited number of additional experiments were conducted with 1 m (3.3 ft) lengths of 1.59 cm (5/8 in.) lead and galvanized steel pipe.

The pipe cleaning procedure used was a modified version of the ASTM procedure. Pipe sections were soaked in 5% HCl for two minutes. These sections were then drained and rinsed with 0.1 N $NaHCO_3$ to neutralize any acidic solution adhering to the pipe. Finally, pipe sections were rinsed copiously with distilled deionized water.

During metal leaching studies, aliquots of solution were placed in pipe sections and the openings covered with parafilm. Solutions were equilibrated with pipe sections at room temperature (22°C), for a given period of time, generally 10 hours. Both pH and metal concentrations of leachate were measured after equilibrium.

SAMPLING AND ANALYTICAL PROCEDURES

General Procedures

The analytical methods used in this study are summarized in Table 10. Samples were collected in air-tight polyethylene containers for major solute and trace metal analysis, in a sterilized glass bottle for bacteriological analysis, and in biochemical oxygen demand bottles for oxygen analysis. Temperature was measured and dissolved oxygen samples were fixed in the field. Samples were transported in a cooler to the water quality laboratory at Syracuse

Table 10 Analytical Methods

METHOD	PROCEDURE	REFERENCE
pH	potentiometrically with glass electrode	Standard Methods, 1975
alkalinity	strong acid titration with Gran plot analysis	Gran, 1952
Ca^{2+}, Mg^{2+}, Na^{+}, K^{+}	atomic absorption spectrophotometry (AAS)	Slavin, 1968
Al, Fe, Mn, Zn, Ca, Pb	filtration 0.4 μm polycarbonate filter, acidification (pH 1 with HNO_3 for 1 hr) analysis by AAS graphic furnace	Slavin, 1968
NO_3^-, Cl^-	ion chromatography	Small et al., 1975
SO_4^{2-}	ion chromotrography; turbidimetric method	Small et al., 1975; Standard Methods, 1975
dissolved inorganic carbon (DIC)	syringe stripping of CO_2 and detection by gas chromatography	Stainton, 1973
dissolved organic carbon (DOC)	filtration, ampoulation, persulfate oxidation, syringe stripping of CO_2 and detection by gas chromatography	Menzel & Vaccaro, 1964
NH_4^{+1}	phenate colorimetry, autoanalyzer	USEPA, 1983
dissolved oxygen (D.O.)	Winkler titration	Standard Methods, 1985
specific conductance	conductivity bridge	Standard Methods, 1985
standard plate count		Standard Methods, 1985
coliform	membrane filter	Standard Methods, 1985
turbidity	nephelometry	Standard Methods, 1985
temperature	thermometer	

University where they were measured for pH, alkalinity, specific conductance, dissolved inorganic carbon, dissolved oxygen, turbidity, coliform and standard plate count, and ampulated for the analysis of dissolved organic carbon within 8 hours of collection. Samples were stored at 4°C and analysis were completed within one week of collection.

Laboratory Contactors

Samples were collected starting at the top sampling point of the column and moving down the column using all the sampling ports provided. Samples were withdrawn by gravity flow and collected in 500 mL polyethylene bottles. To minimize CO_2 exchange, the bottles were completely filled and closed immediately. To minimize disturbance of the flow in the column during sampling, a period of time equal to twice the distance between two sampling ports divided by the interstitial flow velocity was allowed to elapse before the next sample was taken.

The column experiments were conducted at room temperature (15° - 22°C). To minimize microbial growth, the columns were initially rinsed with chlorinated water followed by deionized water. The clear acrylic column was covered with black plastic sheets to reduce exposure to light.

Field Contactors

Water samples were collected from the baffled box contactor and the housekeeping cottages connected to this unit for a period of 2.5 years. The sampling frequency was monthly except when weather conditions restricted access. Samples were also collected from the spring and cottages on the eastern side of the resort. This program included sampling at the cottage with the Culligan unit. A more frequent, sampling schedule was employed when the wound fiberglass unit was installed in Bay Side Cottage to treat Big Moose Lake water during January - April, 1984.

Two types of tap water samples were collected in the field, a flowing grab sample taken when the faucet was first opened and a grab sample obtained after 3 minutes of continuous flow.

Quality Assurance/Quality Control Information Data

An assessment of field data requires an understanding of the precision and accuracy associated with analytical determinations. In this study, both sampling and analytical precision were evaluated. Triplicate samples were

collected for analysis on a minimum of five percent of the total samples collected, and triplicate determinations were performed on a minimum of five percent of the samples collected. A summary of the range and coefficient of variation from the triplicate sampling (an estimate of sampling and analytical precision) program for a variety of water chemistry parameters is provided in Table 11. Moreover, we periodically performed a 4 by 4 analysis in which four samples were collected and split four ways. The resulting 16 solutions were analyzed for major solutes. By a two-way analysis of variance, (Barr et al. 1976) the sampling and analytical precision were evaluated (Table 12).

To evaluate analytical accuracy we performed charge balances, conductivity checks, and alkalinity checks (Figure 15). Also we periodically evaluated blind samples obtained from the USEPA Municipal Environmental Research Laboratory at Cincinnati, Ohio; the USGS Standard Reference Water Sample Program, Denver, Colorado; and the USEPA Long-Term Monitoring Program through Radian Inc. Results of some blind audit samples obtained from the USEPA Municipal Environmental Research Laboratory are summarized in Table 13. Generally the analyses of audit samples from this program were in agreement with reported values. However, this audit program was not designed to evaluate analytical accuracy of the low concentration ranges generally observed in dilute waters. A more reasonable depiction of the accuracy of our analytical methods is available through the analysis of dilute audit samples from the USEPA Long-Term Monitoring Program conducted in May 1985 (Table 14). Although the percent differences between the theoretical and values obtained by Radian Compared to the values reported by Syracuse University were high for some determinations, the actual magnitude of these discrepancies were generally low. These relatively high percent differences may be attributed to the low solute concentrations in this particular sample. Note some decrease in pH and increase in DIC is evident between determinations made by Radian and analyses conducted by Syracuse University, however ANC values were similar. These trends suggest that when this synthetic sample was made-up it was undersaturated with respect to the solubility of atmospheric CO_2. Over storage time, CO_2 equilibration evidently served to depress pH values while increasing DIC concentrations. Some discrepancy in DOC concentrations are also evident, however, given that the source of this synthetic DOC is unknown, this trend is difficult to explain.

TABLE 11
Summary of Sampling and Analytical Precision from Sample Triplicate Program

Parameter	Range of Mean	Range of Standard Deviation	Range of Coefficient of Variation
pH	6.01 - 7.68	0.006 - 0.231	0.079 - 3.0
alkalinity (mg $CaCO_3 \cdot L^{-1}$)	7.7 - 34	0.29 - 1.0	0.85 - 3.6
Sp. Cond. ($\mu mho \cdot cm^{-1}$)	50 - 107	0.12 - 6.2	0.12 - 5.8
DIC (mg $C \cdot L^{-1}$)	4.9 - 7.7	0.06 - 0.60	0.84 - 9.1
DOC (mg $C \cdot L^{-1}$)	0.76 - 2.3	0 - 0.30	5.0 - 10
Turbidity (NTU)	0.31 - 0.53	0.035 - 0.10	11 - 20
DO (mg $O_2 \cdot L^{-1}$)	7.0 - 7.3	0.1 - 0.5	1.4 - 7.6
Standard Plate Count (#·100 mL^{-1})	3.7 - 195	1.1 - 36	20 - 31
Total Coliform (#·100 mL^{-1})	0 - 64	0 - 16	0 - 25
Ca (mg $Ca \cdot L^{-1}$)	5.3 - 12.2	0.08 - 0.67	0.94 - 5.5
Mg (mg $Mg \cdot L^{-1}$)	0.65 - 0.89	0 - 0.016	0 - 1.8
Na (mg $Na \cdot L^{-1}$)	2.4 - 7.2	0.012 - 1.36	0.46 - 19
K (mg $K \cdot L^{-1}$)	0.66 - 2.6	0 - 0.25	0 - 9.4
SO_4 (mg $SO_4 \cdot L^{-1}$)	4.0 - 4.3	0.21 - 0.40	5 - 10
Al (μg $Al \cdot L^{-1}$)	0 - 33	3 - 16	29 - 48
Cu (μg $Ca \cdot L^{-1}$)	0 - 1	0 - 2	0 - 43
Pb (μg $Pb \cdot L^{-1}$)	0 - 123	0 - 7	0 - 55
Zn (μg Zn·L-1)	13 - 42	20 - 32	60 - 76

TABLE 12 Estimates of sample collection and analytical precision from 4 x 4 analysis for Big Moose Lake

Parameter	Sampling Precision		Analytical Precision	
	Std. Dev.	C.V.	Std. Dev.	C.V.
field pH	0.020	0.39	0.0088	0.17
air equilibrated pH	0.028	0.54	0.012	0.23
ANC ($\mu eq \cdot L^{-1}$)	2.6	44	5.1	86
Spec. Cond($\mu mho \cdot cm^{-1}$)	2.1	5.9	0.3	0.84
Ca($\mu mol \cdot L^{-1}$)	0.49	1.0	0.36	0.78
Mg($\mu mol \cdot L^{-1}$)	0.02	1.5	0.003	0.79
Na($\mu mol \cdot L^{-1}$)	0.77	2.8	0.14	0.52
K($\mu mol \cdot L^{-1}$)	0.34	3.2	0.13	1.2
monomeric Al ($\mu mol \cdot L^{-1}$)	0.40	9.6	0.19	4.9
SO_4^{2-}($\mu mol \cdot L^{-1}$)	2.9	4.3	0.61	0.90
NO_3^-($\mu mol \cdot L^{-1}$)	1.3	6.9	0.76	4.0
Cl^-($mol \cdot L^{-1}$)	1.6	19	0.83	9.5
H_2SO_4($\mu mol \cdot L^{-1}$)	5.1	6.9	1.7	2.3
DOC($\mu mol \cdot L^{-1}$)	54	14	21	5.4
DIC($\mu mol \cdot L^{-1}$)	1.6	6.8	1.4	1.9
Free F($\mu mol \cdot L^{-1}$)	0.018	3.4	0.0095	1.8
Total F($\mu mol \cdot L^{-1}$)	0.14	3.2	0.059	1.4

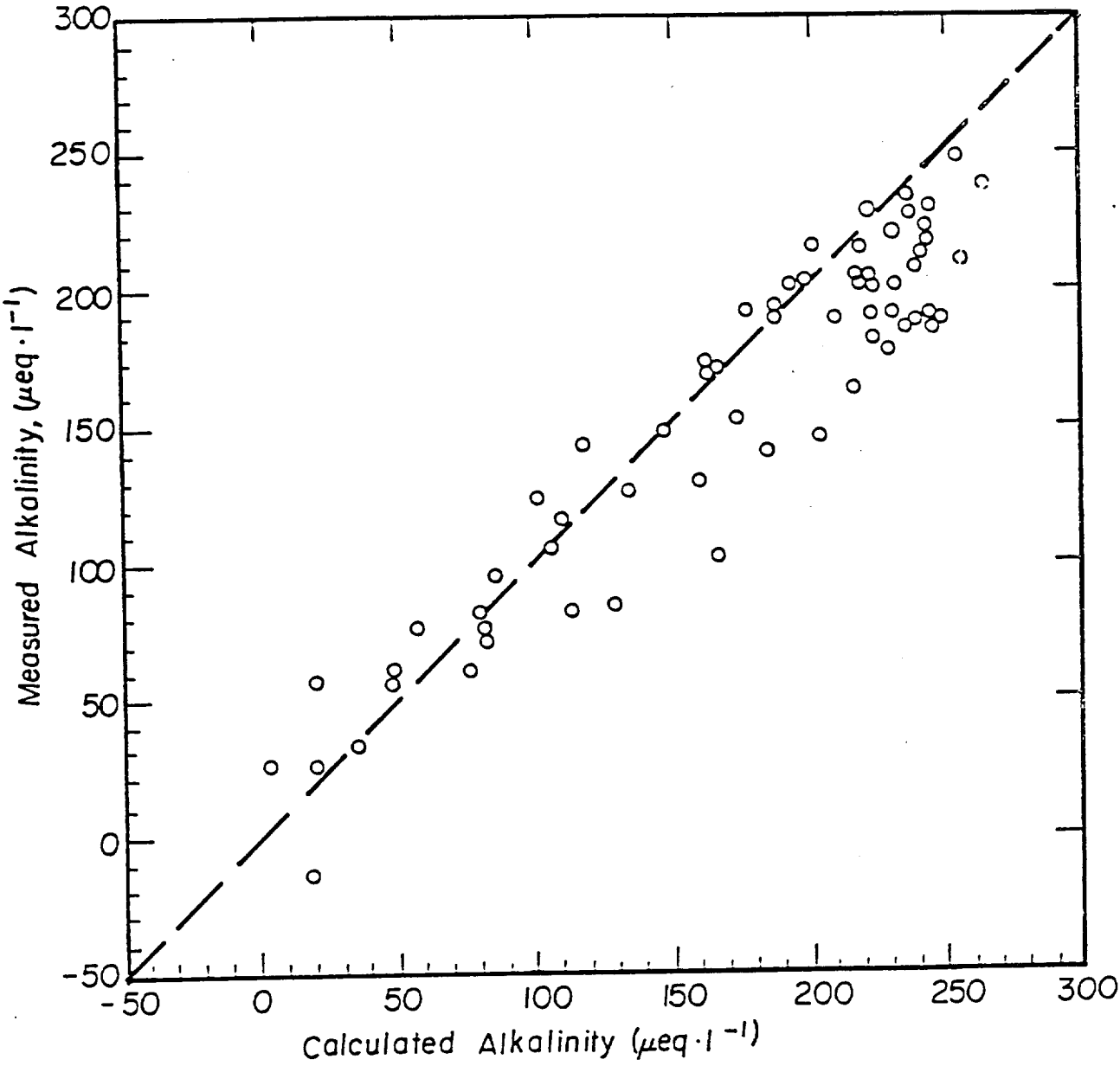

Figure 15. Measured and calculated alkalinity for field measurements. The measured dissolved inorganic carbon concentration and pH were used to determine the "calculated" alkalinity.

TABLE 13

Summary of Blind Sample Analysis Obtained from USEPA Municipal Environmental Research Laboratory

Date	Parameter	True Value	Measured Value	% Difference
7/1/82	Turbidity (NTU)	1.35	1.30	6.7
	Turbidity (NTU)	5.50	5.35	2.7
	NO_3^-(mg $N \cdot L^{-1}$)	0.42	0.42	0
	NO_3^-(mg $N \cdot L^{-1}$)	7.3	7.3	0
	F^-(mg $F \cdot L^{-1}$)	0.12	0.12	0
	F^-(mg $F \cdot L^{-1}$)	1.1	1.1	0
10/1/82	Pb(µg $Pb \cdot L^{-1}$)	25	25	0
	Zn(µg $Zn \cdot L^{-1}$)	15	16	-6.7
	Al(µg $Al \cdot L^{-1}$)	78	78	0
	Mn(µg $Mn \cdot L^{-1}$)	15	16	-6.7
	Mn(µg $Mn \cdot L^{-1}$)	75	68	9.3
	Fe(µg $Fe \cdot L^{-1}$)	80	81	-1.2
	Fe(µg $Fe \cdot L^{-1}$)	900	890	1.1
7/5/83	Turbidity (NTU)	5.9	5.6	5.1
	Turbidity (NTU)	0.42	0.31	26
	Pb(µg $Pb \cdot L^{-1}$)	22	21	4.5
	Pb(µg $Pb \cdot L^{-1}$)	56	43	23
	Cd(µg $Cd \cdot L^{-1}$)	1.2	2.3	-92
	Cd(µg $Cd \cdot L^{-1}$)	22	22	0

TABLE 13 (con't)

Date	Parameter	True Value	Measured Value	% Difference
12/14/83	pH	6.87	6.84	
	pH	8.60	8.45	
	Sp. Cond(μmho$\cdot$cm^{-1})	215	235	-9.3
	Sp. Cond(μmho$\cdot$cm^{-1})	616	685	-11
	Ca(mg Ca$\cdot$L^{-1})	4.8	4.8	0
	Ca(mg Ca$\cdot$L^{-1})	32	32	0
	Mg(mg Mg$\cdot$L^{-1})	1.26	1.20	4.7
	Mg(mg Mg$\cdot$L^{-1})	9.46	9.41	0.5
	Na(mg Na$\cdot$L^{-1})	33.3	35.6	-6.9
	Na(mg Na$\cdot$L^{-1})	68.5	77	1.3
	K(mg K$\cdot$L^{-1})	0.62	1.52	-145
	K(mg K$\cdot$L^{-1})	12.3	17.0	-38
	Cu(μg Ca$\cdot$L^{-1})	78.0	73.0	6.4
	Cu(μg Cu$\cdot$L^{-1})	5.20	5.80	-11
	Pb(μg Pb$\cdot$L^{-1})	158	170	-7.5
	Pb(μg Pb$\cdot$L^{-1})	11.7	30	-156
1/13/84	Turbidity (NTU)	6.0	6.8	-13
	Turbidity (NTU)	0.7	1.2	-71
	Pb(μg Pb$\cdot$L^{-1})	30	45	-50
	Pb(μg Pb$\cdot$L^{-1})	90.1	94	-4.3
7/16/84	Cd(μg Cd$\cdot$L^{-1})	2.1	1.8	14
	Cd(μCd$\cdot$L^{-1})	10.8	8.8	18
	Pb(μg Pb$\cdot$L^{-1})	37.6	29	23
	Pb(μg Pb$\cdot$L^{-1})	105	86	18

[1]%Difference = (True Value - Reported Value)/(True Value) x 100

TABLE 14 Summary of USEPA Corvallis Environmental Research Laboratory Blind Audit Analysis.
All values in $\mu eq \cdot L^{-1}$ except where indicated.

Parameter	Theoretical	Radian Value	Syracuse Univ.		%Difference Theoretical		Radian	
			839	840	839	840	839	840
pH	------	7.31	6.67	6.96	---	---	---	---
alkalinity	------	108	113	110	---	---	---	---
SO_4^{2-}	48	49	44	45	---	---	4	2
NO_3^-	7.4	7.9	7.0	8.2	-9	-7	-11	-9
F^-	2.2	2.2	2.6	2.4	15	8	15	8
Ca^{2+}	9.8	11.1	13	12	25	18	15	8
Mg^{2+}	37	35	39	39	5	5	10	10
Na^+	121	117	118	109	-3	-11	1	-7
K^+	5.2	4.8	5	4	-4	-30	4	-10
NH_4^+	9.3	8.3	12.1	10.7	23	13	31	22
DOC($\mu mol \cdot L^{-1}$)	83	98	140	152	41	45	30	36
DIC($\mu mol \cdot L^{-1}$)	------	98	138	138	---	---	29	29
SiO_2($\mu mol \cdot L^{-1}$)	18	18	20	20	10	10	10	10
Sp. Cond. ($\mu mol \cdot cm^{-1}$)	------	17.3	20	20	---	---	6	6
Cal. Sp. Cond.	------	18.6	19.3	18.5				
sum of cations	------	176	187	175				
sum of anions	------	177	180	179				
Cal. HCO_3^-	------	90	98	99				

Samples were routinely split with other researchers that analyze low ionic strength solutions. Analytical checks on dilute solutions have been made with investigators from Cornell University, McMaster University, University of Virginia, University of California at Los Angeles, the Insitute of Ecosystem Studies Cary Arboretum, and Rensselaer Polytechnic Institute.

COMPUTATIVE ANALYSIS

Thermodynamic calculations involving trace metal solubility were conducted with a modified version of the chemical equilibrium model MINEQL (Westall et al., 1976). Calculations were corrected for the effects of ionic strength using the Davies equations (Stumm and Morgan, 1981) and temperature. The solubility and complexation constants used in our analysis are summarized in Tables 15 and 16, respectively. The results obtained from chemical equilibrium calculations are highly dependent on the thermochemical data used. Data analysis is complicated by inconsistencies in the literature. In this regard, we conducted a thorough review to evaluate if there was consensus among researchers in the use of thermodynamic data relevent to our study (Tables 15 and 16). The results of this literature search suggest that generally there is consensus in the use of thermochemical data. However, some inconsistencies were evident in trace metal reactions.

There is considerable uncertainty in the stability constant for $Cu(OH)_2(aq)$ (Vacenta, 1976). This uncertainty is significant because predictions of total Cu in the neutral pH range are very sensitive to this stability constant. The stability constant for $Cu(OH)_2(aq)$ was evaluated potentiometrically by Quintin (1937), obtaining a value of $\log^* \beta_2 = -13.7$; while Spivakovski and Makouskaya (1968) used a precipitation method to obtain $\log^* \beta_2 = 13.2$. However, Mesmer and Baes (1974) estimated $\log^* \beta_2 = -17.3$, almost four orders of magnitude lower than previous estimates. Vacenta (1976) noted the magnitude and significance in this discrepancy. She evaluated the $Cu(OH)_2(aq)$ stability constant potentiometrically with a Cu ion selective electrode and obtained results consistent with $\log^* \beta_2 = -13.7$. Therefore we followed her lead and used this value in our study.

Another perplexing inconsistency in thermodynamic data involves the solubility of $Pb(OH)_2(s)$. Wagman et al. (1968) reported a value log* Kso

TABLE 15 Equilibrium Constants at 25°C for the Solids Considered in the MINEQL Calculations.

	REACTIONS		log K	REFERENCE
1.	$Cu(OH)_{2(s)} + 2H^+$	$Cu^{+2} + 2H_2O$	- 8.64	Baes and Mesmer 1976
2.	$CuCO_{3(s)}$	$Cu^{+2} + CO_3$-2	- 9.63	Smith and Martell 1976
3.	$Cu_2(OH)_2CO_3 + 3H^+$	$2Cu^{+2} + HCO_3^- + 2H_2O$	5.15	Baes and Mesmer 1976
4.	$Cu_3(OH)_2(CO_3)_2 + 4H^+$	$3Cu^{+2} + 2HCO_3^- + 2H_2O$	3.75	Baes and Mesmer 1976
5.	$CuSO_4$	$Cu^{+2} + SO_4^{-2}$	3.01	Wagman et al 1969
6.	$Pb(OH_{2(s)} + 2H^+$	$Pb^{+2} + 2H_2O$	8.15-13.07	Wagman et al 1969 Topelman 129
7.	$PbCO_{3(s)}$	$Pb^{+2} + CO_3^{-2}$	-13.13	Hem 1976
8.	$Pb_3(CO_3)_2(OH)_{2(s)} + 2H^+$	$3Pb^{+2} + 2CO_3^{-2}$	-17.46	Sillen and Martell 1964
9.	$PbSO_{4(s)}$	$Pb^{+2} + SO_4^{-2}$	- 7.79	Smith and Martell 1976
10.	$Zn(OH)_{2(s)} + 2H^+$	$Zn^{+2} + 2H_2O$	12.45	Baes and mesmer 1976
11.	$ZnCO_{3(s)}$	$Zn^{+2} + CO_3^{-2}$	-10.00	Smith and Martell 1976
12.	$Zn_5(OH)_6(CO_3)_{2(s)} + 6H^=$	$5Zn^{+2} + 2CO_3^{-2} + 6H_2O$	9.65	Sillen and Martell 1964
13.	$ZnSO_{4(s)}$	$Zn^{+2} + SO_4^{-2}$	3.01	Wagmann et al 1969

TABLE 16 REACTIONS AND EQUILIBRIUM CONSTANTS AT 25°C FOR THE AQUEOUS COMPLEXES CONSIDERED IN THE MINEQL CALCULATIONS

	REACTIONS		log K (Ball et al., 1980)		
			Pb	Cu	Zn
1.	$M^{+2} + H_2O$	$\longrightarrow MOH^+ + H^+$	- 7.71	- 8.00	- 8.96
2.	$M^{+2} + 2H_2O$	$\longrightarrow M(OH)_2^0 + 2H^+$	-17.12	-13.68	-16.90
3.	$M^{+2} + 3H_2O$	$\longrightarrow M(OH)_3 + 3H^+$	-28.06	-26.90	-28.40
4.	$M^{+2} + 4H_2O$	$\longrightarrow M(OH)_2^{-2} + 4H^+$	-39.70	-39.60	-41.20
5.	$2M^{+2} + H_2O$	$\longrightarrow M_2OH^{+3} + H^+$	- 6.36	------	- 9.00
6.	$2M^{+2} + 2H_2O$	$\longrightarrow M_2(OH)_2 + 2H^+$	------	-10.36	------
7.	$3M^{+2} + 4H_2O$	$\longrightarrow M_3(OJ)_4^{+2} + 2H^+$	-23.88	-22.05	------
8.	$4M^{+2} + 4H_2O$	$\longrightarrow M_4(OH)_8^{+4} + 4H^+$	-20.88	------	------
9.	$6M^{+2} + 8H_2O$	$\longrightarrow M_6(OH)_8^{+4}$	-43.61	------	------
10.	$M^{+2} + CO_3^{-2} + H^+$	$\longrightarrow MHCO_3^+$	------	13.03	12.43
11.	$M^{+2} + CO_3^{-2}$	$\longrightarrow MCO_3^0$	7.24	6.73	5.30
12.	$M^{+2} + 2CO_3^{-2}$	$\longrightarrow M(CO_3)_2^{-2}$	10.64	9.83	9.63
13.	$M^{+2} + Cl^-$	$\longrightarrow MCL^+$	1.60	0.43	0.43
14.	$M^{+2} + 2Cl^-$	$\longrightarrow MCl_2^0$	1.80	0.16	0.45
15.	$M^{+2} + 3Cl^-$	$\longrightarrow MCl_3^-$	1.70	- 2.29	0.30
16.	$M^{+2} + 4Cl^-$	$\longrightarrow MCl_4^-$	------	- 4.59	0.20
17.	$M^{+2} + SO_4^{-2}$	$\longrightarrow MSO_4^0$	2.75	2.31	2.37

= 8.15. This value has been used throughout the literature in studies of Pb chemistry (e.g. Hem and Durum, 1973; Ball et al., 1980; Faust and Aly, 1981). Topelmann (1929) obtained log* Kso = 13.07 for "freshly precipitated" $Pb(OH)_2$. This latter value has been cited by Feithnecht and Schindler (1963), and ultimately used by Patterson et al. (1977), and Schock (1980, 1984) in studies of Pb corrosion in water distribution systems. Schock (1980) indicated that the discrepancy between the two solubility values represents the difference between "fresh" and "aged" precipitates. However given the magnitude of this discrepancy (5 orders of magnitude), it is doubtful that crystallinity of the precipitate explains the variation. Note that the value obtained by Wagman et al. (1968) was calculated, not experimental. While Topelmann's (1929) work was experimental the magnitude of experimental error in his study in unclear. Therefore one value is not obviously superior to the others; in fact the validity of both values could be challenged. The solubility of $Pb(OH)_2$ is a classic example of thermochemical data finding its way in the literature and gaining acceptance over years of use without the benefit of a critical review. Clearly if we are to improve our understanding of Pb corrosion, better information on the solubility of $Pb(OH)_2$ is desperately needed.

In this study statistical analysis was facilitated by the use of the Statistical Analysis System (SAS; Barr et al., 1976).

SECTION 6

DERIVATION OF CONTACTOR DESIGN EQUATIONS

A set of equations was developed for use in predicting the effect of design and operating variables on the chemistry of the limestone contactor effluent. The following assumptions were made in formulating the model:

- The contactor is a closed system, i.e., as the water passes through the unit there is no exchange of carbon dioxide with the atmosphere,
- The rate of limestone dissolution at any axial location, z, within the column, R_z, is controlled by a mass transfer resistance (calcium ion transport) and a surface reaction acting in series. Eqs. (4) and (5), SECTION 4, were assumed to apply, i.e.,

$$R_z = K_o(C_{eq} - C_{bz}) \tag{19}$$

and

$$K_o = \frac{K_c K_L}{K_c + K_L}, \tag{20}$$

where C_{eq} is the calcium ion concentration when the influent solution and limestone have reached equilibrium, C_{bz} is the bulk solution calcium ion concentration at axial location z, K_c is the first order surface reaction rate constant and K_L is the first order mass transfer rate constant for calcium ion.

- Steady state conditions apply, i.e., the rate of limestone particle shrinkage is negligible, and
- The contactor is essentially a plug flow reactor with limited axial dispersion.

The dispersion (dispersed plug flow) model of Levenspiel (1972) was used to derive the principal design equation. The governing differential equation is

$$N_D \frac{d^2C}{dZ^2} - \varepsilon \frac{dC}{dZ} + r\,\bar{t} = 0, \tag{21}$$

where N_D is the dimensionless dispersion number, C is the reactant concentration, Z is the dimensionless axial distance (Z = z/L), L is the overall depth of limestone in the column, $\bar{t}$ is the mean fluid detention time, ε is the bed porosity and r is the reaction rate expression.

For steady state dissolution of limestone particles in a packed bed, the reactant concentration, C, in Eq. 21 can be replaced by the quantity $(C_{eq} - C_{bz})$ and the reaction rate, r, by

$$r = R_z \; a \; C = K_o \; a \; (C_{eq} - C_{bz}) \tag{22}$$

where a is the interfacial area of limestone particles per unit volume of interstitial fluid in the column. Since the reaction rate expression, Eq. 22, is first order, the solution of Eq. 21 by Wehner and Wilhelm (1956) can be used. The solution is given by;

$$\frac{C_{eq} - C_{bL}}{C_{eq} - C_{bo}} = \frac{4n \exp(1/2N_D)}{(1+n)^2 \exp(n/2\,N_D) - (1-n)^2 \exp(-n/2N_D)} \tag{23}$$

and

$$n = (1 + 4\, K_o\, a\, N_D\, \varepsilon\, L/U_s)^{\frac{1}{2}} \quad . \tag{24}$$

where, in this case C_{bo} and C_{bL} are the influent and effluent calcium ion concentrations for a column of depth L and U_s is the superficial or approach velocity for flow through the column. Note that $\varepsilon\, L/U_s = \bar{t}$.

In packed bed reactors of an overall length which is much greater than the size of the packing the amount of axial dispersion is small ($N_D < 0.01$) and Eqs. 23 and 24 reduce to

$$\frac{C_{eq} - C_{bL}}{C_{eq} - C_{bo}} = \exp\left[-\frac{K_o a L \varepsilon}{U_s} + \left(\frac{K_o\, a\, L\, \varepsilon}{U_s}\right)^2 N_D\right]. \tag{25}$$

Therefore to determine the effluent calcium concentration C_{bL} (Eq. 25), for a column of depth, L, one must know the equilibrium and influent calcium ion concentrations, C_{eq} and C_{bo}, the rate constant for the overall rate of dissolution, K_o, the interfacial area of limestone per unit volume of interstitial water, a, the bed porosity, ε, the superficial velocity, U_s, and the axial dispersion number, N_D. In this study the porosities listed in Table 8 were used and a was determined using Eq. 12,

$$a = \frac{6(1-\varepsilon)}{\bar{d}\ \psi\ \varepsilon} \qquad (12)$$

where $\bar{d}$ and ψ are the mean limestone particle size and sphericity. The magnitude of N_D was estimated using U_s, d, L and Eq. 17,

$$N_D = 2.0\ (\bar{d}/L) \qquad (17)$$

It will be shown in the next section that at least for column-type reactors operating within the range of conditions used in this study the magnitude of K_o can be estimated using well known dimensionless correlations from the mass transfer literature. The equilibrium calcium ion concentration, C_{eq}, was determined using the chemical equilibrium model described below and in Appendix A.

Equilibrium Calcium Concentration, C_{eq}

The equilibrium concentration of calcium ion at the limestone surface, C_{eq}, was determined as a function of the raw water chemistry and temperature. The calculations were based on chemical equilibrium principles which were used to derive the following set of equations.

Charge Balance:

$$2(C_{bo} + S) + C_c + [H^+] = ((DIC)_o + S)\ (\alpha_1 + 2\alpha_2) + C_a + K_w[H^+] \qquad (26)$$

Solubility Product Relationship for $CaCO_3$:

$$(C_{bo} + S)\ ((DIC)_o + S)\ \alpha_2 = K_{sp} \qquad (27)$$

Inorganic Carbon Ionization Fractions:

$$\alpha_1 = \{([H^+]/K_{a1}) + K_{a2}/[H^+]\ \}^{-1} \qquad (28)$$

and

$$\alpha_2 = \{([H^+]^2/K_{a1}\ K_{a2} + ([H^+]/K_{a2}) + 1\}^{-1} \qquad (29)$$

where C_{bo} is the initial (raw water calcium ion concentration, $(DIC)_o$ is the initial dissolved inorganic carbon concentration, S is the amount of

$CaCO_3$ dissolved from the limestone, C_c represents the total concentration of the non-calcium and hydrogen cations, C_a represents the total concentration of the non-inorganic carbon plus hydroxyl anions, K_{a1} and K_{a2} are the first and second ionization constants for carbonic acid, K_w is the ion product of water and K_{sp} is the effective solubility product for the calcium carbonate in limestone.

The magnitude of C_{eq} was determined for each set of initial conditions using a computational procedure in which the pH interval 6 to 10.5 was systematically searched to find the pH and the corresponding value of S at which both the charge balance and $CaCO_3$ solubility product relationships, Eqs. 26 and 27, were satisfied. At equilibrium $C_{eq} = C_{bo} + S$.

At each pH tested in the search procedure the ionic strength was calculated and the activity coefficients were determined using the equations given in Appendix A. The activity coefficients were used to correct the equilibrium constants for changes in ionic strength. These calculations were repeated at each pH until the ionic strength converged to an essentially constant value.

The equilibrium constants at infinite dilution used in this analysis are listed in Appendix A. The enthalpies listed in Appendix A and equations from Plummer and Bussenberg (1982) were used to correct the equilibrium constants for temperature. The effective solubility product for calcium carbonate in limestone was determined experimentally. (See Section 5 and Table 6.)

Calculations were also made to determine the effect of equilibrating the contactor effluent with atmospheric CO_2 on the pH and dissolved inorganic carbon concentration.

The following equations were used:

Charge Balance:

$$2(C_{bo} + S) + C_c + [H^+] = (C_T)\ (\alpha_1 + 2\ \alpha_2) + C_a + K_w/[H^+] \qquad (30)$$

where

$$C_T = K_H\ pCO_2/\alpha_o \qquad (31)$$

and

$$\alpha_o = (1 + K_{a1}/[H^+] + K_{a1}\ K_{a2}/[H^+]2)^{-1} \qquad (32)$$

C_T is the dissolved inorganic carbon concentration after the contactor effluent has equilibrated with atmospheric carbon dioxide, K_H is Henry's Law constant for CO_2, and pCO_2 is the atmospheric partial pressure of carbon dioxide. α_1 and α_2 were determined using Eqs. 28 and 29.

The charge balance expression, Eq. 26, was solved for the equilibrium pH using the search procedure described previously. The equilibrium dissolved inorganic carbon concentration was then determined using Eqs. 31 and 32.

In many cases the concentrations of the ions which determine C_c and C_a in Eqs. 26 and 30 are unknown and it is necessary to estimate the effect of C_c and C_a on the total ionic strength of the solution. It was found in this study that for dilute acidic waters the contribution of the C_c and C_a ions to the total ionic strength was usually small and essentially constant with pH and the dissolution of $CaCO_3$. A method for estimating the contribution of the C_c and C_a ions to the total ionic strength using the measured specific conductivity and the pH and the calcium and DIC concentrations is described in Appendix A.

SECTION 7

RESULTS AND DISCUSSION

MODEL VERIFICATION

Equilibrium Calcium Concentration

A series of laboratory experiments was conducted to test the predictive capability of the chemical equilibrium model. Water of known chemical characteristics was treated using a column containing $\bar{d}$ = 0.96 cm limestone particles and a very low flowrate ($Re \tilde{=} 1$). At this flowrate and limestone particle size, equilibrium conditions were reached or closely approximated in at least the bottom half of the downflow laboratory column.

The water used in these experiments was prepared by adding HCl, $CaCl_2$ and NaCl to deionized water. The raw water pH ranged from 2.3 to 4.5. While most experiments were conducted with no added calcium ion in the raw water five were made with 28 mg Ca/L.

The results obtained using raw water with no added calcium are plotted in Figures 16 to 18. A plot of pH as a function of the distance to the sampling port is indicated in Figure 16 and corresponding plots for $[Ca^{++}]$ and (DIC) are depicted in Figure 17 and 18, respectively. Using each of these figures the equilibrium values of pH, $-\log[Ca^{++}]$ and -log(DIC) were determined for each raw water pH by estimating the magnitude of the asymptotic limit for each parameter at sampling port depths greater than approximately four feet.

pH_{eq}, $-\log[Ca^{++}]$ and -log(DIC) plotted as a function of the raw water pH, pH_o are shown in Figure 19. The data points were determined by the locations of the asymptotes in Figures 16, 17 and 18 and similar plots. The lines shown in Figure 19 were plotted using the chemical equilibrium model and the constants listed in Appendix A. In general the agreement between the model predictions and the column data is good for pH and calcium concentration. In the cases of DIC, for $pH_o > 3.5$ the measured values of DIC are somewhat greater than those predicted by the model. It is possible that some carbon dioxide entered the solutions after the samples had been drawn from the column.

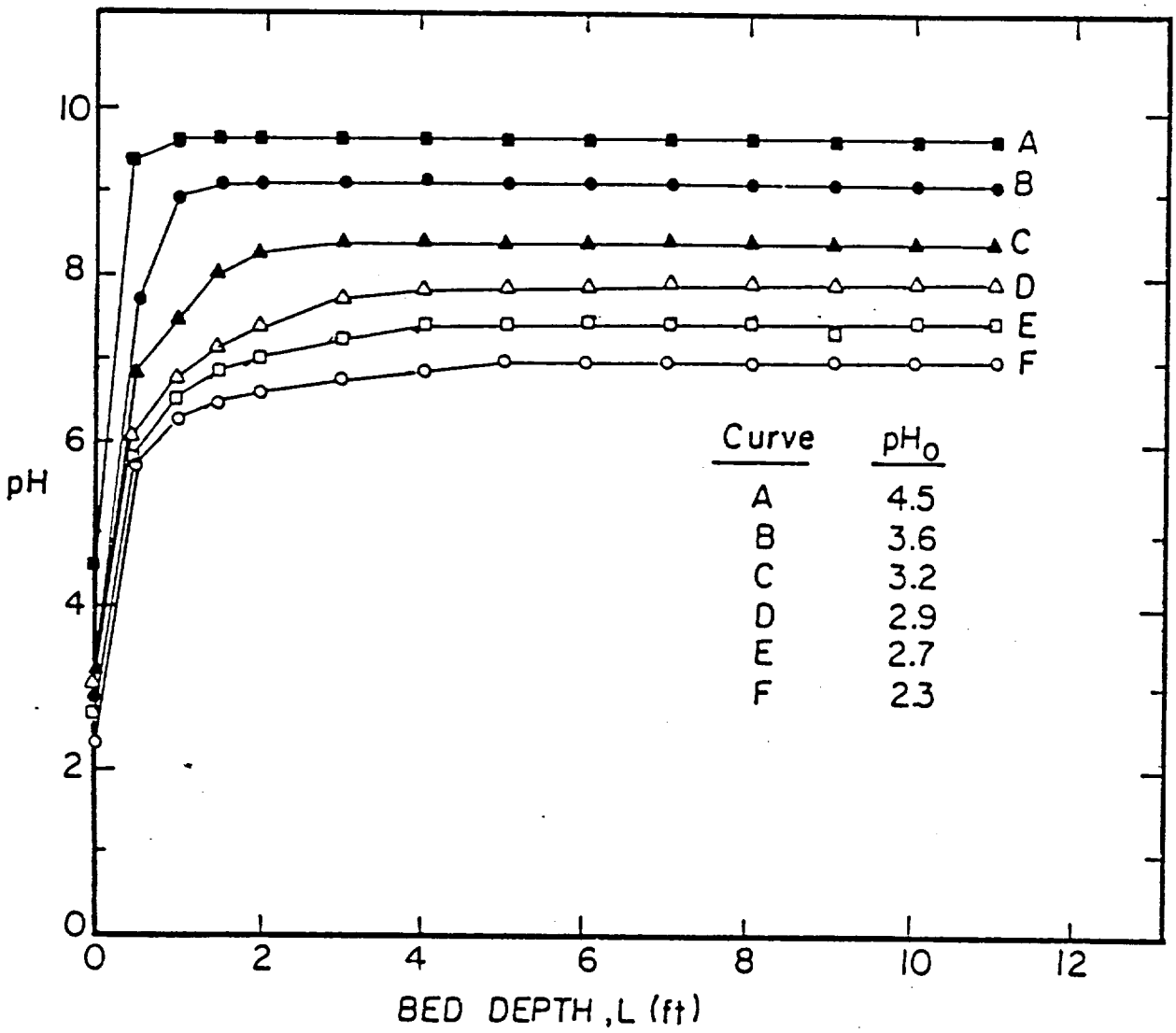

Figure 16. pH plotted as a function of the axial distance to the sampling port and influent pH, pH_o. Results were obtained using Column A, Figure 6.

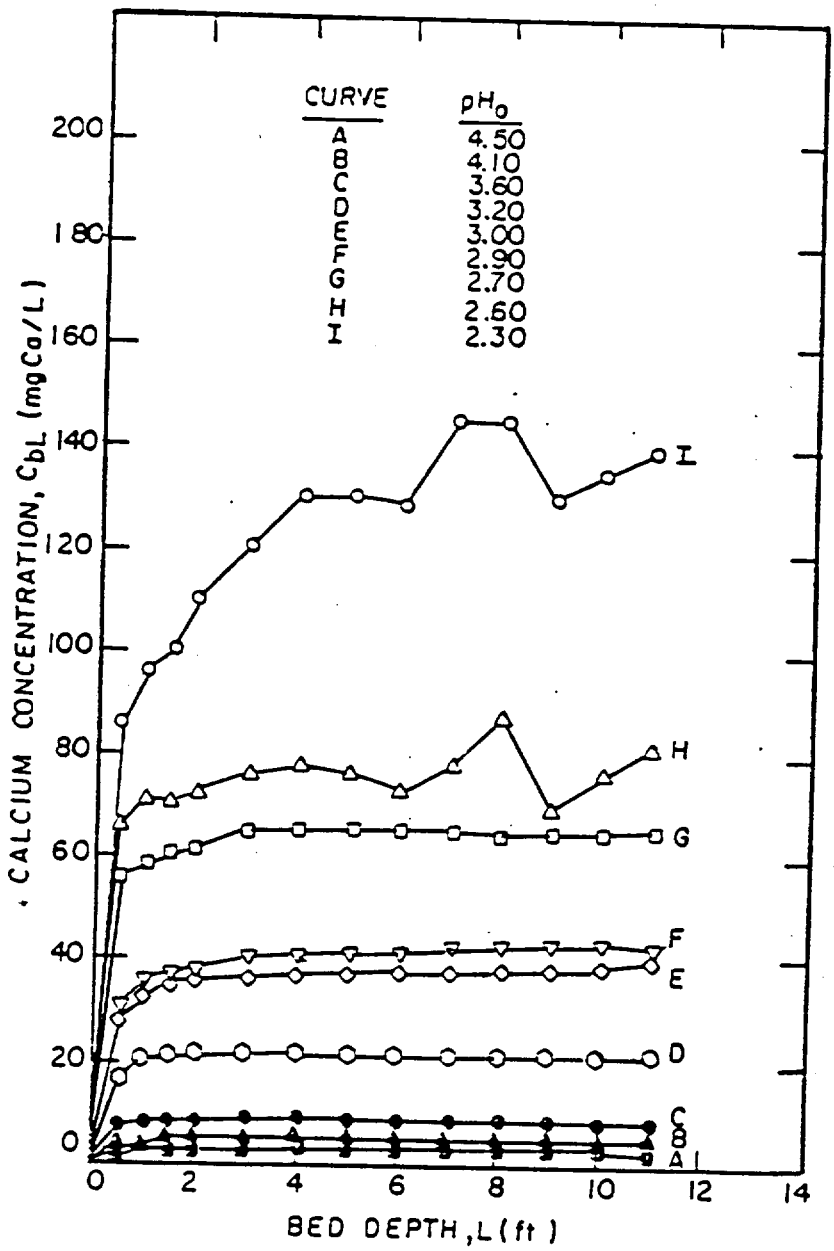

Figure 17. Calcium concentration plotted as a function of the axial distance to the sampling port and influent pH, pH_o. Results were obtained using Column A, Figure 6.

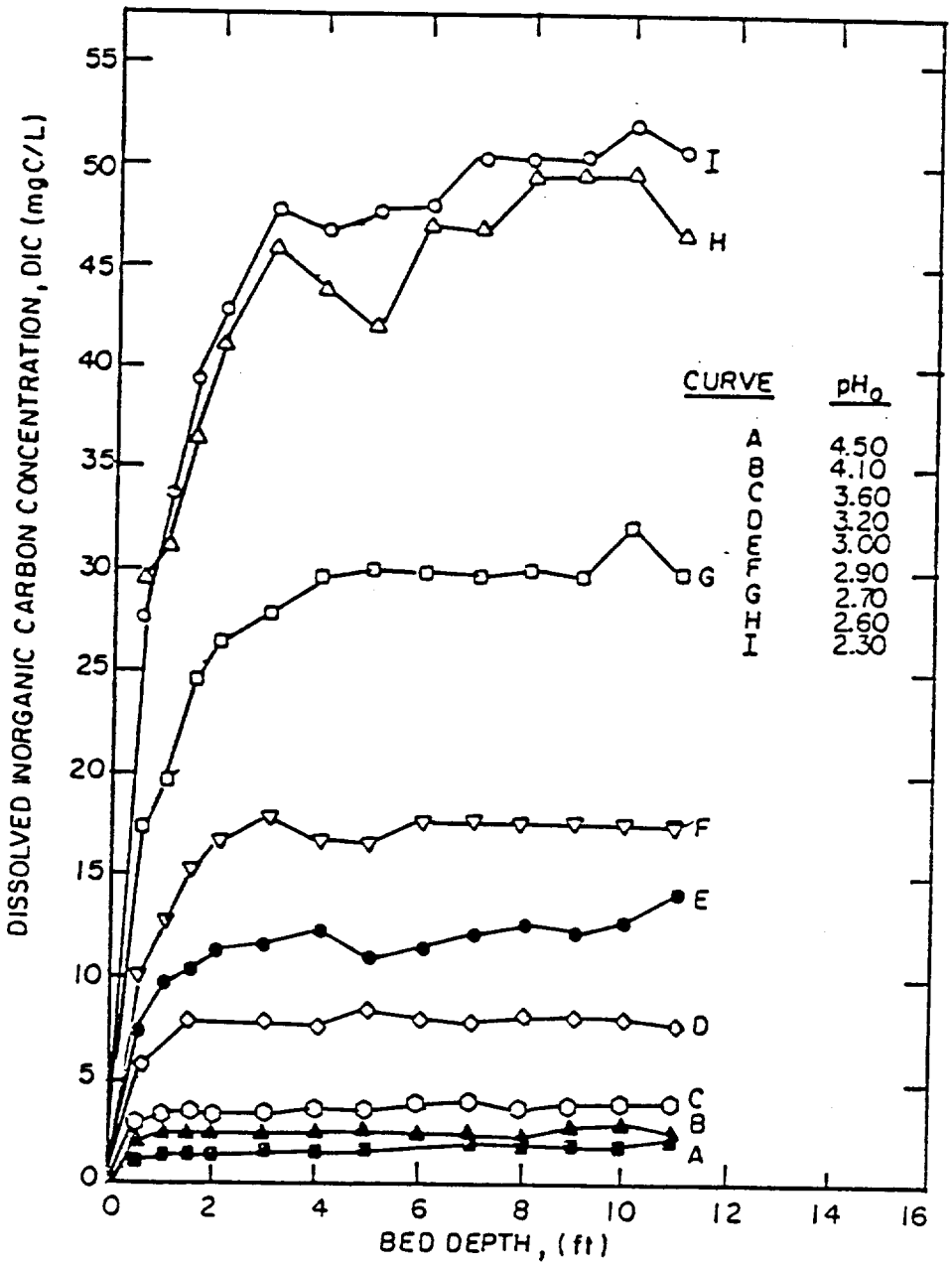

Figure 18. Dissolved inorganic carbon concentration plotted as a function of the axial distance to the sampling port and influent pH, pH_o. Results were obtained using Column A, Figure 6.

The $CaCO_3$ chemical equilibrium model was also used to plot the set of curves in Figure 19 which give the pH, and equilibrium calcium and DIC concentrations for the case when the contactor effluent was equilibrated with atmospheric carbon dioxide. The measured equilibrium DIC concentrations for pH_o > 3.5 were less than the values predicted by the model indicating that if CO_2 uptake by the sample solutions inadvertently occurred, equilibrium with the atmosphere was not reached.

In general, as the raw water pH decreased the maximum effluent pH decreased, from a value which was greater than 9.5 when the raw water pH was greater than 4.5 to approximately 8 when the raw water pH was 3.2. If the effluent pH was 9.5 or greater, equilibrating the contactor effluent with atmospheric carbon dioxide reduced the pH of the solution to slightly less than 7.6.

Decreasing the raw water pH also increased the amount of $CaCO_3$ dissolved at equilibrium. The amount dissolved increased exponentially as the raw water pH was reduced below 4.

The presence of calcium ion in the raw water tended to reduce the dissolution of the $CaCO_3$ by the common ion effect. With 28 mg Ca/L in the influent, the maximum effluent pH was approximately 9.5. For raw water pH values greater than 3 the amount of DIC at equilibrium was also reduced.

An experiment was conducted in which the raw water DIC concentration was adjusted by the addition of sodium bicarbonate. A plastic sheet was used to cover the raw water reservoir. Unfortunately the raw water DIC concentration decreased significantly during the course of the experiment, apparently through the release of carbon dioxide to small pockets of gas which remained under the plastic cover. As the result of this experimental problem the laboratory column data could not be used to test model predictions for variable raw water DIC.

The $CaCO_3$ chemical equilibrium model was used to plot pH_{eq} isopleths on a graph of influent calcium concentration as a function of influent DIC. An influent pH of 6, and a total ionic strength of 4×10^{-4} were used in these calculations. The results are presented in Figure 20.

The influent DIC concentration may have a significant effect on the equilibrium pH (Figure 20). For example, for this initial pH (pH_o = 6.0) and a calcium concentration of 10 mg Ca/L, the equilibrium pH is slightly

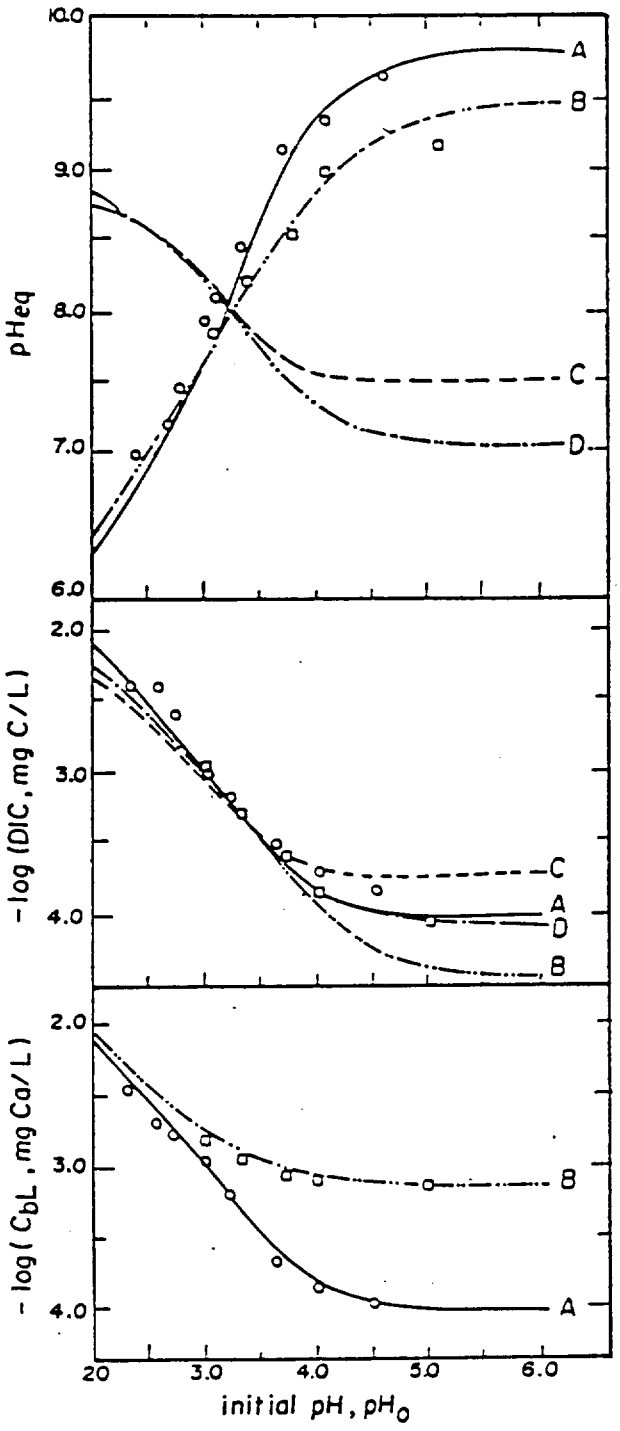

Figure 19. Equilibrium pH, dissolved inorganic carbon and calcium concentrations plotted as a function of the influent pH and the following conditions: Curve A - closed system and C_{bo} = 0; Curve B - closed system and C_{bo} = 28 mgCa/L; Curve C - closed/open system and C_{bo} = 0; Curve D - closed/open system and C_{bo} = 28 mgCa/L. The lines were drawn using the chemical equilibrium model described in Appendix A.

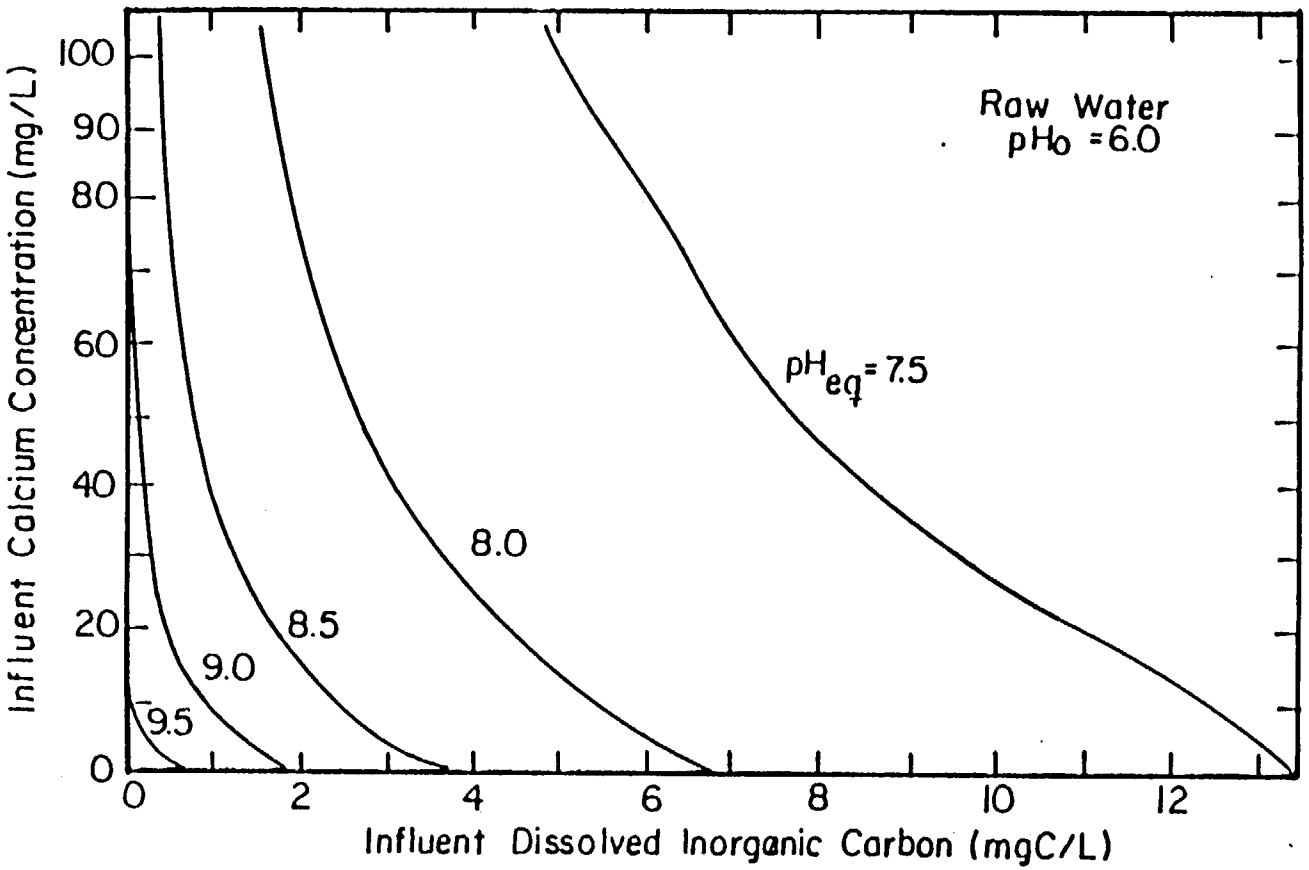

Figure 20. Influent calcium concentration plotted as a function of the influent dissolved inorganic carbon concentration and the equilibrium pH for an influent pH of 6.0.

less than 9.0 when the influent DIC concentration is 1 mg C/L. Increasing the influent DIC concentration to 5.5 mg C/L causes the equilibrium pH to decrease to 8.0. Since the DIC concentration in dilute acidified water usually ranges from 0.5 to 5 mg C/L these results indicate that the raw water dissolved inorganic carbon concentration can be an important parameter in contactor design.

Contactor Design Equations

The contactor design equations and the laboratory column data were used to test the assumption that under the conditions of this study the overall dissolution rate constant, K_o, is equal to the mass transfer coefficient, K_L, i.e.,

$$K_L << K_c$$

and

$$K_o = \frac{K_L K_c}{K_L + K_c} \approx K_L \tag{33}$$

where K_c is the surface reaction rate constant.

A best-fit value of K_o was determined for each laboratory column experiment. For each measured calcium concentration at a given column depth, L, a corresponding model predicted value was determined using L, an assumed value of K_o and the basic design equation, Eq. 25, rearranged to give,

$$C_{bL} = C_{eq} - (C_{eq} - C_{bo})\exp\left[-\frac{K_o\, a\, L\, \varepsilon}{U_s} + \left(\frac{K_o\, a\, L\, \varepsilon}{U_s}\right)^2 N_D\right] \tag{34}$$

C_{eq} was determined using the chemical equilibrium model and the raw water characteristics. N_D and a were calculated using Eqs. 17 and 12 and the known quantities, $\bar{d}$, ψ, L and ε .

The best-fit value of K_o was determined by minimizing the sum of the square of the difference between the measured and the calculated value of the calcium concentration for each depth, L, i.e.,

$$\sum_{i=1}^{n} (C_{bL} - C_{bL}')_i^2 \tag{35}$$

where n is the number of data points for each run. In most cases the total number of data points per run was between 10 and 14.

A plot of $\sum_{i=1}^{n} (C_{bL} - C_{bL}')^2$ as a function of K_o for a typical experiment (number 32) is illustrated in Figure 21. As indicated by the minimum in the curve, the best-fit value of K_o in this case was approximately 0.032 cm/min. The experimental conditions and the best-fit value of K_o for each run in this series are listed in Appendix B.

Calculated and measured values of the calcium concentration for this typical experiment are plotted as a function of the column depth in Figure 22. The best-fit value of K_o (0.032 cm/min) was used with Eq 34 to plot the curve.

The best-fit values of K_o were compared with values of K_o determined by plotting

$$-\ln \frac{C_{eq} - C_{bL}}{C_{eq} - C_{bo}}$$

as a function of the depth of the sampling port, L, for each value of C_{bL}. Only the experimental runs in which there were at least three values of C_{bL} (from the top of the column) where $C_b < 0.9\ C_{eq}$ were used in this comparison. The slope was determined for each set of data by fitting a straight line through the 0.0 point and as many data points as possible. Examples of these plots and fitted lines are given in Figure 23 for superficial velocities of 5.5, 22 and 55 cm/min. Each slope was converted to a value of K_o using

$$K_o = \frac{(\text{slope})U_s}{a\ \varepsilon} \qquad (36)$$

and the known quantities U_s, a and ε.

The correlation coefficient for the comparison of the best-fit values of K_o and the values determined by fitting a straight line to the $\ln [(C_{bL} - C_{eq})/(C_{eq} - C_{bL})]$ points is 0.85 (Figure 24).

Many studies have been conducted in which the object was to measure mass transfer coefficients in packed beds and to formulate predictive relationships using dimensionless parameters (Roberts et al., 1985). Numerous data from a number of investigations have been correlated by plotting the Chilton-Colburn mass transfer factor,

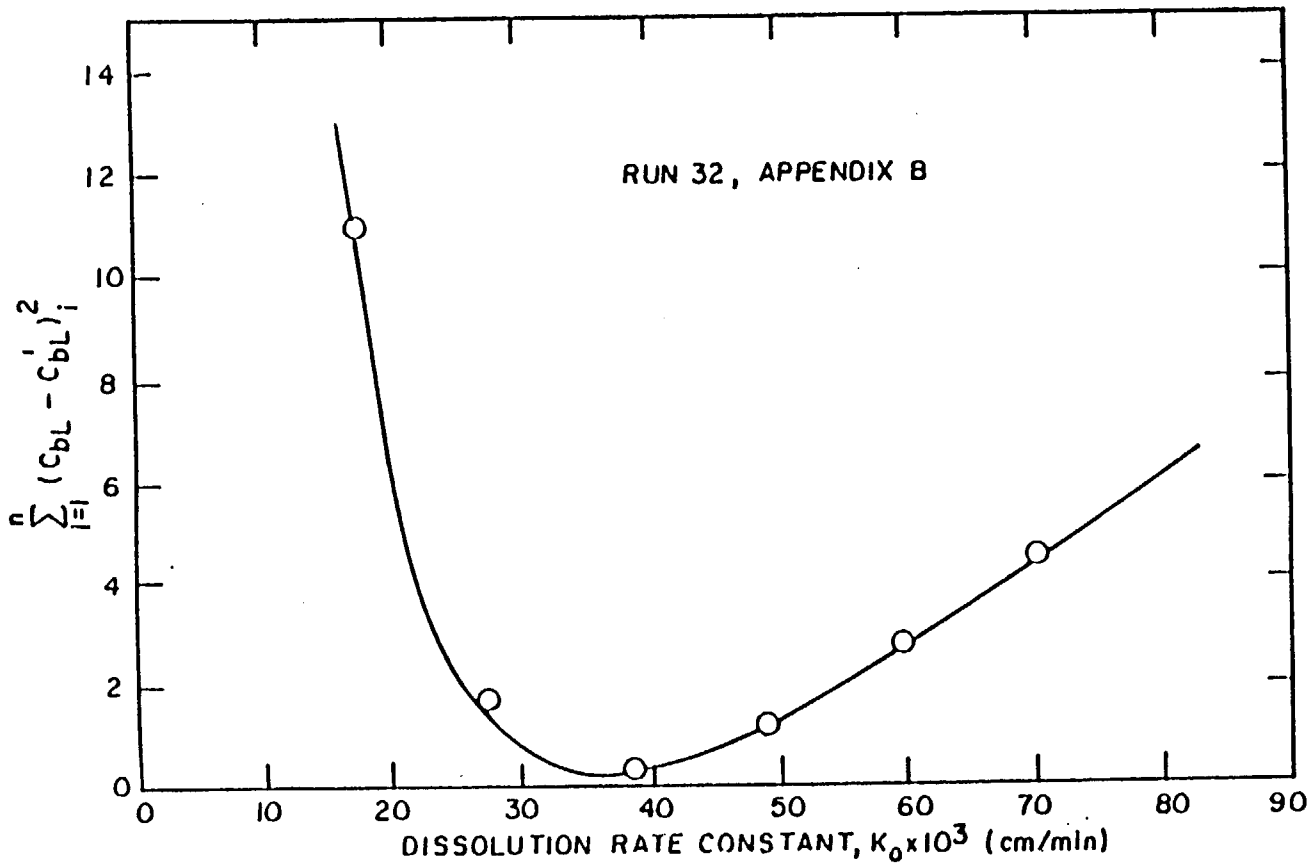

Figure 21. Sum of the square of the difference between the observed and the model predicted calcium concentration plotted as a function of the dissolution rate constant for run number 32, Appendix B. Plot illustrates how best fit values of K_o were determined.

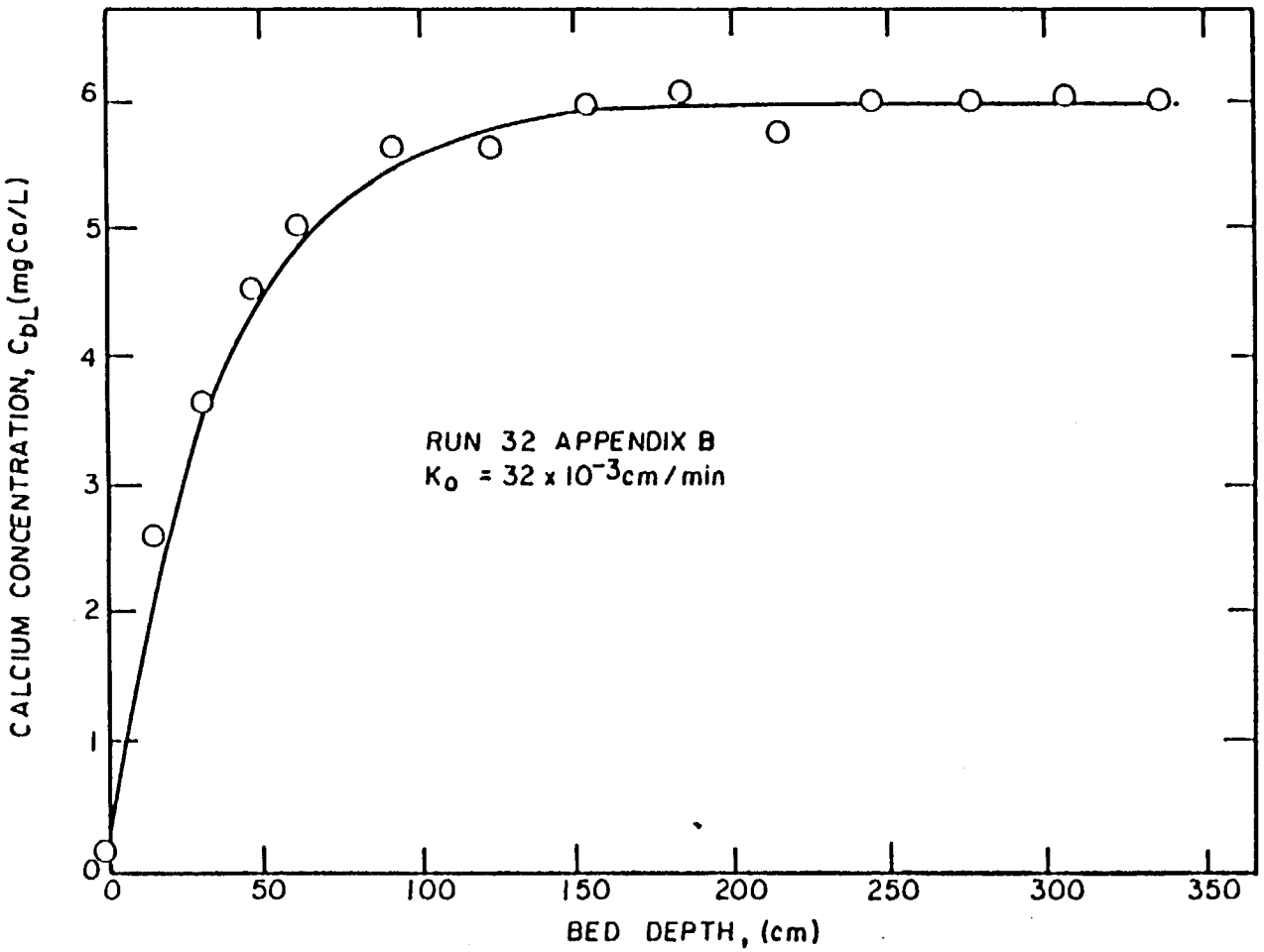

Figure 22. Model predicted and measured calcium concentrations plotted as a function of the axial distance to the sampling port for run number 32 and K_o = 0.032 cm/min.

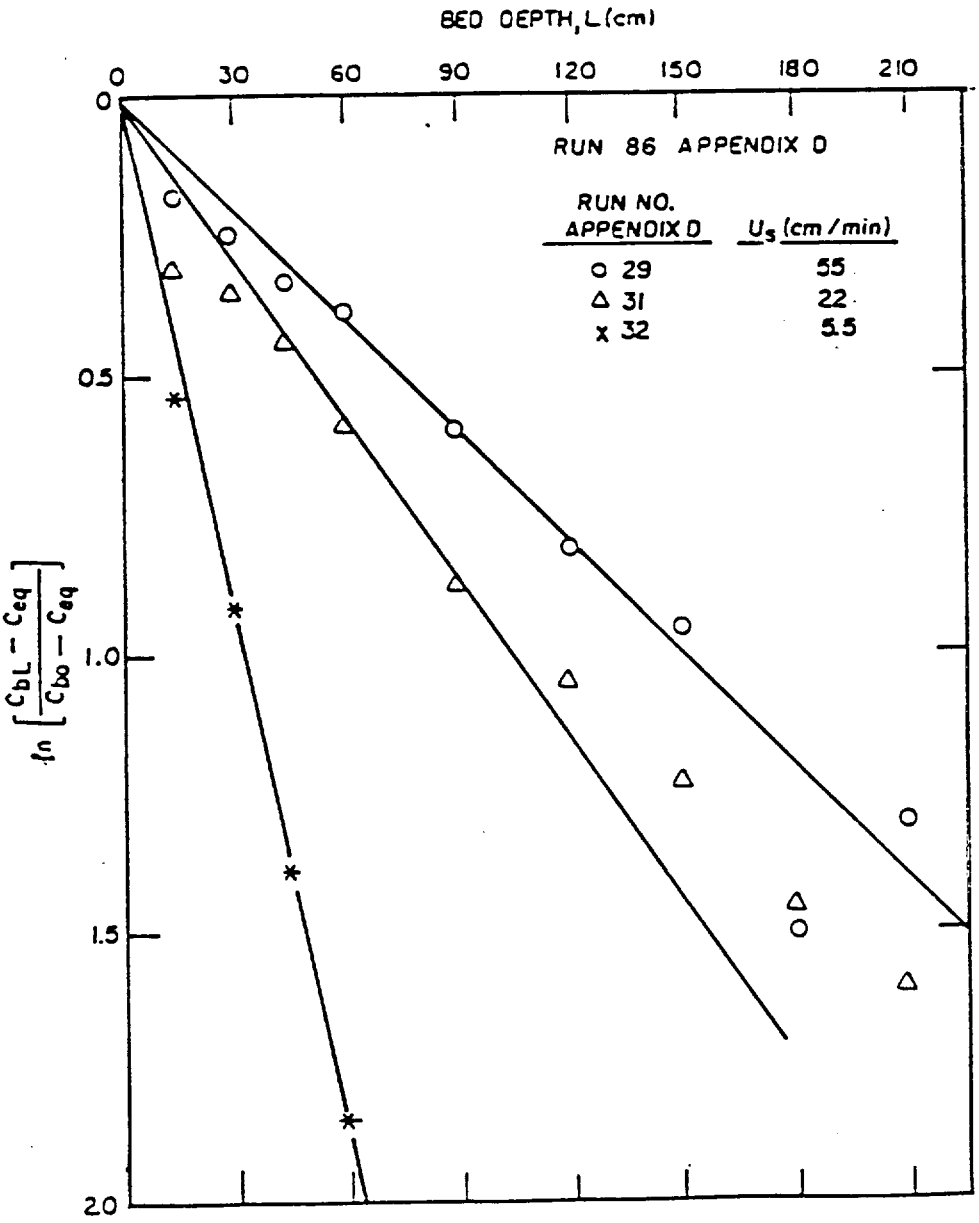

Figure 23. $\ln [(C_{bL} - C_{eq})/(C_{bo} - C_{eq})]$ plotted as a function of the axial distance to the sampling port for runs 29, 31 and 32.

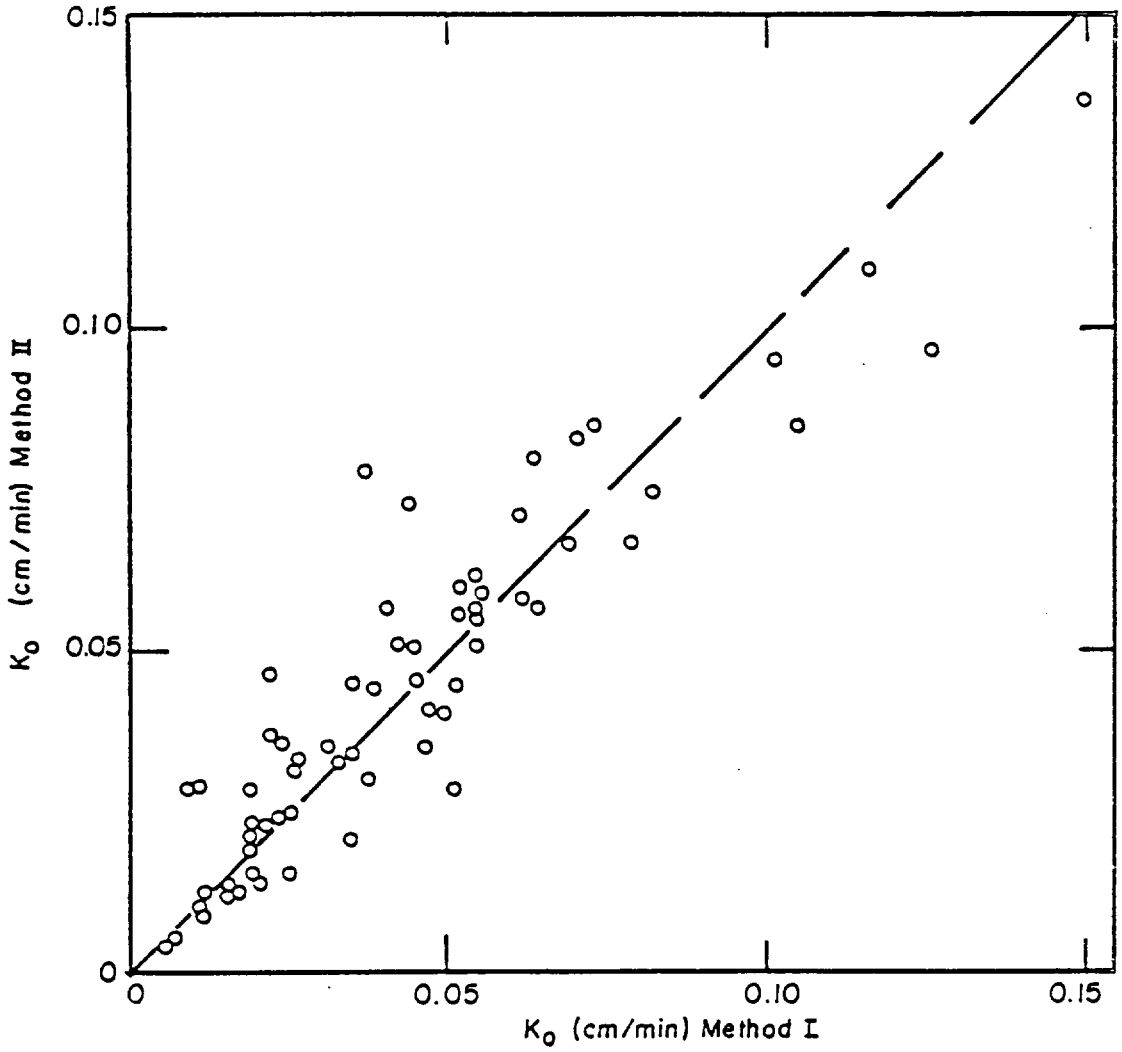

Figure 24. Dissolution rate constant determined by the least squares method (Method II) plotted as a function of the value obtained using plots such as Figure 23 (Method I).

$$j_D = \frac{K_L}{U_s} \left(\frac{\nu}{D}\right)^{2/3} \qquad (37)$$

as a function of a modified Reynolds number

$$MRe = \frac{\bar{d}\ U_s}{\nu(1-\varepsilon)} \qquad (38)$$

Chu and Khalil (1953) found that the following expressions gave a reasonable fit of data compiled from the literature,

$$j_D = 5.70\ (MRe)^{-0.78} \qquad 1 < MRe < 30 \qquad (39)$$

$$j_D = 1.77\ (MRe)^{-0.44} \qquad 30 < MRe < 10{,}000 \qquad (40)$$

j_D is plotted as a function of MRe in Figure 25.

Eqs. 38, 39 and 40 were used in this study to estimate a value of the mass transfer coefficient, K_L, for each experimental run. For example at low values of the modified Reynolds numbers,

$$K_L = 5.70\ (MRe)^{-0.78}\ (U_s)\ (\nu/D)^{-2/3} \qquad (41)$$

In computing a value of K_L for each experimental run the approximate calcium ion diffusivity at 20°C, $D_{20°C}$, was corrected for the temperature, T°C , by,

$$D_{T^o} = D_{20°C} \cdot \frac{T + 273}{293} \cdot \frac{\nu 20°C}{\nu\ T^o} \qquad (42)$$

A corrected value of the kinematic viscosity, ν_{T^o}, was determined for each temperature using equations derived by Blackwell (1984).

Values of K_o (calculated) were calculated using Eqs. 20, 38, 39, 40, and 42 and assumed values of $D_{20°C}$ and K_c and compared with the values of K_o determined by fitting the experimental data, K_o (best-fit) (see Appendix B). A simple variable step grid, search procedure was used to find the values of $D_{20°C}$ and K_c which maximized the correlation coefficient for the comparison of K_o (calculated) with K_o (best-fit). The values determined were

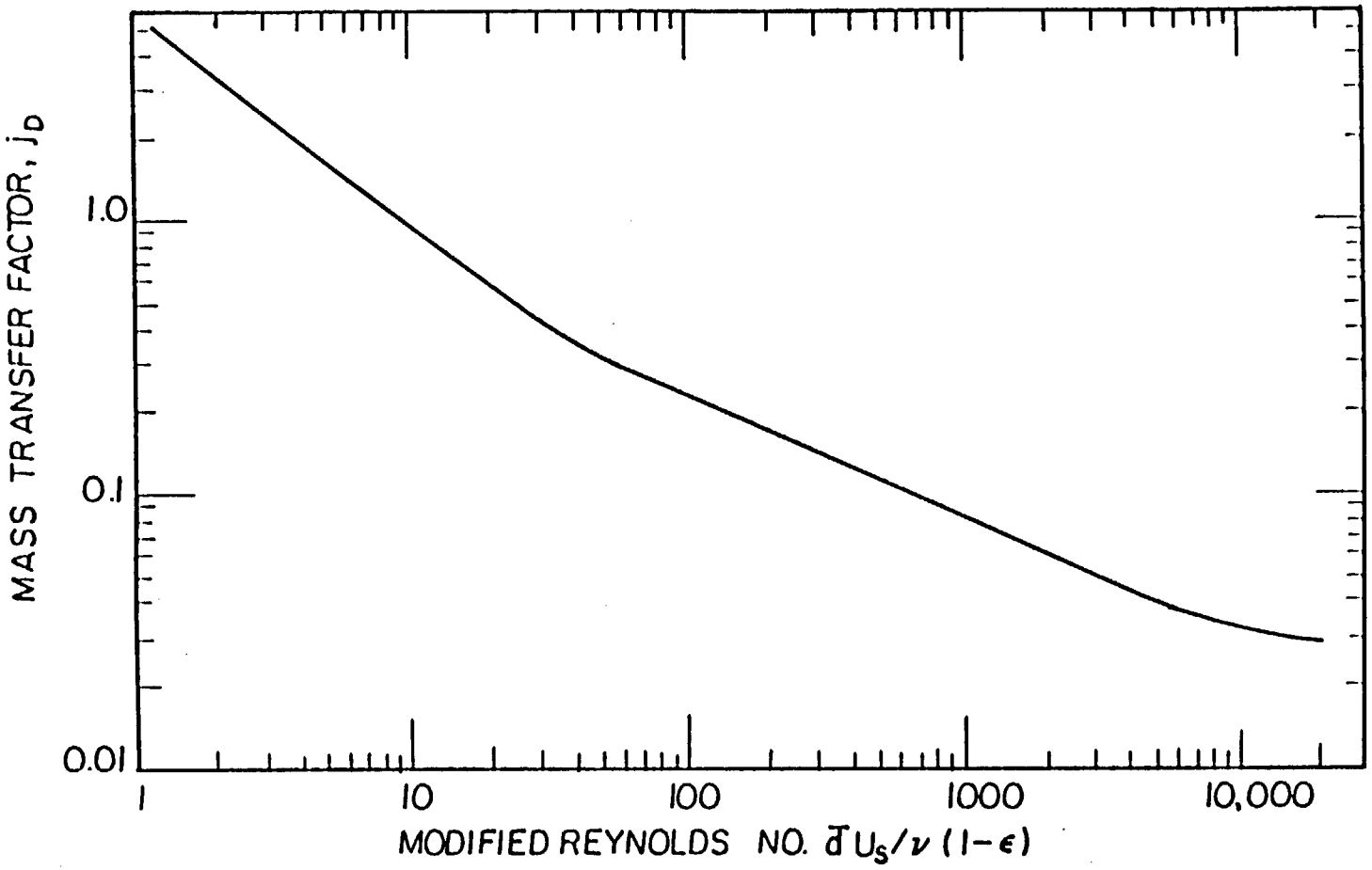

Figure 25. Mass transfer factor, j_D, plotted as a function of a modified Reynolds number using the equations derived by Chu and Khalil (1953).

$$D_{20°C} = 1.2 \times 10^{-5} \text{ cm}^2/\text{s}$$

and

$$K_c = 0.85 \text{ cm/min} \quad .$$

The corresponding maximum correlation coefficient was 0.73. K_o (calculated) is plotted as a function of K_o (best-fit) in Figure 26 using K_c = 0.85 cm/min and $D_{20°C} = 1.2 \times 10^{-5}$ cm^2/s.

The magnitude of K_c, the surface reaction rate constant determined using the optimization procedure was significantly greater than all calculated values of K_L and therefore supports the assumption that under the conditions of this study the effect of the surface reaction was negligible and mass transfer (of calcium ion) controlled the rate of the dissolution process, i.e.,

$$K_o \approx K_L.$$

It should be noted that the use of a constant calcium ion diffusivity, e.g., 1.2×10^{-5} cm^2/s (20°C), in these calculations is an approximation. The diffusivity of a cation such as calcium depends on the nature of the associated anion and the presence of other electrolytes. Diffusion to or from dissolving calcium carbonate in limestone is a complicated process which, in many cases, probably involves changes in ion speciation (particularly the inorganic carbon species) with distance from the surface. Therefore, the principal anion associated with the calcium may change as it diffuses from the surface, and hence, the diffusivity of the calcium ion may be affected.

A plot of measured as a function of model predicted values of the calcium ion concentration is presented in Figure 27 for the runs listed in Appendix B. The points plotted represent measurements and calculations for all sampling port locations (see Figure 6). The model predicted values were determined using the assumption that $K_o \approx K_L$ and that K_L is given by Eq. 39 or 40. The agreement between the measured and model predicted calcium ion concentrations is good except at high calcium concentrations (> 8 mg Ca/L) where all the calculated values tend to be larger than the measured concentrations.

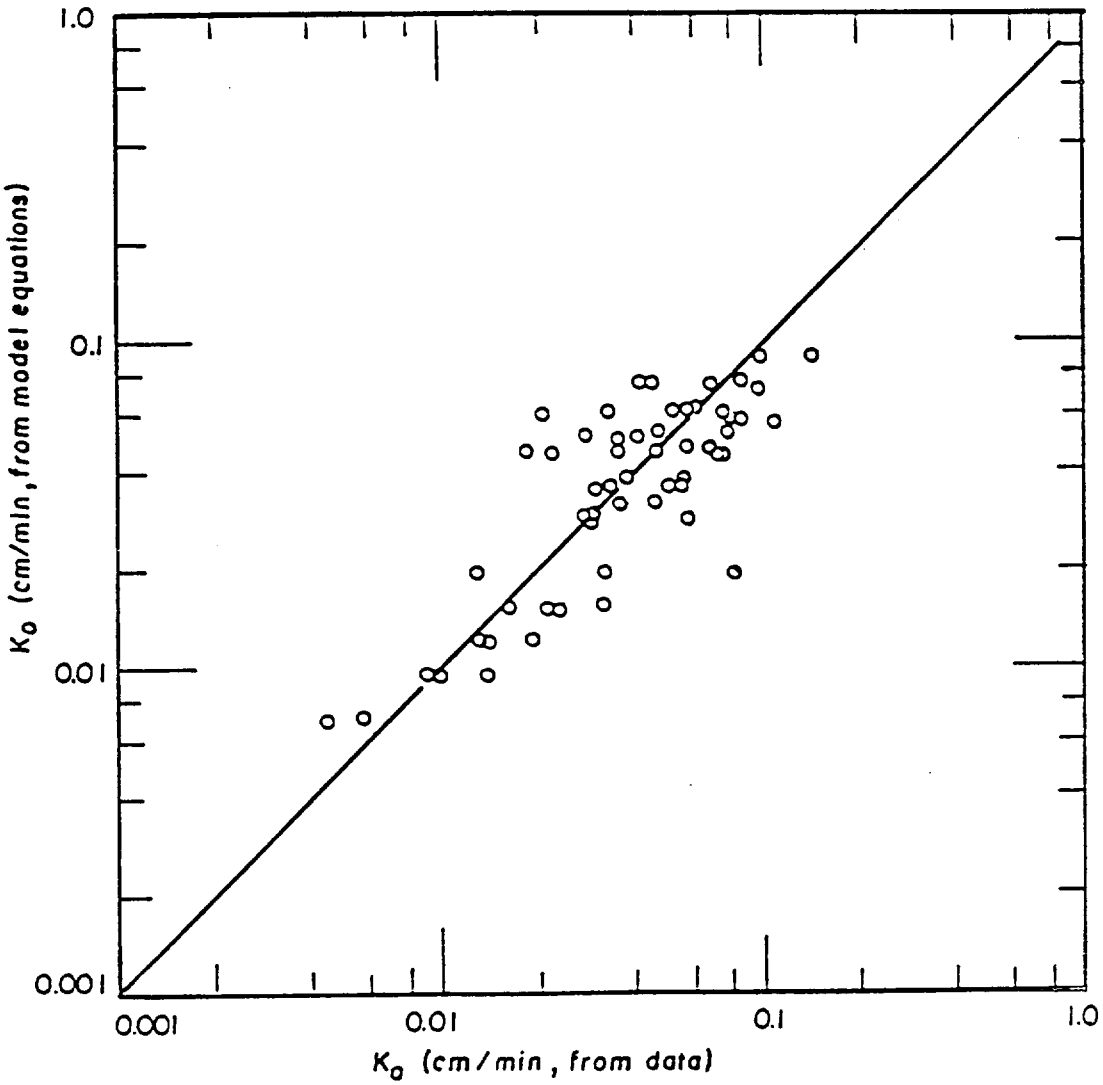

Figure 26. Values of the dissolution rate constant calculated using the model equations plotted as a function of the experimental (best-fit) values listed in Appendix B.

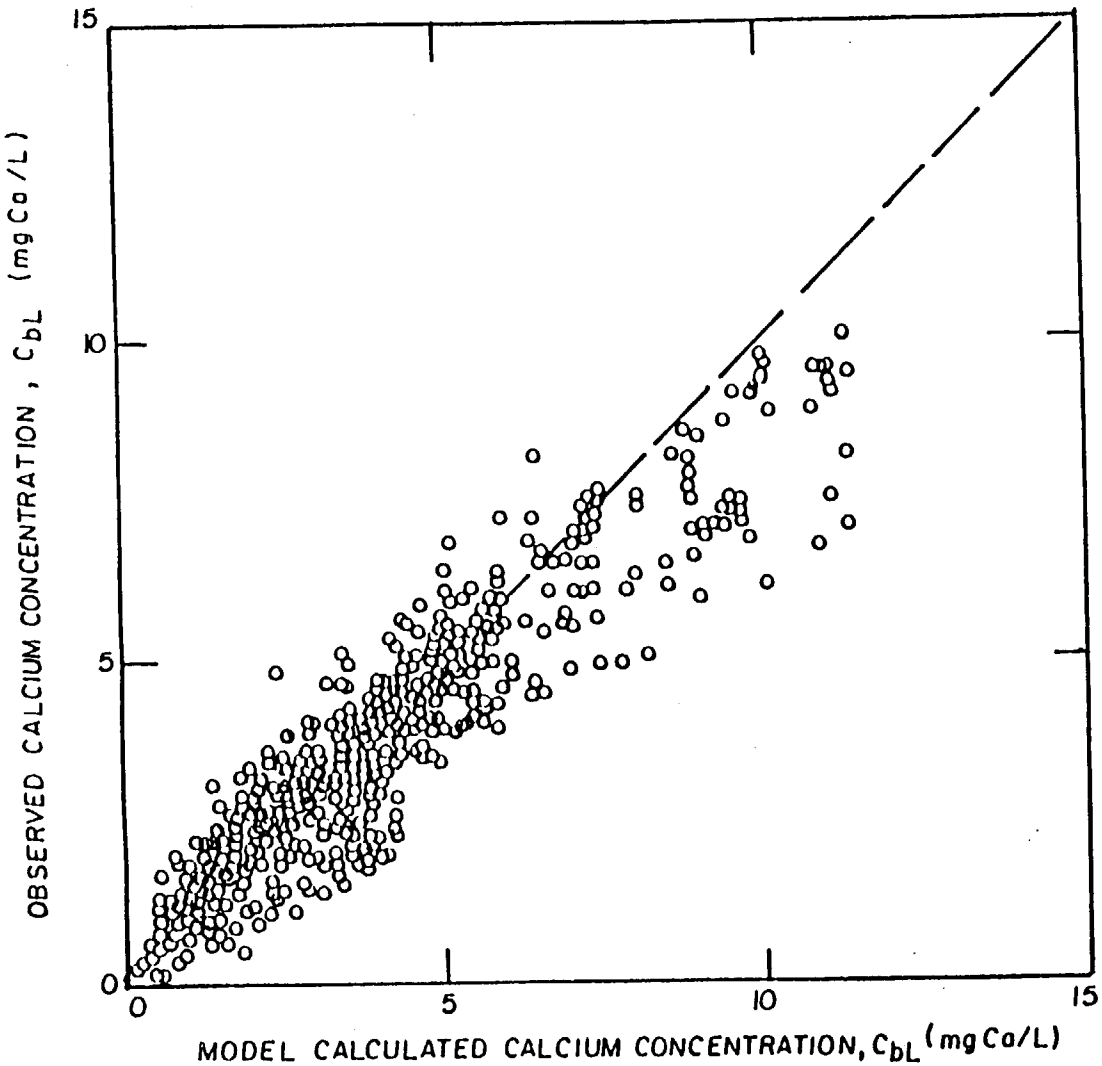

Figure 27. Observed calcium concentration plotted as a function of the model predicted value. The points include all sampling port locations for the runs listed in Appendix B. The model equations were used to determine K_o for each run.

It will be shown in later sections that the pH of the contactor effluent is an important parameter in determining the effect of contactor treatment on metal release. Since the contactor design equations are based on the transport of the calcium ion, the calculated effluent calcium concentration, C_{bL}, must be used with the chemical equilibrium model to determine the corresponding effluent pH. To test the efficacy of this approach, effluent pH values were calculated for each sampling port in a number of experimental runs and then compared with the measured pH values.

The pH at each sampling port was calculated using the charge balance equation and the theoretical amount of $CaCO_3$ dissolved at that port. For example, since the calculated molar concentration of calcium ion at a given depth, L, is C_{bL}, the following substitutions are made in Eq. 26;

$$C_{bo} + S = C_{bL} \tag{43}$$

and

$$(DIC)_o + S = (DIC)_o + (C_{bL} - C_{bo}). \tag{44}$$

The magnitude of the quantity $(C_a - C_c)$ in Eq. 26 was estimated using the raw water conditions (C_{bo}, $(DIC)_o$, pH and temperature) and the basic charge balance assumption, i.e.,

$$(C_a - C_c) = 2\,C_{bo} + [H+] - (DIC)_o\,(\alpha_1 + 2\alpha_2) - K_w\,[H]^+ \tag{45}$$

where α_1 and α_2 are given by Eqs. 28 and 29. The specific conductivity can be used, as suggested in Appendix A, to make approximate ionic strength corrections, if necessary. Using Eqs. 43 and 44 and the estimated quantity $(C_a - C_c)$, Eqs. 26, 28 and 29 were solved for the pH which corresponds to the transport model calculated value of C_{bL}.

A plot of the measured pH as a function of column depth for experimental run number 32 is illustrated in Figure 28. In this run the experimental conditions were $pH_o = 4.0$, $C_{bo} = 0.2$ mg C_a/L, $(DIC)_o = 0$ and $T = 10°C$. The initial ionic strength was approximately 4×10^{-4}M. The calculated equilibrium concentration of calcium ion and the equilibrium pH are 6.0 and 9.6, respectively. The model calculated effluent pH values plot somewhat above the measured values.

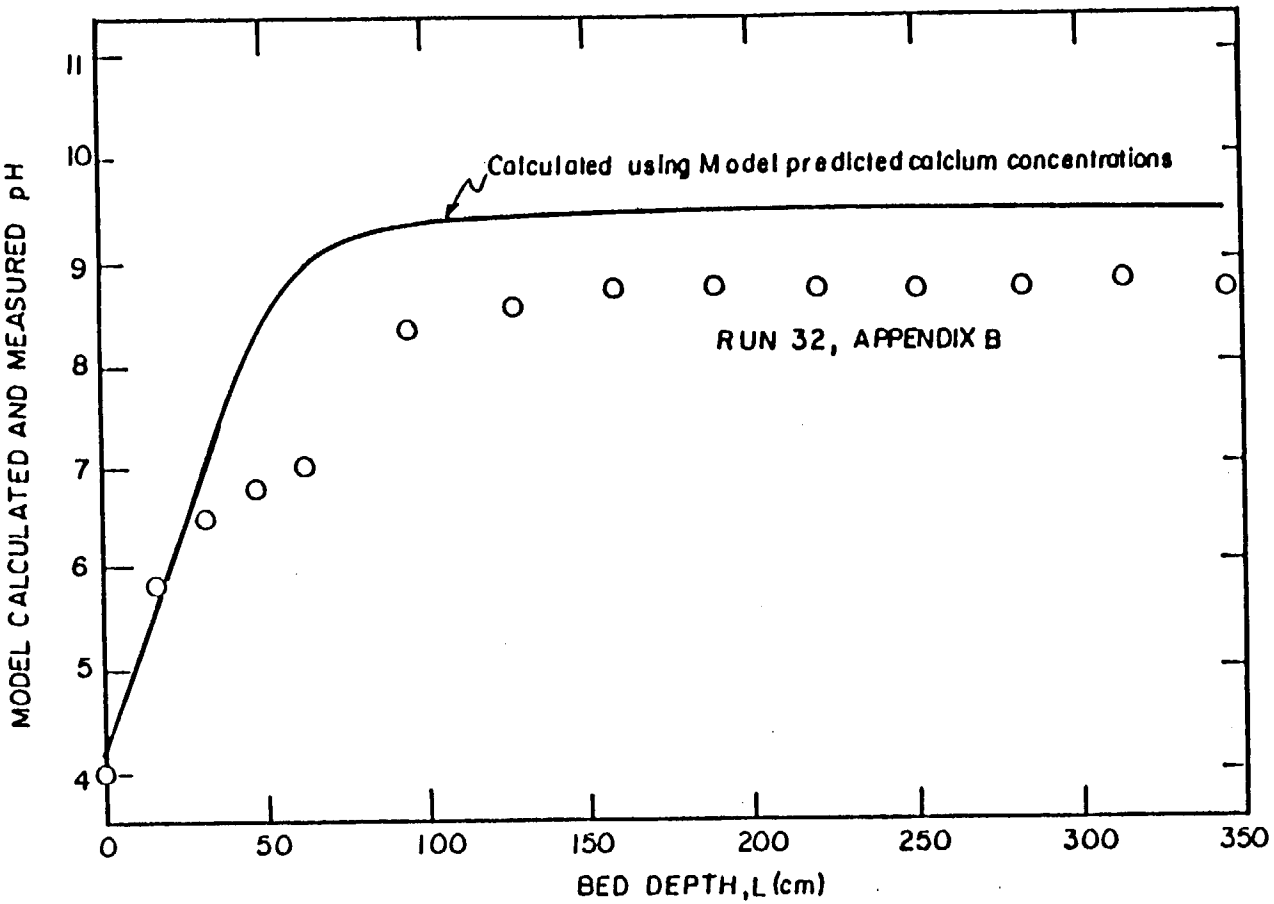

Figure 28. Model predicted and measured pH plotted as a function of the axial distance to the sampling port for run number 32 and K_o = 0.032 cm/min.

A plot of the measured pH as a function of the calculated pH for the runs listed in Appendix B is shown in Figure 29. The poor agreement obtained between the measured and the model calculated pH values may be due to the inadvertent uptake of carbon dioxide in samples during collection and pH measurement. The uptake of carbon dioxide would result in pH values less than those predicted using the mathematical model with the closed-to-the-atmosphere assumption.

The conclusion that carbon dioxide entered at least some of the samples is supported by the results plotted in Figure 30 where the dissolved inorganic carbon concentration has been plotted as a function of column depth for experimental run number 32. The equilibrium concentration of DIC for this run is approximately 1.8 mg C/L. A number of points are 20 percent greater than the equilibrium value (Figure 30).

The model calculated calcium concentrations were used to determine the alkalinity for each sampling port location using

$$\text{Alkalinity } (\mu\text{eq/L}) = \text{influent alkalinity } (\mu\text{eq/L}) + (50,\ \mu\text{eq/mg})\ (C_{bL},\ \text{mg/L}) \quad (46)$$

The model calculated and measured alkalinities for run number 32, Appendix B, are plotted in Figure 31.

Measured alkalinities plotted as a function of the model calculated values for the runs listed in Appendix B are illustrated in Figure 32. The alkalinities are given as the change in alkalinity between the influent and each sampling port. The agreement obtained between the model calculated and measured alkalinities supports the use of the model as a predictive tool. It is apparent, however, that alkalinity and calcium ion concentration are significantly better parameters for model calibration than pH.

FIELD STUDY RESULTS

Baffled Box Contactor

The baffled-box contactor was sampled at regular intervals during the period June 1982 to October 1984. Twenty-three sampling visits were made to the unit. During the period January to April 1984, the main pipe between the contactor and the cottages became frozen and no samples were collected.

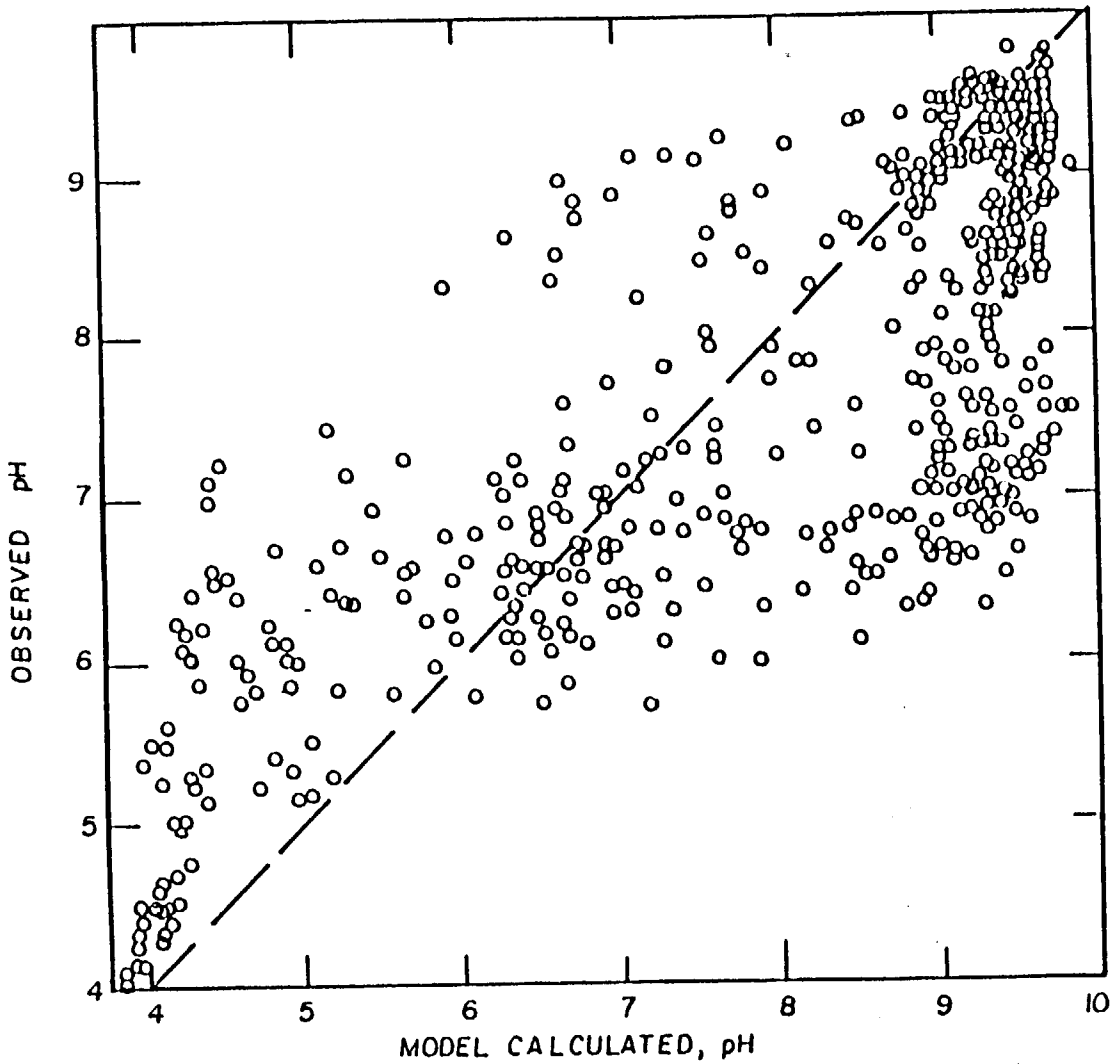

Figure 29. Observed pH plotted as a function of the model predicted values for all sampling port locations for the runs listed in Appendix B. The model equations were used to determine K_o for each run.

The first samples in this study were collected on June 24, 1982. The first data point in each plot of the field study results is for the samples obtained on this date. At that time the contactor contained limestone which has been in place approximately one year. On June 28, 1982 the limestone in the contactor was replaced with fresh stone and the results plotted for 6/28/82 (the second point on each graph) are for this condition.

On September 26, 1983 the contactor was opened to obtain samples of limestone and to measure the amount of the limestone that had dissolved during the 455 day period since June 28, 1982. Before the unit was put back into operation, each compartment was filled to the top with fresh stone. The partially dissolved stone was not replaced.

Results obtained from the baffled box unit are plotted in Figures 33 to 38. In plotting these data points "influent" depicts sample location 1, the sampling compartment at the inlet, Figure 6, and "effluent" represents sample location 6, the compartment at the outlet.

The influent water temperature is plotted in Figure 33. The temperature during the sampling period ranged from 2.5°C in February to 13°C in August. The average water temperature for the 24 month period, June 1982 to July 1984 was 7.5°C.

The baffled-box contactor increased the pH on average by about 1 unit. An effluent pH of 8.5 was measured immediately after fresh limestone was installed in June, 1982. During the next month the pH decreased to about 7. The average effluent pH for the study period was 7.33 and the average influent pH was 6.34. The pH values are plotted in Figure 34.

A significant amount of the variability in the effluent pH (and in other effluent characteristics such as the calcium concentration) can be attributed to the variability in the influent chemistry and temperature as well as the flowrate through the units. It was not possible to routinely measure the instantaneous flowrate at the baffled-box contactor. The estimated average daytime flowrate is approximately 10 L/min. It is possible the flowrate ranges from near zero at times in the fall and spring to approximately 20 L/min during the summer months when the seven cottages served by the unit were occupied by families. In the winter the resort owner attempts to maintain a constant minimum flowrate through the system to minimize the chance that the pipeline will freeze.

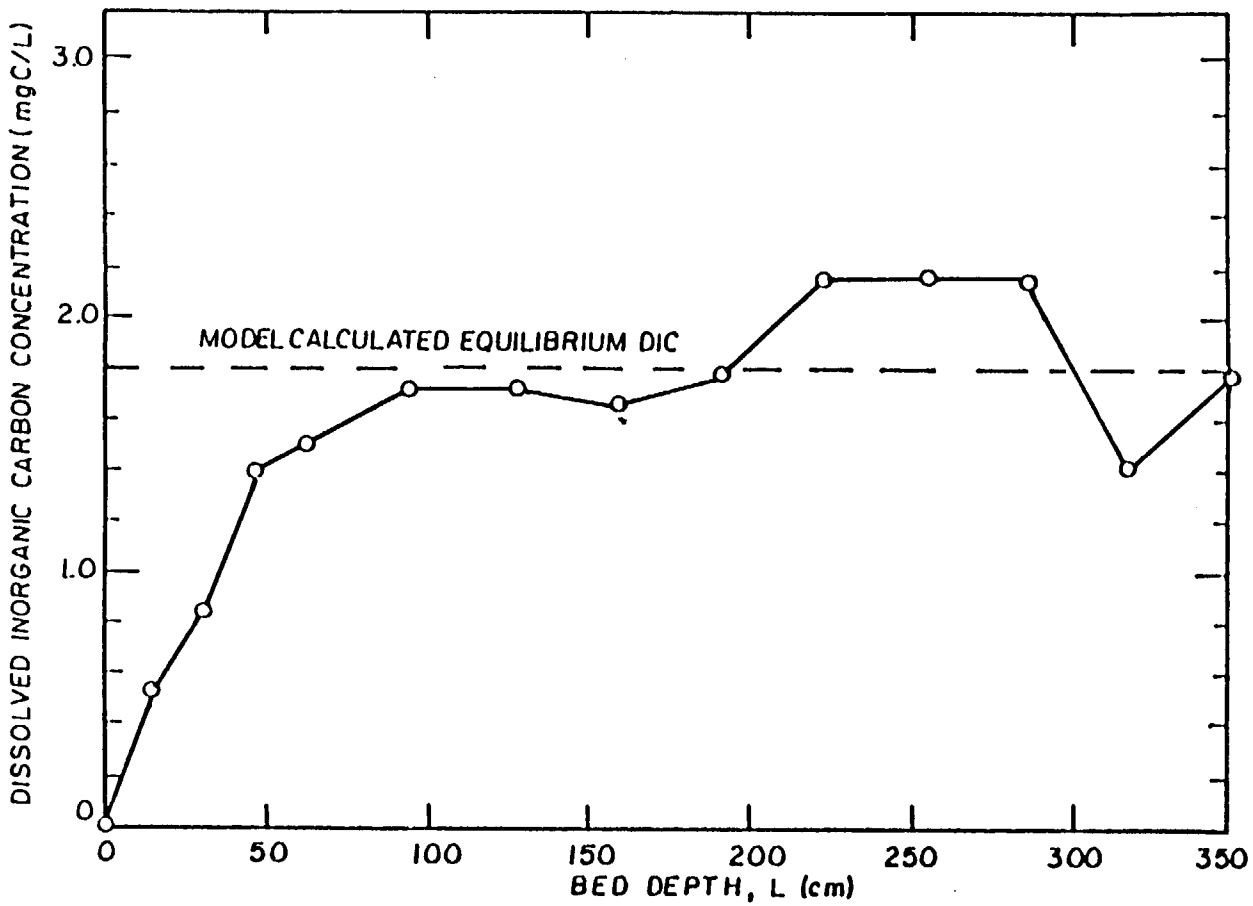

Figure 30. Model predicted and measured dissolved inorganic carbon concentrations plotted as a function of the axial distance to the sampling port for run number 32 and K_o = 0.032 cm/min.

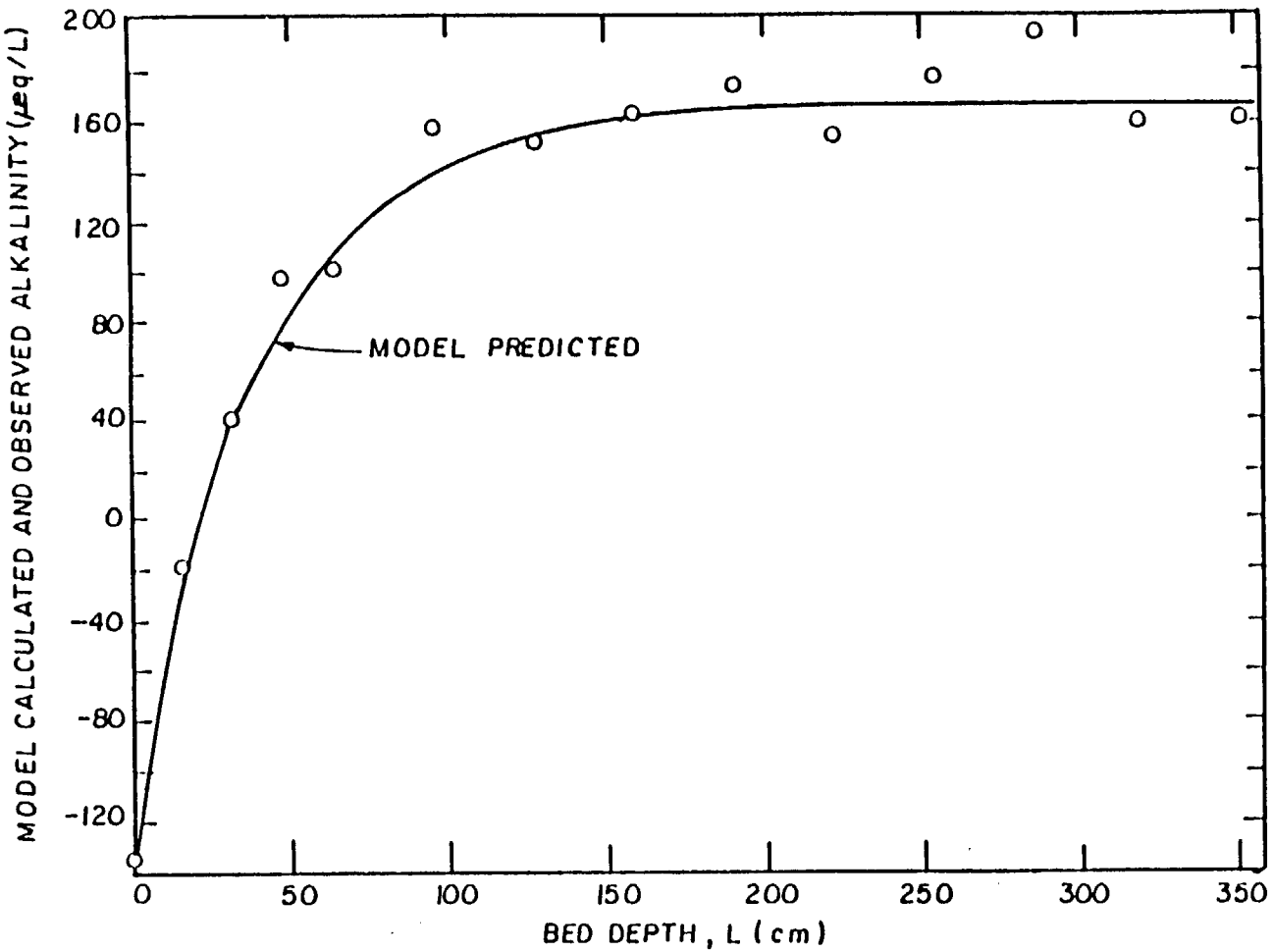

Figure 31. Model predicted and measured alkalinity plotted as a function of the axial distance to the sampling port for run number 32 and K_o = 0.032 cm/min.

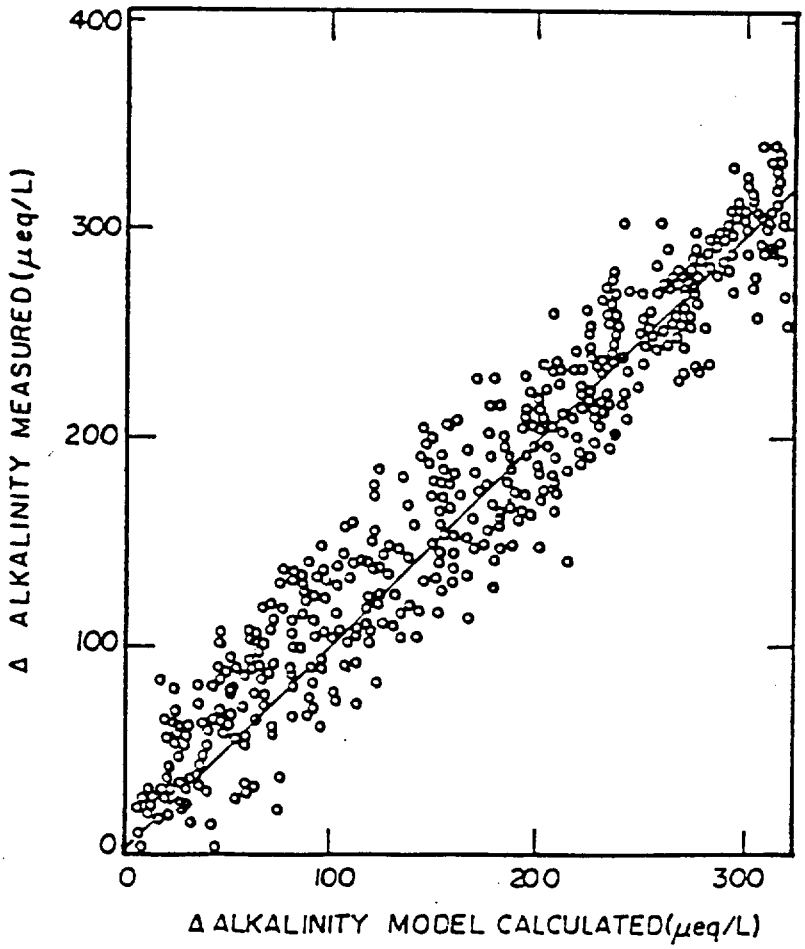

Figure 32. Measured change in alkalinity within the laboratory contactors plotted as a function of the model predicted change. The data obtained for the runs listed in Appendix B (all sampling ports) were used. The model equations were used to determine K_o for each run.

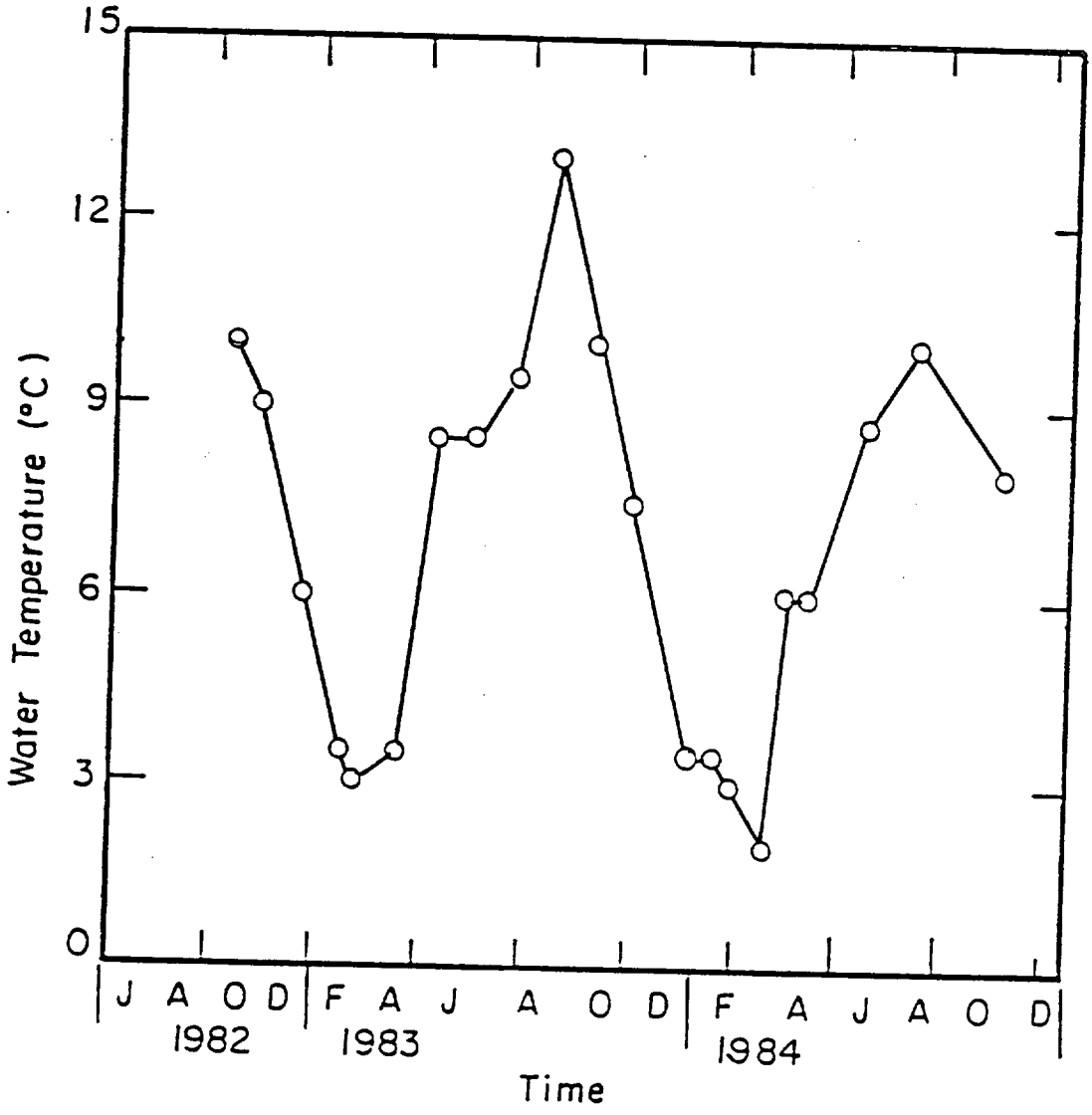

Figure 33. Water temperature plotted as a function of time for the baffled-box contactor.

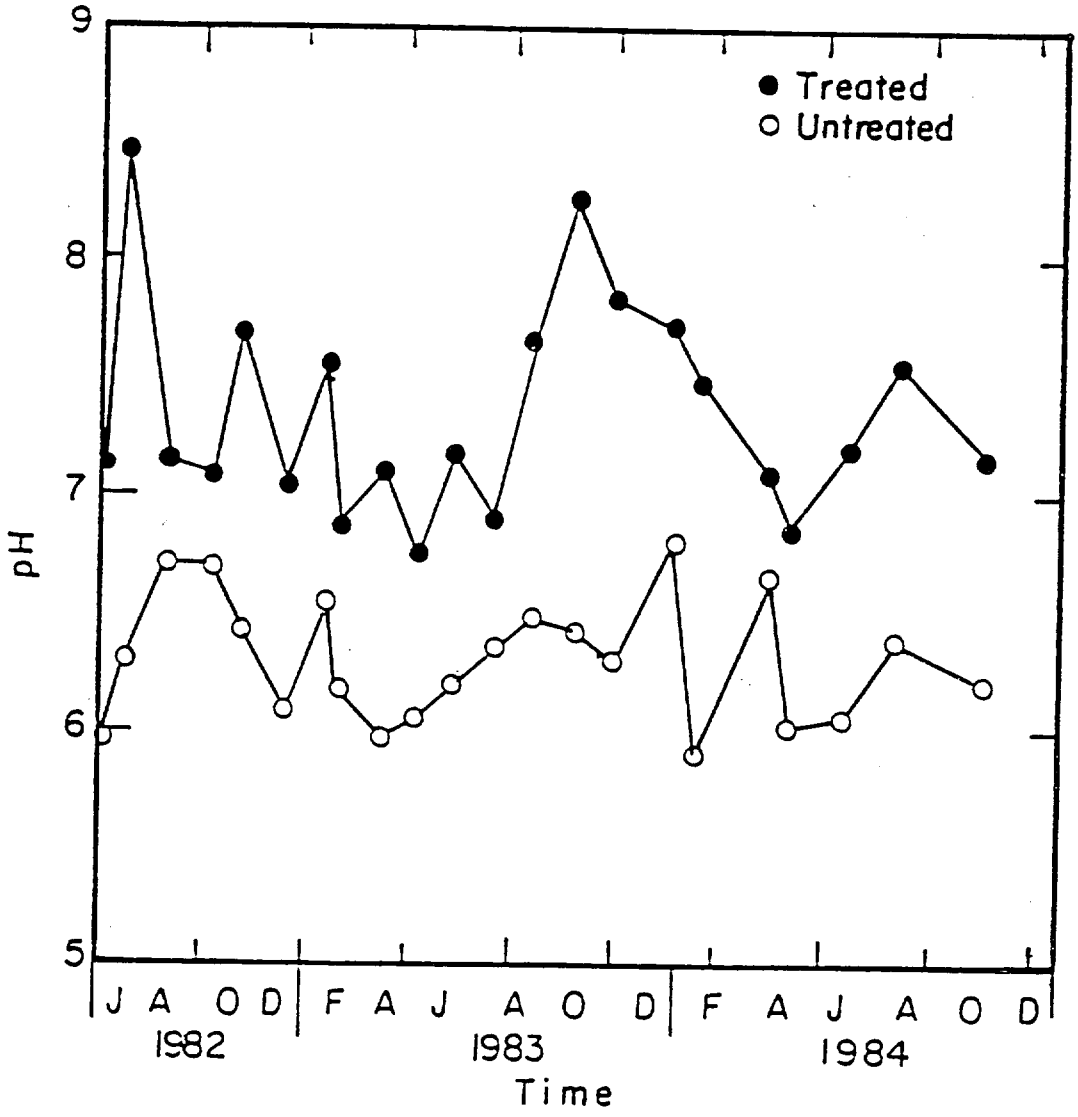

Figure 34. Influent and effluent pH plotted as a function of time for the baffled-box contactor.

The calcium concentration results are plotted in Figure 35. The average influent and effluent calcium concentrations for the study period were 4.1 and 11.3 mg Ca/L, respectively. The highest effluent calcium concentration, 24 mg Ca/L, was measured in January 1984 when flow through the contactor was at a minimum.

The average influent and effluent magnesium concentrations were 0.67 and 0.80 mg Mg/L, respectively. The average increase in the magnesium concentration across the contactor was 0.13 mg Mg/L, or 5.4×10^{-6}M magnesium.

The average dissolved aluminum concentrations in the influent and effluent were 0.071 and 0.066 mg Al/L, respectively. Given the variation in the measured aluminum concentrations the difference between these values is not significant.

The alkalinity is plotted in Figure 36. The average influent and effluent alkalinities for the study period were 0.15 and 0.57 meq/L (7.5 and 28.5 mg $CaCO_3$/L), respectively.

The average influent and effluent DIC concentrations were 3.7 and 7.0 mg C/L, respectively. The DIC data are plotted in Figure 37. There are no obvious trends in this data.

The influent and effluent standard plate count bacteria results are plotted in Figure 38. The SPC results correlate with water temperature, the highest counts were obtained during the summer months. While there was considerable variability in both the influent and effluent measurements it appears that the effluent counts were somewhat higher than those of the influent. The average values for the influent and effluent for the study period were 89 and 170 per 100 ml, however, the statistical significance of this difference is negligible.

Total coliform measurements were initiated in November 1982 in response to a request by the resort owner and the New York State Department of Health. High coliform densities, (Figure 39), correspond as expected to periods with high surface runoff, i.e., late fall 1982 and spring snowmelt, 1983. In general, transport through the contactor seemed to have no effect on the measured total coliform density. In early 1984 the resort owner installed an on-line ultra-violet light disinfection unit downstream of the contactor unit.

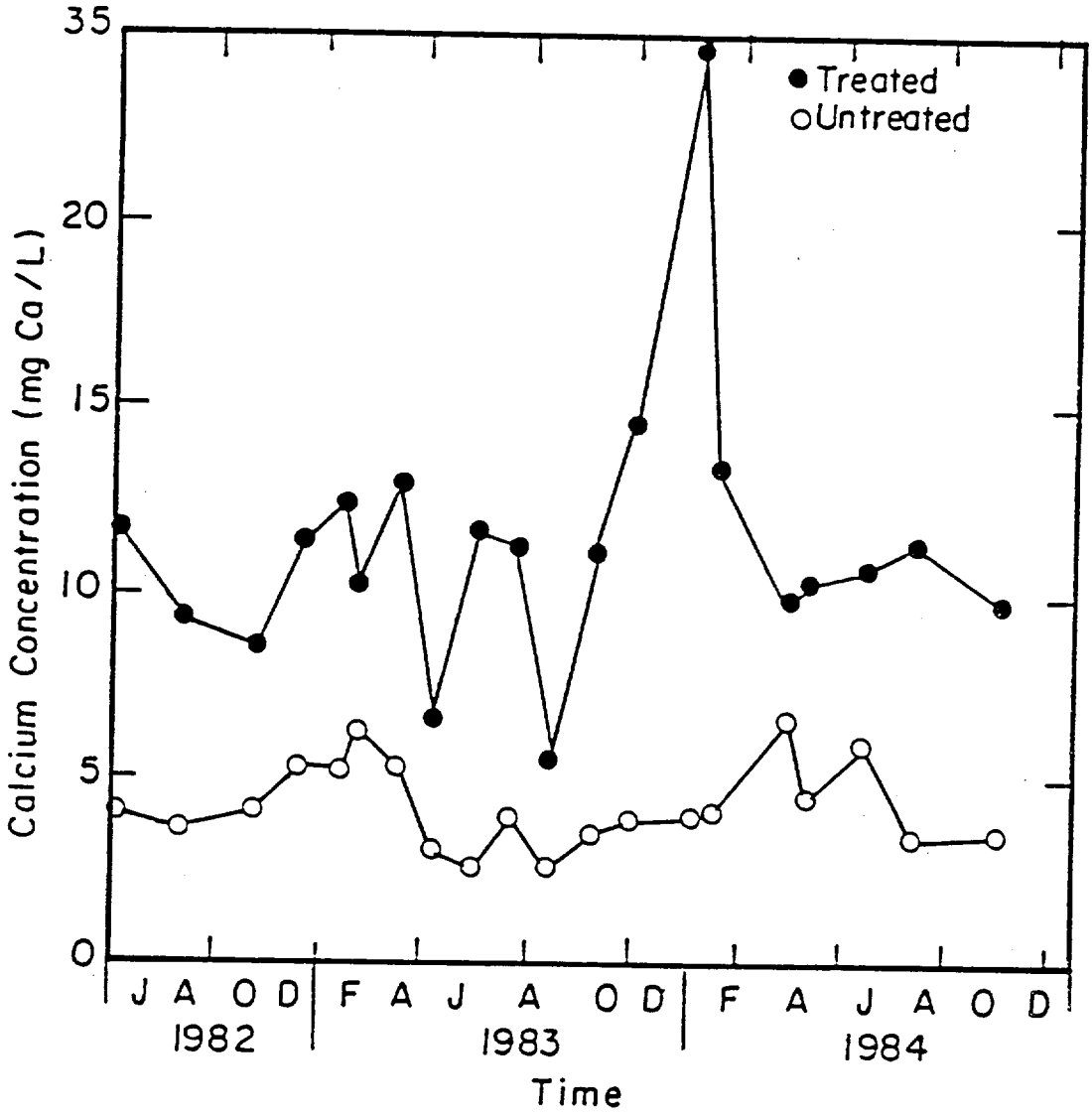

Figure 35. Influent and effluent calcium concentration plotted as a function of time for the baffled-box contactor.

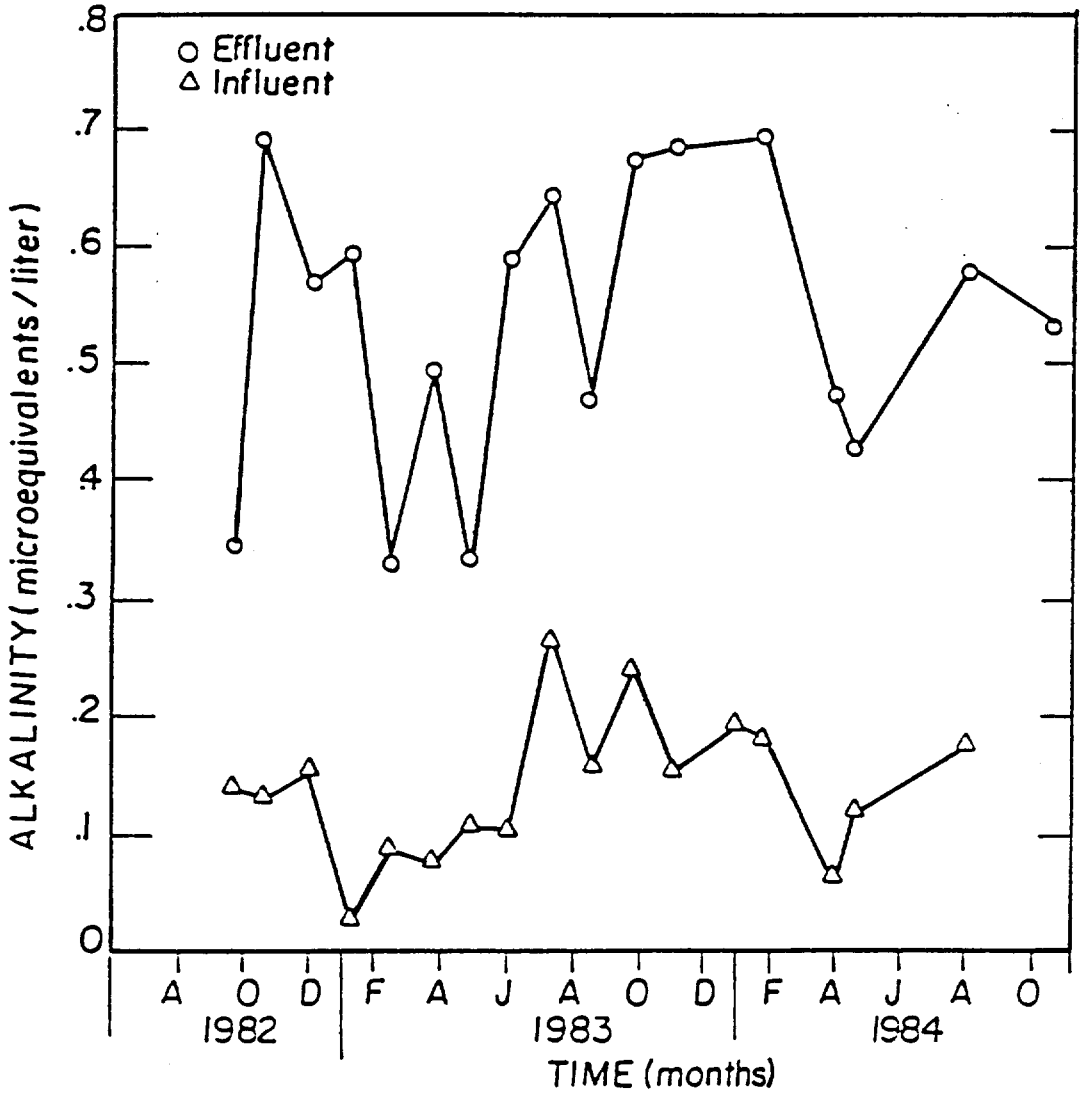

Figure 36. Influent and effluent alkalinity plotted as a function of time for the baffled-box contactor.

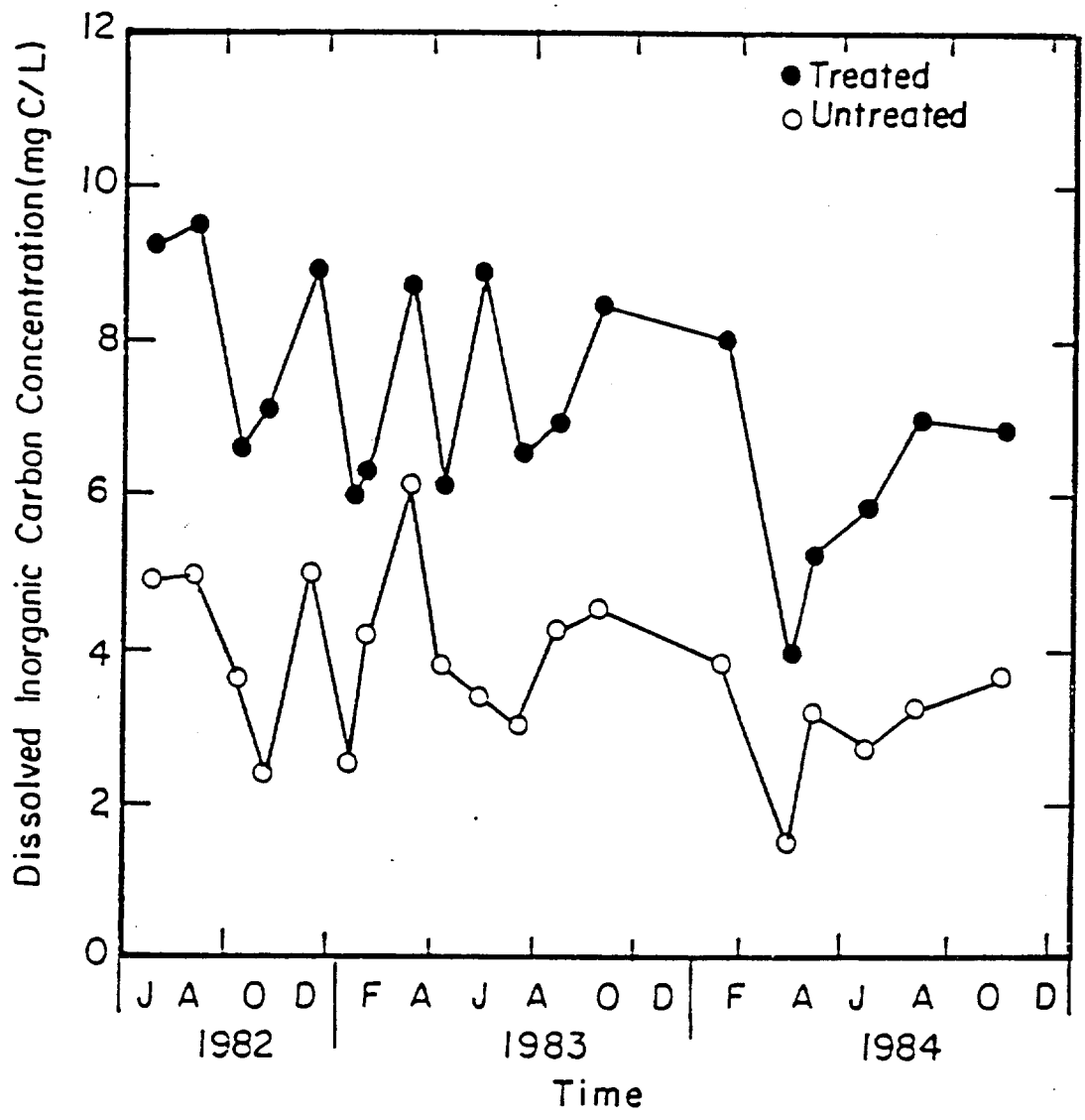

Figure 37. Influent and effluent dissolved inorganic carbon concentration plotted as a function of time for the baffled-box contactor.

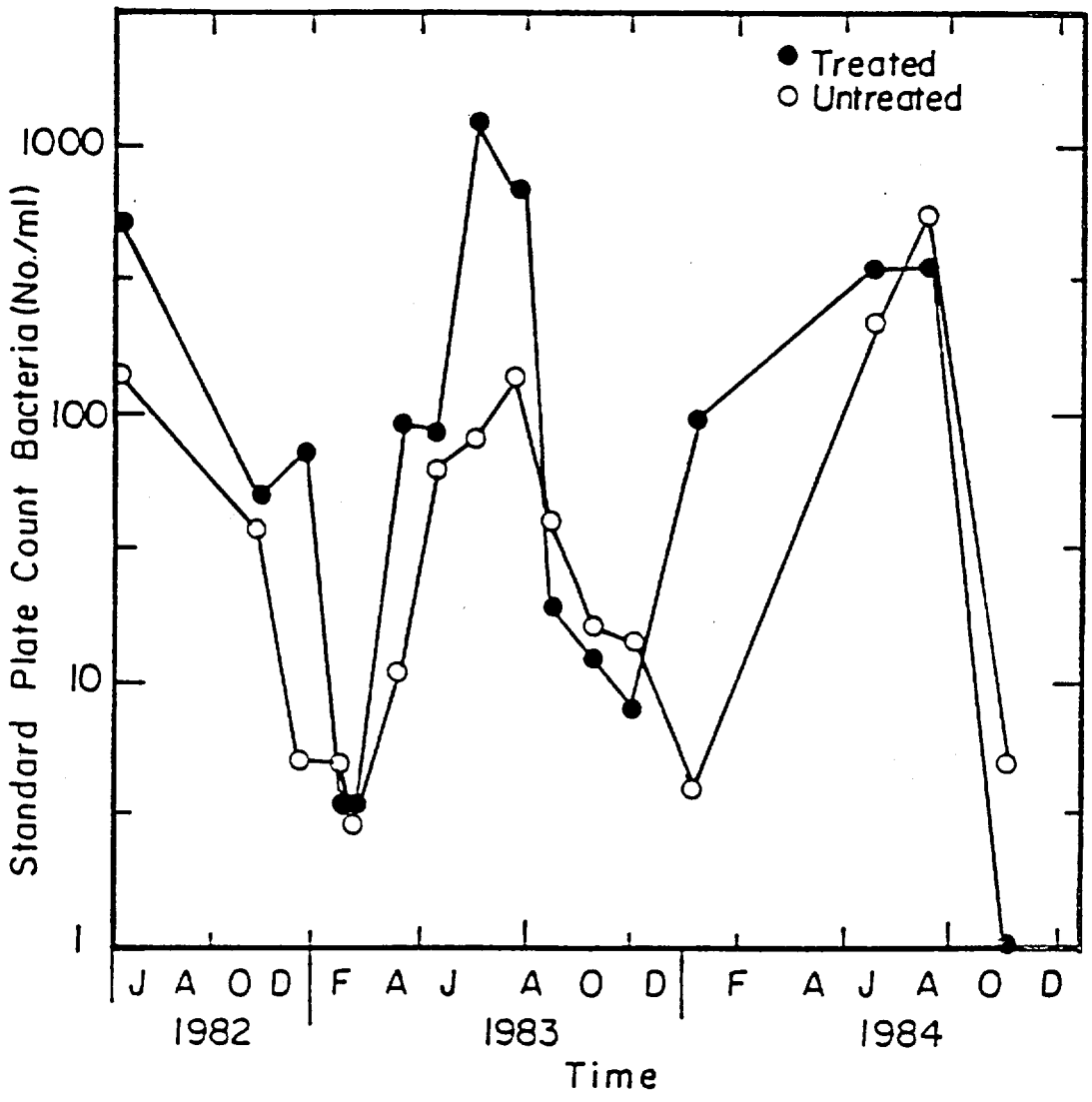

Figure 38. Influent and effluent standard plate count bacteria concentration plotted as a function of time for the baffled-box contactor.

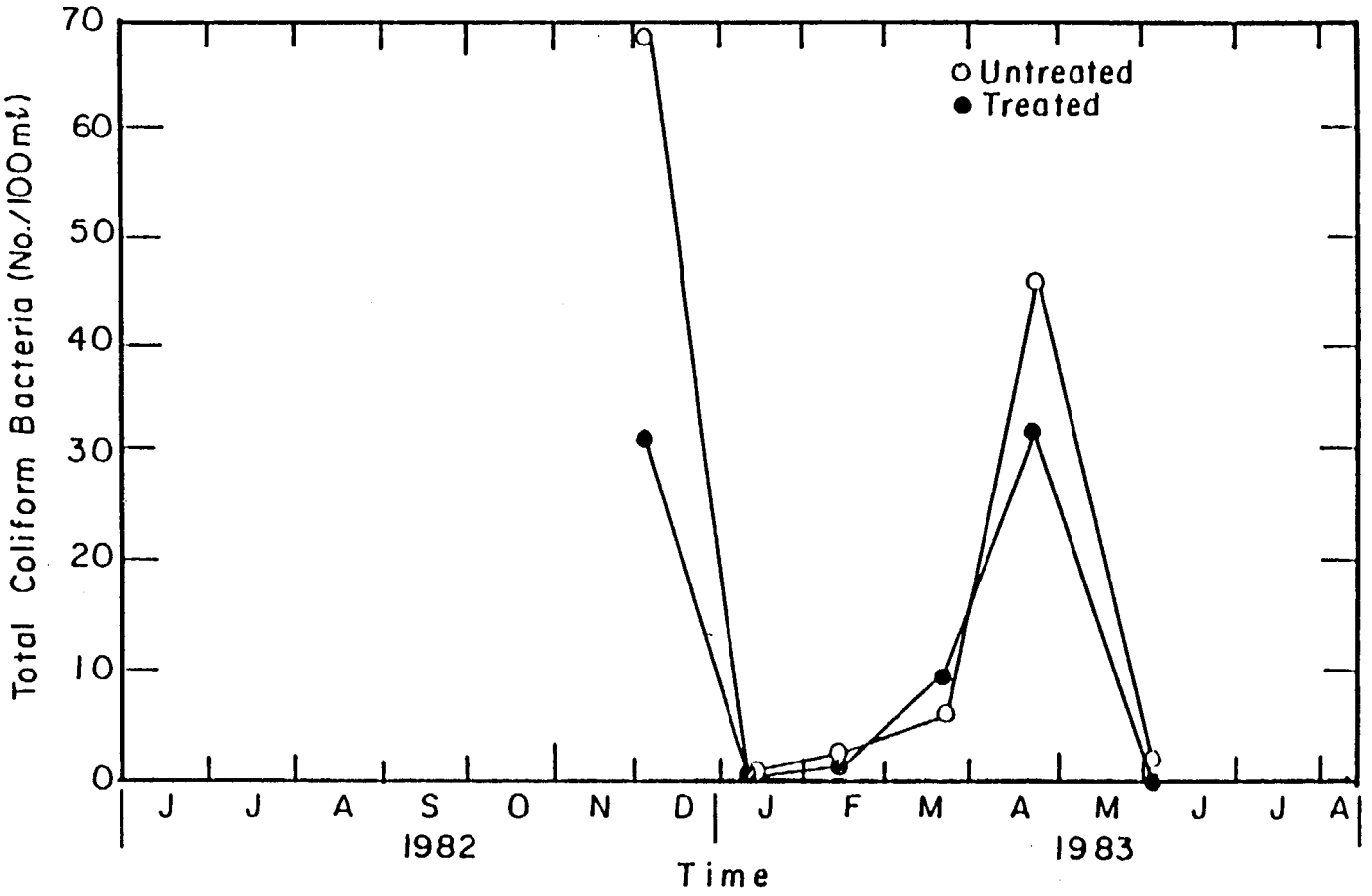

Figure 39. Influent and effluent total coliform bacteria concentration plotted as a function of time for the baffled-box contactor.

The results obtained in monitoring the baffled box contactor are summarized in Table 17. The mean, standard deviation and total number of data points are listed for each measured quantity. The average change in the calcium concentration through the contactor (7.2 mg Ca/L or 1.8×10^{-4}M calcium) is in reasonable agreement with the average change in the alkalinity. (0.42 meq/l or, in terms of the calcium ion molar concentration, 2.1×10^{-4}M). The average increment in the DIC, 3.3 mg C/L, is equivalent to a 2.8×10^{-4} molar increment in the calcium concentration. This lack of agreement between the average incremental change in the DIC and changes in calcium and alkalinity suggests that DIC may be produced within the contactor by microbial respiration or that gaseous carbon dioxide entered the samples after they were collected.

The results listed in Table 17 indicate that the fluid contact time within the box contactor during the sampling period was apparently long enough to produce an effluent which was essentially in equilibrium with the $CaCO_3$ in the limestone. If the average influent water chemistry is used with the chemical equilibrium model (with a closed-to-the-atmosphere assumption) to predict the equilibrium calcium concentration the result obtained (10.9 mg Ca/L) is close to the average measured effluent calcium concentration (11.3 mg Ca/L).

The chemical equilibrium model, however, predicts an equilibrium pH (pH_{eq} = 9.18) which is significantly greater than the average measured value for the contactor effluent (7.33). This discrepancy is apparently the result of the uptake of gaseous carbon dioxide by the effluent samples or possibly by the production of carbon dioxide within the sample bottles by microbial respiration.

The negative logarithm of the carbon dioxide partial pressure, pCO_2, was calculated for each measured pH value and alkalinity. The following equations were used:

$$pCO_2 = \frac{\alpha_o(DIC)}{K_H} \quad , \tag{47}$$

and

$$DIC = \frac{alk_m - 10(-pK_w - pH_m) + 10^{-pHm}}{\alpha_1 + 2\alpha_2} \tag{48}$$

Table 17 Summary of Baffled-Box Contactor Results
Field Measurements

	Influent			Effluent		
Parameter	Mean	Std. Dev.	n	Mean	Std. Dev.	n
pH	6.34	0.26	23	7.33	0.46	23
Calcium(mg Ca/L)	4.1	1.0	20	11.3	3.8	20
Magnesium	0.67	0.12	21	0.80	0.19	22
Aluminum	0.071	0.087	10	0.066	0.066	10
Alkalinity(Meq/L)	0.15	0.06	18	0.57	0.20	18
Alkalinity(mg $CaCO_3$/L)	7.5	30	18	28.5	10.0	18
Dissolved Inorganic Carbon(mg C/L)	3.7	1.1	19	7.0	1.6	20
Specific Conductivity (μmhos/cm)	56	9	12	87	16	13
Standard Plate Count (No/ml)	89	142	15	170	365	16
Dissolved Organic Carbon (mg C/L)	1.4	0.5	6	1.5	0.6	6
Dissolved Oxygen (mg O_2/L)	7.2	0.6	8	7.4	0.8	9
Turbidity (NTU)	0.6	0.5	9	0.7	0.2	9

where alk_m and pH are the measured alkalinity and pH, K_H is Henry's Law constant and α_o, α_1, and α_2 are the ionization fractions for H_2CO_3 (see Eqs. 28, 29 and 32). The calculated values of pCO_2 are plotted in Figure 40.

The CO_2 partial pressure values plotted in Figure 40 were all significantly greater than the partial pressure of atmospheric carbon dioxide, $10^{-3.5}$ or $pCO_2 = 3.5$ (20°C). The average pCO_2 values for the influent and effluent were 2.55 adn 2.90, respectively. Both values are consistent with CO_2 partial pressures determined for soil-water systems and indicate that the water flowing through the contactor is supersaturated with respect to atmospheric carbon dioxide.

The pH calculated using the equilibrium model for contactor effluent equilibrated with atmospheric CO_2 is 7.87, a value which is greater than the average observed value of 7.33. This result supports the contention that the effluent samples were not maintained as intended, in a closed-to-the-atmosphere condition and that microbial respiration within the bed may have been an additional factor.

The influent and effluent dissolved oxygen concentrations, 7.2 and 7.4 mg/L, were essentially the same (Table 17). The influent and effluent dissolved organic carbon and turbidity measurements also showed essentially no change across the contactor.

On September 26, 1983, after 455 days of continuous operation the spring was partially drained and the lid was removed from the box contactor unit. Measurements were carefully made with a ruler to determine how much of the total volume of each compartment was still occupied by the limestone bed. (On June 26, 1982, each of the five compartments had been completely filled with fresh stone.) Representative samples of stone were removed from each compartment to determine the mean particle diameter by the water displacement technique (see Section 5). Two additional samples from the first and second compartments were obtained for size analysis by sieving. Representative samples were removed from the first and last compartments for particle surface analysis by scanning electron microscopy (SEM) and x-ray energy spectrometry (XES).

The general physical condition of the limestone was similar to that of fresh limestone, however, some differences were noted. In the first several

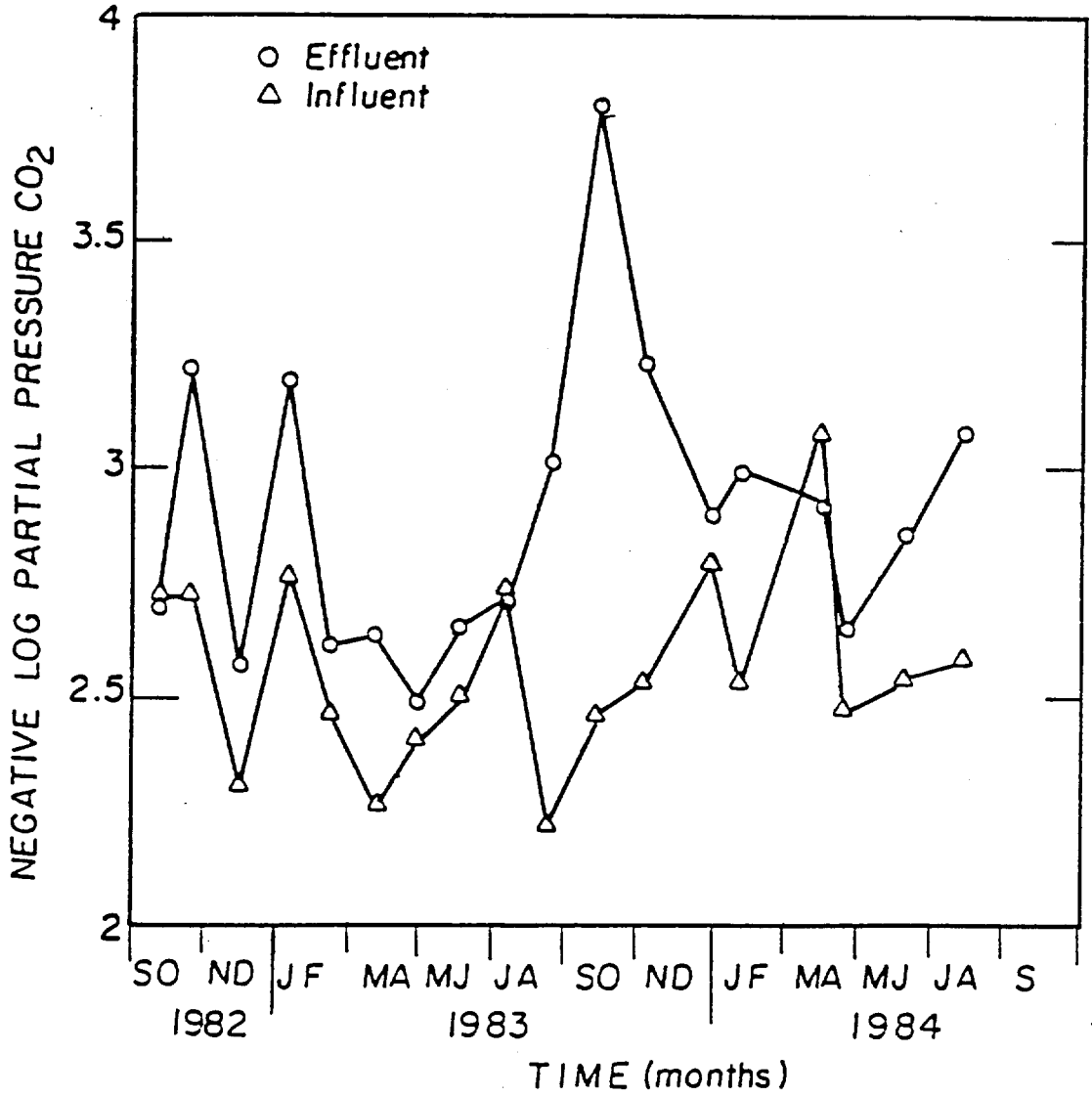

Figure 40. Calculated partial pressure of carbon dioxide plotted as a function of time for the influent and effluent of the baffled-box contactor.

compartments a brown, humous-like material was evident in the interstitial spaces. The bed did not appear to be clogged by this material but when the stone layer was disturbed the water in the compartment became turbid with coarse, brown particulate matter. It seems reasonable to assume that because the spring is in a hardwood forest most of the material was decomposing leaf litter.

The used, wet limestone from the contactor seemed to have a slightly "slimy" feel when rubbed between the fingers. A cursory microscopic examination of the surface (SEM and light microscope) did not yield any obvious indications of microbiological contamination. The XES analysis (which will be discussed in more detail later) did not indicate the presence of major amounts of metal hydroxide precipitates on the particle surfaces. A reasonable assumption seems to be that although the microscopic examination was essentially negative, the sliminess was due to some microbiological contamination and possibly deposited particles of soil material.

The amount of limestone dissolved during the 455 day period was sufficient to cause a measurable decrease in the volume occupied by the bed and a decrease in the average size of the stones, particularly the material in the first two compartments. The percent of the total compartment volume occupied by the limestone bed and the mean particle diameter for each of the five compartments is given in Table 18.

The final volume occupied by the bed ranged from 83 percent in the compartment at the inlet to 93 percent of the total compartment volume in the fifth compartment (Table 18). The mean limestone particle diameter varied from a low value of 0.78 cm in Compartment 1 at the inlet to 0.98 cm in Compartment 5. The initial mean particle diameter was 0.97 cm in all compartments.

The measured particle diameters indicate that very little dissolution occurred in the fourth and fifth compartments. However, during the test period there was apparently some consolidation of the stone in these compartments. The final volumes occupied by the limestone bed in the fourth and fifth compartments were 92 and 93 percent, respectively, of the total volume occupied when the compartments were filled.

The calculated final porosity of the limestone bed in each of the compartments is listed in the fourth column of Table 18. The final porosity, ε', was calculated using the initial porosity, ε, the initial and final limestone particle diameters, $\bar{d}$ and $\bar{d}'$, and the initial and final volumes filled by the limestone bed, V and V'. It was assumed that the number of limestone particles in each compartment remained constant during the dissolution process, i.e.,

$$\frac{(1-\varepsilon)\ V}{\frac{\pi}{6}(\bar{d})^3} = \frac{(1-\varepsilon')\ V'}{\frac{\pi}{6}(\bar{d})^3} \tag{49}$$

or

$$\varepsilon' = 1 - (1 - \varepsilon)\ (V/V')\ (\bar{d}'/\bar{d})^3 \tag{50}$$

The quantities V/V' and $(\bar{d}'/\bar{d})^3$ were determined using the percent volume occupied and mean particle diameter values listed in Table 18. For example, in the case of Compartment 1, $(V/V') = 1/0.83 = 1.20$, $(\bar{d}'/\bar{d})^3 = (0.78/0.97)^3 = 0.52$, $\varepsilon = 0.44$ and therefore, according to Eq. 50, $\varepsilon' = 0.66$.

The final porosity values for the first two compartments in the contactor were significantly greater than the initial porosity of 0.44. This trend suggests that while under these conditions the limestone bed tended to consolidate somewhat as the limestone particles became smaller (the bed volume decreased in every compartment), the porosity increased in the first two compartments. It is possible that the brown humous-like deposit which was found in the compartments near the inlet tended to prevent the bed from collapsing as the particles dissolved.

The amount of limestone dissolved from the first compartment of the box contactor was estimated using the measurements listed in Table 18. This value was compared with an amount determined using a mass balance calculation and measured increases in the calcium ion concentration across the chamber.

According to the results listed in Table 18 the mass of limestone dissolved from the first compartment during the 455 day test period was approximately 25 kg. This amount was determined using the following relationships:

Table 18 Baffled-Box Contactor - Limestone Dissolution
June 28, 1982 - September 26, 1983

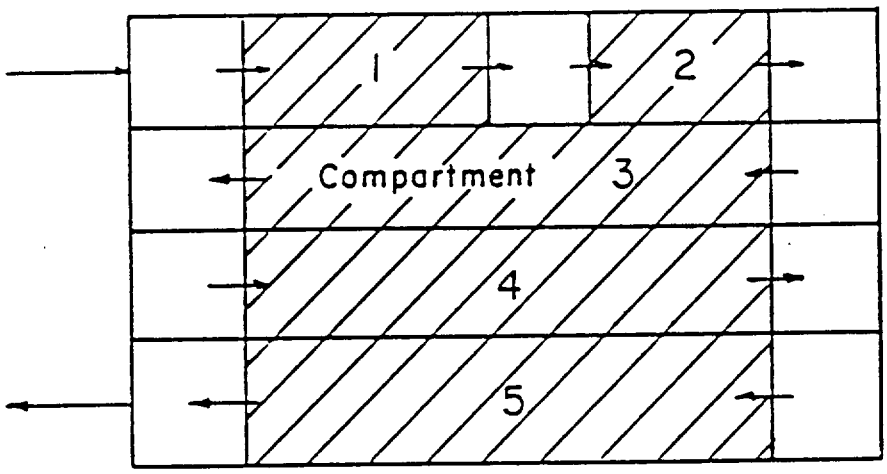

Compartment Number	Percent of Total Compartment Volume Occupied by the Limestone Bed	Mean Limestone Particle Diameter (cm)[2]	Final Porosity of the Limestone Bed[3]
1	83	0.78[4]	0.66
2	84	0.79[4]	0.66
3	87	0.95	0.42
4	92	0.97	0.42
5	93	0.98	0.42

NOTES:

1. Original Volume Occupied was 100 percent in all compartments.
2. Original Mean Diameter was 0.95 cm.
3. Original Porosity was 0.44.
4. A sieve analysis of the stone in Compartments 1 and 2 yielded median stone diameters of 0.71 and 0.84 cm., respectively.

initial mass of limestone in the compartment = (compartment volume)(1-porosity)(limestone density)

= $(36{,}203\ cm^3)(1-0.44)(2.64\ g/cm^3)(10^{-3}\ kg/g)$

= 52 kg

final mass of limestone in the compartment = final volume occupied by limestone (1-porosity)(limestone density)

= $(36{,}203\ cm^3)(0.827)(1-0.66)(2.64\ g/cm^3)(10^{-3}\ kg/g)$

= 27 kg

[Mass of Limestone Dissolved] = 52 - 27 = 25 kg.

In a special series of constant flowrate experiments using the expected range of operating flowrates (1-4 gpm, 4-15 liters/min) the increase in calcium ion concentration across the first compartment ranged from 3 mg Ca/L at 4 liters/min to 1 mg Ca/L at 15 liters/min. Since the limestone in this study contained 79 percent $CaCO_3$ and $CaCO_3$ is 40 percent calcium (by mass) the amount of limestone dissolved for a given increase in calcium ion concentration, Ca, and flowrate, Q, is given by:

Mass of Limestone Dissolved = (ΔCa, g/L)(Q, L/min)(1440 min/day)(455 days) x (10^3 kg/g)(3.13 kg limestone/kg Ca)

For $\Delta Ca = 0.003$ g/L and Q = 4 L/min, the mass of limestone dissolved during the 455 day period is 25 kg. For $\Delta Ca = 0.001$ g/L and Q = 15 L/min, the mass dissolved is 31 kg. Given the assumptions upon which these calculations are based the agreement obtained between the mass dissolved calculated by the two methods (25 kg and 25 to 31 kg) is not unreasonable.

A qualitative analysis was made of the surface chemical characteristics of limestone samples using an ISI scanning electron microscope with a Kevex x-ray energy spectrometer attachment. In this instrument the electron beam is used to provide an image of the sample through electron scattering and to cause characteristic x-rays to emanate from the surface layer of the sample. The measurement of the energy of the characteristic x-rays indicates the presence of certain elements and their relative abundance on the sample surface.

Four elements were detected and identified in one or more of the four samples; calcium, silicon, aluminum and iron. The x-ray energy spectra for the four samples are given in Figure 41, A-D.

Calcium was the dominant identifiable element in the fresh limestone sample. A lesser peak, characteristic of silicon was also apparent. It is possible that aluminum is present in the fresh limestone surface (Figure 41A), however, the peak which is characteristic of aluminum is partially obscured by the silicon peak.

Prolonged contact of the limestone with the spring water in the box contactor reduced the amount of calcium and increased the amount of silicon and aluminum on the limestone particle surface (Figures 40B and 40C). A small peak attributable to iron also appears after prolonged use in the contactor. A comparison of the results obtained for samples from the first and fifth compartments (Figures 41B and 41C) shows that the decrease in the prominence of the calcium peak is much greater in the case of the first compartment where more of the limestone was dissolved.

The results obtained using the SEM/XES system suggest that as the calcium carbonate was dissolved from the limestone particles the relative abundance of aluminum and silicon on the surface increased. Apparently alumino-silicate (clay) impurities in the limestone remained as a thin "residue" coating after the $CaCO_3$ was leached from the limestone matrix.

There is no evidence that the source of the aluminum, silicon and iron was the spring water. The x-ray energy spectrum obtained for the sample from the laboratory column (treating a high purity acidified water; Figure 41D) was very similar to that obtained for the first compartment of the box contactor unit (Figure 41A).

Bay Side Cottage Wound Fiberglass Column

In December 1983, the water line between the box contactor and the winterized cottages became frozen and the resort owner had to pump water from Big Moose Lake directly to the cottages. Column 1, a wound fiberglass, ion exchange type column, Figure 8, was installed in the heated basement of Bay Side Cottage (Figure 9). The unit was operated during the months of January to April 1984. The temperature of the water was 3 to 4°C during this period.

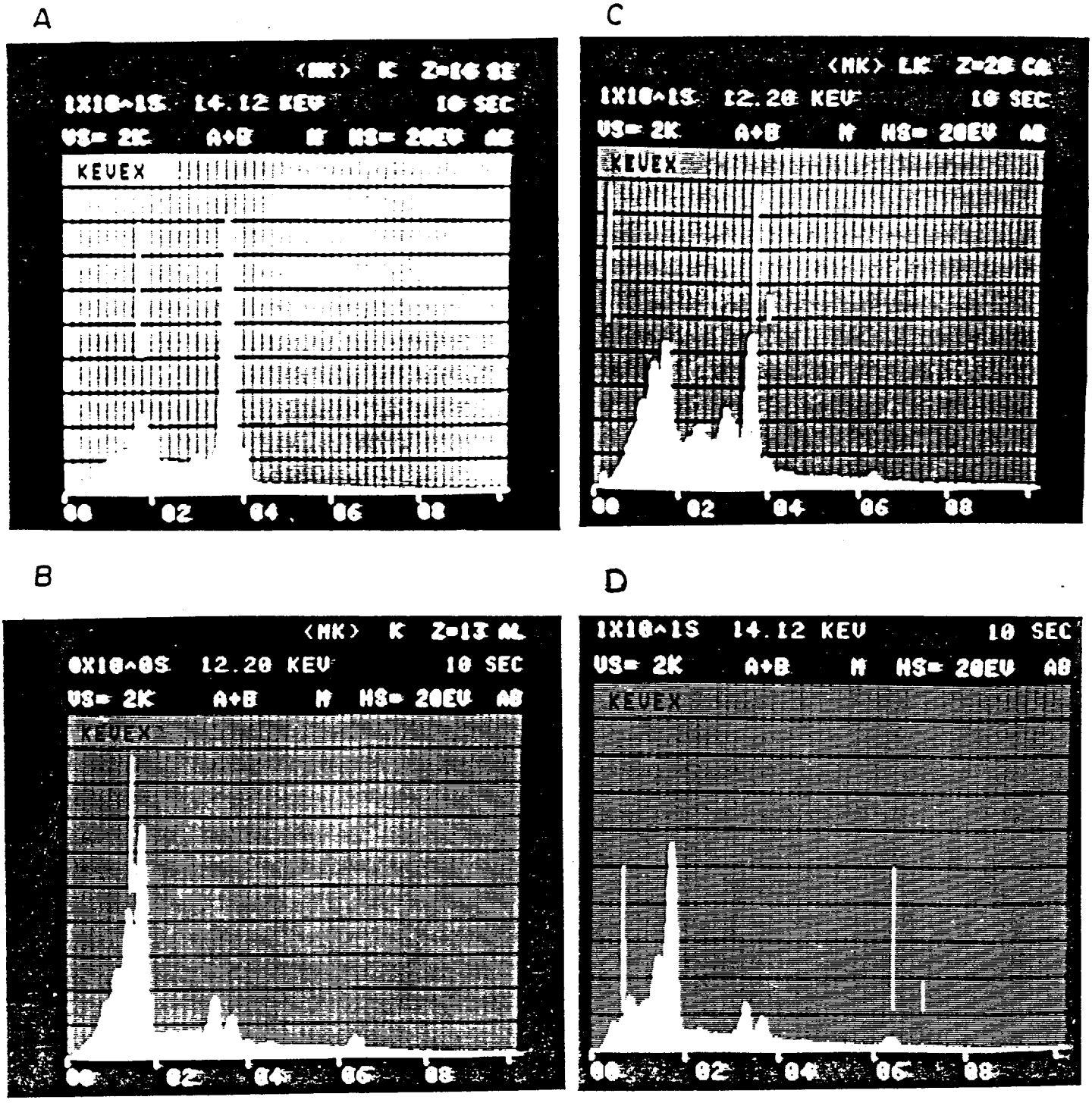

Figure 41. X-ray energy spectra for the following samples; A - fresh limestone, B - limestone after prolonged dissolution in the baffled-box contactor, compartment 1, C - same as B except compartment 5, D - limestone after prolonged dissolution in the laboratory.

The results obtained from the wound fiberglass column are plotted in Figures 42 to 45. In these figures influent means water drawn from a sample tap located near the inlet to the unit and effluent means a sample taken from the cold water tap in the kitchen of Bay Side Cottage.

The pH results are plotted in Figure 42. The wound fiberglass column increased the pH from 4.6 to approximately 7.0. Some of the variability which was evident in the effluent results is probably due to our inability to maintain a constant flowrate through the unit during routine operation. Inadvertent uptake of CO_2 by some of the water samples may also have affected the results.

A plot of influent and effluent calcium concentrations for the 86 day sampling period is presented in Figure 43. The average increase in calcium ion concentration across the column was 5.5 mg Ca/L. On average the calcium ion concentration increased form 1.8 to 7.3 mg Ca/L.

The alkalinity was increased from an average influent value of -0.03 meq/L (-1.5 mg $CaCO_3$/L) to an average influent value of 0.26 meq/L (13 mg $CaCO_3$/L). The results are plotted in Figure 44.

The dissolved inorganic carbon concentration showed significant variability, probably due to the uptake or (in the case of the influent samples), release of carbon dioxide. The average influent DIC concentration was 1.0 mg C/L and the average effluent concentration was 3.2 mg C/L. The DIC results are plotted in Figure 45. The results obtained in monitoring the wound fiberglass column are summarized in Table 19.

The chemical equilibrium model (with the closed-to-the-atmosphere assumption and using the average influent water chemistry (Table 19)) predicts an equilibrium pH of 9.8 and an equilibrium calcium concentration of 9.1 mg Ca/L. It is apparent that the wound fiberglass unit did not produce an effluent which was in equilibrium with the $CaCO_3$ in the limestone. The average effluent calcium concentration was 7.3 mg Ca/L and the average effluent pH was 6.9.

The low magnitude of the average effluent pH suggests that in this case, as in the case of the box contactor unit, the effluent pH was depressed below the value associated with a truly closed system, apparently through the uptake of gaseous carbon dioxide.

The average increase in alkalinity across the wound fiberglass column was 0.30 meq/L (Table 19). This trend corresponds to a calculated average increase in DIC of 1.8 mg C/L. The observed increase in DIC according to Table 19 was 2.2 mg C/L, a value which was larger than the calculated increment and, hence, in support of the assumption that the measured effluent pH values were depressed by the uptake of carbon dioxide.

A sample of limestone was taken from the wound fiberglass unit at the conclusion of the experiment in April. The chemistry of the surface layer was analyzed, as in the box contactor case, using x-ray energy spectrometry. The energy spectrum for one analysis is shown in Figure 46. The spectrum is very similar to that obtained with fresh (undissolved) limestone, Figure 41A. Apparently the 3 month period of operation in the wound fiberglass unit was insufficient to alter the elemental make-up of the surface layer to a measureable extent.

Culligan (Cullneu)® Contactor

Access to the basement of Henry Covey cottage was limited due to use by tourists and therefore the influent and effluent of the Culligan contactor were sampled infrequently. The results obtained are listed in Table 20.

The average increase in the calcium ion across the Culligan unit was 3.2 mg Ca/L and the average increase in the alkalinity was 240 μeq/L. The average influent pH was 6.52 and the average effluent pH was 7.1.

The depth of Cullneu medium in the Culligan contactor was 15 in. (40 cm.). The mean particle size of the Cullneu material was approximately 2 mm (sieve analysis) and therefore it was estimated that the particle surface area per unit volume of interstitial water (a) was approximately 50 cm^{-1}. This value is about 5 times greater than the value for the 0.97 cm diameter limestone particles used in the box contactor and wound fiberglass units. The higher specific surface area of the Cullneu medium explains why the incremental change in water chemistry was as high as it was given that the depth of the medium was only 15 inches (versus 48 inches in the wound fiberglass unit).

The Culligan contactor was monitored for 9 months. During this period there was no evidence of fouling or other operational problems. In the fall

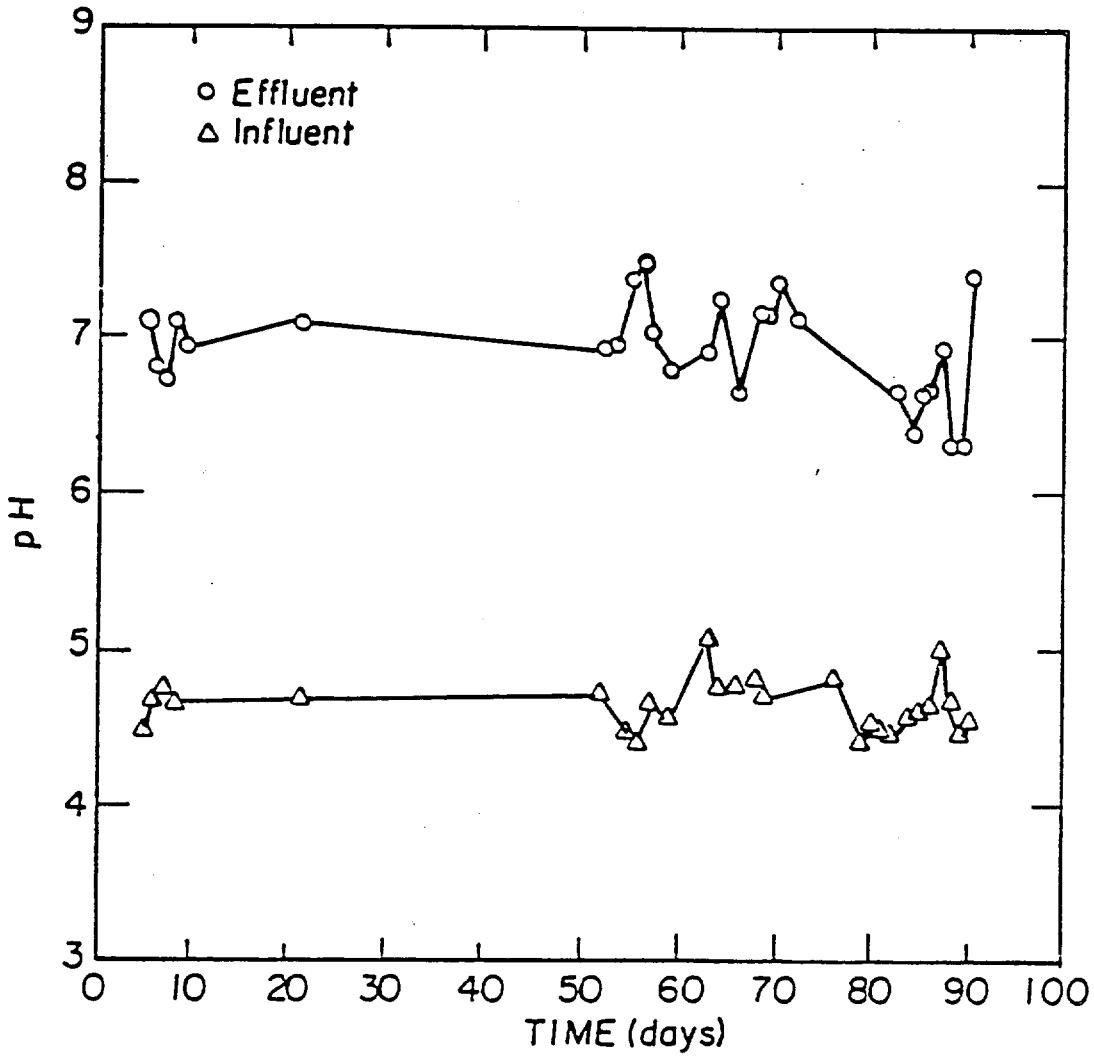

Figure 42. Influent and effluent pH plotted as a function of time for the wound-fiberglass contactor in Bayside Cottage.

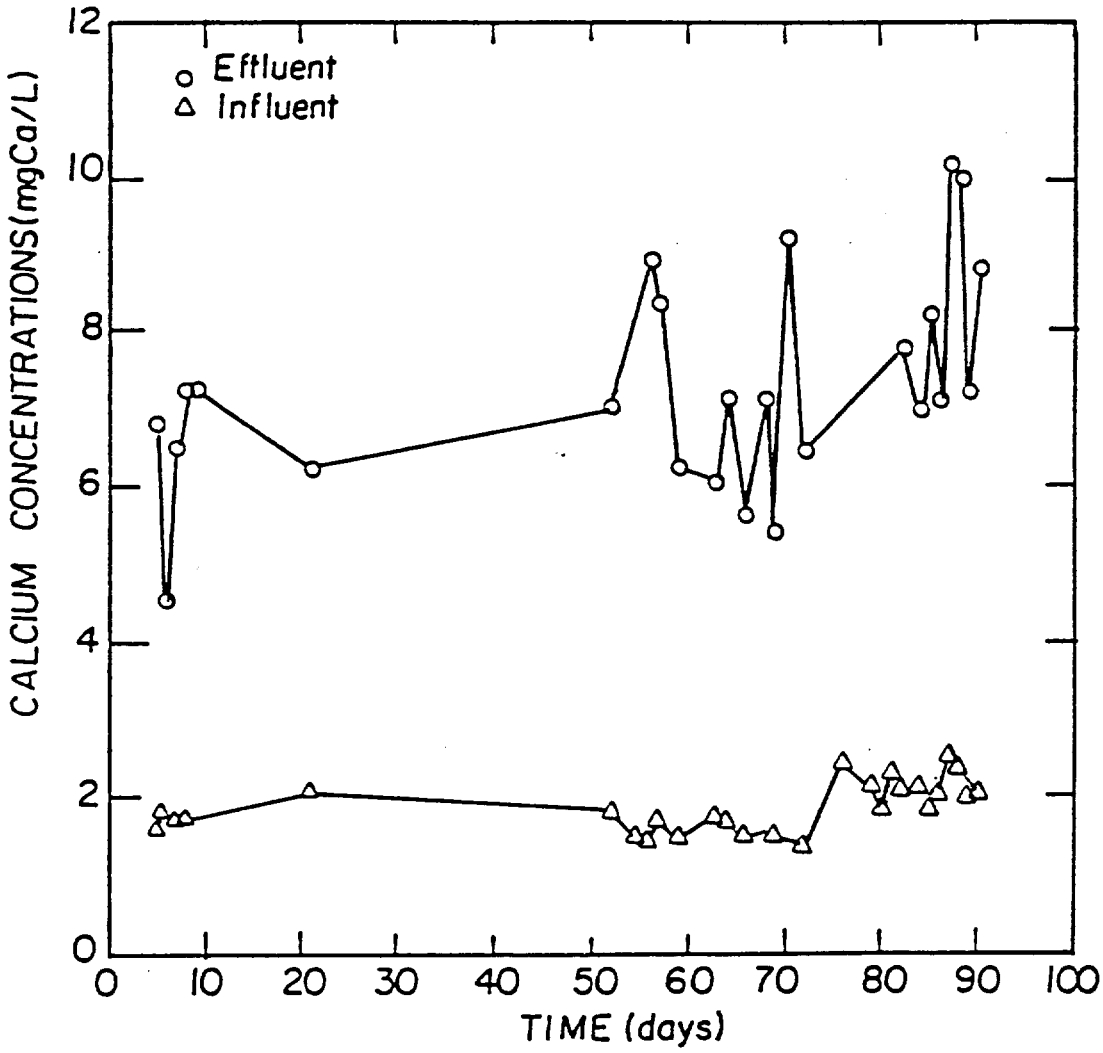

Figure 43. Influent and effluent calcium concentration plotted as a function of time for the wound-fiberglass contactor in Bayside Cottage.

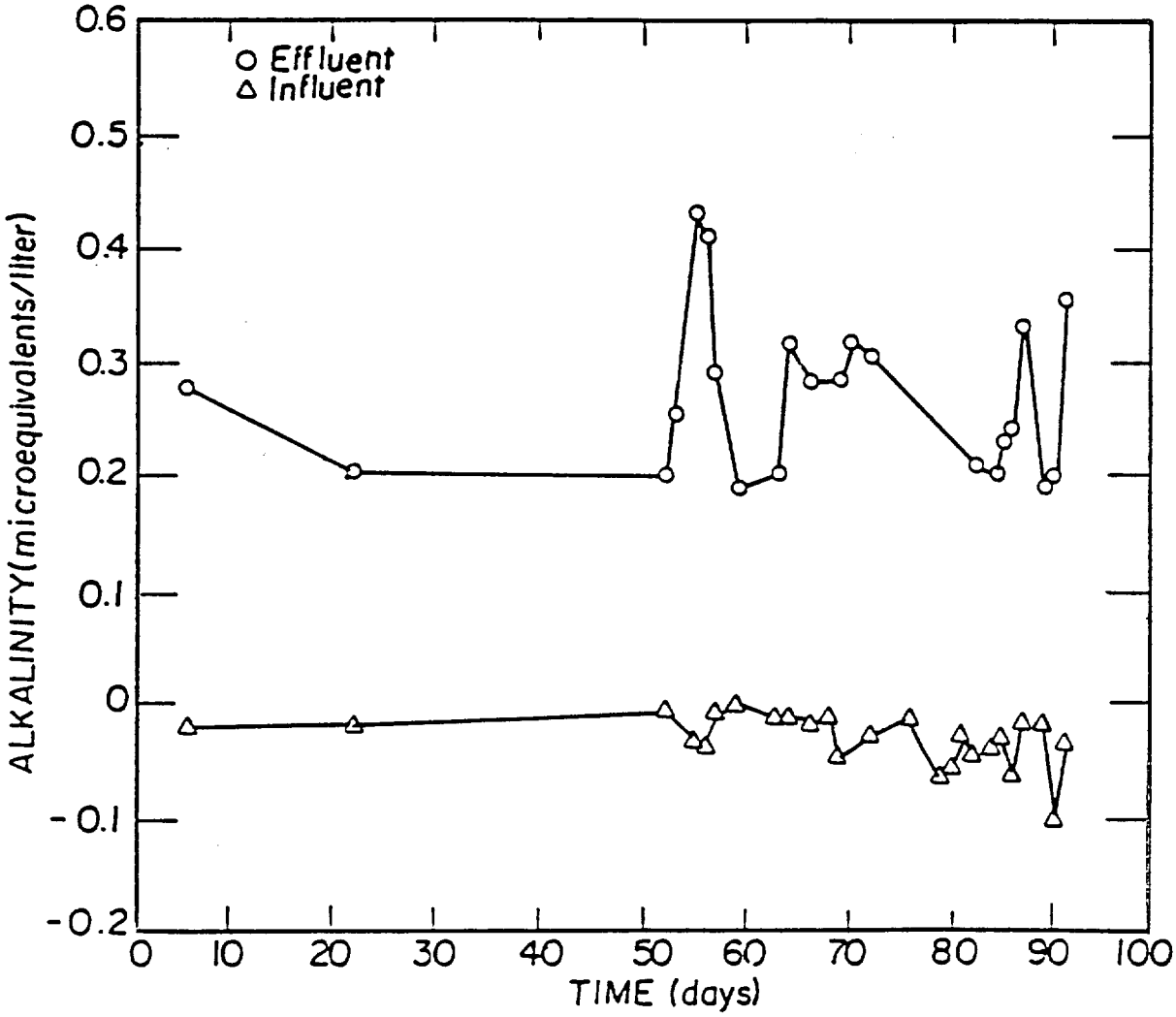

Figure 44. Influent and effluent alkalinity plotted as a function of time for the wound-fiberglass contactor in Bayside Cottage.

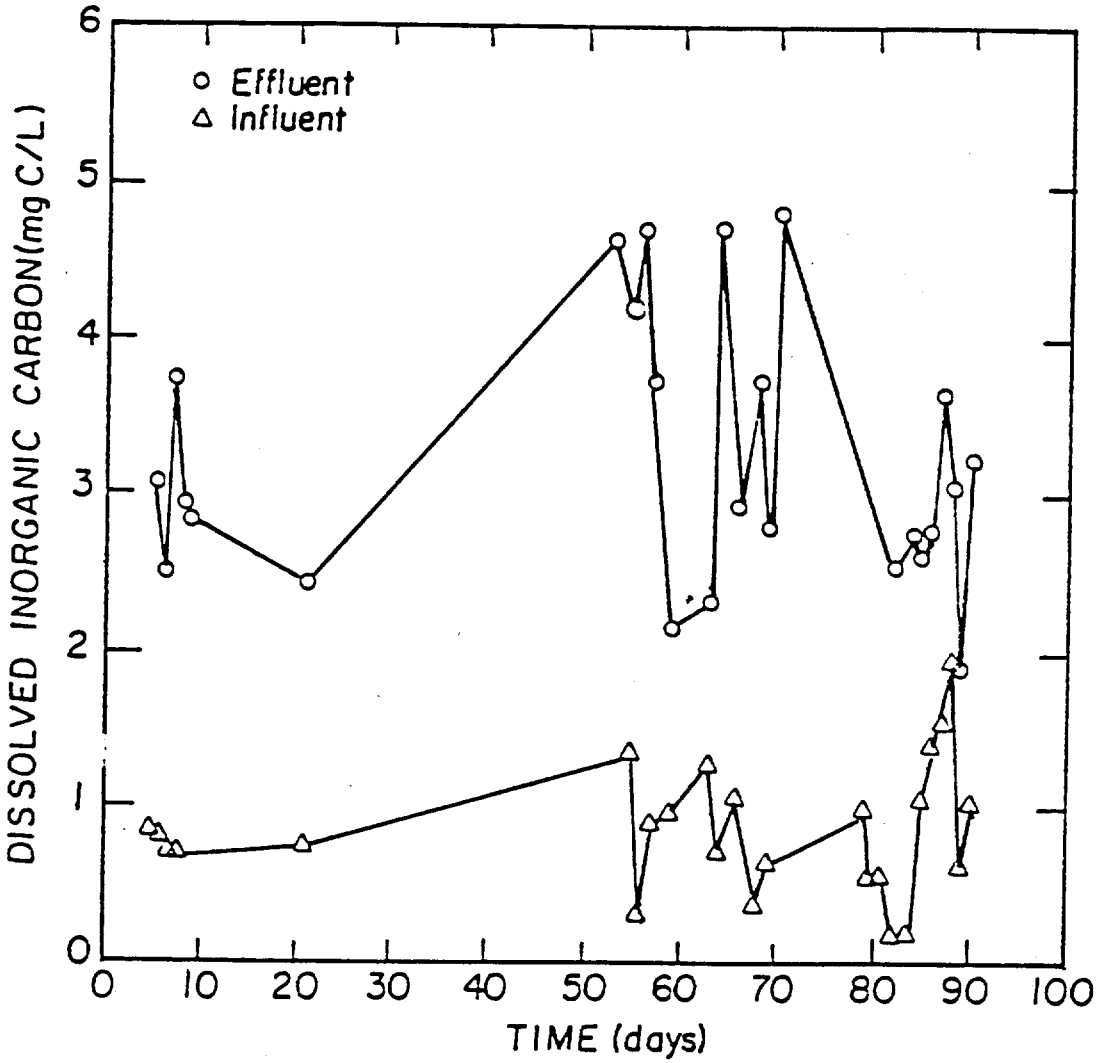

Figure 45. Influent and effluent dissolved inorganic carbon concentration plotted as a function of time for the wound-fiberglass contactor in Bayside Cottage.

Table 19 Summary of Bay Side Cottage
Wound Fiberglass Column Results

Jan. 25, 1984 to April 20, 1984

	Influent (Big Moose Lake)			Effluent		
Parameter	Mean	Std. Dev.	n	Mean	Std. Dev.	n
pH	4.64	0.17	28	6.93	0.32	27
calcium (mg Ca/L)	1.82	0.33	28	7.27	1.37	25
magnesium (mg Mg/L)	0.37	0.03	28	0.49	0.11	26
alkalinity (meq/L)	-0.03	0.02	25	0.26	0.07	23
alkalinity (mg $CaCO_3$/L)	-1.5	1.0	25	13.0	3.5	23
dissolved inorganic carbon (mg C/L)	0.99	0.52	25	2.33	0.85	25

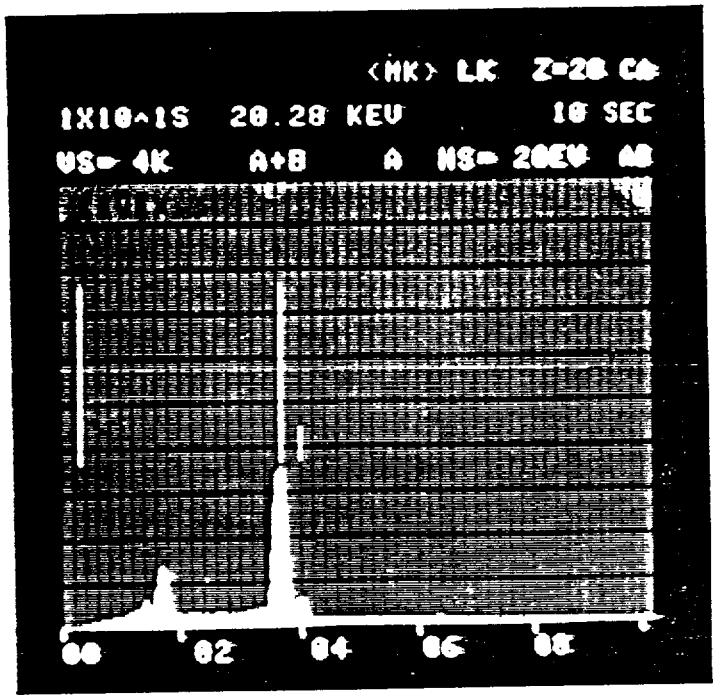

Figure 46. X-ray energy spectrum for a limestone sample taken from the wound-fiberglass contactor at the end of the experiment.

TABLE 20 Culligan Contactor - Summary of Results
November 3, 1983 - July 31, 1984

Date	Influent			Effluent		
	pH	Calcium (mgCa/L)	Alkalinity (μeq/L)	pH	Calcium MgCa/L	Alkalinity eq/L
Nov. 3, 1984	6.76	9.95	376	7.16	13.3	811
Dec. 30	6.42	7.64	312	6.79	10.6	458
Jan. 25, 1984	6.25	8.64	270	6.57	10.3	439
Feb. 10	--	--	--	7.53	11.10	834
June 13	--	--	--	7.40	19.10	--
July 31	6.64	11.40	590	7.08	15.2	726

of 1984 the unit was drained and a sample of medium was extracted for a sieve analysis and for particle surface analysis by x-ray energy spectrometry (XES). The sieve analysis result was not significantly different than that obtained before the material was used. The results of the XES analysis are presented in Figure 47.

The XES scan for unused Cullneu (Figure 47A) shows a significant calcium peak, but unlike the fresh limestone, no evidence of silicon or aluminum. The used Cullneu (Figure 47B) has XES peaks which indicate the presence of aluminum, calcium and copper on the particle surface. It is not known whether the aluminum came from the influent water or was a contaminate in the Cullneu material. The copper peak suggests that copper released from several short sections of copper tubing upstream of the contactor unit was adsorbed on the medium.

EVALUATION OF THE CONTACTOR DESIGN EQUATIONS USING FIELD MEASUREMENTS

The contactor design equations (Section 6) were evaluated using data obtained in experiments conducted in the field. The wound fiberglass and box contactors were disconnected from the effluent piping and valves were installed to control the flowrate. Samples of the influent and effluent were collected after the units had been operating at constant flowrate for at least fifteen minutes. In the case of the box contactor, effluent samples were obtained for limestone depths of 39 and 78 cm. The depth of limestone in the wound fiberglass unit was 122 cm. The experimental conditions and the results are listed in Tables 21 to 23.

The overall dissolution rate constant, K_o, was calculated for each experimental run using a simplified version of Eq. 25, Section 6, i.e.,

$$K_o \simeq \frac{-\ln[(C_{bL} - C_{eq})/(C_{bo} - C_{eq})]U_s}{L\ a\ \varepsilon} \qquad (51)$$

where C_{bo} and C_{bL} are the measured influent and effluent calcium concentrations, C_{eq} is the model calculated equilibrium calcium concentration, U_s is the superficial velocity, L is the depth of limestone, a is the interfacial area of limestone per unit volume of bed and ε is the bed porosity. The magnitude of a was determined using the limestone particle mean diameter, $\bar{d}$, and sphericity, ψ, and Eq. 12 Section 6.

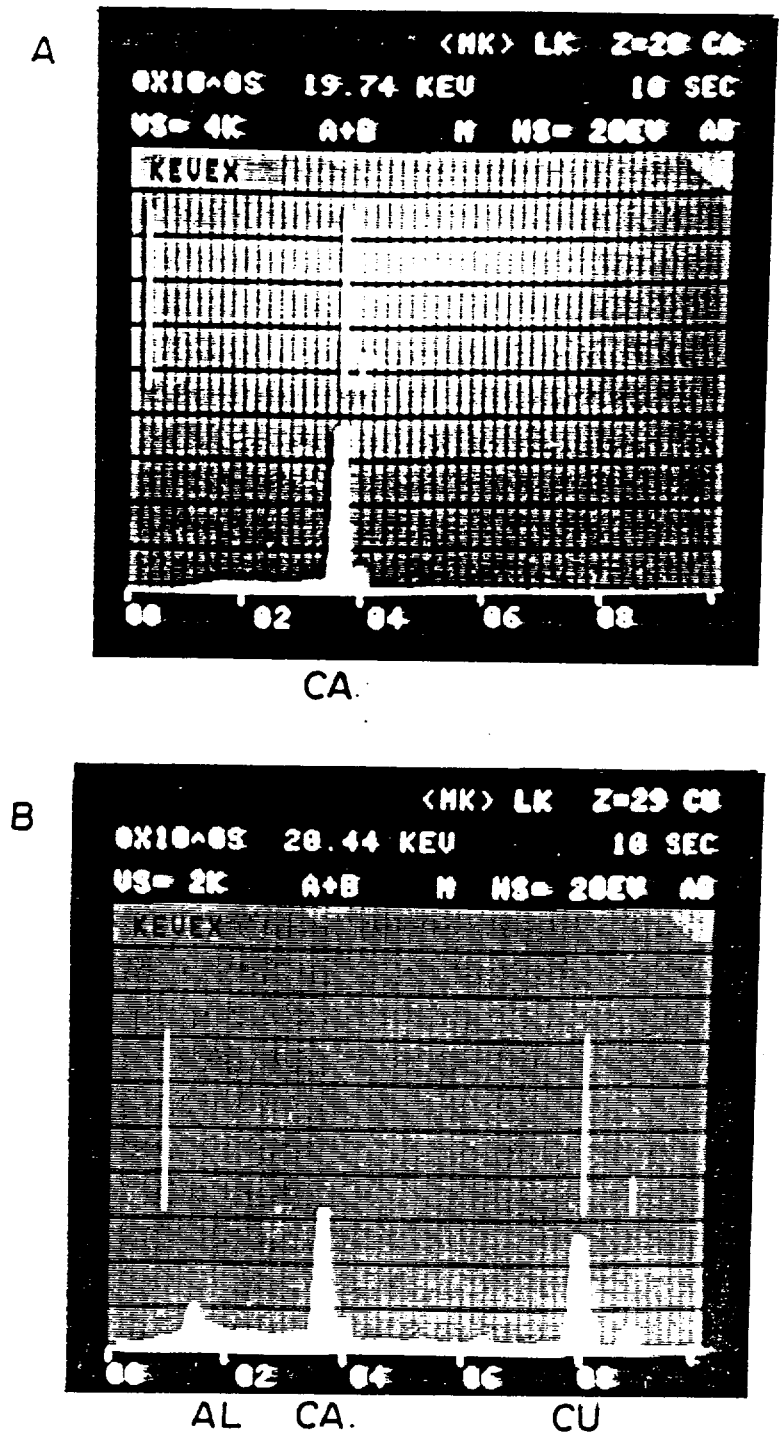

Figure 47. X-ray energy spectra for fresh cullneu medium (A) and Cullneu used in the Culligan contactor for 9 months (B).

Table 21 Baffled-Box and Wound Fiberglass Contactors
Special Test of Model Equations
Experimental Conditions and Results

INFLUENT CHARACTERISTICS

	Wound Fiberglass Contactor Big Moose Lake	Box Contactor Covewood Spring
pH, pH_o	4.7	6.4
Calcium, C_{bo}(mg Ca/L)	1.8	4.0
Dissolved Inorganic Carbon, DIC_o (mg C/L)	1.0	3.6
Temperature (°C)	3	10
$C_a - C_c$(moles/L)	1.1×10^{-4}	5.1×10^{-5}

CONTACTOR DESIGN AND OPERATING CONDITIONS

	Big Moose Lake	Covewood Spring
Limestone diameter, $\bar{d}$(cm)	0.97	0.97
Limestone particle sphericity, ψ	0.79	0.79
Bed Porosity, ε	0.44	0.44
Superficial flow velocity, U_s(cm)	3.0, 12.3	5.4, 10.8, 16.2, 21.5, 26.9
Bed depth, L(cm)	122	39, 78
Kinematic viscosity, ν(cm^2/s)	1.62×10^{-2}	1.31×10^{-2}

MEASURED EFFLUENT CALCIUM CONCENTRATIONS

	Calcium Concentration (mg Ca/L)	
Big Moose Lake	L = 122 cm	
U_s = 3.0 cm/min	8.7	
U_s = 12.3 cm/min	6.9	
Covewood Spring	L = 39 cm	L = 78 cm
U_s = 5.4 cm/min	7.0	8.2
U_s = 10.8	6.6	6.7
U_s = 16.2	5.0	5.6
U_s = 21.5	5.7	6.3
U_s = 26.9	5.8	5.5

TABLE 22 Special Test of Model Equations
Calculated Equilibrium pH and Calcium Concentration

MODEL CALCULATED EQUILIBRIUM (Closed-to-the-Atmosphere)CONCENTRATIONS

	Big Moose Lake	Covewood Spring
pH, pH_{eq}	9.8	9.2
calcium concentration, C_{eq}(mg Ca/L)	9.1	10.9

TABLE 23 Results of Special Test
of Model Equations

BIG MOOSE LAKE RESULTS - WOUND FIBERGLASS CONTACTOR

	Superficial Velocity U_s(cm/min)	
	3.0	12.3
$K_o \times 10^{-3}$(cm/min) (from experimental results)	15	25
$K_o \times 10^{-3}$(cm/min) (from contactor design equations)	19	26

COVEWOOD SPRING RESULTS - BOX CONTACTOR

	Superficial Velocity U_s(cm/min)				
	5.4	10.8	16.2	21.5	26.9
$K_o \times 10^{3}$(cm/min) (from experimental results)*	17	23	14	31	38
$K_o \times 10^{3}$(cm/min) (from contactor design equations)	31	36	41	47	54

*Average values for L = 39 and 78 cm.

The use of Eq. 51 instead of Eq. 25, section 6, is appropriate because in the case of these field experiments, the dispersion number, N_D, was small,

$$N_D \left(\frac{K_o\ a\ L\ \varepsilon}{U_s}\right)^2 \quad << \quad \left(\frac{K_o\ a\ L\ \varepsilon}{U_s}\right)$$

and therefore ideal plug flow can be assumed.

The equilibrium calcium concentration, C_{eq}, was determined for a closed-to-the-atmosphere condition using the influent characteristics listed in Table 15 and the equations and thermodynamic constants discussed in Section 6 and Appendix A. The results, pH_{eq} and C_{eq}, are given in Table 22. Only the equilibrium calcium concentration, C_{eq}, is used in the calculation of K_o.

Model calculated values of K_o were determined for each set of experimental conditions using Eqs. 38 to 40, Section 7. For example for modified Reynold's numbers (MRe) less than 30, i.e.,

$$\frac{\bar{d}\ U_s}{\nu(1-\varepsilon)} < 30,$$

The magnitude of K_L is given by Eq. 39,

$$K_L = 5.70(MR_e)^{-0.78}\ U_s(\nu/D)^{-2/3} \qquad (41)$$

The calcium ion diffusivity determined in the laboratory experiments, $D_{20°C} = 1.2 \times 10^{-5} cm^2/5$, was used with Eq. 42, Section 7 to estimate D at the influent water temperature.

To determine the overall dissolution rate constant, K_o, it was assumed that the surface reaction rate constant, K_c, was significantly larger than K_L (as was observed in the laboratory experiments) and therefore $K_o = K_L$. The model calculated values of K_o are listed in Table 23 next to those determined using the experimental data.

The agreement between the values of K_o calculated using the experimental results and those determined using the design equations is reasonable in the case of the wound fiberglass unit treating water from Big Moose Lake. In the case of the box contactor results the agreement is less satisfactory;

the model calculated values of K_o are essentially two times the values derived from the experimental results. An exact reason for this discrepancy has not been determined, however, one possible explanation will be discussed.

It is possible that the presence of a microbial film on the surface of the limestone reduced the interfacial area available for mass transfer and consequently, reduced the overall dissolution rate. To explain the average difference between the values of K_o, the interfacial area per unit volume of interstitial water, a, would have to be reduced by a factor of about two. As noted earlier, a limited examination of the surface with light and scanning electron microscopes did not give a positive indication of significant biological fouling of the surfaces. However, the "sliminess" of the limestone particles which was noted when the unit was opened after one year, and the higher than expected dissolved inorganic carbon concentrations in the effluent, suggest that there was significant biological activity within the box contactor.

The box contactor and the wound fiberglass units had both been in operation about 3 months when the experiments were conducted to determine K_o. A biological film may not have formed on the limestone in the wound fiberglass unit because of the low temperature (3°C) of the lake water influent. The box contactor was operating during the summer months (June to September) with a water temperature of about 12°C immediately before the test was conducted. This fact combined with the proximity of the unit to the soil may have enhanced the formation of a microbiological film.

SENSITIVITY ANALYSIS - DESIGN EQUATIONS

The design equations (transport and chemical equilibrium) were used to determine the effect of a number of physical and chemical parameters on the depth of limestone required to achieve an effluent pH of 8.5. The "average" conditions above and below which each parameter was incremented (one at a time) are listed below:

Influent water characteristics:

pH, pH_o	5.5
Calcium Concentration, C_{bo}	3.0 mg Ca/L
Dissolved Inorganic Carbon concentration, DIC_o	3.0 mg C/L

Temperature	10°C
Contactor Design Parameters:	
Superficial velocity	20.4 cm/min
Limestone particle size	0.96 cm

The effect of pH_o, C_{bo}, DIC_o and temperature on the magnitude of the equilibrium calcium concentration, C_{eq}, and the calcium concentration, C_{bL}, which corresponds to an effluent pH of 8.5 was determined for the average and the high and low parameter values using the chemical equilibrium model (Appendix A). The results are listed in Table 24. Items A and B in Table 24 were used in the following equations to calculate the required depth of limestone. Line C, the effluent pH which would be obtained if the closed system effluent (initially at pH = 8.5) was equilibrated with the atmosphere, shows the significant effect that opening the effluent to the atmosphere can have on the pH. In general as the effluent equilibrates with the atmosphere the pH decreases from 8.5 to a value in the range 7.5 to 8.2.

The calculation of the limestone depth involved the following equation from Section 5,

$$-\ln\left[\frac{C_{eq} - C_{bL}}{C_{eq} - C_{bo}}\right] = \left(\frac{K_o\, a\, L\, \varepsilon}{U_s}\right) - \left(\frac{K_o\, a\, L\, \varepsilon}{U_s}\right)^2 N_D \qquad (25)$$

It was assumed based on the laboratory experiments that

$$N_D = 2(\bar{d}\,/L), \qquad (17)$$

$$K_o = K_L, \qquad (52)$$

and

$$D_{20°}(\text{calcium ion}) = 1.2 \times 10^{-5}\ cm^2/s$$

$D_{20°}$ was corrected for temperature using Eq. 42.

The magnitude of K_L was determined using the Chu and Khalil (1953) equations (Eqs. 37 to 40) and a, the interfacial area of limestone per unit volume of interstitial water and ε, the bed porosity, were assumed to be equal to the measured values listed in Table 8.

The depth of limestone, L, was calculated by combining Eqs. 25, 17 and 52, i.e.,

$$L = \frac{-\ln\left[\frac{C_{eq} - C_{bL}}{C_{eq} - C_{bo}}\right]}{\left(\frac{K_L\, a\, \varepsilon}{U_s}\right) - 2\,\bar{d}\,\left(\frac{K_L\, a\, \varepsilon}{U_s}\right)^2} \qquad (53)$$

Table 24 Results of Chemical Equilibrium Model Calculations

A = calcium concentration at equilibrium, C_{eq} (mg Ca/L)

B = calcium concentration in contactor effluent when pH = 8.5 (mg Ca/L)

C = effluent pH if effluent was equilibrated with atmospheric CO_2

	pH_o		
	4.0	5.5	7.0
A	17.5	12.9	6.8
B	17.1	12.3	5.4
C	7.9	7.9	7.8

	C_{bo} (mg Ca/L)		
	0	3.0	10.0
A	10.0	12.9	19.5
B	9.3	12.3	19.3
C	7.9	7.9	8.2

	DIC_o (mg C/L)		
	0.5	3.0	6.0
A	6.9	12.3	21.6
B	4.8	12.3	----*
C	7.5	7.9	7.9

	Temperature °C		
	2	10	20
A	13.8	12.9	12.2
B	12.4	12.3	11.8
C	7.9	7.9	7.9

*$pH_{eq} < 8.5$

The results of the sensitivity analysis calculations are listed in Table 25. The depth of the limestone bed required to achieve a pH of 8.5 increases with;

(1) decreasing influent pH

(2) increasing influent calcium concentration

(3) increasing influent dissolved inorganic carbon concentration

(4) increasing superficial velocity and

(5) increasing limestone particle size.

The effect of temperature on L is complex. With increasing temperature between 2 and 10°C, L increases slightly and between 10 and 20°C it decreases. This complexity is due to the opposing effects of temperature on the mass transfer coefficient, K_L, and the equilibrium and effluent calcium ion concentrations (C_{eq} and C_{bL}).

When the influent dissolved inorganic carbon concentration is increased to 6.0 mg C/L, the equilibrium pH is 8.26 and the target pH of 8.5 can not be reached.

Increasing the influent calcium ion concentration can have an effect similar to that of increasing the influent DIC. For example, if DIC_o is 3.0 mg C/L and the calcium concentration is increased to values greater than approximately 5 mg Ca/L the equilibrium pH becomes less than 8.5 and a contactor which will meet the pH = 8.5 objective is infeasible. (See Figure 20, Section 6).

The effect of ionic strength of the influent on the depth of limestone required to achieve an effluent pH of 8.5 was evaluated using the previously described average conditions. The ionic strength was adjusted by assuming that the background electrolyte (C_a and C_c, Eq. A-10, Appendix A and Eq. 26, Section 6) is NaCl. The results of the chemical equilibrium model calculations are listed in Table 26. In general, as the amount of NaCl is increased the equilibrium and effluent (at pH = 8.5) calcium concentrations (C_{eq} and C_{bL}) increase. The ionic strength of the column effluent (pH = 8.5) is also listed in Table 26.

Table 25 Sensitivity Analysis Results

L is the Depth of Limestone in meters required to obtain an effluent pH of 8.5.

	L		
	Low Value	Average Value	High Value
pH, pH_o	4.0	5.5	7.0
L(m)	3.5	2.4	0.8
Calcium, C_{bo} (mg Ca/L)	0	3.0	10.0
L(m)	2.4	2.4	3.9
Dissolved Inorganic Carbon DIC_o(mg C/L)	0.5	3.0	6.0
L(m)	0.5	2.4	----
Temperature (°C)	2	10	20
L(m)	2.2	2.4	2.1
Superficial Velocity, U_s (cm/min)	8.2	20.4	40.8
L(m)	1.3	2.4	3.3
Limestone Particle Size $\bar{d}$ (cm)	0.54	0.96	3.2
L(m)	1.0	2.4	14.8

The results listed in Table 26 were used with Eq. 53 to calculate the required depth of limestone. It was assumed that the ionic strength does not affect the mass transfer coefficient, K_L. The depth of limestone bed is plotted as a function of the influent ionic strength in Figure 48. The plotted results show that when the influent ionic strength is attributable to a simple 1:1 electrolyte such as NaCl and is less than approximately 2 x 10^{-3}M the effect on the depth of limestone needed to reach an effluent pH of 8.5 is negligible.

It was noted in Section 5 that the mean value of the dispersion number based on the results of the tracer experiments was equal to 2 $\bar{d}/L$. The upper and lower limits on this quantity, based on the standard deviation of the Peclet number, were approximately 3.3 $\bar{d}/L$ and 1.4 $\bar{d}/L$, respectively. The "average" conditions were used with the chemical equilibrium model and Eq. 53 to calculate the effect of the variability in the dispersion number on the depth of limestone required to achieve an effluent pH of 8.5. The following results were obtained.

$N_D = 0$	L = 2.2 m
$N_D = 1.4\ \bar{d}/L$	L = 2.2 m
$N_D = 2.0\ \bar{d}/L$	L = 2.3 m
$N_D = 3.3\ \bar{d}/L$	L = 2.3 m

The variability in the dispersion number has an essentially negligible effect on the depth of limestone required to reach pH = 8.5. For many cases, particularly when the limestone particle diameter is less than 1 cm, it is reasonable to assume that $N_D = 0$ and plug flow exists.

THERMODYNAMIC CALCULATIONS OF TRACE METAL CHEMISTRY

A series of thermodynamic calculations was performed with the chemical equilibrium model, MINEQL, to evaluate the solubility of trace metals and the stability of passivation films. Calculations were made over a range of pH values and dissolved inorganic carbon concentration; the latter including both constant dissolved inorganic carbon concentrations (closed-to-atmospheric CO_2) and equilibrium (open) with gaseous CO_2. To facilitate an evaluation of the conditions for which passivation films are stable, a series of predomin-

Table 26 Effect of Ionic Strength on the Equilibrium and Contactor Effluent (pH = 8.5) Calcium Concentrations

Influent Ionic Strength, M	Equilibrium Calcium Concentration, C_{eq} (mg Ca/L)	Effluent Calcium Concentration when pH = 8.5 C_{bL} mg Ca/L
8.6×10^{-4}	12.9	12.4
1.9×10^{-3}	13.0	14.4
5.9×10^{-3}	13.1	12.5
1.1×10^{-2}	13.4	12.5
5.1×10^{-2}	15.0	12.8

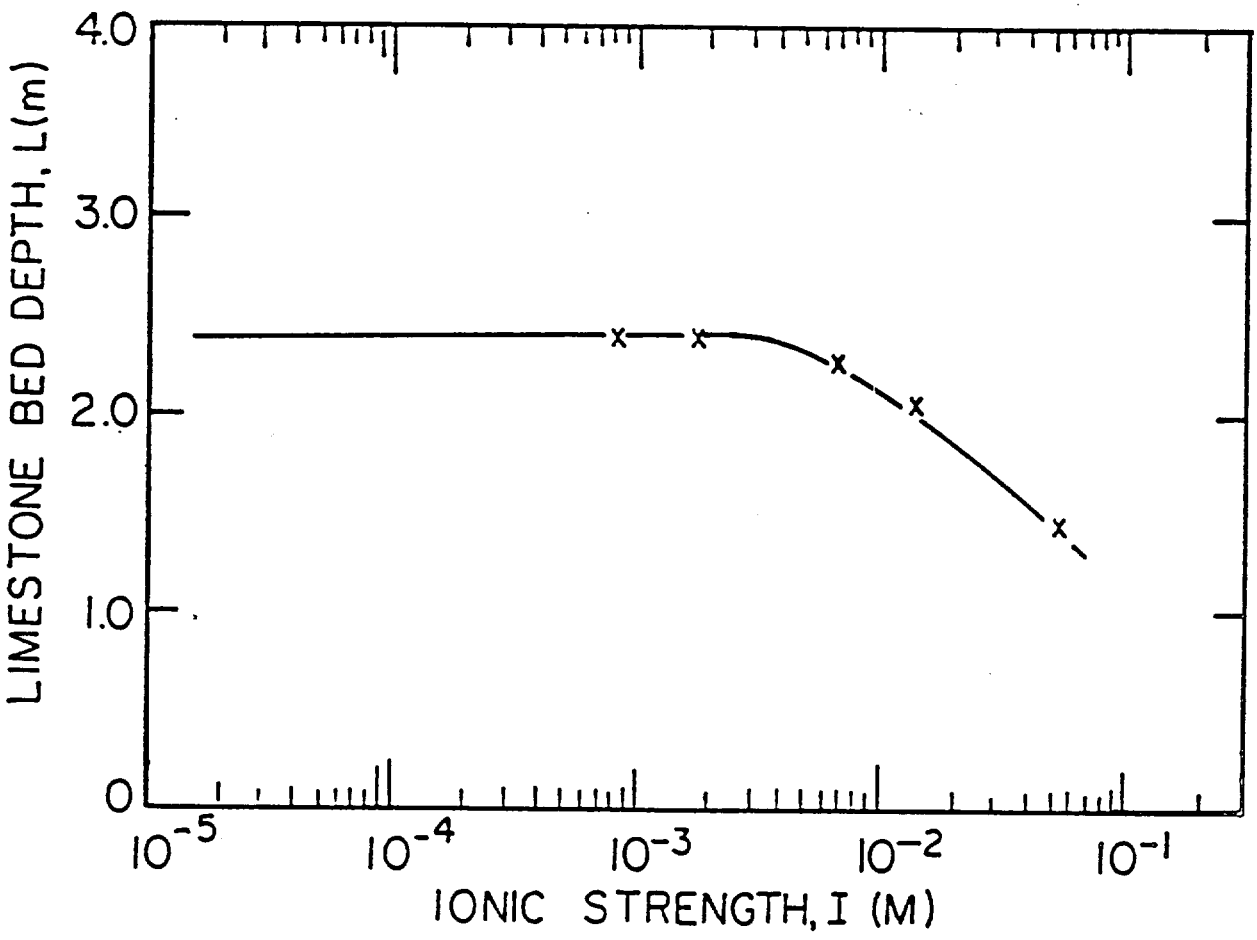

Figure 48. Total depth of limestone required to obtain an effluent pH of 8.5 plotted as a function of the ionic strength. The influent was assumed to have the average conditions used in the sensitivity analysis calculations.

ance area diagrams were made. These diagrams were constructed over a range of pH values and either various dissolved inorganic carbon concentrations (closed to gasesous CO_2) or partial pressures of CO_2 (open system).

As discussed previously, there is considerable uncertainty in the thermodynamic solubility of $Pb(OH)_2$. As a result, predominant area diagrams were constructed for both proposed values of the solubility constant (log*Kso = 8.15, Wagman et al., 1969; log*Kso = 13.07, Topelman, 1929). For constant dissolved inorganic carbon systems (closed atmospheric), $PbSO_4$ is the stable mineral phase under acidic (pH < 6) conditions with low dissolved inorganic carbon concentrations (Figure 49 and 50). Note that the solubility of lead increases substantially with decreases in pH. It is unlikely that equilibrium with $PbSO_4$ would ever be obtained below pH 6. Therefore under these conditions, concentrations of lead are likely controlled by dissolution kinetics.

In the neutral pH range $PbCO_3$ becomes the stable lead-controlling solid phase at modest dissolved inorganic carbon concentrations (10^{-5} mol·l^{-1}). With increases in dissolved inorganic carbon concentrations, the pH range over which $PbCO_3$ controls solubility increases. In the alkaline pH range, the lead regulating solid phase is in doubt. If a $Pb(OH)_2$ solubility constant (log*Kso) of 13.07, is assumed then $Pb_3(OH)_2(CO_3)_2$ is the thermodynamically stable solid phase. This condition is similar to that proposed by Schock (1980). However, if a $Pb(OH)_2$ solubility constant of 8.15 (log*Kso) is assumed then this lower solubility constant suggests that $Pb(OH)_2$ is the thermodynamically stable passivation film under high pH, low dissolved inorganic carbon conditions. Unfortunately, because of this uncertainty in thermochemical data it is impossible to evaluate the lead controlling solid phase by thermodynamic calculations.

Both variations in pH and dissolved inorganic carbon concentrations have a profound influence on the solubility of lead (Figure 51). Lead concentrations are highest under low pH conditions and generally decrease with increasing pH. When a $Pb(OH)_2$ log*Kso of 8.15 is assumed, the theoretical solubility of Pb can be reduced below the MCL above the pH range 7.5 to 8.5 (Figure 51). Variations in dissolved inorganic carbon concentrations alter the pH-dependent solubility trend of lead. Note that under acidic conditions (pH <7), however, dissolved inorganic carbon acts to enhance lead solubility through the formation of soluble lead carbonate complexes. actually, pH 7?

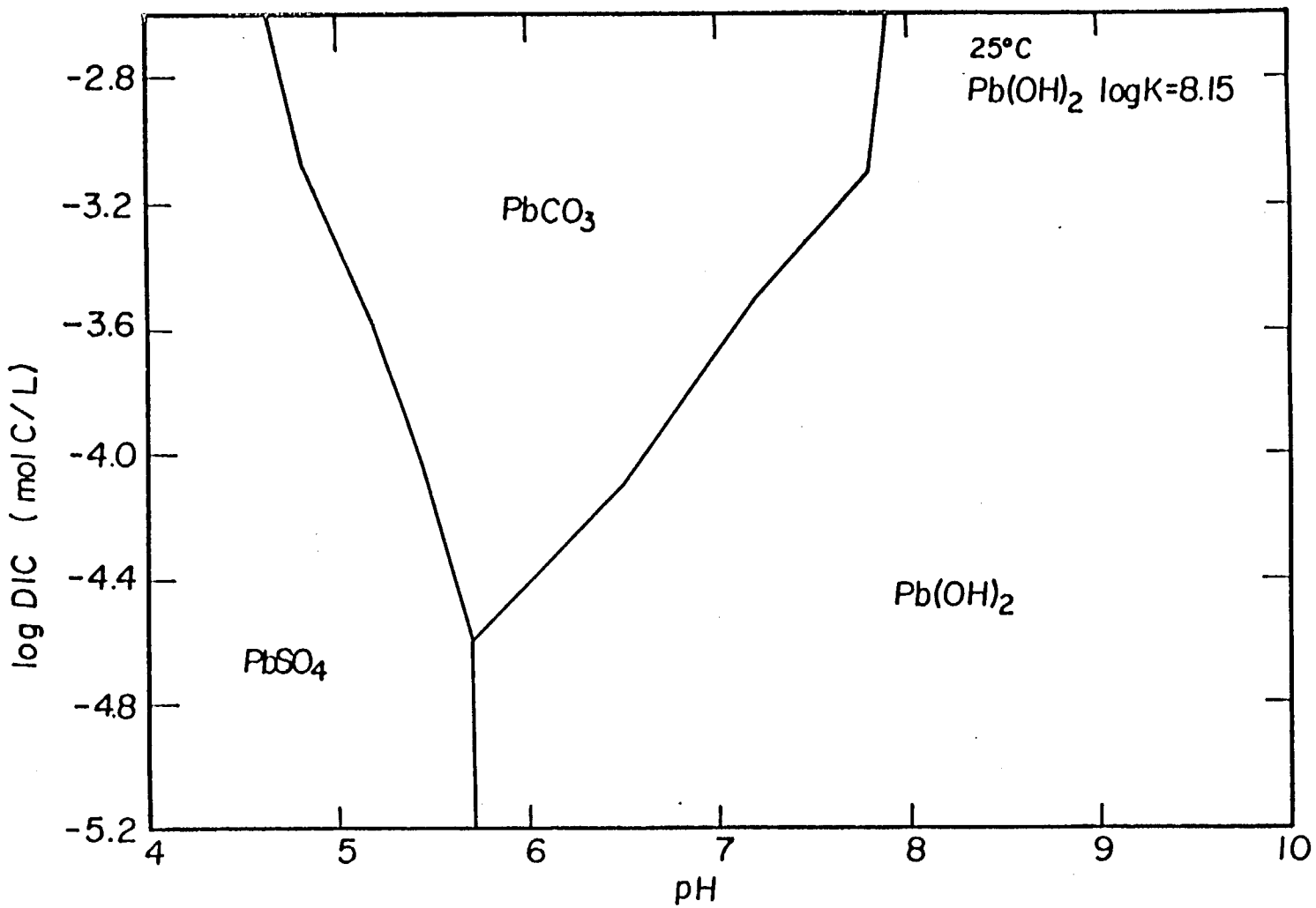

Figure 49. Predominance area diagram for the stability of lead passivation films over a range of pH and dissolved inorganic carbon concentrations at 25°C. A p*Kso of -8.15 for the solubility of $Pb(OH)_2$ was assumed.

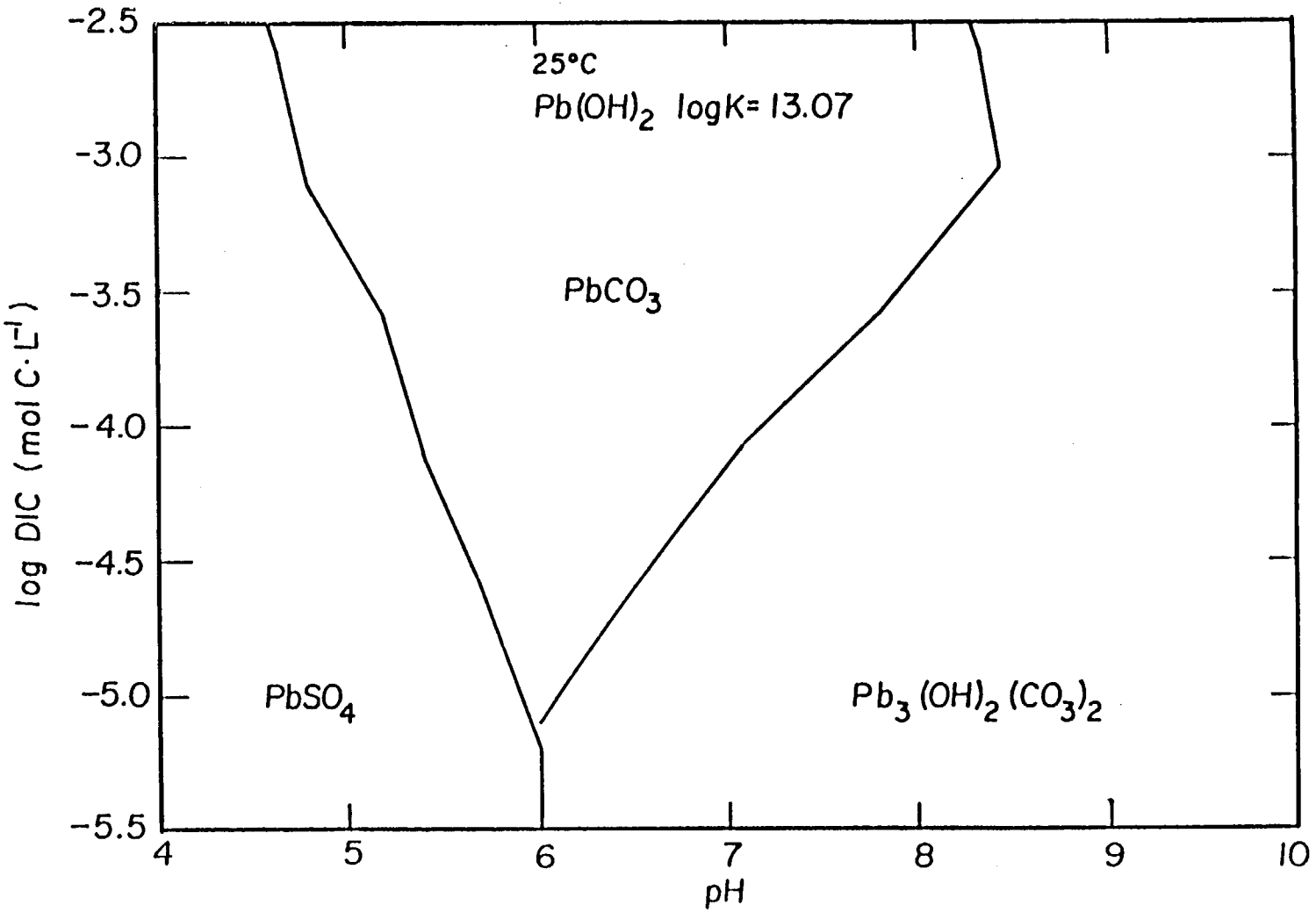

Figure 50. Predominance area diagram for the stability of lead passivation films over a range of pH and dissolved inorganic carbon concentrations at 25°C. A p*Kso of -13.07 for the solubility of $Pb(OH)_2$ was assumed.

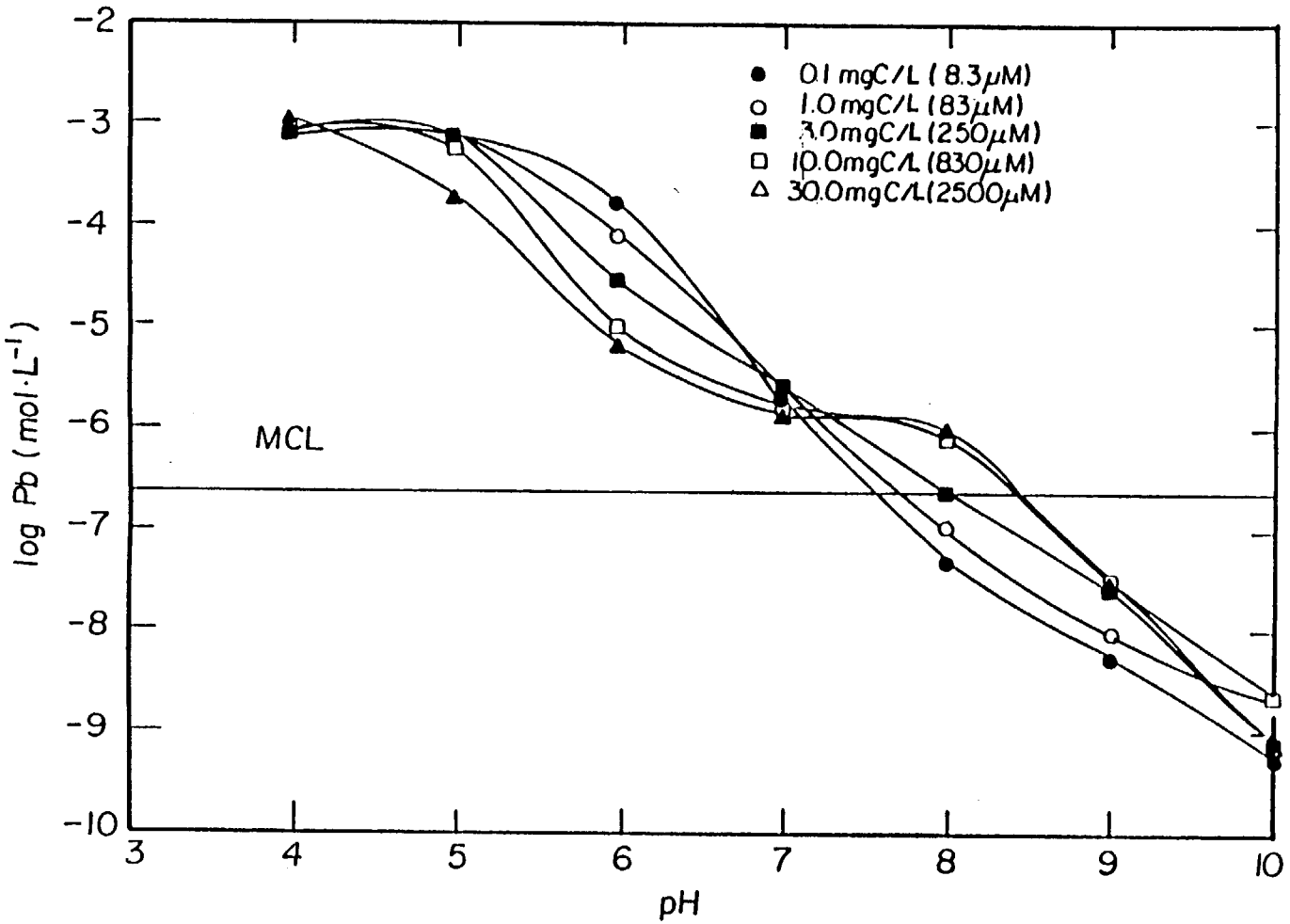

Figure 51. Lead concentrations calculated with the chemical equilibrium model MINEQL as a function of pH for several concentrations of dissolved inorganic carbon. The maximum contaminant level (MCL) for lead is indicated.

In systems that are in equilibrium with gaseous CO_2 the formation of $PbCO_3$ is the predominant stable mineral phase under essentially all but very acidic conditions (pH < 5.5; Figures 52 and 53). However, note that when the solubility of $Pb(OH)_2$ (log*Kso) is assumed to be 8.15, then $Pb(OH)_2$ becomes the solubility controlling mineral phase under low partial pressures of CO_2 Figure 52). Like under conditions of constant dissolved inorganic carbon concentrations, variations in the partial pressure of CO_2 alter the pH dependent solubility of lead (Figure 54). At pH values below 7 elevated partial pressures of CO_2 serve to reduce lead concentrations through the formation of $PbCO_3$, while at pH values above 7 increased partial pressure of CO_2 enhances lead solubility through the formation of soluble lead carbonate complexes. Note that even at atmospheric levels of CO_2 ($10^{-3.5}$ atm), the solubility of lead in equilibrium with gaseous CO_2 exceeds the MCL (Figure 54).

Variations in water chemistry also influence the stability of copper passivation films (Figure 55). Under low pH and high dissolved inorganic carbon concentrations $Cu_2(OH)_2CO_3$ is the thermodynamically stable passivation film, while under high pH, low dissolved inorganic carbon concentrations $Cu(OH)_2$ appears to regulate copper solubility. Variations in dissolved inorganic carbon concentrations do not alter the solubility of copper to the same extent as lead (Figure 54). At pH values below 7 to 8, increased concentrations of inorganic carbon, either under constant dissolved inorganic carbon (closed atmosphere) or through the solubility of gaseous CO_2, act to reduce copper concentrations by the formation of $Cu_2(OH)_2CO_3$. Unlike lead, copper does not form strong carbonate complexes. Therefore copper solubility at elevated pH is only enhanced at extremely high carbonate concentrations associated with high partial pressures of CO_2 (Figure 57). Note that reductions in copper below the MCL can be accomplished by increasing pH values above 7.

As discussed by Schock (1984), under most conditions the solubility of zinc is regulated by $Zn_5(OH)_6(CO_3)_2$ (Figure 58 and 59). Only with high inorganic carbon concentrations can $ZnCO_3$ become the stable passivation film. Trends in the pH-dependent solubility of Zn at different dissolved inorganic carbon concentrations (Figure 60) or partial pressure of CO_2 (Figure 61) are similar to copper. The solubility of zinc generally decreases with in-

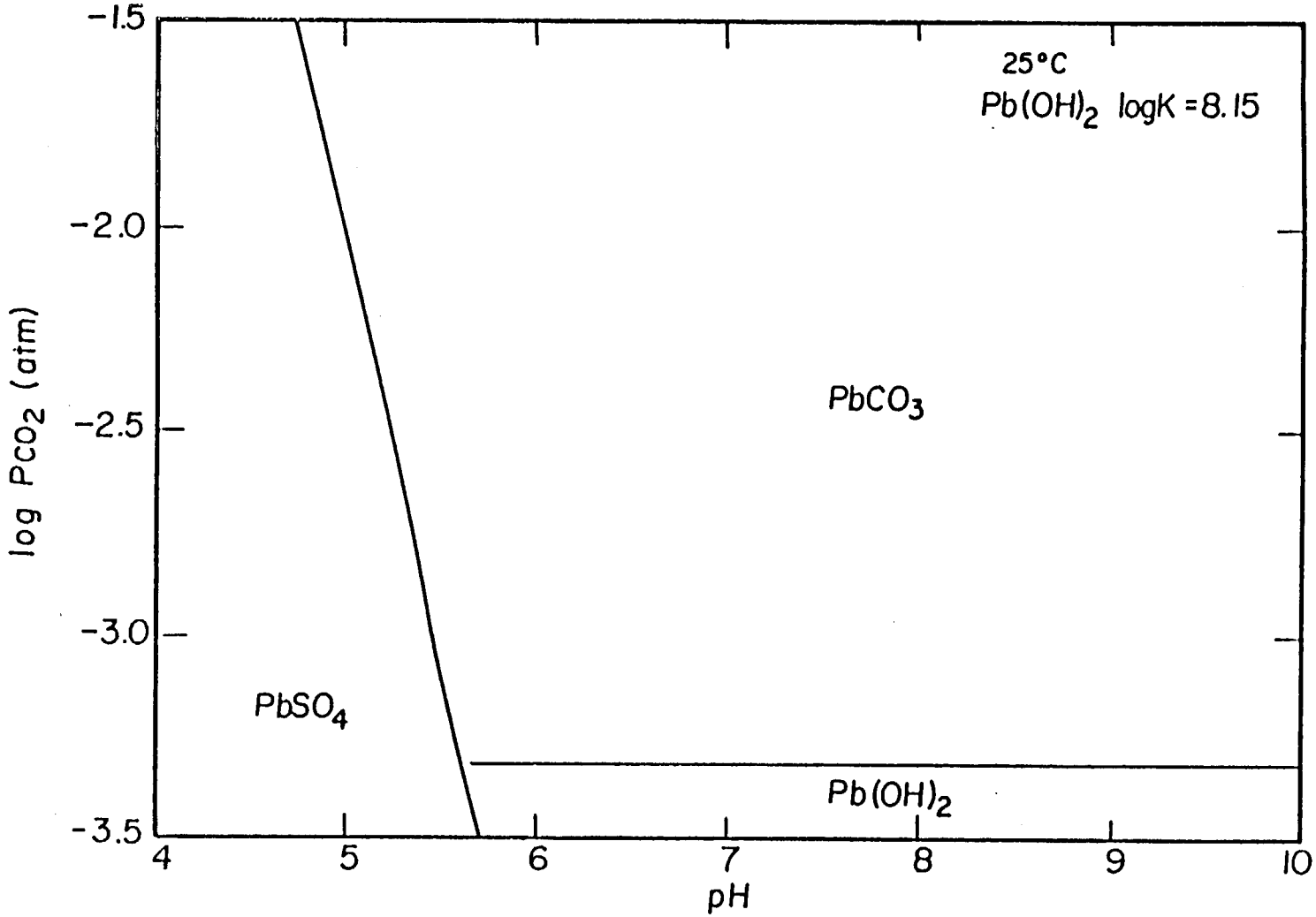

Figure 52. Predominance area diagram for the stability of lead passivation films over a range of pH and partial pressures of CO_2 at 25°C. A p*Kso of -8.15 for the solubility of $Pb(OH)_2$ was assumed.

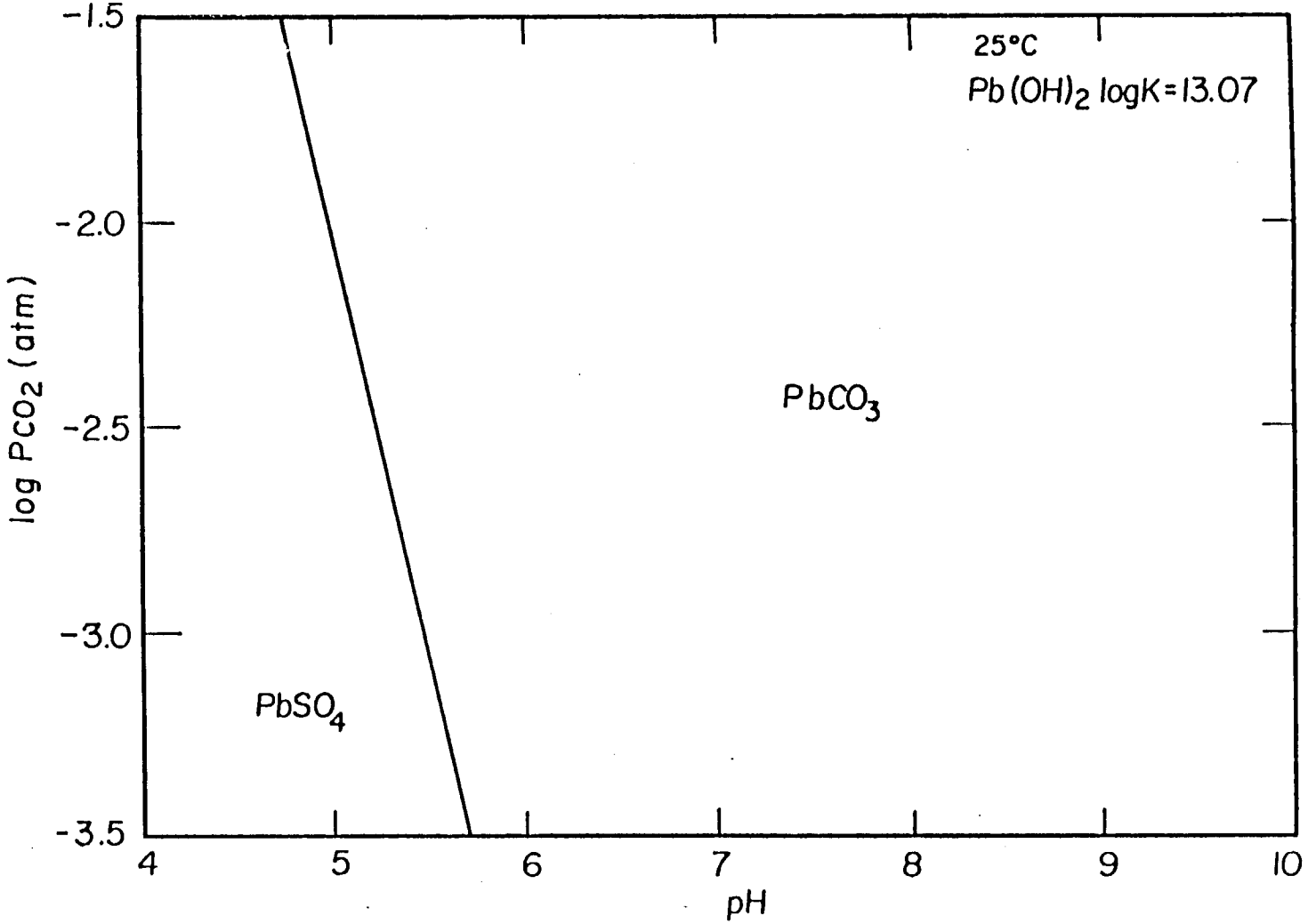

Figure 53. Predominance area diagram for the stability of lead passivation films over a range of pH and partial pressures of CO_2 at 25°C. A p*Kso of -13.07 for the solubility of $Pb(OH)_2$ was assumed.

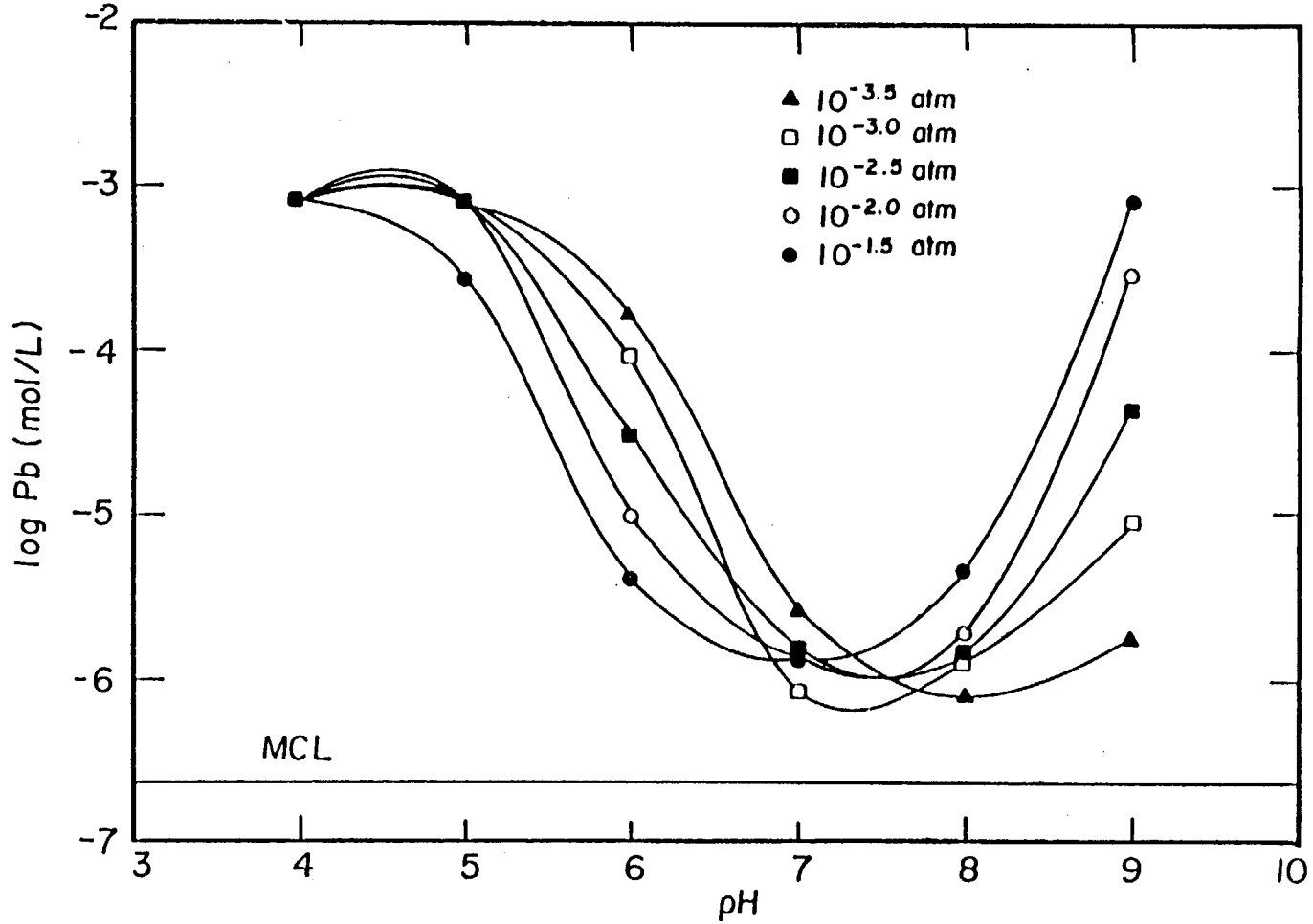

Figure 54. Lead concentrations calculated with the chemical equilibrium model MINEQL as a function of pH for several partial pressures of CO_2. Calculations are in equilibrium with gaseous CO_2. The maximum contaminant level (MCL) for lead is indicated.

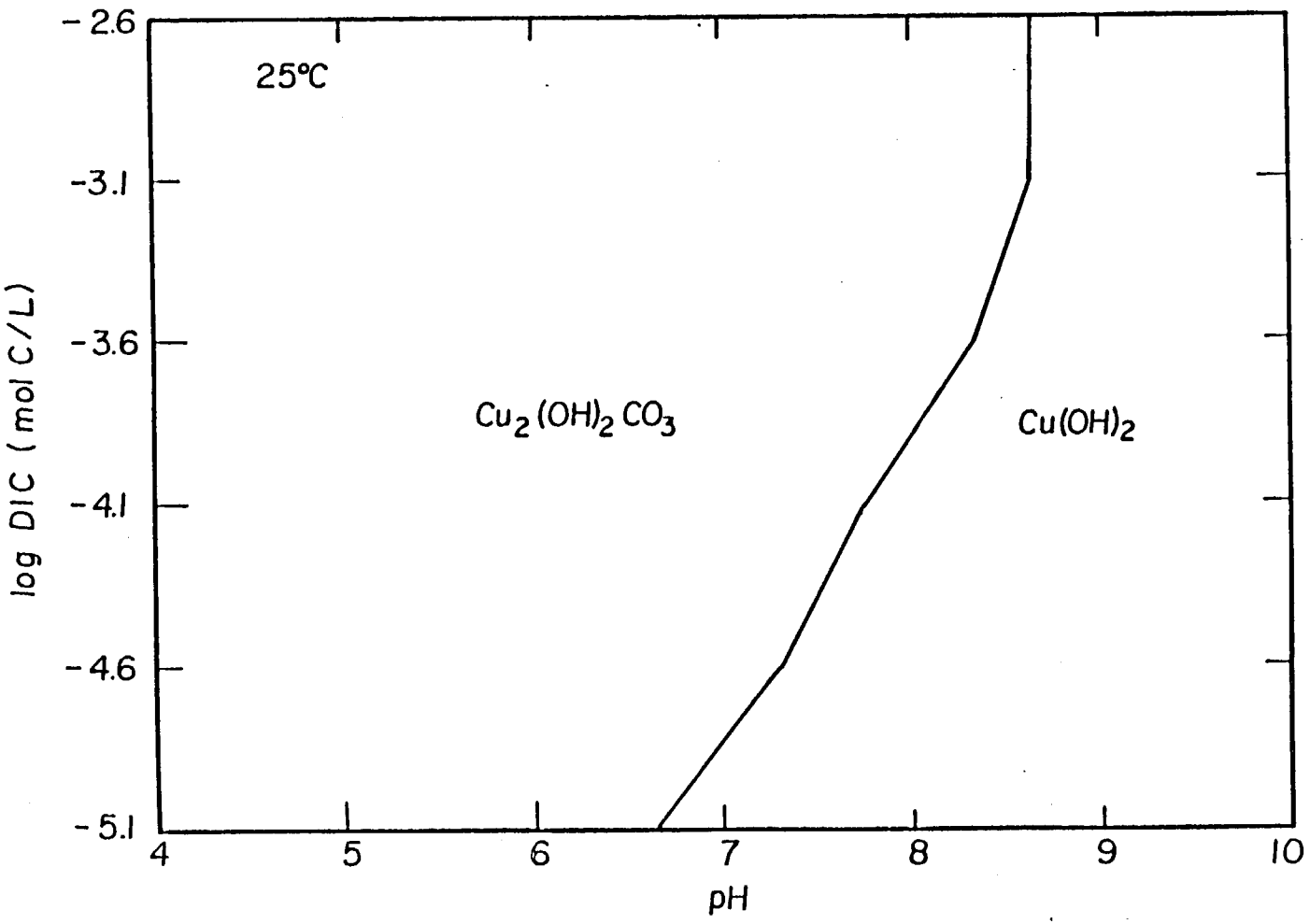

Figure 55. Predominance area diagram for the stability of copper passivation films over ranges of pH and dissolved inorganic carbon concentrations at 25°C.

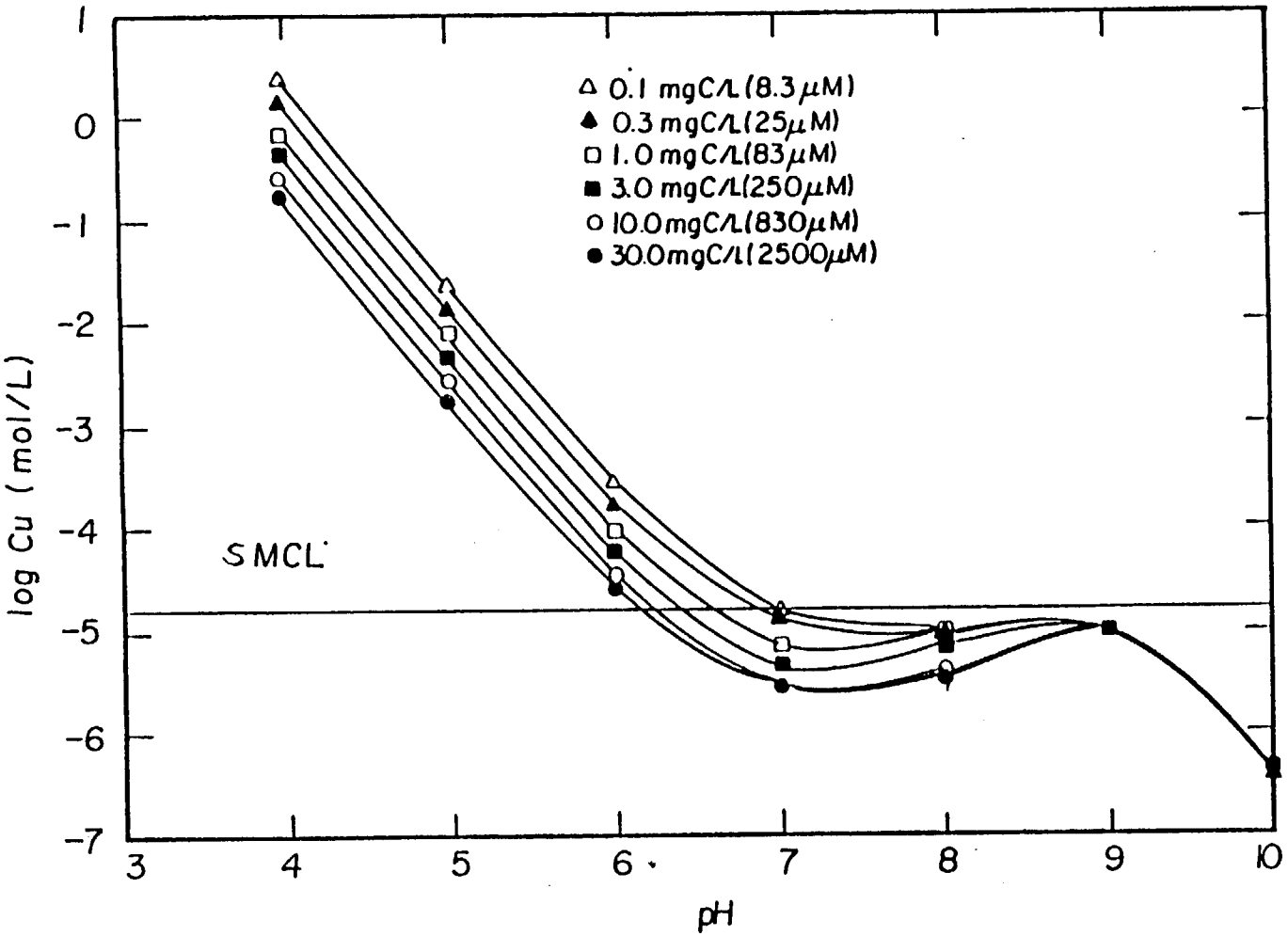

Figure 56. Copper concentrations calculated with the chemical equilibrium model MINEQL as a function of pH for several concentrations of dissolved inorganic carbon. The secondary maximum contaminant level (SMCL) for copper is indicated.

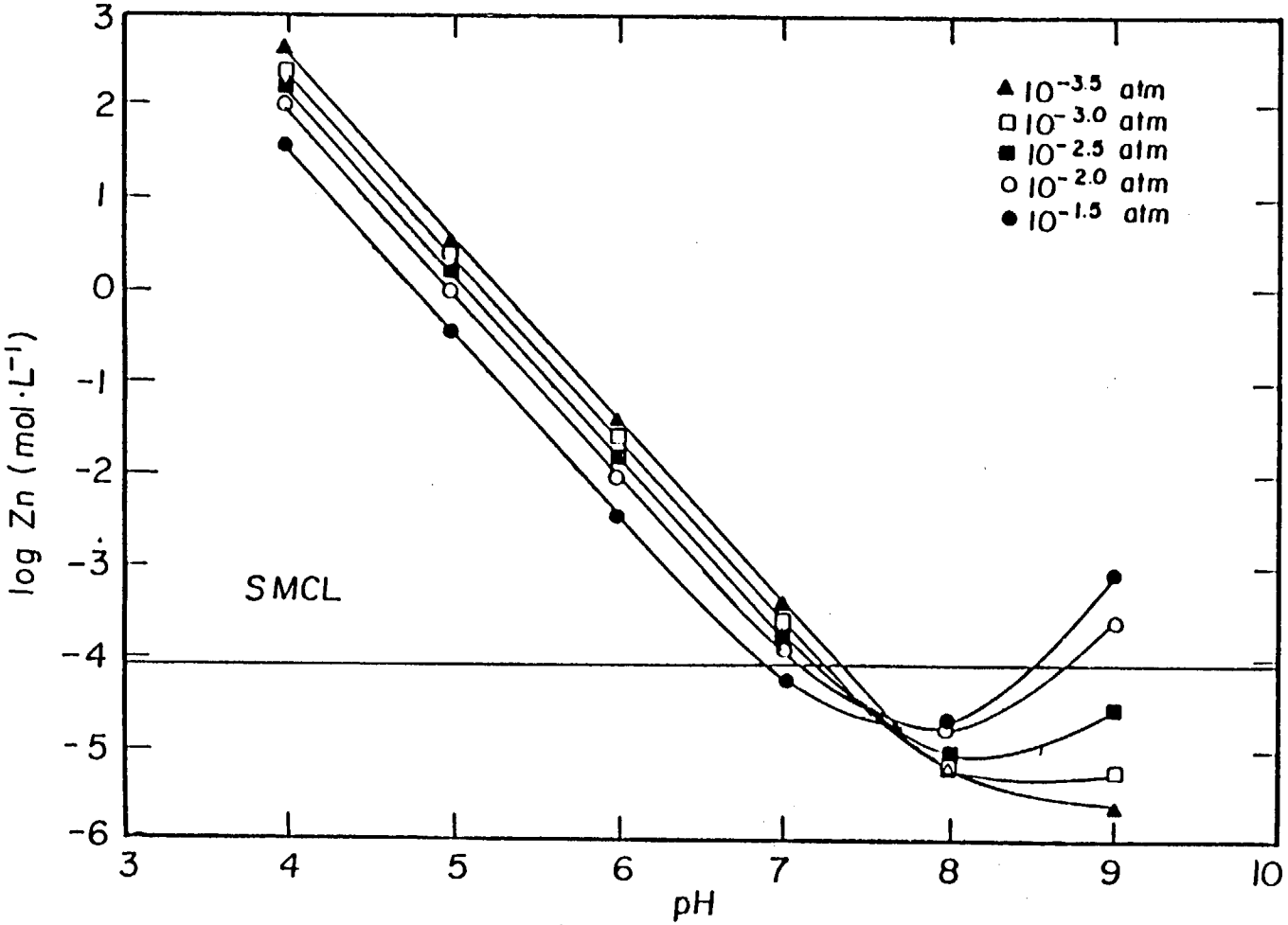

Figure 57. Copper concentrations calculated with the chemical equilibrium model MINEQL as a function of pH for several partial pressures of CO_2. Equilibrium with gaseous CO_2 is assumed. The secondary maximum contaminant level (SMCL) for copper is indicated.

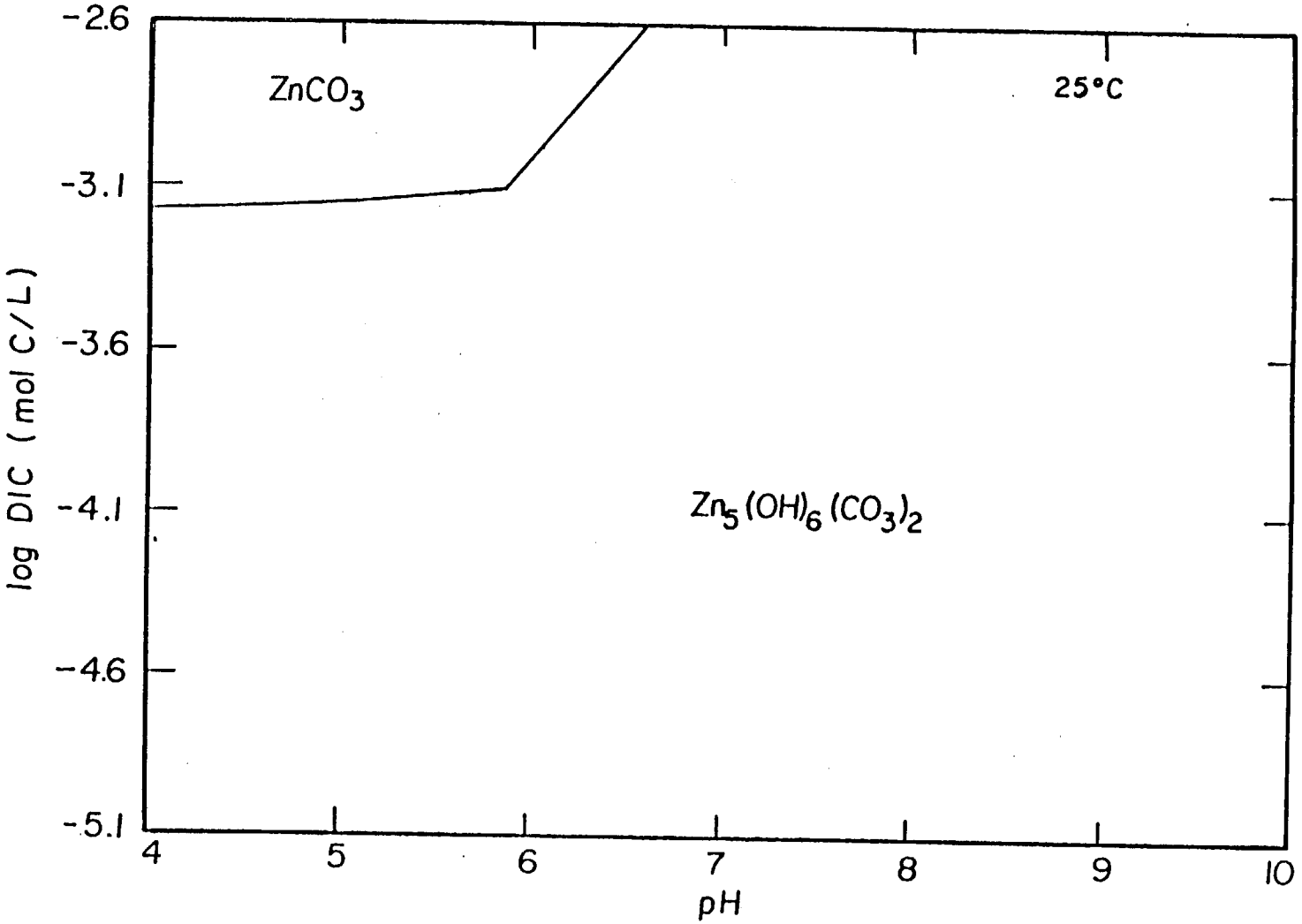

Figure 58. Predominance area diagram for the stability of zinc passivation films over a range of pH and dissolved inorganic carbon concentrations at 25°C.

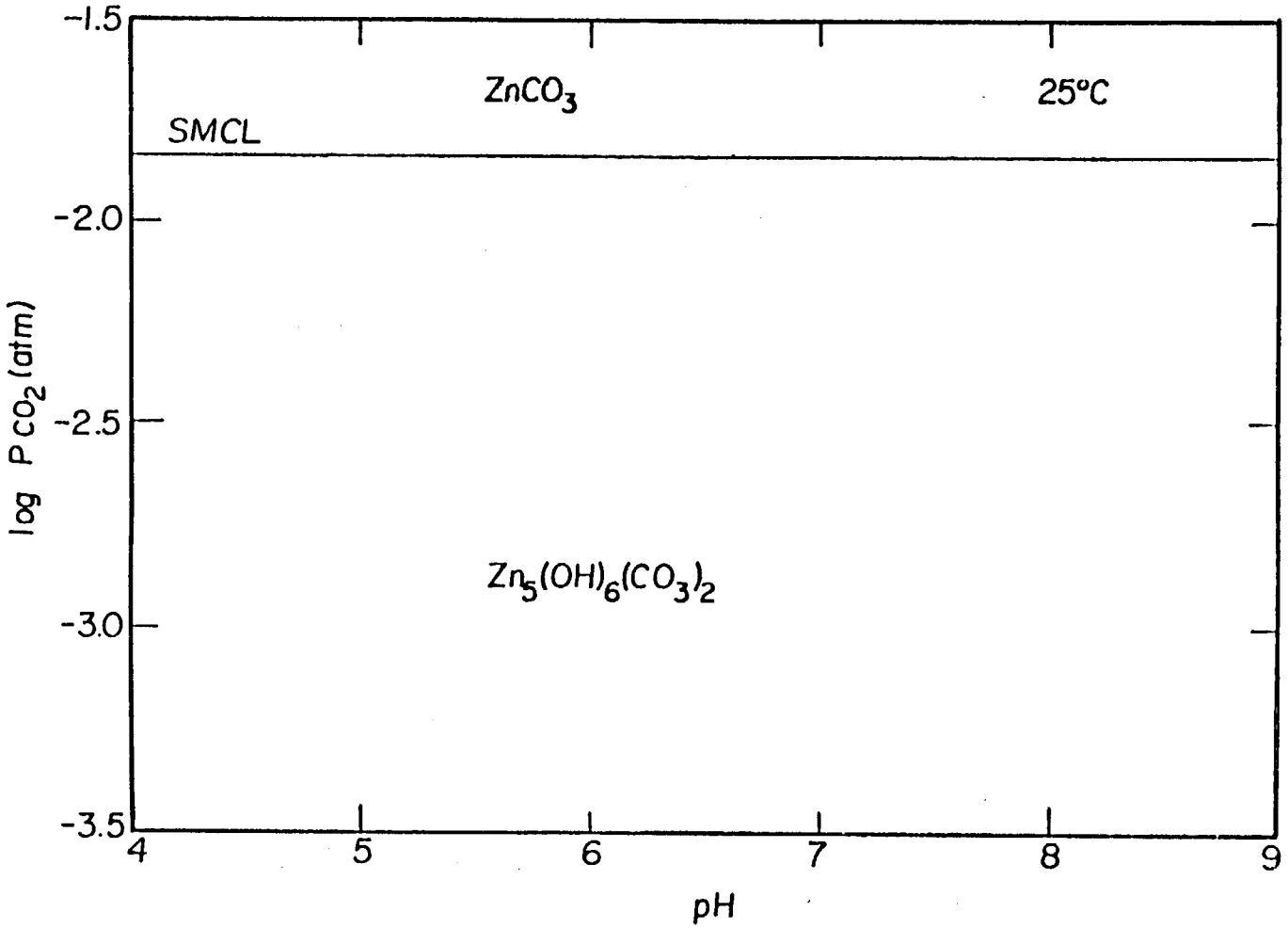

Figure 59. Zinc concentrations calculated with the chemical equilibrium model MINEQL as a function of pH for several dissolved inorganic carbon concentrations. The secondary maximum contaminant level (SMCL) for zinc is indicated.

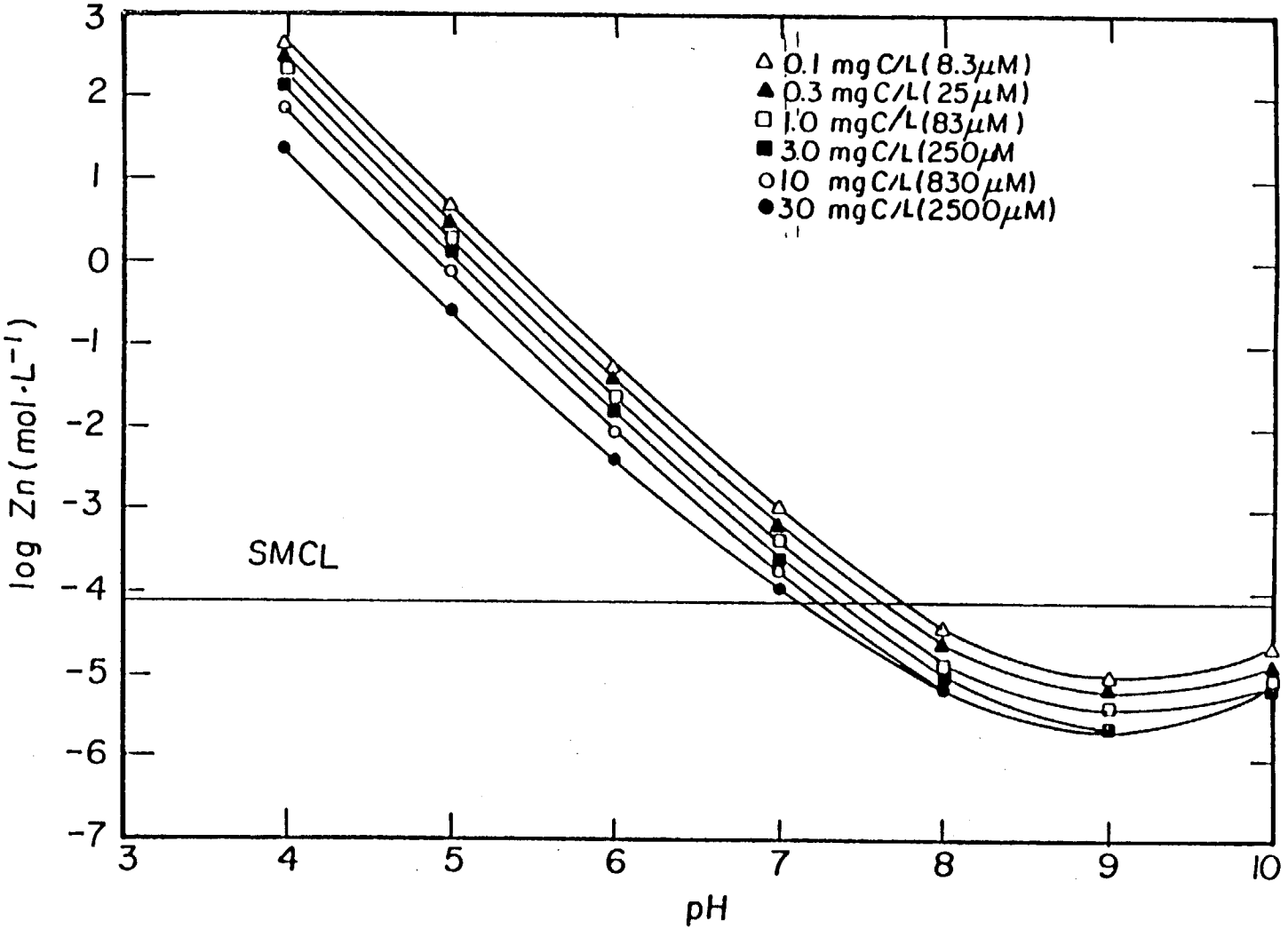

Figure 60. Predominance area diagram for the stability of zinc passivation films over ranges of pH and partial pressures of CO_2 at 25°C.

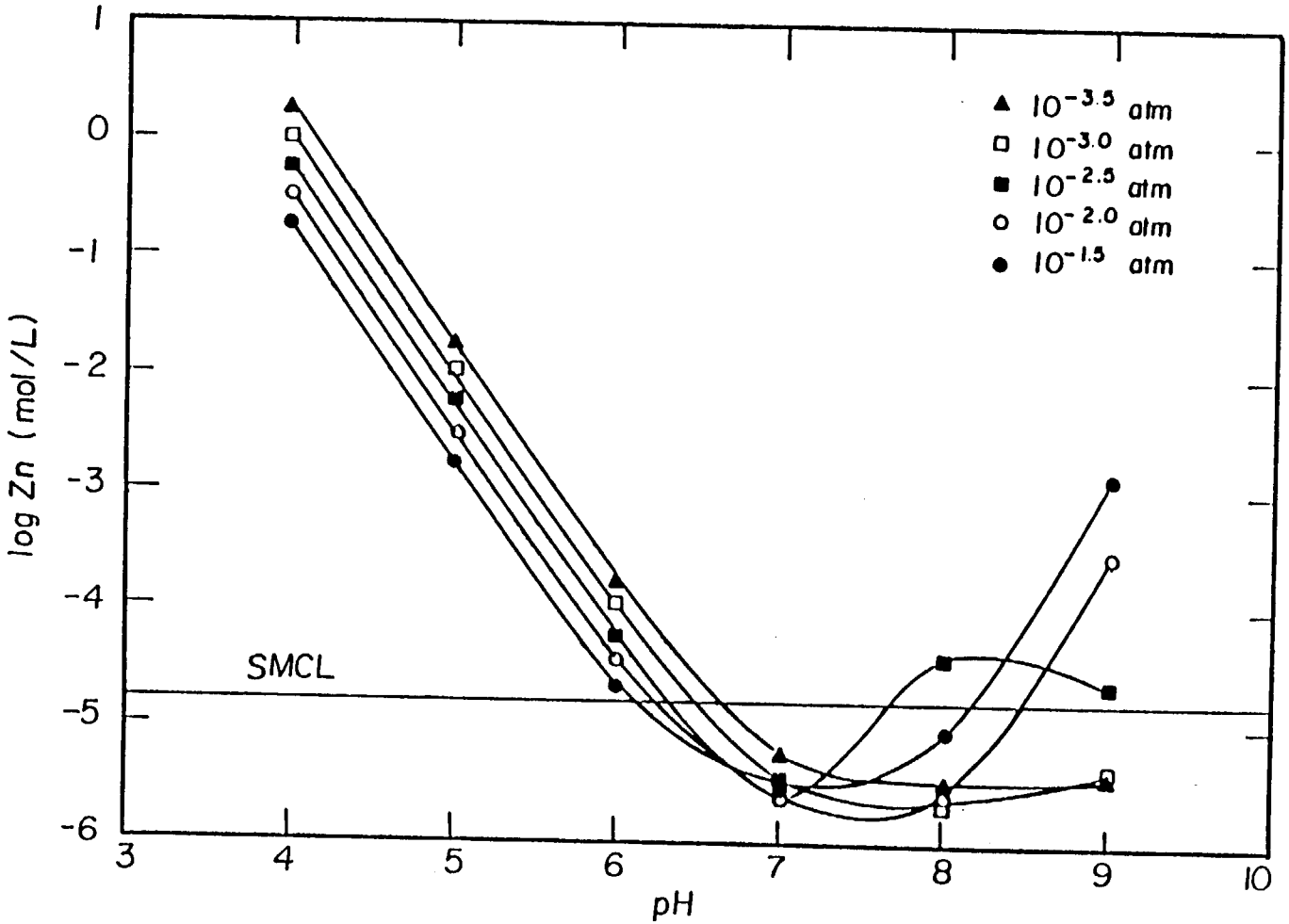

Figure 61. Zinc concentrations calculated with the chemical equilibrium model MINEQL as a function of pH for several partial pressures of CO_2. Calculations are in equilibrium with gaseous CO_2. The secondary maximum contaminant level (SMCL) for zinc is indicated.

creasing pH. If pH values are above 7 to 8, zinc concentrations generally fall below the MCL. Increases in dissolved inorganic carbon concentrations (or partial pressure of CO_2) generally result in a decrease in the solubility of Zn. Like copper, zinc forms relatively weak aqueous complexes with carbonate so the solubility of zinc is only enhanced when the carbonate concentrations are extremely high due to high pH values and elevated partial pressure of CO_2.

PIPE LEACHING EXPERIMENTS

A series of experiments was conducted to evaluate the extent to which calcium carbonate treatment could reduce the corrosivity of dilute acidic waters. Aliquots of water obtained from the ports of the laboratory limestone column were sealed in one meter pipe sections for ten hours and analyzed for trace metals. Results of lead (Figure 62) and zinc leaching experiments (Figure 63) with lead and galvanized steel pipe sections, respectively, yielded inconsistent results. Concentrations of both metals were highly variable and demonstrated no systematic trends with the level of treatment of pH. As mentioned previously, both lead and zinc may form non-adhering passivation films. The extremely high scattered concentrations observed for these experiments may be a reflection of this condition. The lead pipe experiments, were repeated (Figure 64) and aliquots of leachate were analyzed for both total and filtered (Filtration through 0.40 μm polycarbonate filter) lead. In some samples considerable discrepancy was evident between total and filtered lead concentrations. Note that very fine particulate lead, capable of passing a 0.40 μm filter, may be released from lead pipe. It appears that the release of particulate metal was a complicating factor in the lead and galvanized steel pipe leaching experiments.

Additional leaching experiments were conducted by applying aliquots of water from various stages of laboratory contactor treatment with sections of copper pipe and copper pipe with lead-tin solder joints. To illustrate results from these experiments measured water chemistry parameters as a function of limestone column depth (0.96 diameter particle) at a flow rate of 5 liters/minute are plotted in Figure 65. As discussed earlier with increasing contact with calcium carbonate pH (Figure 65a) and dissolved inorganic carbon

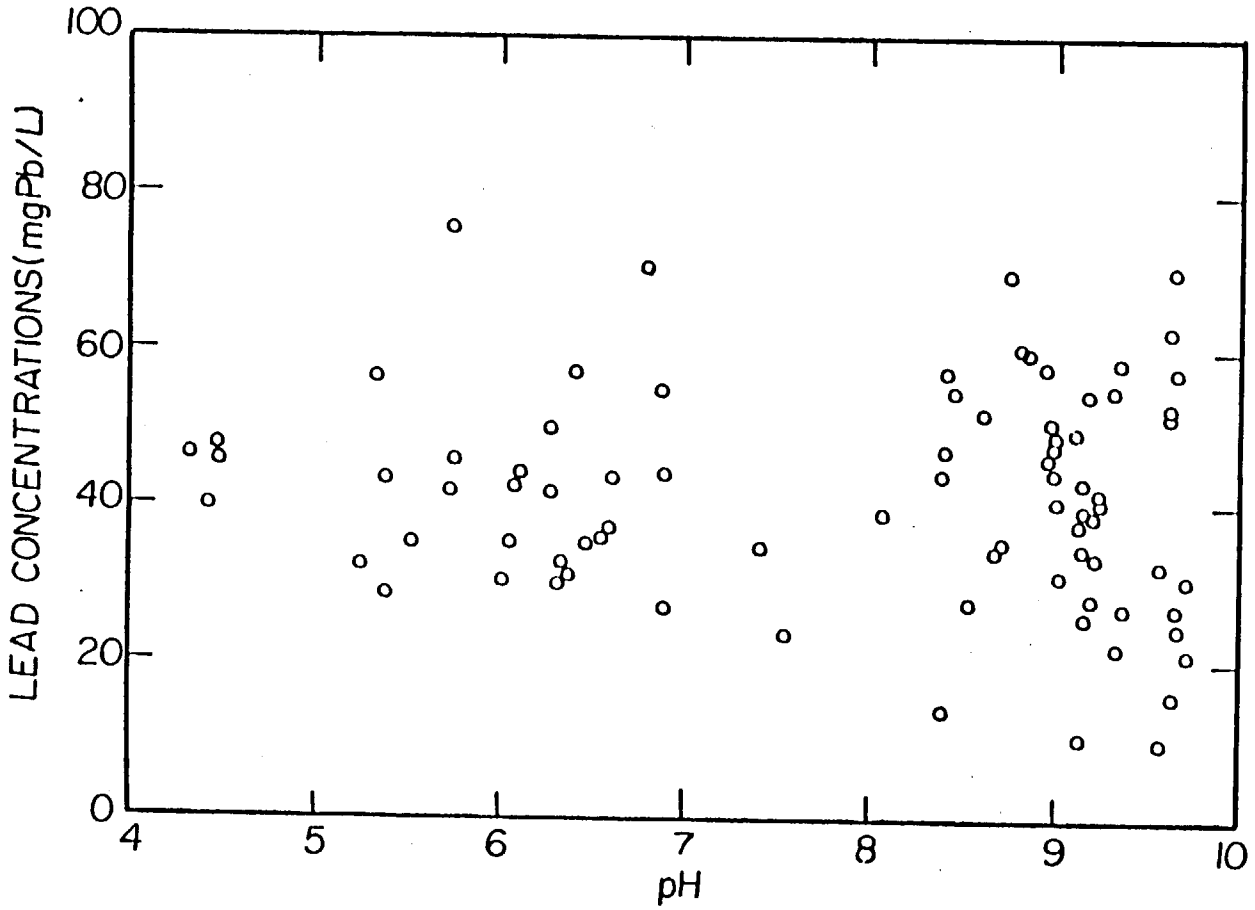

Figure 62. Lead concentrations from lead pipe section leaching experiments.

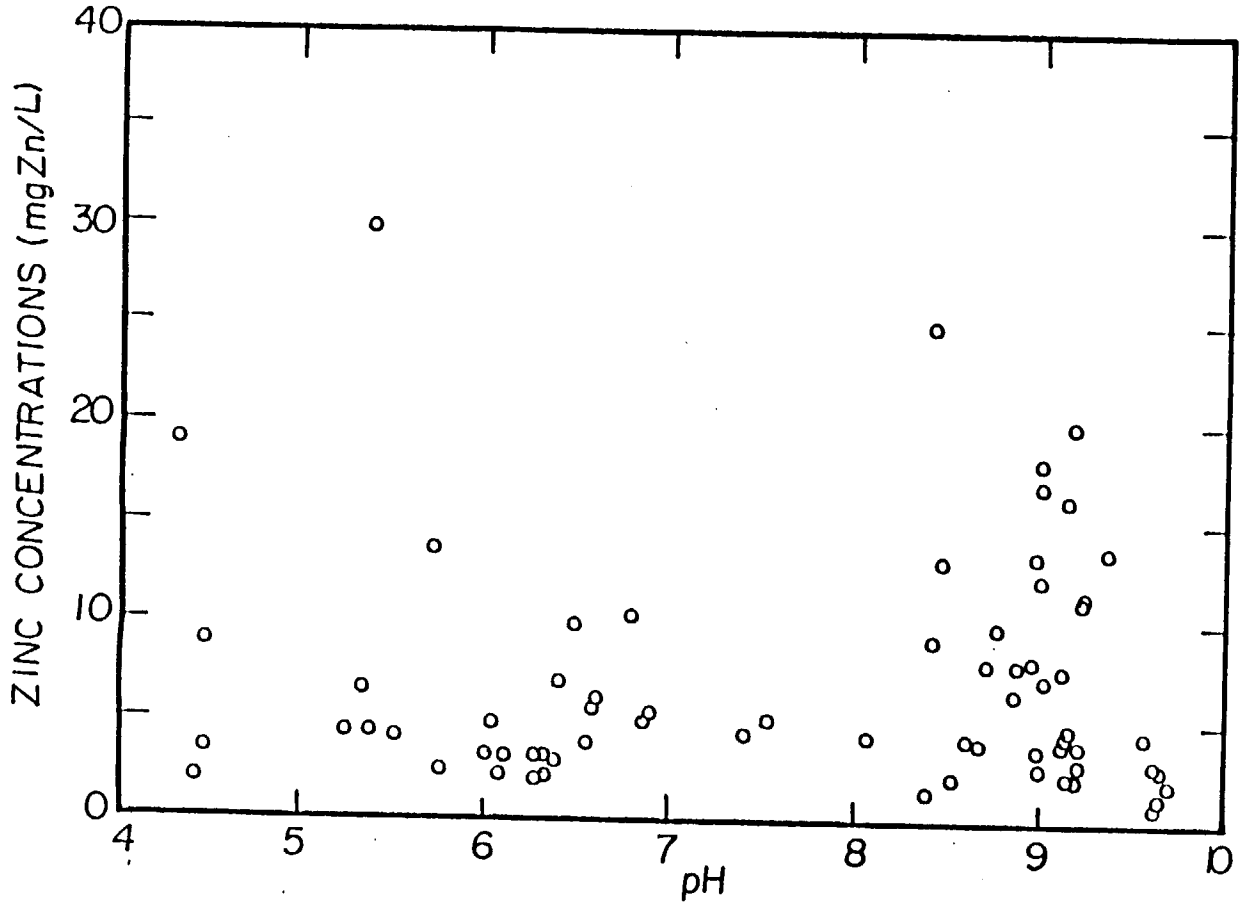

Figure 63. Zinc concentrations from galvanized steel pipe section leaching experiment.

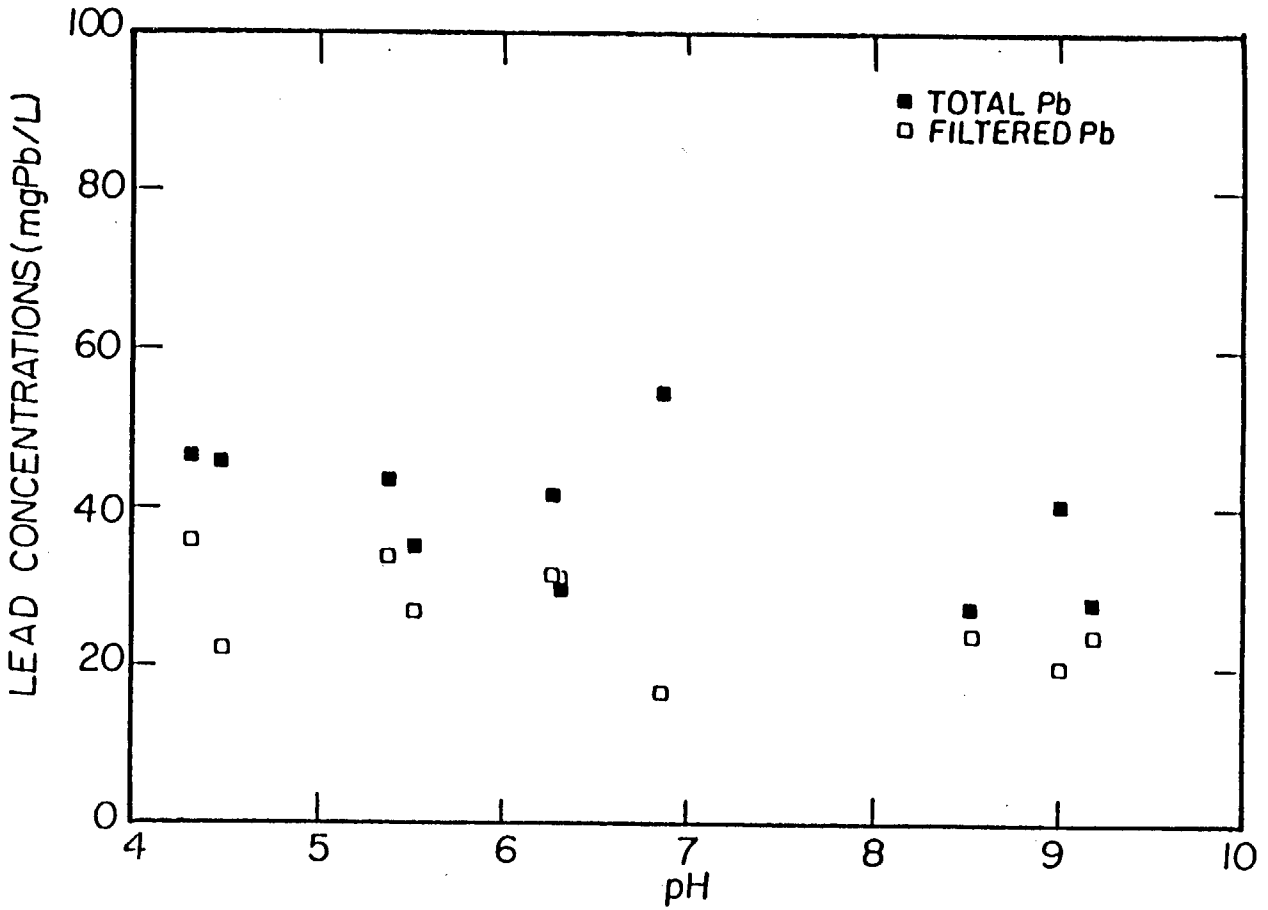

Figure 64. Total and filtered concentrations of lead from lead pipe section leaching experiments.

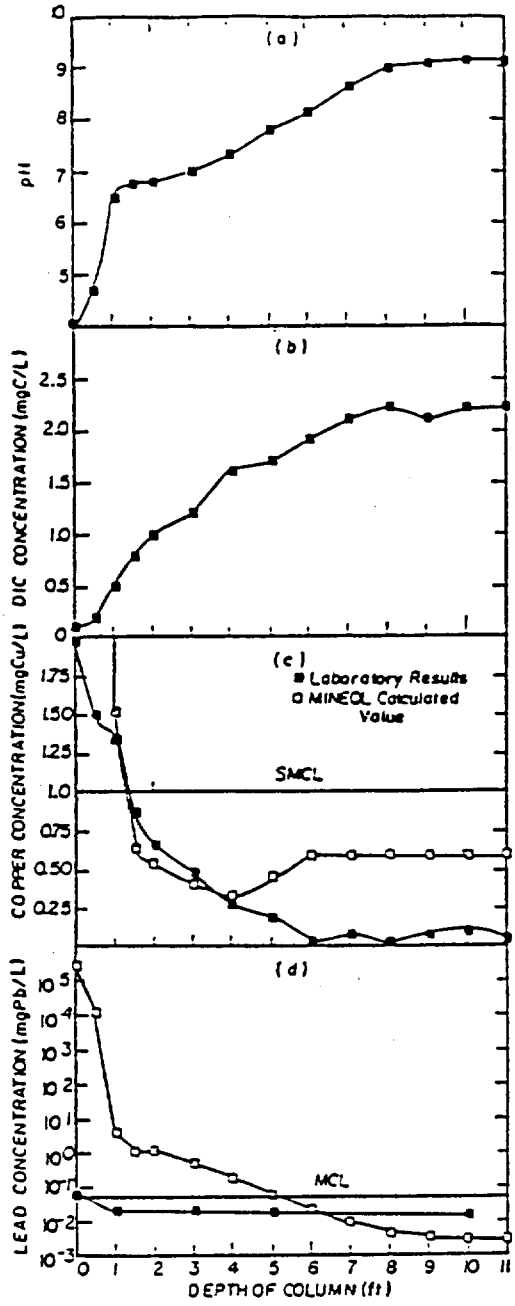

Figure 65. Variations in pH (a), dissolved inorganic carbon (DIC) concentrations (b), and measured copper (c) and lead (d) concentrations from pipe section leaching experiments as a function of column treatment by $CaCO_3$. The experimental conditions were 0.96 cm diameter $CaCO_3$ and a flow rate of 5 liters/min. Calculated values of copper (c) and lead (d) obtained from MINEQL calculations are plotted for comparison. The secondary maximum contaminant level (SMCL) for copper and the maximum contaminant level (MCL) for lead are indicated.

concentrations (Figure 65b) increased resulting in a pronounced decrease in copper concentrations from pipe section leachates (Figure 65c). Unlike copper, lead concentrations from lead-tin solder joints did not exhibit marked variations (Figure 65d), although lead concentrations did decrease somewhat with increased contactor treatment. Superimposed on the results of trace metal leaching experiments (Figures 65c, 65d) are predicted concentrations from measured water chemistry (e.g. pH: Figure 65a, dissolved inorganic carbon; Figure 65b) using the chemical equilibrium model MINEQL. Note that generally the MINEQL calculations followed measured copper concentrations (Figure 65c). However, some discrepancy was evident under acidic conditions, associated with minimum calcium carbonate treatment, and under the higher pH conditions (pH 7.5 to 9.5), associated with greater contactor treatment. The former may be attributed to non-equilibrium conditions. Acidic water chemistry resulted in measured copper concentrations that were highly undersaturated with respect to the solubility of $Cu_2(OH)_2CO_3$, probably due to insufficient contact time with the copper pipe. Under these conditions, aqueous copper concentrations were probably controlled by dissolution kinetics. There is also an apparent deviation between measured predicted concentrations associated with the higher level of treatment. Again laboratory results were highly undersaturated with respect to anticipated mineral phase solubility. This discrepancy is most likely due to one of two considerations. First, the deviation coincides with the shift from $Cu_2(OH)_2CO_3$ to $Cu(OH)_2$ passivation films. Second, the predominant form of aqueous copper under these conditions is $Cu(OH)_2(aq)$. Uncertainity in thermodynamic data of one or both of these copper forms may be responsible for the deviation between measured and predicted values.

There was poor agreement between measured values of lead from lead-tin solder leaching experiments and values predicted from MINEQL (Figure 65d) (MINEQL calculations were made by assuming $\log^*K_{so} = 8.15$). Note that under low pH conditions lead concentrations were highly undersaturated with respect to anticipated lead mineral phase solubility. These results are not surprising given the relatively small contact area associated with lead-tin solder joints.

Results of all copper pipe and lead-tin solder leaching experiments from limestone contactor treated water are summarized in Figure 66 and 67,

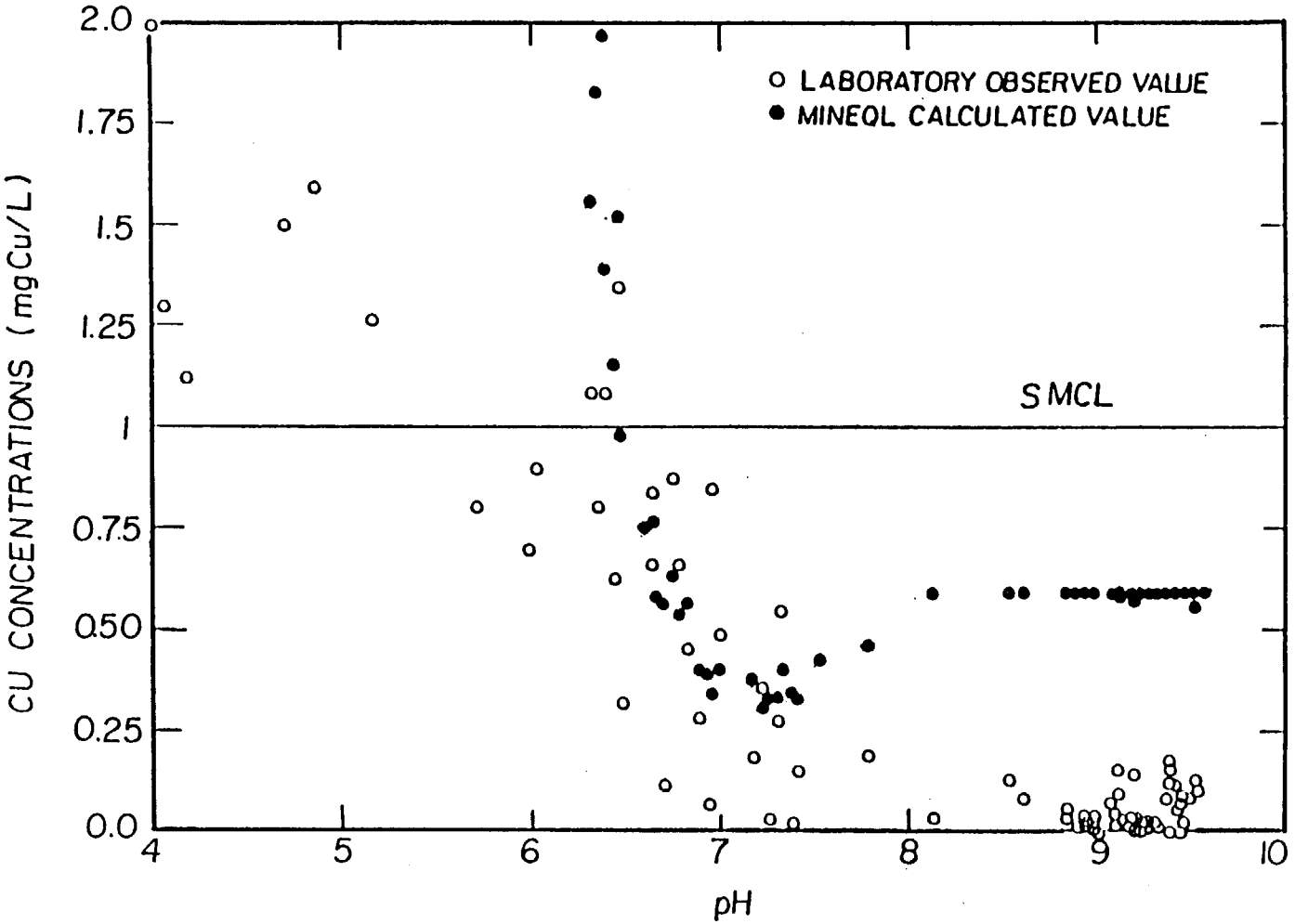

Figure 66. Copper concentrations from copper pipe section leaching experiments at various levels of $CaCO_3$ treatment (variations in pH). The corresponding values of copper calculated with the chemical equilibrium model MINEQL are indicated. The secondary maximum contaminant level (SMCL) for copper is indicated.

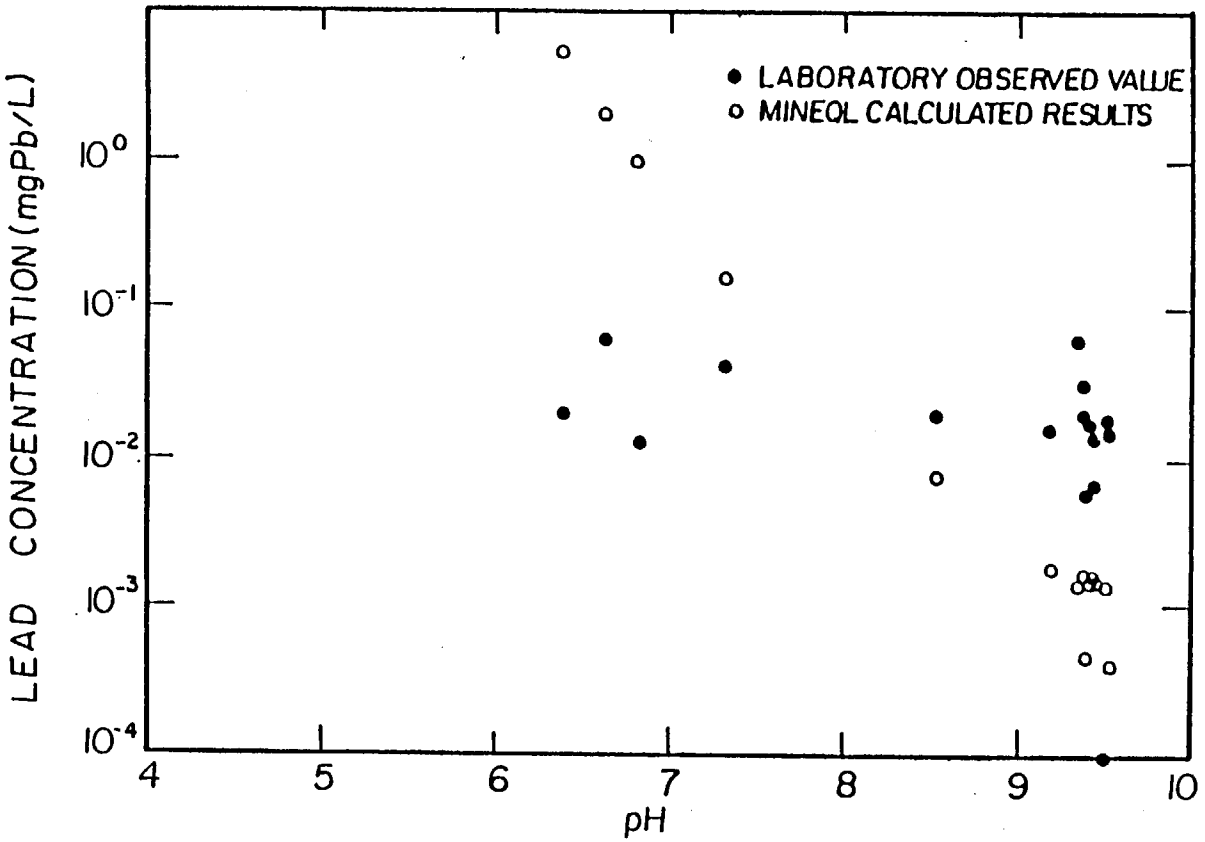

Figure 67. Lead concentrations from copper pipe section with lead-tin solder leaching experiments at various levels of laboratory $CaCO_3$ treatment (variations in pH). The corresponding values of lead calculated with the chemical equilibrium model MINEQL are indicated.

respectively. Again measured copper concentrations systematically increased with decreasing pH. Measured results were qualitatively consistent with MINEQL predictions however again a discrepancy was evident under low pH (pH < 6; low $CaCO_3$ treatment) and under higher pH (pH > 7.5, greater $CaCO_3$ treatment) conditions. As discussed previously unlike MINEQL predictions, measured lead concentrations were relatively insensitive to changes in pH and calcium carbonate treatment (Figure 67).

METAL RELEASE FROM FIELD SITE

Trace metal concentrations were monitored in inlet spring and lake water, as well as tapwater from two cabins, Hillside and Bay Side (Figure 9). During most of the study period, water to these cottages was obtained from the spring and was treated with the box contactor. During certain times it was possible to collect untreated tapwater at Covewood (Figure 9). Therefore, trace metal concentrations from Covewood tapwater served as reference values for treated spring tapwater at Hillside and Bay Side. During the spring 1984, lake water was used as a water supply to Bay Side. This water was treated with a wound fiberglass column contactor. During this latter study both treated and reference (untreated) samples were collected from Bay Side tapwater.

Spring Contactor Treatment

Copper, lead and zinc concentrations were elevated (significant at the 0.05 level; two tailed t-test) in tapwater samples relative to untreated spring water (Table 27). The source of zinc was probably largely leaching from two 400 gallon water storage tanks, made of galvanized steel, located immediately down flow of the spring with the box contactor. Although fewer samples were analyzed for concentrations of other trace metals, there was no statistically significant evidence of leaching (or deposition) of cadmium, manganese, iron or aluminum within the water distribution system relative to the influent spring water (Table 27).

As reported in other studies (e.g. Meranger et al., 1984) trace metal concentrations were highest with the "first-flush" after tapwater had been in contact with the distribution system overnight. Copper and lead concentrations were significantly reduced (at the 0.05 level; two tailed t-test) in tapwater which had been flushed for three minutes (Table 28).

TABLE 27 Comparison of trace metal concentration (as mg/L) in spring water and from the first flush of treated (Hillside, Bay Side) and untreated (Covewood) cottages.

Metal	Spring		Hillside		Bay Side		Covewood	
	n	mean ± std. dev.	n	mean ± std. dev.	n	mean ± std. dev.	n	mean ± std. dev.
Copper	19	0.0047 ± 0.0087	8	0.087 ± 0.049	14	0.030 ± 0.37	4	1.9 ± 0.31
Lead	13	0.0027 ± 0.0043	7	0.018 ± 0.024	13	0.0084± 0.0084	3	0.046 ± 0.0040
Cadmium	6	0.0014 ± 0.0012		---	4	0.0010 ± 0.0010		---
Zinc	8	0.025 ± 0.017	2	0.26	6	0.26 ± 0.18		---
Manganese	8	0.0044 ± 0.006	2	<0.001	6	0.0043 ± 0.005		---
Iron	10	0.07 ± 0.11	4	0.11 ± 0.15	7	0.13 ± 0.19	1	0.11
Aluminum	10	0.064 ± 0.074	4	0.016 ± 0.014	7	0.018 ± 0.018	1	0.056

TABLE 28 Comparison of copper and lead concentrations (mean ± std. dev. as mg/L) from first flush and three minutes of flowing tapwater derived from the box contactor treated spring.

	Hillside			Bayside		
	n	First Flush	Three Minutes	n	First Flush	Three Minutes
Copper	(7)*	0.091 ± 0.052	0.007 ± 0.011	(10)*	0.32 ± 0.38	0.031 ± 0.050
Lead	(6)	0.021 ± 0.025	0.0074 ± 0.0096	(8)*	0.0069 ± 0.0084	0.0049 ± 0.0045
Zinc	(2)	0.26	0.07	(6)*	0.26 ± 0.16	0.061 ± 0.041

*Indicates three minute flowing samples were significantly lower than first flush samples at 0.05 level (two tailed t-test).

Contactor treatment appeared to diminish the corrosivity of the spring water (Table 27). Concentrations of copper and lead at both Hillside and Bay Side were significantly lower (at the 0.05 level; two-tailed t-test) than the reference tapwater at Covewood. The apparent decrease in both copper and lead solubility may be attributed to the increase in pH and dissolved inorganic carbon concentrations associated with $CaCO_3$ treatment (Table 17). These trends are consistent with the theoretical solubility of copper and lead passivations films discussed previously (e.g Figures 56 and 51, respectively).

Substantial variation was evident in trace metal concentrations. To illustrate this variability the probability distribution of copper and lead concentrations in first-flush tapwater were plotted for both treated and untreated springwater (Figures 68 and 69, respectively). The probability of treated springwater exceeding the secondary MCl for copper was low ($\sim$ 4%), particularly in comparison with the untreated spring supply. However, note that relatively few observations were available for untreated first-flush tapwater.

Our results suggest that the probability of first-flush tapwater, derived from the treated spring, exceeding the MCL for lead was extremely low (Figure 69). (None of the first-flush tapwater samples from the treated spring supply exceeded 0.05 mg Pb/L). Note however, that some of our untreated spring tapwater samples (2 out of 3 collected) exceeded th MCL for lead.

The variability of trace metal concentrations in this field phase of study is not surprising. Cottages were generally in use during sample collection. While we attempted to collect tap water samples in the early morning to obtain maximum metal concentration from an overnight leaching period, this controlled collection was not always possible. Moreover, lead in tapwater samples was largely derived from lead-tin solder joints. Given that two joints are present on the average at every 2 m of pipe, it is not surprising that the concentrations were so variable.

Lake Contactor Treatment

Both treated and untreated tapwater at Bay Side were also greatly enriched in both copper and lead concentrations relative to the lake water supply

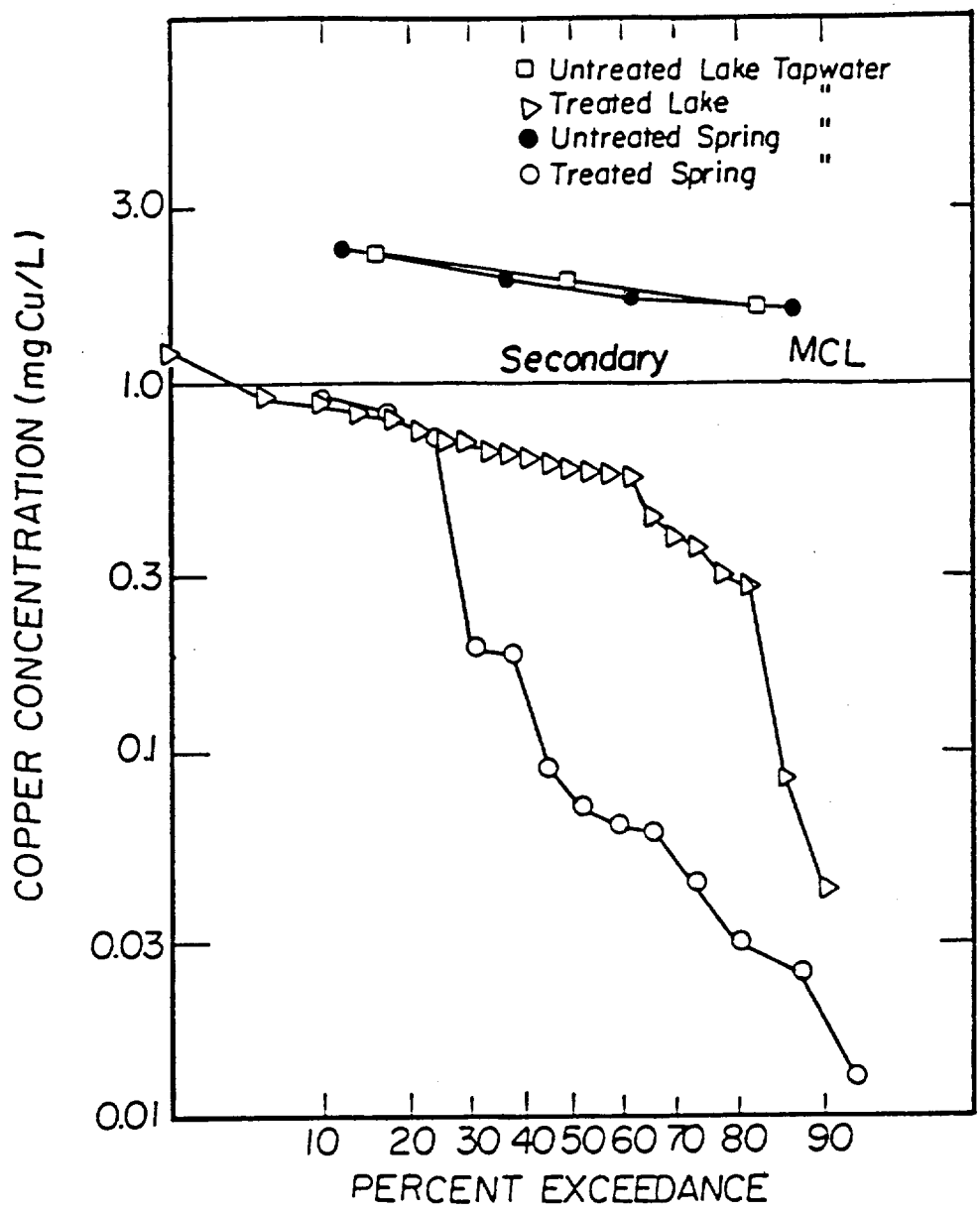

Figure 68. The probability of copper concentrations in untreated and $CaCO_3$ treated lake and spring waters exceeding a given concentration. The secondary maximum contaminant level (SMCL) for copper is indicated.

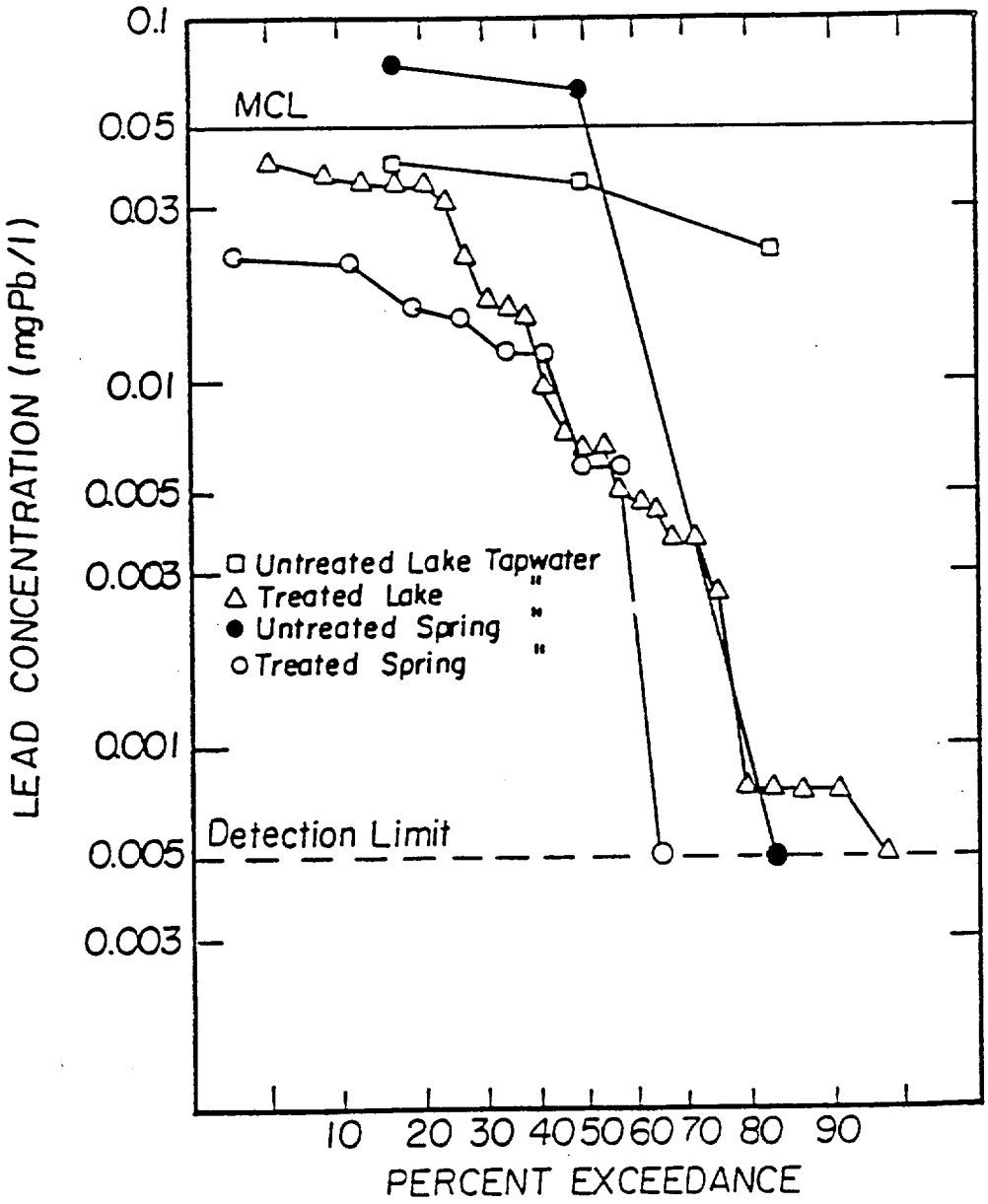

Figure 69. The probability of lead concentrations in untreated and $CaCO_3$ treated lake and spring waters exceeding a given concentration. The maximum contaminant level (MCL) for lead is indicated.

(Table 29). However, again tapwater treated with the limestone contactor were significantly lower (at the 0.05 level; two tailed t-test) than untreated lakewater samples, for both copper and lead. As we observed from the spring water supply, metal concentrations were generally greatly reduced in tapwater that had been flowing for three minutes relative to the first flush (Table 30). The exception to this trend was that no statistically significant difference in lead concentrations were evident between first flush and three minute flowing samples in the treatment cottage.

To evaluate the applicability of chemical equilibrium modeling to the field observations, theoretical concentrations of both copper and lead were calculated using measured water chemistry (e.g. pH, DIC) with the equilibrium model MINEQL. These calculations were then compared to first-flush tapwater concentrations obtained from the lake contactor equipment. Results from the lake contactor experiment were better suited to evaluate the chemical equilibrium model than the spring contactor experiments because sample collection was conducted under more controlled conditions. We have confidence that the first-flush tapwater collected from this phase of the study had been in contact with the cottage piping system for a prolonged period of time (.e.g overnight) and therefore may be used to depict equilibrium conditions.

Untreated lakewater samples were highly acidic (pH = 4.60 $\pm$ 0.1) and therefore it is not surprising that measured concentrations of both copper and lead were highly undersaturated with respect to mineral phase solubility. (The theoretical solubility of copper and lead for untreated lake water were 370 $\pm$ 1500 mg Cu/L and 69 $\pm$ 1.0 mg Pb/L, respectively). These results are similar to the metal pipe experiments discussed previously and suggest that under highly acidic conditions metal concentrations were regulated by kinetics rather than equilibrium solubility.

Copper concentrations of treated lakewater, however, were qualitatively consistent with MINEQL calculations (Figures 70 and 71). Although measured and calculated copper concentrations were similar for the treated lakewater, there were considerable scatter in the measured values. Unlike MINEQL predictions, measured first-flush copper concentrations did not demonstrate a systematic increase in copper concentration with decrease in pH over the pH range measured (pH 6.3 to 7.5).

TABLE 29 Metal Concentrations (as mg/L) in lake influent, untreated and treated first flush tapwater at Bay Side

	Lakewater		Untreated		Treated	
	n	mean ± std. dev.	n	mean ± std. dev.	n	mean ± std. dev.
Copper	27	<0.0005	3	1.9 ± 0.35	25	0.54 ± 0.30
Lead	27	0.0034 ± 0.0049	3	0.033 ± 0.009	26	0.015 ± 0.014

Table 30 Comparison of copper and lead concentrations (mean ± std. dev. as mg/L) from first flush and after three minutes of flowing tapwater derived from both $CaCO_3$ treated and untreated lakewater.

	Untreated			Treated		
	n	First Flush	Three Minutes	n	First Flush	Three Minutes
Copper	3*	1.92 ± 0.35	0.082 ± 0.072	5*	0.63 ± 0.099	0.027 ± 0.040
Lead	3*	0.033 ± 0.009	0.013 ± 0.007	5	0.005 ± 0.0009	0.011 ± 0.012

*Indicates three minute flowing samples were significantly lower than first flush samples at 0.05 level (two tailed t-test).

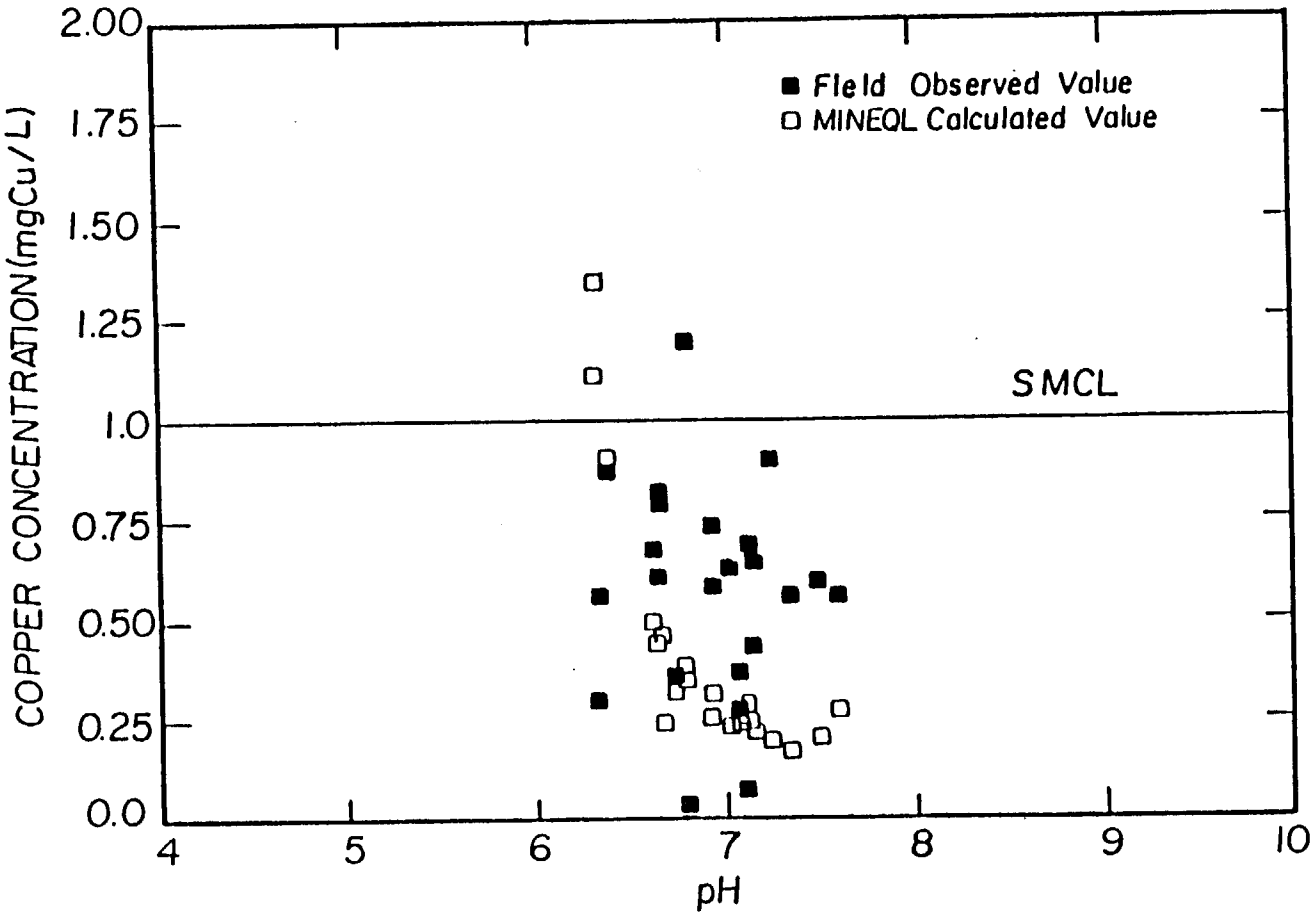

Figure 70. A comparison of measured copper concentrations from first flush tapwater derived from $CaCO_3$ treated lakewater and calculated values from the chemical equilibrium model MINEQL as a function of pH. The secondary maximum contaminant level (SMCL) for copper is indicated.

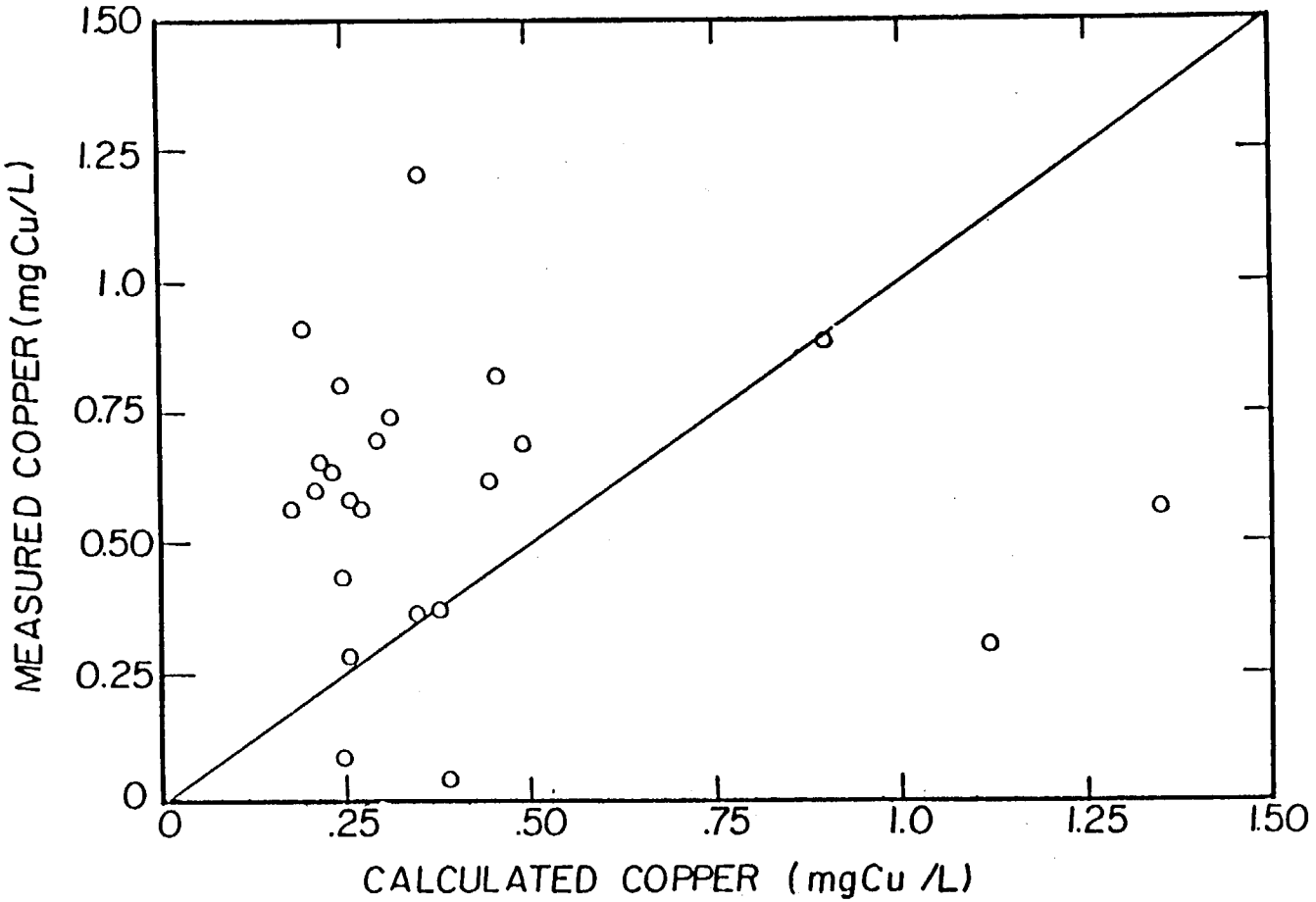

Figure 71. A comparison of measured copper concentrations from first flush tapwater derived from $CaCO_3$ treated lakewater and calculated values from the chemical equilibrium model MINEQL. One-to-one line is indicated.

As observed in laboratory pipe section experiments, measured lead concentrations were highly undersaturated with respect to the solubility of anticipated lead passivation films (Figure 72). Again these results are not surprising in view of the fact that tapwater lead was largely derived from lead-tin solder on joints.

As we reported for tapwater derived from spring supplies, the probability of copper exceeding the SMCL was high for untreated lakewater while it was low for treated lakewater (Figure 68). It is also evident that concentrations of copper at Bay Side tapwater were generally higher for treated lake water than treated spring water (significant at the 0.1 level; two tailed t-test). Although the reason for this discrepancy is not clear, differences in the level of treatment of the two water supplies may have contributed. The influent lakewater was considerably more acidic and had a lower dissolved inorganic carbon concentration than the spring water (Tables 17 and 18). These influent chemical characteristics coupled with the longer path length of the spring box contactor resulted in higher pH, alkalinity and dissolved inorganic carbon concentrations in the spring treated water relative to lake treated water (Tables 17 and 18). As mentioned previously, both increased pH and dissolved inorganic carbon concentrations theoretically result in lower copper solubility and may have contributed to the apparent difference (Figure 56).

First-flush tapwater concentrations of lead in treated lake water were always below the MCL for lead (Figure 69). Likewise, untreated tapwater was also below the MCL for all observations. However, relatively few untreated samples were collected and concentrations were generally close to the 0.05 mg Pb/L standard.

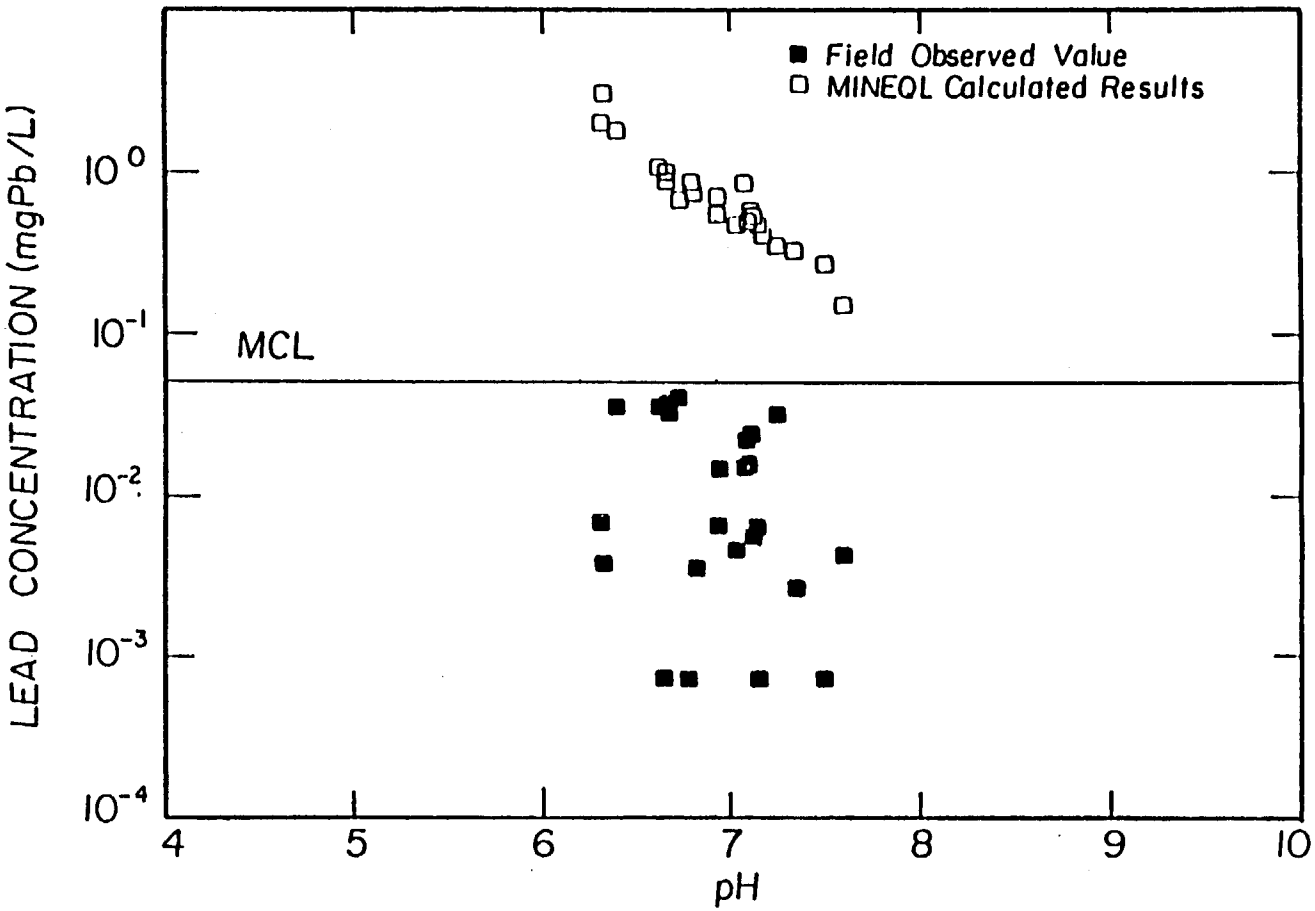

Figure 72. A comparison of measured lead concentrations from first flush tap-water derived from $CaCO_3$ treatment and calculated values from the chemical equilibrium model MINEQL as a function of pH. The maximum contaminant level (MCL) for lead is indicated.

REFERENCES

Anderson, R. and D. Berry. 1981. Regulating Corrosive water. Wat. Resour. Res., 17:1571-1577.

ASTM, 1972. Manual on Test Sieving Methods, ASTM-STP447A, Philadelphia, Pa.

Baes, C. F. and R. E. Mesmer. 1976. The Hydrolysis of Cations. John Wiley, NY. 458 p.

Beevers, D. G., E. Erskine, and M. Robertson. 1976. Blood Lead and hyper-Tension. The Lancet 2:1-3.

Ball, J. W., D. K. Nordstrom and E. A. Jenne. 1980. Additional and Revised Thermochemical Data and Computer Code for WATEQ2-A Computerized Chemical Model for Trace and Major Element Speciation and Mineral Equilibria of Natural Waters. Resour. Invest., WRI 78-116, U. S. Geological Survey.

Barr, A. J., J. H. Goodnight, J. P. Sail and J. T. Helwis. 1976. A User's Guide to SAS76. SAS Institute, Raleigh, NC.

Barton, P., T. Vatanatham. 1975. Kinetics of Limestone Neutralization of Acid Waters. Environ. Sci. and Tech., 10:262-266.

Berner, R. A., J. W. Morse, 1974. Dissolution Kinetics of Calcium Carbonate in Sea Water: Theory of Calcite Dissolution. Am. J. Sci., 274:108-134.

Bjerle, I., G. Rochelle. 1982. Limestone Dissolution in Acid Lakes. Vatten, 38:156-163.

Blackwell, W. W. 1984. Chemical Process Design on a Programmable Calculator. McGraw-Hill Inc., pp. 370-371.

Boynton, R. S. 1980. Chemistry and Technology of Lime and Limestone. Second Edition, John Wiley and Sons.

Cameron, W. R. and R. C. Wunderlich. 1976. Trace Element Toxicity Associated with a Public Water Supply. In: D. D. Hemphill (ed.). Trace Substances in Environmental Health-X. Columbia, MO.

Campbell, B. C., A. D. Beattie, M. R. Moore, A. Goldbert and A. G. Reid. 1977. Renal Insufficiency Associated with Excessive Lead Exposure. British Medical J. 1:482-485.

Chu, I., J. Khalil. 1953. Mass Transfer in Fluidized Beds. Chem. Eng. Prog., 49:141-149.

Dangel, R. A. 1976. Study of Corrosion Products in the Seattle Water Department Tolt Distribution System. USEPA Rep. EPA-67012-75-036.

Doull, J., C. D. Klaassen anfd M. G. Andur (eds.). 1980. Toxicology: The Basic Science of Poisons. 2nd ed. Macmillan, NY 778 p.

Driscoll, C. T., J. White, G. Schafran, J. Rendall. 1982. $CaCO_3$ Neutralization of Acidified Surface Waters. J. of ASCE-Environ. Eng. Div., 108:NO. EE6.

Eden, G. E., G. A. Truesdale. 1950. Treatment of Waste Water from the Pickling of Steel. J. of Iron and Steel Institute. pp 281.

Edwards, M. F., and J. F. Richardson, 1968. Gas Dispersion in Packed Beds. Chem. Eng. Sci., 23:109.

Erga, O., S. G. Terjesen. 1956. Kinetics of the Heterogeneous Reaction of Calcium Bicarbonate Formation. Acta Chem. Scand., 10:872-874.

Faust, S. D., and O. M. Aly. 1981. Chemistry of Natural Waters. Ann Arbor Science. 400 p.

Feithnecht, W. and P. Schindler. 1963. Solubility Constants of Metal Oxides, Metal Hydroxides and Metal Hydroxide Salts in Aqueous Solution. Pure and Applied Chemistry 6:134-197.

Frear, G. L., and J. Johnson. 1929. The Solubility of $CaCO_3$ in Certain Aqueous Solutions at 25 C. J. Am. Chem. Soc., 51:2082-2093.

Galloway, R. E., and J. F. Colville. 1970. Treatment of Spent Pickling Plant Liquors. Management of Water in the Iron and Steel Industry. Iron and Steel Institute Publication.

Gehm, H. W. 1944. Neutralization of Acid Waste Waters with an Up-Flow Expanded Limestone Bed. Sewage Work Journal, 16:104-120.

Gortikova, V. M., and L. I. Panteeva. 1937. Kinetics of Solvation of Calcium Carbonate. Journal of General Chemistry-USSR, 7:56-64.

Gran, G.. 1952. Determination of the Equivalence Point in Potentiometric Titrations. Intern. Cong. Anal. Chem., 77:661-671.

Haddad, M. 1983. Neutralization of Corrosive Waters Using a Packed Bed of Crushed Limestone. M.S. Thesis, Syracuse University.

Hem, J. D. and W. H. Durum. 1973. Solubility and Occurrence of Lead in Surface Water. J. Am. Water Works Assoc., 65:562-568.

Hem, J. D. 1976. Geochemical Controls on Lead Concentrations in Stream Water and Sediments. Geochim. Cosmochim. Acta. 40:599-609.

Herrera, C. E., J. F. Ferguson and M. M. Benjamin. 1982. Evaluating the Potential for Contaminating Drinking Water from the Corrosion of Tin-Antimony Solder. J. Am. Water Works Assoc., 74:368-375.

Hilburn, R. D. 1983. Modelling Copper Corrosion in Water with Low Conductivity by Using Electrochemical Techniques. J. Am. Water Works Assoc. 75:149-154.

Hoak, R. D., C. J. Lewis, and W. W. Hodge. 1945. Treatment of Spent Pickling Liquors with Limestone and Lime. Ind. and Eng. Chem., 37:553-559.

Hoak, R. D., C. J. Lewis, C. J. Sindlinger, and B. Klein. 1947. Lime Treatment of Waste Pickle Liquor. Ind. and Eng. Chem., 39: No. 2.

Hoak, R. D., C. J. Lewis, W. W. Hodge. 1944. Basicity Factors of Limestone and Lime - Evaluation as Neutralizing Agents. Ind. and Eng. Chem., 36: No. 3.

Hudson, H. E, and F. W. Gilcreas. 1976. Health and Economic Aspects of Water Hardness and Corrosiveness. J. Am. Water Works Assoc., 68:201-204.

Jacobs, H. L. 1947. Acid Neutralization. Chem. Eng. Progress, 43:247-254.

Jarrett, R. E. 1966. Porous Limestone Barriers for Neutralization of Acid Streams. M. S. Thesis, Pennsylvania State University at University Park.

Karalekas, P. C., C. R. Ryan and F. B. Taylor. 1983. Control of Lead, Copper and Iron Pipe Corrosion in Boston. J. Am. Water Works Assoc., 75:92-94.

Kaye, C. A. 1957. The Effect of Solvent Motion on Limestone Solution. J. Geol., 65:34-36.

King, C. V., and C. L. Liu. 1933. The Rate of Solution of Marble in Dilute Acid. J. Am. Chem. Soc., 55:1928-1940.

Levenspiel, O., and W. K. Smith. 1957. Notes on the Diffusion-Type Model for the Longitudinal Mixing of Fluids in Flow. Chem. Eng. Sci., 7:227-233.

Levenspiel, O. 1972. Chemical Reaction Engineering. Wiley, NY.

Levenspiel, O., and K. B. Bishchoff. 1963. Patterns of Flow in Chemical Process Vessels. Advances in Chemical Engineering, 4:95-198.

Lund, K. H. C. Folger, C. C. McCune, and J. W. Ault. 1975. The Dissolution of Calcite in Hydrochloric Acid. Chem. Eng. Sci. 30:825-835.

Maessen, O., B. Freedman and R. McCurdy. 1985. Metal Mobilization in Home Well Water Systems in Nova Scotia. J. Am. Water Works Assoc., 77:73-80.

Meranger, J. C., T. R. Khan, C. Vario, R. Jackson, and W. C. Li. 1983. Lake Water Acidity and the Quality of Pumped Cottage Water in Selected Areas of Northern Ontario. Intern. J. Environ. Anal. Chem., 15:185-212.

Mesmer, R. E. and C. F. Baes. 1974. The Hydrolysis of Cations: A Critical Review of Hydrolytic Species and their Stability Constants in Aqueous Solution. Oak Ridge National Laboratory, ORNL-NSF-EATC-3. Part III.

Miadokova, M. and H. Bednarova. 1968. Einfluss der lonen und Organischer Molekule auf die Kinetic der Kalcitauflosung in der Bronwasserstoffsaure. Acta Fac. Rerum., Nat. Univ. comenianae - Chimia, 12:35-44.

Mihok, E. A., et al. 1968. Mine Water Research - the Limestone Nautralization Process. Report No,. 7191, U. S. Bureau of Mines, Pittsburgh, PA.

Morse, J. W. and R. A. Berner, 1972. Dissolution Kinetics of Calcium Carbonate in Sea Water II: A Kinetic Origin for the Lysocline. Am. J. Sci., 272:840-851.

Morse, J. W. 1974. Dissolution Kinetics of Calcium Carbonate in Sea Water III: A New Method for $CaCO_3$ Reaction Kinetics. Am. J. Sci., 274:97-107.

Morse, J. W. 1978. Dissolution Kinetics of Calcium Carbonate in Sea Water IV: The Near Equilibrium Dissolution Kinetics of CaCO3-Rich Deep Sea Sediments. Am. J. Sci., 278:344-353.

Morse, J. W. 1974. Dissolution Kinetics of Calcium Carbonate in Sea Water V: Effects of Natural Inhibitors and the Position of the Chemical Lysocline. Am. J. Sci., 274:638-647.

Murray, J. A., et al. 1954. Shrinkage of High Calcium Limestones During Burning. J. A. Ceram. Soc., 37:323-328.

National Academy of Science. 1977. Drinking Water and Health. Report of the National Research Council. Washington, DC. 939 p.

Nestaas, I., and S. J. Terjessen. 1969. The Inhibiting Effect of Scandium Ions upon the Dissolution of Calcium Carbonate. Acta. Chem. Scand., 23:2519-2531.

Nierode, D. E. , and B. B. Williams. 1971. Characteristics of Acid Reaction in Limestone Formation. Soc. Petrol. Journal, Trans. 251:406-418.

Patterson, J. W., H. E. Allen and J. J. Scala. 1977. Carbonate Precipitation for Heavy Metal Pollutants. J. Water Pollut. Con. Fed., 49:2397-2410.

Patterson, J. W. , and J. O'Brien. 1979. Control of Lead Corrosion. J. Am. Water Works Assoc., 71:264-271.

Pearson, F. H., and A. J. McDonnel. 1975. Limestone Barriers to Neutralize Acidic Streams. ASCE J. of Environ. Eng. Div., 101: No. EE3.

Pearson, F. H., and A. J. McDonnel. 1975. Use of Crushed Limestone to Neutralize Acid Wastes. J. Environ. Eng. Div. ASCE, 101:No. EE1.

Plummer, L. N., T. M. L. Wigley, and D. L. Parkhurst. 1978. The Kinetics of Calcite Dissolution in CO_2 Water Systems at 5 to 60 C and 0 to 1.0 atm. CO_2. Am. J. Sci., 278:179-216.

Plummer, L. N., and T. M. L. Wigley. 1976. The Dissolution of Calcite in CO_2 Saturated Solutions at 25 C and 1 Atm. Total Pressure. Geochemica et Cosmochemica Acta, 40:191-202.

Plummer, L. N., and E. Bussenberg. 1982. The Solubility of Calcite, Arogonite, and Veterite in CO_2-H_2O solutions between 0 and 90 C and an Evaluation of the Aqueous Model for the System $CaCO_3$-CO_2-H_2O. Geochemica et Cosmochemica Acta, 46:1011-1040.

Quintin, M. 1937. Sur l'hydrolyse du benzene sulfonate de cuivre. Compt. Rend., 204:968.

Reidl, A. L. 1947. Limestone Used to Neutralize Acid Waste. Chem. Engineering, 100-101.

Rickard, D., and E. L. Sjoberg. 1983. Mixed Kinetic Control of Calcite Dissolution Rates. Am. J. Sci., 283:815-830.

Roberts, P. V., P. Cornel, and R. Scott. 1985. External Mass-Transfer Rate in Fixed-Bed Adsorption. Journal of Environmental Engineering, ASCE, 111:891-905.

Robinson, R. A., and R. H. Stokes. 1959. Electrolyte Solutions. Butterworth, London.

SAS User's Guide-Statistics. 1982. SAS Institute Inc., Cary, NC.

Schock, M. R. 1980. Response of Lead Solubility to Dissolved Carbonate in Drinking Water. J. Am. Water Works Assoc., 73:695-704.

Schock, M. R. 1984. Treatment of Water Quality Adjustment to Attain MCL's in Metallic Potable Water Plumbing Systems. Proceedings: Seminars on Plumbing Materials and Drinking Water Quality, USEPA, Environmental Research Center, Cincinnati, OH. May 16-17.

Schock, M. R. and M. C. Gardels. 1983. Plumbosolvency Reduction by High pH and Low Carbonate-solubility Relationships, J. Am. Water Works Assoc. 75:87-91.

Sillen, L. G. and A. E. Martell. 1964. Stability Constants of Metal-ion Complexes. The Chemical Society Special Publication 17, London. 754 p.

Sjoberg, E. L. 1976. A Fundamental Equation for Calcite Dissolution Kinetics. Geochemica et Cosmochemica Acta, 40:441-447.

Sjoberg, E. L., and D. Rickard. 1983. The Influence of Experimental Design on the Rate of Calcite Dissolution. Geochemica et Cosmochemica Acta, 47: 2281-2285.

Sjoberg, E. L., and D. Rickard. 1984. Calcite Dissolution Kinetics: Surface Speciation and the Origin of Variable pH Dependence. Chem. Geol., 42:119-136.

Sjoberg, E. L. and D. Rickard. 1984. Temperature Dependence of Calcite Dissolution Kinetics between 1 and 62 C at pH 2.7 to 8.4 in Aqueous Solutions. Geochemica et Cosmochimica Acta, 48:485-493.

Slavin, W. 1968. Atomic Absorption Spectroscopy. John Wiley Interscience, New York.

Small, H., T. S. Stevens and W. C. Bauman. 1975. Novel Ion Exchange Chromatographic Method Using Conductimetric Detection. Anal. Chem. 47:1801-1809.

Smith, R. M. and A. E. Martell. 1976. Critical Stability Constants Vol. 4. Inorganic Complexes. Plenum Press, NY. 257 p.

Snoeyink, N., and D. Jenkins. 1980. Water Chemistry. John Wiley and Sons, NY.

Spivakovskii, V. B. and G. V. Makovskaya. 1968. Copper Hydroxide Chlorides, Hydroxide and Hydroxo-complexes. A New Version of the Method of Three Variables. Russ. J. Inorg. Chem., 13:815.

Stainton, M. P. 1973. A Syringe Gas-stripping Procedure for Gas-chromatography Determination of Dissolved Inorganic and Organic Carbon in Freshwater and Carbonate in Sediments. J. Fish. Res. Bd., Canada, 30:1441-1445 .

Standard Methods for the Examination of Water and Wastewater. 1985. 16th ed. American Public Health Association, Washington, DC.

Stumm, W. and J. J. Morgan. 1981. Aquatic Chemistry, Wiley-Interscience, New York, NY.

Sverdrup, H., and I. Bjerle. 1982. The Calcite Utilization Efficiency and the Long Term Effect on Alkalinity in Several Swedish Liming Projects. Lund Inst. Publication No. S-220.

Terjesen, S. G., O. Erga, G. Thorsen, and A. Ve. 1961. Phase Boundary Processes as Rate Determining Steps in Reactions Between Solids and Liquids. Chem. Eng. Sci., 14:277-289.

Topelmann, H. 1929. J. Prakt. Chem. 121:320.

Treweek, G. P., J. Glicker, B. Chow and M. Sprinkler. 1985. Pilot-plant Simulation of Corrosion in Domestic Pipe Materials. J. Am. Water Works Assoc., 77:74-82.

USEPA. 1983. Methods for Chemical Analysis of Water and Wastes. Environmental Monitoring and Support Laboratory, Cincinnati, OH, EPA-600/4-79-02G, 350.1-1 to 350.1-6.

Vaceta, J. 1976. Adsorption of Lead and Copper on Quartz from Aqueous Solutions: Influence of pH Ionic Strength and Complexing Ligands. PhD thesis California Institute of Technology. 206 p.

Vaillencourt, G. W. 1981. Crushed Limestone Neutralization of Dilute Acidified Adirondack Surface Waters. M. S. Thesis, Cornell University.

Vatanatham, T. 1975. Kinetics of Limestone Neutralization of Mine Drainage. M.S. Thesis, Penn. State University, University Park, PA.

Volpocili, V. , C. L. Santoro, and P. Ciambeli. 1981. Neutralization of Acid Water Containing Aluminum Ions by Means of Limestone. Chem. Eng. Journal, 21:29-38.

Wagman, D. D., W. H. Evans, V. B. Parker, I. Halow, S. M. Bailey, and R. H. Schumm. 1968. Selected Values of Chemical Thermodynamic Properties. National Bureau of Standards Technical Note 270-3 to 270-6.

Waldbott, G. L. 1978. Health Effects of Environmental Pollutants. The C. V. Mosby Company, St. Louis.

Wehner, J. F., and R. H. Wilhelm. 1956. Boundary Conditions of Flow Reactors. Chem. Eng. Sci., 6:89-93.

Wentzler, T. H., and F. F. Aplan. 1972. Kinetics of Limestone Dissolution by Acidic Wastewater. Environmental Control AIME, NY.

Wentzler, T. H. 1971. A Study of the Interaction of Limestone in Acid Solution. M.S. Thesis, Penn. State University, University Park, PA.

Westall, J. C., J. L. Zachary, and F. M. Morel. 1976. MINEQL-A Computer Program for the Calculation of Chemical Equilibrium Composition of Aqueous Systems. TN-18 Parson Laboratory, MIT, Cambridge, MA.

Weyl, P. K. 1958. The Solution Kinetics of Calcite. J. Geol. 66:163-176.

Wilhelm, R. H. 1962. A Priori Design of Chemical Reactors. Pure Applied Chemistry, 5:403-409.

Appendix A

Chemical Equilibrium Model
Used in Contactor Design Calculations

INTRODUCTION

Determination of the limestone contactor effluent chemistry requires knowledge of the chemical equilibrium conditions in the solution which is immediately adjacent to the limestone surface (see Figure 2 and Eq. 25).

The equilibrium water chemistry at the limestone surface was determined for two cases:

1. When a complete chemical analysis of the raw water is available, and,
2. When only a partial knowledge of the chemical composition of the raw water is available.

Three operational conditions were also considered:

a. Closed system: The contactor and the contactor effluent are closed to the atmosphere and therefore there is no exchange of carbon dioxide between the solution and the atmosphere.

b. Open system: The water in the contactor is continuously in equilibrium with atmospheric carbon dioxide.

c. Closed/Open system: The water in the contactor is closed to the atmosphere but the effluent is open to the atmosphere.

The three operational conditions are illustrated schematically in Figure A.1.

In the description of the computational procedure which follows the knowledge of the raw water chemistry and the operational conditions which pertain to a given procedure are designated by a number and a letter, e.g., "1a" indicates that a complete chemical analysis of the raw water is available and the system is closed to the atmosphere.

The solute species Ca^{++}. H_2CO_3, $CO_3^{=}$, H^+ and OH^- in the solution which is immediately adjacent to the limestone particle surface are unknown. To define the solution composition and to determine the unknown species the following equations were used:

- Charge balance equation:

$$\sum_{i=1}^{n} Z_i C_i = 0 \qquad (A.1)$$

where Z_i and C_i are the charge and molar concentration of specie (i).

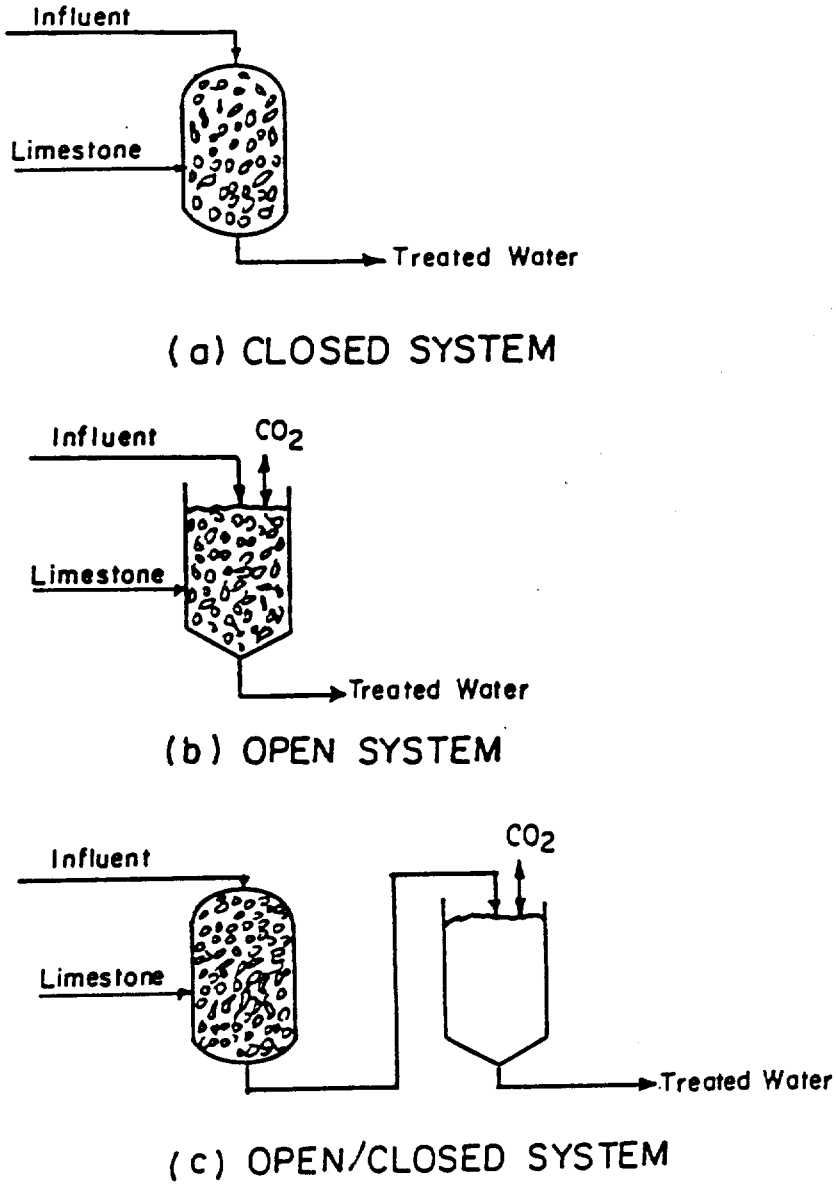

Figure A.1. Operational conditions used in the chemical equilibrium modelling.

- Mass action expressions for the deprotonation of carbonic acid:

$$K_{a1} = \frac{\{H^+\}\{HCO^-_3\}}{\{H_2CO_3\}} \qquad (A.2)$$

$$K_{a2} = \frac{\{H^+\}\{CO_3^{2-}\}}{\{HCO_3^-\}} \qquad (A.3)$$

where {i} is the activity of specie (i).

- Solubility product expression for $CaCO_3(s)$:

$$K_{sp} = \{Ca^{2+}\}\{CO_3^{2-}\} \qquad (A.4)$$

- Ion product expression for water:

$$K_W = \{H^+\}\{OH^-\} \qquad (A.5)$$

- Henry's law expression for carbon dioxide dissolved in water:

$$K_H = \frac{H_2CO_3^*}{pCO_2} \qquad (A.6)$$

where pCO_2 is the partial pressure of carbon dioxide.

- Mass balance equations:

$$DIC = [H_2CO_3^*] + [HCO_3^-] + [CO_3^{2-}] \qquad (A.7)$$

where

$$[H_2CO_3^*] = DOC \times \alpha_o, \qquad (A.8.1)$$

$$[H_2CO_3^-] = DIC \times \alpha_1, \qquad (A.8.2)$$

$$[CO_3^{2-}] = DIC \times \alpha_2, \qquad (A.8.3)$$

DIC is the dissolved inorganic carbon concentration and α_o, α_1 and α_2 are the ionization fractions for the carbonate system (Stumm and Morgan, 1981):

$$\alpha_o = \left(1 + \frac{K_{a1}}{[H^+]} + \frac{K_{a1}K_{a2}}{[H^+]^2}\right)^{-1} \qquad (A.9.1)$$

$$\alpha_1 = \left(1 + \frac{[H^+]}{K_{a1}} + \frac{K_{a2}}{[H^+]}\right)^{-1} \qquad (A.9.2)$$

$$\alpha_2 = \left(1 + \frac{[H^+]^2}{K_{a1}K_{a2}} + \frac{[H^+]}{K_{a2}}\right)^{-1} \qquad (A.9.3)$$

For a dilute acidic water flowing into the contactor, equation (A.1) becomes:

$$2[Ca^{2+}] + C_c + [H^+] = [HCO_3^-] + 2\,[CO_3^{-2}] + C_a + [OH^-] \qquad (A.10)$$

where C_c is the total concentration of non-calcium and hydrogen ion cations, in equivalents per liter, C_a is the total concentration of non-inorganic carbon and hydroxyl ion anions in equivalents per liter, and the brackets denote molar concentration.

As water flows through the contactor $CaCO_3$ is dissolved from the limestone and the calcium and DIC concentrations increase, i.e.,

$$C_{bL} = C_{bo} + S \qquad (A.11.1)$$

and

$$DIC = DIC_o + S \qquad (A.11.2)$$

where C_{bL} and S are the molar concentrations of calcium ion and calcium carbonate dissolved from the limestone at an axial location, L, in the contactor bed, C_{bo} is the calcium concentration in the influent and DIC_o is the influent DIC concentration.

With the substitution of Eqs. (A.8.2), (A.8.3) and (A.11) in the solubility product equation, (A.4), and charge balance equation, (A.10), the following expressions are obtained:

$$2[C_{bo} + S] + C_c\,[H^+] = (DIC_o + S)\,(\alpha_1 + 2\alpha_2) + C_a + [OH^-] \qquad (A.13)$$

$$\{C_{bo} + S\}\,\{(DIC_o + S)\,\alpha_2\} = K_{sp} \qquad (A.14)$$

or

$$S = -\left(\frac{C_{bo} + DIC_o}{2}\right) + \left(\frac{C_{bo} + DIC_o}{2}\right)^2 - \left((C_{bo} \times DIC_o) - \frac{K_{sp}}{\alpha_2\,\gamma_2^{\,2}}\right)\Big]^{\frac{1}{2}} \qquad (A.15)$$

where γ_2 is the activity coefficient for divalent ions, in this case the Ca^{2+} and the CO_3^{2-} ions.

Computational Procedure

The equilibrium calculations assume that the influent water is dilute, i.e., the ionic strength, I, is less than 0.01 and negligible complexing of ions occurs.

The equilibrium calcium concentration, C_{eq}, was determined for each set of raw water chemical conditions and temperature using an algorithm in which the pH is systematically varied to find the point at which both the charge

balance, equation (A.13), and the solubility product relationship, equation (A.14) are satisfied.

The search procedure was conducted using three computational loops:

-First loop: the pH interval 6 to 10.5 was searched in steps of 0.25 pH units and the point (pH_1) at which equations (A.13) and (A.14) were satisfied was found.

-Second loop: the pH interval ($pH_1 \pm 0.30$) was searched in steps of 0.05 pH units and the point (pH_2) at which equations (A.13) and (A.14) were satisfied was found.

-Third loop: the pH interval ($pH_2 \pm 0.06$) was searched in steps of 0.01 pH units and the point (pH_3) at which equations (A.13) and (A.14) were satisfied was found. At this point:

$$pH_3 = pH_{eq}$$
$$C_{eq} = C_{bo} + S \qquad (A.16)$$
$$DIC_{eq} = DIC_o + S$$

In the above calculations the following were considered:

-Equations derived by Plummer and Bussenburg (1982) were used to calculate the equilibrium constants K_{a1}, K_{a2}, and K_H at infinite dilution as a function of temperature. Plummer's equations are given in Table (A.1)..

-The effective $CaCO_3$ solubility product ($K_{sp\ 20°}$) of 1.9×10^{-9} at 20°C (Section 5) was corrected for temperature using the following relationship (Snoeyink and Jenkins, 1980):

$$K_{sp} = K_{sp\ 20°} \{\exp [-\frac{H}{R} (\frac{1}{T} - \frac{1}{293})]\} \qquad (A.17)$$

where K_{sp} is the $CaCO_3$ solubility product at temperature, T. Values for the enthalpy, H, and the Boltzmann constant, R, were taken from Snoeyink and Jenkins,

$$\frac{H}{R} = 1484.5 \text{ (degree Kelvin)}$$

Values of the equilibrium constants, K_{a1}, K_{a2} and K_H and the effective $CaCO_3$ solubility product, K_{sp}, (Equation A.17) for a range of temperature (1 to 25°C) are presented in Table A.2.

Table A-1 Equations Used to Calculate the Equilibrium Constants, K_{a1}, K_{a2} and K_H as a Function of Temperature (Plummer and Bussenburg, 1982)

$$\log K_{a1} = -356.3094 - (0.0609196 \times T) + (2.834.37/T) + (126.8339 \times \log T) - (168491/T^2)$$

$$\log K_{a2} = -107.8871 - (0.03252849 \times T) + (515179/T) + (38.92561 \times \log T) - (563713.9/T^2)$$

$$\log K_H = 108.3865 + (0.0198507 \times T) + (669365/T^2) - (6919.53/T) - (40.45154 \times \log T)$$

where, T, is in degrees Kelvin

-At each pH in the search procedure the ionic strength, I, and the activity coefficients, γ_i, were calculated using

$$I = 1/2(\Sigma Z_i^2 C_i) \qquad (A.18)$$

and

$$\text{Log } \gamma_i = -A Z_i^2 \quad I^{\frac{1}{2}} \quad \text{for } I < 10^{-2.3} \qquad (A.19)$$

or

$$\text{Log } \gamma_i = \frac{- A Z_i^2 \quad I^{\frac{1}{2}}}{1 + \quad I^{\frac{1}{2}}} \qquad \text{for } I < 10^{-1} \qquad (A.20)$$

where A = 0.509.

The calculations were made using a computer program written in APL. Outlines of the program calculations are given below for conditions 1a, 1b, 1c, 2a, 2b and 2c.

1.a Closed-to-the-Atmosphere System (Complete Influent Water Chemistry is Known).

After the water chemical composition and temperature are input, the program is used to compute the temperature corrected values of the equilibrium constants K_{a1} and K_{a2} (see Table A.2) and the effective $CaCO_3$ solubility product K_{sp} (Equation A.17).

-Ionization fractions for the carbonate and bicarbonate ions are then estimated for the first pH value in the interval being searched and the carbonate and bicarbonate concentrations are calculated using equations (A.9.2), (A.9.3), (A.8.2) and (A.8.3).

-The ionic strength, I, is estimated using Eq. A.18 and accordingly the activity coefficients for monovalent, γ_1, and divalent, γ_2, ions are calculated using Eq. A.19 or A.20. With the known activity coefficients, the equilibrium constants, K_{a1} and K_{a2} are corrected for ionic strength as follows:

$$K'_{a1} = \frac{K_{a1}}{\gamma_1^2} \qquad (A.21)$$

$$K'_{a2} = \frac{K_{a2}}{\gamma_2} \qquad (A.22)$$

-New values of the ionization fractions for carbonate and bicarbonate ions are calculated, using the corrected equilibrium constants, K'_{a1} and K'_{a2} (Eqs. A.9.2 and A.9.3). At this point the amount of limestone dissolved, S, is calculated using Eq. A.15 and the value is entered in the charge balance

equation, Eq. A.13. A quantity, DEL, defined as the difference between the left and the right side of the charge balance equation is then calculated:

$$DEL = \{2[C_{bo} + S] + C_c + [H_i^+]\} - \{((DIC_o + S)(\alpha_1 + 2\alpha_2)) + C_a + [OH_i^-]\} \quad (A.23)$$

-The program then repeats the above calculations using the next pH in the interval. The pH in the search interval at which DEL is a minimum is the point where the solubility product and the charge balance equations (Eqs. A.13 and A.14) are essentially satisified. In the first loop the pH at the point where DEL is a minimum is pH_1.

After pH_1 is obtained the second loop begins. The calculations in the second and third loop are the same as those in the first loop except, as noted, smaller pH intervals are searched and smaller pH increments are used in the search across each interval.

To use the contactor design equations the calcium concentration in the contactor effluent C_{bL}, must be determined for the case when the effluent is not in equilibrium with the limestone, i.e., $pH < pH_{eq}$ and $C_{bL} < C_{eq}$. Usually a target effluent pH is known and one must then calculate the corresponding effluent calcium concentration.

The magnitude of C_{bL} for a given effluent pH is determined using the charge balance equation, Eq. A.13. The target effluent pH is used to determine α_1, α_2, $[H^+]$ and $[OH^-]$ and these quantities are used with C_{bo}, DIC_o, C_c and C_a to solve Eq. A.13 for the quantity, S. The desired effluent calcium concentration is equal to $C_{bo} + S$. Note that this value of S is less than the equilibrium value from Eq. A.15.

1.b - Open-to-the-Atmosphere System

For an open to the atmosphere system the computational procedure was the same as that used for a closed-to-the-atmosphere system except that the value of the dissolved inorganic carbon concentration in equations A.13 and A.14 was estimated at each pH using equations A.8.1 and A.6. Combining equations A.8 and A.9 yields,

$$DIC = \frac{K_H \, pCO_2}{\alpha_o} \quad (A.24)$$

Table A-2 Values of K_{a1}, K_{a2}, K_H and $K_{sp}(CaCO_3)$ for a Range of Temperatures. The Equations of Plummer and Busśenburg (1982) were used to Calculate these Quantities.

T°C	log K_{a1}	log K_{a2}	log K_H	log K_{sp}
1	-6.56	-10.61	-1.12	-8.56
2	-6.55	-10.59	-1.14	-8.57
3	-6.54	-10.58	-1.15	-8.58
4	-6.53	-10.56	-1.17	-8.59
5	-6.51	-10.55	-1.19	-8.60
6	-6.50	-10.54	-1.20	-8.61
7	-6.49	-10.52	-1.22	-8.61
8	-6.48	-10.51	-1.23	-8.62
9	-6.47	-10.50	-1.25	-8.63
10	-6.46	-10.48	-1.26	-8.64
11	-6.45	-10.47	-1.28	-8.65
12	-6.44	-10.46	-1.29	-8.65
13	-6.43	-10.45	-1.31	-8.66
14	-6.42	-10.44	-1.32	-8.67
15	-6.41	-10.42	-1.34	-8.68
16	-6.41	-10.41	-1.35	-8.69
17	-6.40	-10.40	-1.36	-8.69
18	-6.39	-10.39	-1.38	-8.70
19	-6.38	-10.38	-1.39	-8.71
20	-6.38	-10.37	-1.40	-8.72
21	-6.37	-10.36	-1.41	-8.72
22	-6.36	-10.35	-1.43	-8.73
23	-6.36	-10.34	-1.44	-8.74
24	-6.35	-10.33	-1.45	-8.75
25	-6.35	-10.32	-1.46	-8.75

An equation derived by Plummer and Bussenburg (1982) for determining Henry's Law constant for carbon dioxide (see Table A.1) was used with a partial pressure of atmospheric CO_2 of $10^{-3.5}$.

1.c - Closed/Open System

The closed/open system calculation involved the pH interval search procedure and Eq. A.23 with the following substitutions;

$$S = 0$$

$$C_{bo} = C_{bL}$$

and from Eq. A.24,

$$DIC_o + S = \frac{K_H \, pCO_2}{\alpha_o} \quad .$$

C_{bL} is the calcium concentration in the contactor effluent. Eq. A.15 is omitted from the pH interval search calculations because the effluent is not in contact with solid $CaCO_3$.

2 - A procedure for the case when there is limited information on the chemistry of the raw water

The availability of a well equipped laboratory and trained technical personnel in a small water supply system may be limited. In order to proceed with the determination of the chemical equilibrium conditions at the limestone surface, knowledge of the total anion, C_a, and cation, C_c concentrations and their effects on the total ionic strength is necessary to estimate the activity coefficients for individual ions. A procedure was developed for use when only the measured specific conductance, K_m, initial calcium concentration, C_{bo}, initial pH, pH_o, and alkalinity are known.

An equation relating the portion of the total ionic strength contributed by C_c and C_a ions, I_{AB}, to the corresponding specific conductivity, K_{AB}, was derived using data from the analysis of water from 34 lakes in the Adirondack Region of New York State. The equation is given by:

$$I_{AB} = \text{constant} \times K_{AB}. \qquad (A.25)$$

The complete chemical analyses for these lakes were obtained from the results of a survey conducted by the U.S. EPA (Kanciruck et al. 1985). The data for the 34 lakes were chosen at random from a list of over 100 lakes.

The MINEQL chemical equilibrium program (Westall et al. 1976) was used to calculate the total ionic strength, I, for each of the 34 sets of data. The total component concentrations and temperature for each lake were entered in the MINEQL program. The values of the ionic strength obtained from MINEQL for the 34 lakes ranged from 2×10^{-4} to 9×10^{-4} M.

The contributions of Ca^{++}, H^+, OH^-, HCO_3^-, and $CO_3^=$ to the total ionic strength I, was estimated using:

$$I' = 1/2\ (4[Ca^{++}] + [H^+] + [HCO_3^-] + 4[CO_3^{2-}] + [OH^-])\ . \qquad (A.26)$$

The ionic strength attributable to C_c and C_a was determined by calculating the difference between the total ionic strength, I, and I', i.e.,

$$I_{AB} = I - I'. \qquad (A.27)$$

The specific conductance attributable to C_a and C_c ions, K_{AB}, was estimated for each lake by computing the difference between the measured specific conductance, K_m, and the sum of the specific conductances attributable to Ca^{++}, H^+, HCO_3^-, CO_3^{2-}, and OH^-, i.e.,

$$K_{AB} = K_m - K_1 \qquad (A.28)$$

where

$$K_1 = [Ca^{++}]\ \lambda_{Ca^{++}} + [H^+]\ \lambda_{H^+} + [HCO_3^-]\ \lambda_{HCO_3^-} + [CO_3^{-2}]\ \lambda_{CO_3} + [OH]\ \lambda_{OH^-} \qquad (A.29)$$

and, λ, is the specific ionic conductance in water at 25°C, in micromhos/cm.

The values of the specific conductance used in the analysis were taken from Robinson et al. (1959) and are listed in Table A.3. The values of I, K_m, I_{AB}, K_{AB} for the 34 lakes are listed in Table A.4.

TABLE A.3 Individual ion specific conductance

Ion	Specific Conductance, λ
H^+	349.8
HCO_3^-	44.5
$CO_3^=$	69.3
Ca^{++}	59.5
OH^-	198.3

To determine the value of the constant in Equation A.25 a nonlinear least squares procedure which produces least squares or weighted least squares esti-

mates of the parameters of the model was used (SAS 1982). This procedure uses the modified Gauss-Newton iterative method. The analysis gave the following equation:

$$I_{AB} = 1.31 \times 10^{-5} K_{AB} \quad (r^2 = 0.55) \qquad (A.30)$$

The low value of R^2 might have resulted from errors in the pH and/or DIC measurements which were used in estimating I_{AB} (see equations A.26 and A.27).

The computational procedure for conditions 2a, 2b and 2c was the same search algorithm as was used for conditions 1a, 1b and 1c. The only difference between the two procedures is in the determination of the ionic strength of the solution at each pH. Determination of the ionic strength of the solution at each pH when limited information is available on the ionic constituents of the raw water can be summarized as follows:

-According to the charge balance equation (A.10):

$$C_{AB} = C_a - C_c = (2[C_{bo}] + [H^+] - (DIC_o(\alpha_1 + 2\alpha_2)) - K_w[OH^-]) \qquad (A.31)$$

Since this analysis is intended for use in dilute, low ionic strength systems, it was assumed that the magnitude of C_{AB} is essentially constant during the limestone dissolution process, i.e., its contribution to the total ionic strength of the system is constant and equal to I_{AB}.

The specific conductance attributable to C_a and C_c, K_{AB}, was calculated by combining equations A.28 and A.29, i.e.,

$$K_{AB} = K_m - ([Ca^{++}]\ Ca^{++} + [H^+]\ \lambda H^+ + [CO_3^{2-}]\lambda CO_3 = \\ +[HCO_3^-]\ \lambda HCO_3^- + [OH^-]\lambda OH^-) \qquad (A.32)$$

and I_{AB} was calculated using equation A.30.

The contribution to the ionic strength by Ca^{++}, H^+, OH^-, HCO_3^-, and $CO_3^=$ at each pH was determined by Equation A.18 as follows:

For Condition 2.a,

$$I' = 1/2(4(C_{bo} + S) + [H^+] + ((DIC_o + S)(\alpha_1 + 4\ \alpha_2)) + K_w[H]) \qquad (A.33)$$

For Condition 2.b,

$$I' = 1/2(4(C_{bo} + S) + [H^+] + (DIC(\alpha_1 + 4\alpha_2)) + K_w[H]) \qquad (A.34)$$

where, DIC is estimated using equation A.24.

Table A.4 Ionic Strength and Specific Conductivity for 34 Adirondack Region Lakes

Ref. #	1×10^4 [M]	K_{AB} micromhos/cm	$I_{AB} \times 10^4$ [M]	K_{AB} micromhos/cm
1	3.81	23.70	3.14	16.36
2	1.97	22.70	1.41	13.85
3	4.23	26.00	2.63	19.20
4	2.21	28.00	1.81	17.35
5	2.16	33.70	1.48	17.03
6	2.63	16.60	1.79	13.44
7	2.98	17.60	1.89	13.16
8	3.10	22.40	1.94	18.17
9	2.3	24.50	1.78	15.26
10	2.94	27.10	1.99	17.82
11	3.08	24.10	2.08	18.89
12	3.41	21.00	2.42	16.90
13	2.80	19.90	1.91	15.86
14	4.14	22.60	3.32	16.63
15	6.47	33.40	3.87	20.71
16	7.18	40.40	4.28	26.56
17	7.09	50.50	5.30	43.68
18	6.76	41.10	3.33	23.64
19	7.61	44.00	4.59	39.87
20	8.36	54.80	4.82	38.97
21	6.00	33.40	3.32	20.95
22	6.96	44.90	3.83	30.09
23	8.71	81.30	4.87	63.26
24	5.84	34.80	3.61	25.00
25	5.48	18.00	4.78	13.08
26	4.77	24.10	3.15	16.60
27	2.47	20.90	1.67	16.40
28	2.99	27.00	3.08	18.15
29	5.36	29.00	3.13	19.09
30	4.44	19.06	3.27	14.65
31	4.51	24.20	2.90	17.70
32	4.83	32.80	3.06	24.97
33	6.11	34.20	3.18	21.18
34	7.34	24.7	6.34	14.67

For Condition 2.c,

Equation A.33 was used to calculate the chemistry of the contactor effluent (closed system) and then equation A.34 was used for the condition when the contactor effluent is opened to the atmosphere.

For all conditions, once I_{AB} and I' are known, the total ionic strength of the solution can be estimated using equation A.27,

$$I = I_{AB} + I' \qquad (A.35)$$

and the computational procedure for the three conditions (2.a, 2.b and 2.c) proceeds in the same manner as was described for the case when the detailed chemistry (C_a and C_c) is known.

Appendix B
Dissolution Rate Data
from Column Experiments

Run Number	Column[1]	Superficial Velocity (cm/min)	Influent Water Characteristics[2]				Overall Dissolution Rate Constant, $K_o \times 10^3$ (cm/min)
			pH	Calcium (mg Ca/L)	Dissolved Inorganic Carbon (mg C/L)	Water Temperature °C	
1	A	5.5	4.19	0	0.1	16	35
2	A	11.0	4.19	0	0.1	16	54
3	A	16.5	4.19	0	0.1	16	61
4	A	22.0	4.08	0	0.2	16	37
5	A	27.5	4.08	0	0.2	16	54
6	A	5.5	3.92	3.0	0.3	16	37
7	A	11.0	4.00	1.7	0.1	16	22
8	A	16.5	4.00	1.7	0.1	16	44
9	A	22.0	3.92	3.0	0.3	16	51
10	A	27.5	4.00	4.3	0.2	16	62
11	A	27.5	4.34	0.3	0.1	10	46
12	A	41.2	4.50	0	0.1	10	54
13	A	55.0	4.50	0	0.1	10	54
14	A	72.0	4.50	0.3	0.1	10	69
15	A	5.5	4.50	0	0.2	10	18

[1] See Figure for limestone particle diameter and sphericity and bed porosity

[2] Background electrolyte concentration was 20 mg NaCl/L

Run Number	Column[1]	Superficial Velocity (cm/min)	Influent Water Characteristics[2]				Overall Dissolution Rate Constant, $K_o \times 10^3$ (cm/min)
			pH	Calcium (mg Ca/L)	Dissolved Inorganic Carbon (mg C/L)	Water Temperature °C	
16	A	5.5	3.89	3.2	5.5	22	12
17	A	5.5	3.90	5.2	0	22	9
18	A	16.5	3.90	5.2	0	22	22
19	A	5.5	3.91	0.1	0.5	22	55
20	A	16.5	3.91	0.1	0.5	22	82
21	A	27.5	3.91	0.1	0.5	22	101
22	A	27.5	3.89	0.2	1.8	22	64
23	A	16.5	3.89	0.2	1.8	22	49
24	A	5.5	3.89	0.2	1.8	22	23
25	A	54.8	5.45	0	0.3	10	47
26	A	38.4	5.45	0	0.3	10	33
27	A	21.9	5.45	0	0.3	10	16
28	A	5.5	5.45	0	0.3	10	25
29	A	55.0	4.00	0.2	0	10	73
30	A	38.4	4.00	0.2	0	10	52

[1] See Figure for limestone particle diameter and sphericity and bed porosity

[2] Background electrolyte concentration was 20 mg NaCl/L

Run Number	Column[1]	Superficial Velocity (cm/min)	Influent Water Characteristics[2]				Overall Dissolution Rate Constant, $K_o \times 10^3$ (cm/min)
			pH	Calcium (mg Ca/L)	Dissolved Inorganic Carbon (mg C/L)	Water Temperature °C	
31	A	22.0	4.00	0.2	0	10	38
32	A	5.5	4.00	0.2	0	10	32
33	D	8.8	5.99	0.4	0	9	35
34	D	6.1	5.99	0	0	9	15
35	D	3.5	5.48	0	0	9	11
36	D	0.9	5.48	0	0	9	7
37	D	8.8	3.86	0.4	0	9	19
38	D	6.1	3.86	0.4	0	9	17
39	D	3.5	3.88	0.7	0.1	9	11
40	D	0.9	3.98	0.3	0.2	9	6
41	D	8.8	3.41	0.0	0.2	9	21
42	D	6.1	3.41	0.0	0.2	9	18
43	D	3.5	3.56	0.3	0.3	9	20
44	C	54.8	6.12	2.4	0.2	10	105
45	C	38.4	6.12	2.4	0.2	10	52

1 See Figure for limestone particle diameter and sphericity and bed porosity

2 Background electrolyte concentration was 20 mg NaCl/L

Run Number	Column[1]	Superficial Velocity (cm/min)	Influent Water Characteristics[2]				Overall Dissolution Rate Constant, $K_o \times 10^3$ (cm/min)
			pH	Calcium (mg Ca/L)	Dissolved Inorganic Carbon (mg C/L)	Water Temperature ^oC	
46	C	21.9	6.12	2.4	0.2	10	42
47	C	5.5	6.12	2.4	0.2	10	26
48	C	54.8	4.02	0.5	0.2	10	116
49	C	38.4	4.02	0.4	0.2	10	78
50	C	21.9	4.02	0	0.2	10	54
51	C	5.5	4.38	0	0.2	10	23
52	C	54.8	3.53	0.2	0.2	10	63
53	C	38.4	3.53	0.2	0.2	10	40
54	C	21.9	3.53	0.2	0.2	10	27
55	C	5.5	3.53	0.2	0.2	10	12
56	B	54.8	5.45	0	0.3	10	126
57	B	38.4	5.45	0	0.3	10	52
58	B	22.0	5.45	0	0.3	10	25
59	B	5.5	5.45	0	0.3	10	19
60	B	55.0	4.00	0.2	0	10	150

1 See Figure for limestone particle diameter and sphericity and bed porosity

2 Background electrolyte concentration was 20 mg NaCl/L

Run Number	Column[1]	Superficial Velocity (cm/min)	Influent Water Characteristics[2]				Overall Dissolution Rate Constant, $K_o \times 10^3$ (cm/min)
			pH	Calcium (mg Ca/L)	Dissolved Inorganic Carbon (mg C/L)	Water Temperature ^oC	
61	B	38.4	4.00	0.2	0	10	70
62	B	21.9	4.00	0.2	0	10	45
63	B	5.5	4.00	0.2	0	10	45
64	B	5.5	3.51	0.3	0	10	35

1 See Figure for limestone particle diameter and sphericity and bed porosity

2 Background electrolyte concentration was 20 mg NaCl/L

APPENDIX C

Estimates of Limestone Contactor Cost

The Culligan contactor unit (see Figure 8) with 100 lb (45 kg) of Cullneu medium (2ft^3 (57 L) of medium) costs $672 installed (March 1986). A 50 lb (23 kg) bag of Cullneu costs $50.40. Culligan recommends that the unit be used with a flow rate of less than 5 gpm (0.3 L/s) and that the medium be backwashed periodically. The piping supplied with the unit enables one to backwash using the influent flow. Culligan also suggests that the Cullneu medium be replenished by the addition of small amounts ("handfulls") at frequent intervals (monthly).

The box contactor, depicted in Figure 7, was constructed by graduate students at Syracuse University. The materials used in its construction, (plywood, acrylic plastic, fiberglass, etc.) were purchased for approximately $800. About 80 man-hours of labor were required. The unit contained about 800 lb (363 kg) of limestone. The empty box weighed approximately 400 lbs (182 kg) and therefore installation of the box contactor in the mountain-side spring was a very time-consuming laborious process.

The least expensive approach involves the purchase of a fiberglass pressure vessel and filling it with crushed limestone. This is what was done in the case of the wound-fiberglass column (Column 1, Figure 8). It is recommended that the limestone be analyzed to determine amounts of chemical contaminants and $CaCO_3$ purity before it is used. The cost of limestone is negligible ($\sim$\$0.01/lb, \$0.02/kg) compared to the cost of a container. The cost of fiberglass pressure vessels is given in Table C.1. Depending on the size of the unit the cost ranges from \$3 to \$7/L (\$85 to \$198/ft^3)capacity.

TABLE C.1 Cost of Fiberglass Pressure Vessels

Vessel Volume	Dimensions Diameter	Length	Approximate Cost (March 1984)	Approximate Cost Dollars/Liter
14L	15 cm	46 cm	$ 92	6.6
28L	20 cm	100 cm	$137	4.9
57L	20 cm	132 cm	$198	3.5
100L	33 cm	137 cm	$296	3.0
142L	36 cm	165 cm	$410	2.9